FIELD MEASUREMENT OF SELF-AERATED HIGH SPEED OPEN CHANNEL FLOW

A thesis presented for
the degree of Doctor of Philosophy
in Civil Engineering
in the University of Canterbury,
Christchurch, New Zealand.

---

by

R.J. KELLER

February 1972

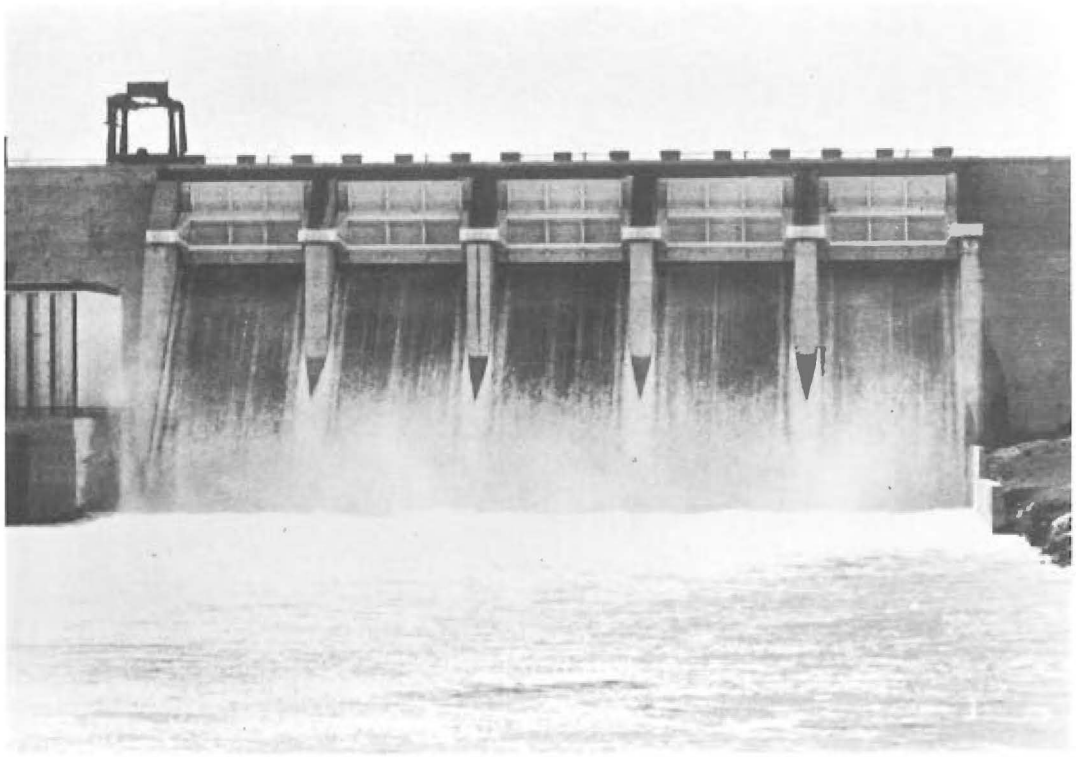

FRONTSPIECE : SELF AERATED FLOW ON SPILLWAY OF AVIEMORE DAM, WAITAKI RIVER, NEW ZEALAND.

ABSTRACT

This thesis is concerned with the measurement of self-aerated flow on the spillway of a large dam.

The major part of the project involved the development of an air concentration probe and a velocity meter suitable for use under field conditions. The air concentration probe basically measures the electrical conductivity of a small filament of the flowing air-water mixture. The velocity meter measures the stagnation pressure at a point in the flow and relates this to the velocity and air concentration.

Results subsequently obtained with the instruments on the spillway of the Aviemore Dam are presented.

During testing, it was noted that the "critical point", where aeration commenced, moved downstream with increasing flow discharge. Furthermore, it was found that its position could be predicted by means of a formula derived from a previous experimental study of model overflow spillways.

An analysis of model data, obtained in a previous model study, was carried out and found to correlate well with the prototype data obtained on the Aviemore spillway. A design method for partially - aerated developing flows is presented.

It was found that the governing criterion in spillway design is the extent of wall-induced aeration. Further development of the instruments to enable measurements to be made near the spillway side wall is discussed.

ACKNOWLEDGEMENTS

This study was undertaken within the Civil Engineering Department, University of Canterbury, under the overall guidance of Professor H.J. Hopkins, Head of Department.

Many staff members and others assisted in the execution of this study. In particular the writer expresses his grateful thanks to the following;

Professor F.M. Henderson, formerly of this University, who first inspired the writer's interest in hydraulics, and initiated this study.

Mr R.F. Hince, formerly of this University, who acted as supervisor throughout the greater part of this study. He provided inspiration and made many constructive suggestions and the writer is particularly indebted to him.

Professor I.R. Wood, who supervised the result analysis phase of this study. His experience and encouragement are greatly appreciated.

Dr D. Rowell, formerly of this University, who acted as consultant during the development of the electronic equipment.

Mr G.F. Archer, whose technical ability enabled high quality instruments to be constructed.

Mr H.S. Pearce, who assisted with the field testing and was responsible for many of the photographs in this thesis.

Mr W.M. Duncan, of the Ministry of Works, and Mr K.D. McCool of the New Zealand Electricity Department, for their interest and cooperation.

Mr S.M.J. Smith, Project Engineer, Ministry of Works, Otematata, and Mr G. Symes, Station Superintendent, New Zealand Electricity Department, Aviemore, and members of their staffs for assistance during the field testing.

Miss K. Evans, Mr W. McClelland, Mr H. Patterson and Miss S. Ruffell for assistance in the preparation of this thesis.

The University Grants Committee, the University of Canterbury, and the Ministry of Works for financial assistance.

My wife, Judy, for her love and support.

CONTENTS

LIST OF FIGURES

LIST OF TABLES

LIST OF COMMONLY USED SYMBOLS

Each symbol is defined where it first appears in the text.

Separate notations are used for the spillway flow simulator design, and the analysis of the velocity meter testing procedure. These are presented on pages 13 and 67 respectively.

Symbol	Definition
a	Diaphragm radius
B	Width of spillway bay
$B_1 - B_8$	Turbulent fluctuation terms
C	Air Concentration
CF	Velocity meter calibration factor
E	Error value
E_o	Supply voltage
E_p	Voltage across probes
E_s	Voltage across series resistance (represents O/P reading)
h	Diaphragm thickness
I	Electric current
k_s	Roughness height
P	Stagnation pressure
P_{stat}	Static pressure
p	Volume concentration of suspended material
Q	Air-water mixture discharge
Q_w	Water discharge
q	Water discharge/unit width
R	Electrical resistance of mixture
R_1	Electrical resistance of suspending liquid

R_p	Equivalent resistance across probes in mixture
R_s	Series resistance
r	Specific resistivity of suspension
r_1	Specific resistivity of suspending liquid
r_2	Specific resistivity of suspended spheres
U	Free stream velocity
u	Velocity within boundary layer
v	Velocity
w	Ratio R_1/R_s
x	Distance down spillway
Y	Depth of air-water mixture
y	Distance normal to spillway face
z	Ratio E_o/E_s for de-aerated water
α	Spillway slope
γ	Specific weight of water
δ	Boundary layer thickness
δ_1	Boundary layer displacement thickness
ϵ	Measured diaphragm strain output
θ	Tapping coefficient
μ	Poisson's ratio
ρ	Density of air-water mixture
ρ_w	Density of water
σ_{max}	Maximum allowable diaphragm stress

CHAPTER ONE

INTRODUCTION

Self-aeration in open channel flow is the natural phenomenon whereby atmospheric air is drawn into and mixed with the water to create a white appearance and a violently agitated and ill-defined free surface. This condition is possible only in high speed open channel flow and can frequently be observed in spillways (see frontspiece).

The practical importance of research in this field is involved with the economical design of steep channels or chutes. As air is drawn into the flow the mixture increases in volume or "bulks". This implies that aerated flow requires higher side walls than non-aerated flows. However, a complete lack of information from full-scale structures has meant that spillways have been designed assuming pure water flow with an over-conservative margin, to allow for air bulking, when setting wall heights.

The self-aeration phenomenon is related to the conditions of turbulence within the flow which, in turn, are dependent on the shear at the flow boundaries.

The physical process of aeration may be described with reference to Figure 1.1 .

The growth of the turbulent boundary layer, due to the movement of water over the spillway face, commences at a point on the upstream face of the dam. The boundary layer thickness increases with distance down the spillway, growing into the inviscid flow, and transmitting the turbulence generated at the bed towards the surface.

A boundary layer also forms on the upstream face of the spillway gate. However, due to the short length of the gate, the layer remains very thin. It is, thus, insignificant compared to the boundary layer which forms at the spillway face.

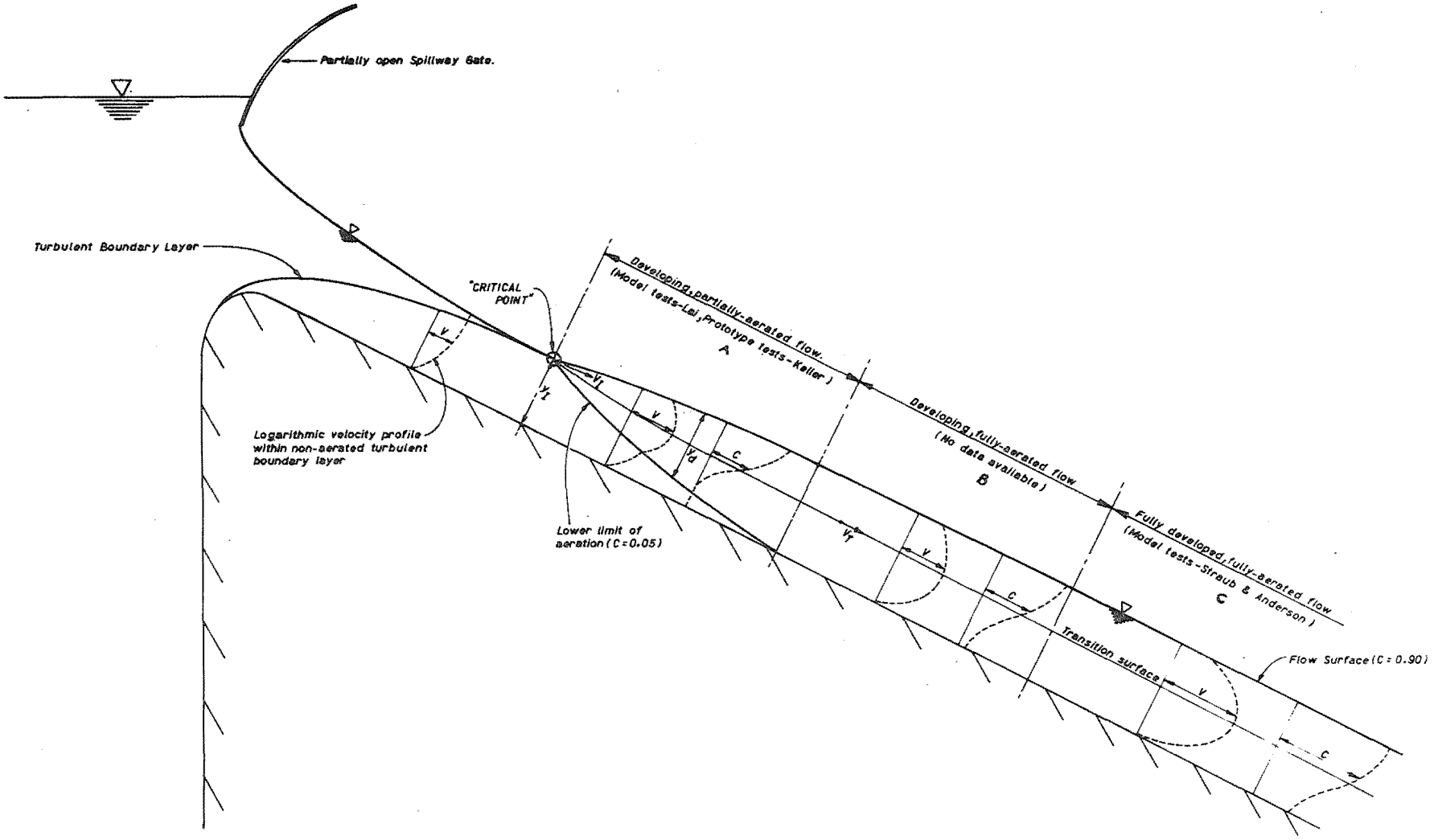

FIG.1.1: TYPICAL SECTION OF FLOW DOWN A STEEP SPILLWAY
(showing expected shapes of velocity (V) and air concentration (C) profiles in each region)

Downstream of the gate, a boundary layer forms at the air-water interface due to atmospheric drag. Because the overlying air is free to move with the water, and is of a considerably lower density and dynamic viscosity, the velocity gradient in the stream is very much less at the surface than at the bed. Thus, the turbulence intensity is also very much less.

The growth of the surface boundary layer has not yet been completely analysed. Ellison[1] assumed that the components of the turbulence which contribute to the eddy viscosity near the surface are determined entirely by local quantities and showed that the velocity profile near the surface could be expressed in the form

$$u = U - \frac{2}{m} V_S \left(1 - \frac{y}{d}\right) \qquad \ldots 1.1$$

where

- u is the velocity at an elevation y above the channel bed
- U is the maximum (free stream) velocity
- m is a constant ($= 0.8$) analagous to von Karmans constant, k, near a rigid wall
- V_S is the shear velocity
- d is the flow depth

By assuming values for the surface drag coefficient, he showed that, for large scale flow conditions, the surface layer is extremely thin. Considering also the comparatively small velocity gradient in the layer, it is, thus, reasonable to ignore its influence on the flow.

The flow surface, then, is not considered to become turbulent until the so called "critical point" (see Figure 1.1) is reached, where the bed-induced boundary layer reaches the flow surface.

Aeration commences at the critical point if the transverse velocity fluctuations, due to the turbulence within the boundary layer, are sufficiently strong to overcome the surface tension and throw particles of water into the air. The falling back of these particles into the main stream with attendant splashing and breaking into a spray is associated with the entrainment of air into the flow.

If the velocity fluctuations are not strong enough for aeration to occur, the flow surface downstream of the critical point, has a characteristically roughened but unbroken appearance.

Downstream of the critical point, the entrained bubbles are carried into the flow by turbulent transport. The penetration is counteracted by the buoyant force on each bubble, so that a balance is reached between the volume of air leaving the flow and the volume being drawn into it. This aeration balance can be compared to the suspended load balance on a reach of a sediment-carrying stream where neither aggradation or degradation occurs.

Normally, the aerated layer continues to thicken with distance downstream until a point is reached where the entire depth of flow is aerated. This point represents the downstream limit of region "A" shown in Figure 1.1.

The flow continues to develop until it has entrained as many air bubbles as it can retain. Beyond this point (the boundary between regions "B" and "C" in Figure 1.1) the air concentration and velocity profiles are similar with distance down the spillway. The stream is then said to have reached the fully aerated, developed state for the given channel slope, roughness, and discharge.

In cases where the turbulent velocity fluctuations at the surface are comparatively weak, the entrained air bubbles are not thrust as violently into the flow. This implies that a fully developed flow condition may be reached without the stream becoming fully aerated. Such cases can occur, for

example, where the flow is in a channel with a smooth bed, or where the flow depth is comparatively large. In the first case, the turbulent fluctuations generated at the bed have been shown to be comparatively weak.[2] In the latter situation the intensity of the turbulence generated at the bed can be considerably weakened by the time it has propogated to the surface.[2]

In such cases the longitudinal delineation of the aerated stream differs from Figure 1.1 in that it consists of only two regions: a region of developing, partially aerated flow, and one in which the flow is fully developed, but not fully aerated.

Above the surface of the air entrained flow a portion of the water discharge flows in the form of droplets which have become detached from the main stream and move through the air by virtue of their initial momentum. Depending on the intensity of the turbulent fluctuations at the surface, this spray region can extend to a considerable distance above the main stream, and, consequently, should be considered in calculations of freeboard in channel design. The surface of the air entrained region is called the "transition" surface between the two flow regimes and is shown in Figure 1.1. The flow "surface" is defined as the level where the air concentration has reached an arbitrary limit (usually 90 or 95 percent.)

In the upper region, the moving water droplets have an appreciable velocity relative to the air. Together with the high velocity at the turbulent transition surface, this has the effect of dragging a considerable volume of air into motion above the flow. A velocity deficiency can be expected in the vicinity of the transition surface because of the drag necessary to sustain this air motion.

The formation of vortices can complicate the picture presented. Vortices may form at the lake surface upstream of the gate or at irregularities on the gate lip. It can be shown[3] that as a vortex stretches in the

direction of the flow, its angular velocity increases, and, hence, its internal pressure is reduced. Consequently, when the stretched vortex reaches the surface downstream of the gate, air may be entrained in its core. This is thought to be the explanation for the streaky nature of the flow, upstream of the critical point, in the photographs of Figure 1.2(Pxxiii)

The problem of vortex formation is a transient phenomenon and the bulking effect associated with the aeration is unlikely to be significant. The phenomenon is not considered further in this thesis.

A further possible cause of bulking in the flow is the mass transfer of oxygen across the liquid-air interface. This possibility was investigated using a penetration theory[4], simplified by assuming that the concentration of dissolved oxygen in the flow, before mass transfer from the atmosphere, was zero. The theory indicated a negligible volume increase of the order of only 0.0017% and no further account was taken of the phenomenon.

The published literature indicates that an awareness of special problems involved in the design of structures, where aerated flows may be expected, has been present throughout the last half century. During the past twenty years the demand for a more comprehensive definition of these flows has intensified in relation to the increase in knowledge about other factors of hydraulic design.

The volume of published material is considerable and the following brief survey covers only those publications which have reported significant advances in the state of the art.

Pioneer laboratory research was carried out by R. Ehrenberger[5] in 1926. He carried out a series of experiments using a smooth, rectangular wooden channel at various slopes. His apparatus for measuring local air concentrations and velocities was ingenious but crude compared with modern

electronic methods. Consequently, the empirical equations he published relating air concentration, flow depth, and channel slope can now be considered of historical interest only.

By observing initial aeration along the sides of steep gradient flows and then aeration across the whole surface, Lane[6], in 1939, first made the qualitative proposal that the onset of aeration was dependent upon the state of the turbulent boundary layer. Later and more elaborate discussions [29, 30] substantiated the hypothesis.

Evidence for the hypothesis is provided by the observation that for increasing gate openings, and, thus, flow depths, the first appearance of white water moves downstream (Figure 1.2).

In 1943, Hall[31] reported on a series of experiments carried out on large field chutes. He suggested that open channel flow equations, such as those of Chezy and Manning, could be applied to aerated flows with modifications to the "non-aerated" values of the Chezy "C" and Mannings "n". His data and conclusions were of limited significance, however, due to the crudeness of his measuring techniques and the relatively small range of conditions covered by the tests.

Bauer[32], in 1954 , carried out an experimental investigation into the development of the turbulent boundary layer on smooth and rough, model overflow spillways. From the results of his investigation, Halbronn [33] showed that

$$\delta = 0.0447\, k_s^{0.154} \times x^{0.846} \quad \text{(rough)} \qquad \ldots 1.2$$

and

$$\delta = \frac{0.0104}{S^{0.0485}} \times x^{0.8515} \quad \text{(smooth)} \qquad \ldots 1.3$$

where

δ is the boundary layer thickness at a distance x from 0 in the direction of flow (see Figure 1.3)

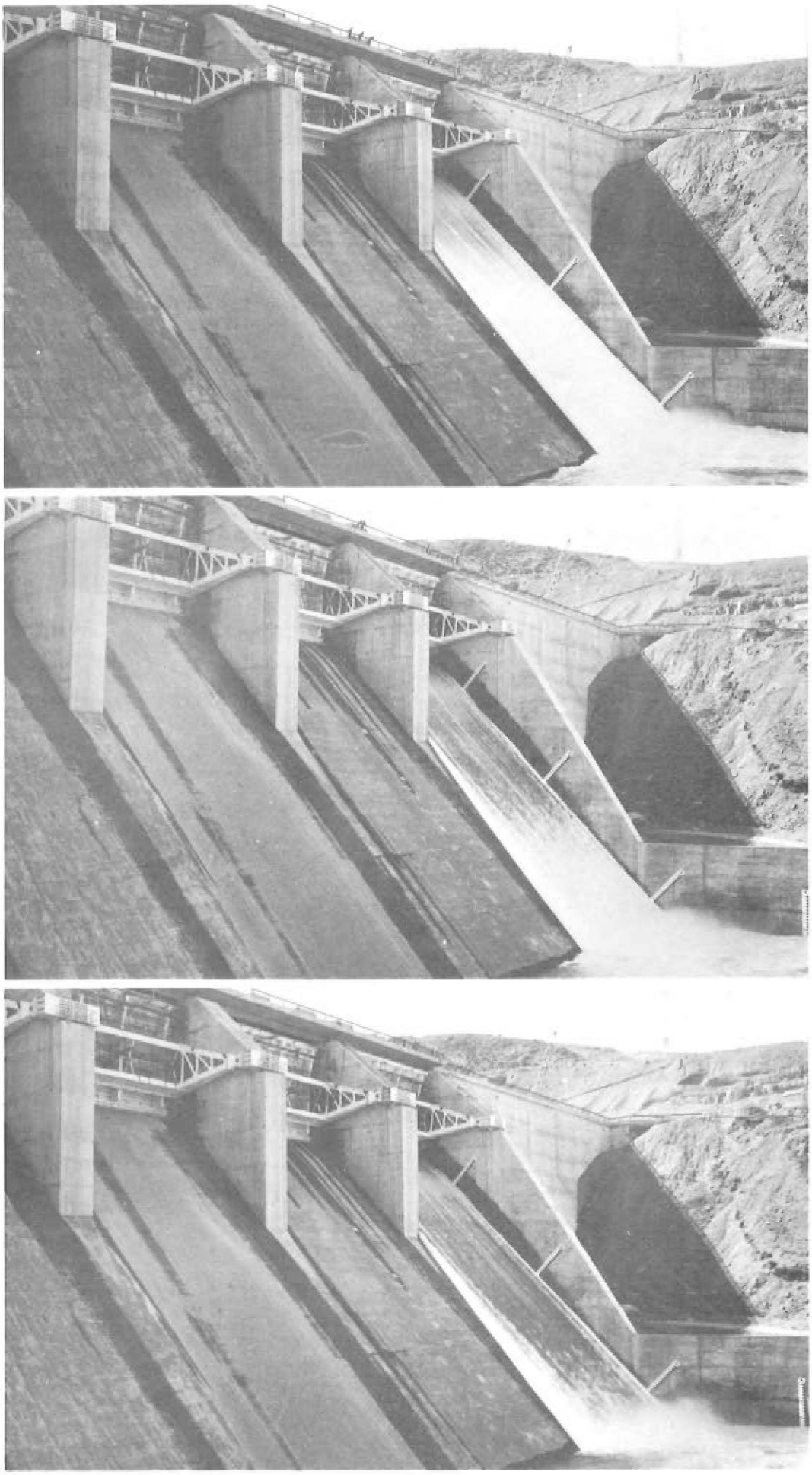

Fig.1.2 : FLOW ON AVIEMORE SPILLWAY FOR GATE OPENINGS 1ft.(Top), 2ft.(Centre) AND 3ft. (Bottom)

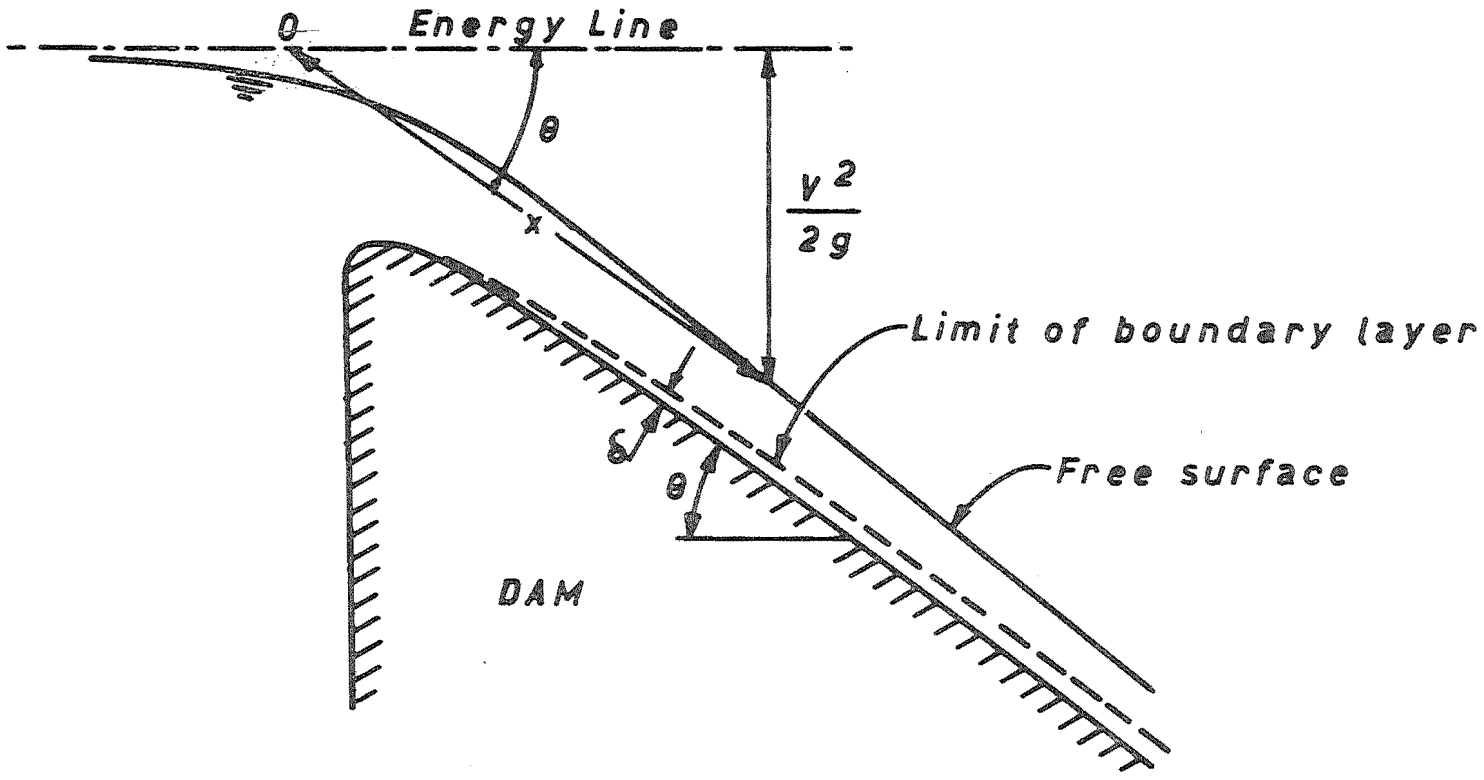

Fig. 1.3 : DEFINITION SKETCH FOR EQ. 1.1

k_s is the roughness height (ft)

S is the channel slope

Bauer further proposed an approximate but practical method of locating the "critical point" for a particular discharge on a concrete overflow spillway. The water surface profile is calculated as the sum of the potential flow thickness (given by $\frac{q}{U}$ where q is the discharge per unit width, and U the free stream velocity computed from the velocity head $\frac{U^2}{2g}$) and the "displacement thickness" (defined as the distance from the boundary that the potential flow has been displaced by the presence of the boundary layer, and calculated to be 10% of the thickness of the boundary layer - see Appendix V). The water surface and boundary layer profiles are plotted as functions of x on the same graph. The "critical point" is then the point of intersection of the two profiles.

A major advance in the experimental study of self-aeration was the development by Lamb and Killen[7], in 1950, of an electronic meter for measuring the air concentration at a point in an aerated flow. The meter measures the electrical conductivity of the air-water mixture relative to that of water alone.

This was followed in 1954 by the successful development by Straub, Killen and Lamb[8] of a velocity meter suitable for measuring point velocities in model self-aerated flows. The meter operated on the direct "time-distance" principle and measured the time for a small slug of salt solution to travel a known distance between two pairs of electrodes.

These developments led to a series of classical experiments carried out at the St Anthony Falls Hydraulic Laboratory, Minnesota, United States; the results of which were published in 1958 by Straub and Anderson[9].

These experiments were notable for their clarification of the detailed structure of fully developed, self-aerated flow (i.e. flow where a terminal air concentration profile has been reached). Straub and Anderson found that the flow can be considered as two distinct regions - a lower region in which discrete air bubbles are suspended in a turbulent stream and are distributed by the mechanism of turbulence, and an upper region consisting primarily of independent droplets and larger agglomerations of water that move independently of the stream proper.

They investigated the distribution of air bubbles in the lower region by using a theory which is commonly used to examine the distribution of suspended sediment in stream flow. The two problems are essentially similar although air bubbles tend to rise and sediment tends to fall. In each case a drift in one direction is balanced by transport in the other direction due to the interaction of fluid turbulence and a continuous change in concentration in the direction normal to the channel bed.

The upward volumetric rate of bubble movement per unit area at a distance y above the bed is given by $C V_b$, where C is the air concentration at an elevation y and V_b is the rising velocity of the air bubbles in flowing water. The rate of downward movement depends on the concentration gradient and on a coefficient ϵ_b representing the intensity of the turbulence.

The resulting equilibrium equation is

$$- C V_b + \epsilon_b \frac{dC}{dy} = 0 \qquad \ldots 1.4$$

Integration of Equation 1.4 requires knowledge of ϵ_b as a function of y.

Straub and Anderson made the assumption that air bubbles are transported in the same manner as momentum; i.e. ϵ_b is proportional to ϵ_m, the eddy viscosity.

By a combination of theory and experiment, it has been shown[10] that ϵ_m has a parabolic form and can be expressed by the equation

$$\epsilon_m = k V_s y \left(\frac{d_T - y}{d_T}\right) \qquad \ldots 1.5$$

where

k is the von Karman universal constant

V_s is the shear velocity

d_T is the elevation of the transition surface above the channel bed.

By writing $\epsilon_b = \beta \epsilon_m$ (where β is a proportionality constant), substituting Equation 1.5 into Equation 1.4, and integrating, Straub and Anderson showed that

$$C = C_1 \left(\frac{y}{d_T - y}\right)^z \qquad \ldots 1.6$$

where

C_1 is a constant whose value is the concentration at $y = \frac{d_T}{2}$

$z = \frac{V_b}{\beta k V_s}$

In the upper region, drops of water are projected upwards by turbulent velocity fluctuations at the transition surface. Straub and Anderson assumed that these fluctuations follow a Gaussian probability distribution. They then showed that the frequency, $f(y')$, with which particles were projected a distance y' above the transition surface could be expressed as

$$f(y') = \frac{2}{h \pi} e^{-\left(\frac{y'}{h}\right)^2} \qquad \ldots 1.7$$

where

h is a measure of the mean distance that the particles are projected above d_T.

They expressed the ratio of the number of drops reaching an elevation y' above d_T to the number leaving the transition surface in terms of the water concentrations at the two depths and deduced from Equation 1.6 that

$$\frac{1-C}{1-C_T} = \frac{2}{h\sqrt{\pi}} \int_{y'}^{\infty} e^{-\left(\frac{y'}{h}\right)^2} dy' \qquad \ldots 1.8$$

where

C is the air concentration at an elevation y' above d_T

C_T is the air concentration at d_T.

They showed further that at the transition level ($y' = 0$) the concentration gradient, $\frac{dC}{dy}$, is a maximum.

Equations 1.6 and 1.8 were found to agree well with the form of the experimental curves. However, although Straub and Anderson's analyses appear to adequately explain the physical structure of aerated flow, the equations are of limited design use because, at the present state of the art, the terms C_T, h, d_T, C_1 and z can be predicted only from the experimental data. Furthermore, their conclusions were limited by the fact that uniform flow was produced artificially in all the experiments by the adjustment of an upstream gate. It follows that Straub and Anderson's results are not strictly applicable unless the flow becomes uniform before reaching the spillway toe, which is not necessarily always the case.

In addition to the emergence of the turbulent boundary layer at the free surface, it is necessary, for aeration to occur, that the kinetic energy of the turbulent eddies at the surface be greater than the surface tension energy.

The latter condition was investigated by Gangadharaiah, Lakshmana Rao, and Seetharamiah[11].

They developed a criterion for a surface eddy, in the form of a water particle, to leave the free surface; based on an investigation carried out by Hino[12].

Hino showed that the mean size of a particle projected into the atmosphere, is proportional to the microscale of the turbulent eddies - regarded as a measure of the diameters of the smaller eddies - near the surface (λ), and may be expressed by

$$\lambda_1 = \pi\lambda = \chi\,\pi\sqrt{\frac{\nu y}{V_S}} \qquad \ldots 1.9$$

where

χ is a constant

ν is the kinematic viscosity of water

y is the flow depth

V_S is the bed shear velocity

The authors expressed the kinetic energy of a particle of water at the surface as

$$K.E = \tfrac{1}{2}\left[\rho\,\tfrac{4}{3}\,\pi\left(\frac{\lambda_1}{2}\right)^3\right]\left[\sqrt{\overline{v^2}}\right]^2$$

$$= \beta_1\left[\rho\left(\frac{\nu y}{V_S}\right)^{\frac{3}{2}}\bar{U}^2\right] \qquad \ldots 1.10$$

where

$\sqrt{\overline{v^2}}$ is the root mean square of the transverse velocity fluctuations, and is expressed as a linear function of the mean water velocity, $\bar{U}$ ($\sqrt{\overline{v^2}} = \beta\,\bar{U}$ where β is a constant).

$$\beta_1 = (\pi^4\,\chi^3\,\beta^2)\,/\,12\ .$$

The surface tension energy was expressed as

$$S.E. = \pi\lambda_1^2\,\sigma = \beta_2\left(\frac{\nu y}{V_S}\,\sigma\right) \qquad \ldots 1.11$$

where

σ is the surface tension

$\beta_2 = \pi^3 \chi^2$

For aeration to occur

$$\frac{K.E.}{S.E.} > 1 \qquad \ldots 1.12$$

Substitution of Equations 1.10 and 1.11 into 1.12 and simplification yields

$$\frac{K.E.}{S.E.} = \frac{I}{\beta_3} > 1$$

where

$I = (\rho y \bar{U}^2 / \sigma) / (V_S y / \nu)^{\frac{1}{2}}$ is defined as the "inception number"

$\beta_3 = \beta_2 / \beta_1$

They carried out a series of model experiments and showed that I has a crtical value of 56 , below which aeration will not occur. From limited prototype observations, they established further that the value of I in full scale channels is generally far in excess of this figure.

The authors did not put forward any theoretical basis for the critical value of inception number, nor is any consideration given to the variation (if any) in β_3 . The concept is not of great importance on full scale structures, where the surface velocity fluctuations at the critical point appear to be always sufficiently large to overcome the surface tension energy and entrain air. Nevertheless, it represents a useful tool in predicting whether or not aeration will occur in small-scale or model channels.

In 1971 Lai[26] carried out a series of experiments on model aerated flows and obtained profiles of air concentration and velocity within the partially-aerated developing region (see Figure 1.1) . These results represent the first comprehensive data obtained in this region.

Lai carried out a theoretical analysis, considering the developing flow as consisting of two layers : 1.) from the channel bed to the transition surface, 2.) from the transition surface to the flow surface.

The lower region was treated as a boundary layer, making the rather extreme assumption that the influence of the air below the transition surface was negligible.

He analysed the upper region by considering it as a free turbulent flow, using a kinematic eddy viscosity to correlate the shear stress with other characteristics of the flow.

In both regions, Lai used simplified air concentration and velocity profiles which did not agree well with the shape of his experimental curves.

The writer considers that a better basis for analysis is to treat the aerated region as a separate phenomenon. An analysis based on this concept is presented in Chapter Five of this thesis.

Most investigators have experienced difficulty in fitting their experimental data to a generally acceptable relationship. The empirical approach used in most of the studies reported rendered varying relationships among slope, flow depth, velocity, and air concentration which appear to define the data from that study but do not always agree well with results of other investigations. Consequently, even in the most comprehensive recorded investigations, there are qualifying limitations placed on the proposed relationships.

Furthermore, it is known that flow down the face of a high, open spillway is not well represented in the conventional hydraulic model,

mainly due to disproportionate resistance effects. Thus the application of the research to practical design problems clearly depends on detailed corroborative information from large spillways. Despite this dependence, such information has not yet been obtained.

Undoubtedly the main reasons for the lack of research on large scale flows have been the problems of instrumentation and non-availability of suitable large spillways. The difficulty of holding measuring instruments in full scale high velocity flows is severe in itself, let alone the problems posed by the requirements of remote control, limited space, and independence from continual calibration.

Moreover, testing on large scale flows is expensive and unattractive to researchers because of the restricted availability of water and the relatively small range of test conditions that can be studied on a single installation.

Nevertheless, a full understanding of the phenomenon of self-aeration, as applied to spillway design, must await a comprehensive series of tests carried out on many large spillways and covering a wide range of flow conditions.

The investigation reported in this thesis was initiated to study the effect of aeration on the flow in the spillway of the Aviemore Dam on the Waitaki River, and represents the first known attempt to obtain detailed information from a full-scale structure.

The major part of the project involved the development of instrumentation to measure accurately various spillway flow parameters. This development included the design of a special field unit by means of which depth profiles of air concentration and velocity could be obtained at various positions on the spillway. Laboratory equipment capable of simulating the spillway flow under variable and measureable conditions of turbulence, air concentration and velocity was a pre-requisite to instrument design.

The development of the instrumentation is described in detail in Chapter Two of this thesis.

In Chapter Three, the experimental programme carried out on the Aviemore Spillway is described. The programme was designed with two objects - firstly the obtaining of depth profiles of mean (time average) air concentrations and velocities at different points on the spillway; secondly the investigation of the time dependence of air concentration and stagnation pressure at different points in the spillway flow.

Representative results from the experimental programme are presented in Chapter Four. An error analysis is included and the significance of the results themselves discussed.

In Chapter Five a re-analysis of Lai's data is presented. This enables a comparison to be made between his model data and the writer's prototype data. On the basis of this analysis, a design method is proposed whereby the air concentration and velocity profiles within the partially-aerated developing flow region may be predicted.

Chapter Six completes the thesis by drawing conclusions from the results of the experimental programme, and the correlation with Lai's data, and by commenting on the suitability of the developed instrumentation. The chapter incorporates, also, suggestions for the improvement of the developed instruments and for further experimental work.

CHAPTER TWO

INSTRUMENT DESIGN

SYNOPSIS

The experimental programme carried out necessitated the development of the equipment detailed in this chapter. This work involved the design of instruments which would measure accurately air concentrations and velocities at points in the flow. Furthermore a pier assembly had to be developed which would be strong enough to hold the instruments under the very demanding high speed flow conditions, yet light enough to be readily portable between stations on the spillway.

Laboratory equipment capable of simulating the spillway flow under variable and measurable conditions of turbulence, air concentration, and velocity was a prerequisite to instrument design.

This chapter is devoted to a detailed explanation of each part of the equipment.

2.1 SPILLWAY FLOW SIMULATOR

2.1.1 Introduction

This section describes in detail the spillway flow simulator constructed for use in the design of the field instruments.

It was of great importance that the simulator reproduced the true spillway flow as accurately as possible with regard to velocity, air concentration, and degree of turbulence. In order that the full

range of field conditions could be covered, it was also important that the three parameters be independently adjustable.

It was felt that the best method of satisfying these conditions lay with the construction of a jet pump using water in the pressure line, air in the suction line, and the effluent air-water mixture as the test flow.

In an earlier Ph.D. project, C.F. Bathurst[13] developed the theory and method of design of a jet pump suitable for use with the high pressure water source available in the University of Canterbury Fluid Mechanics Laboratory. Although an accurate design was not necessary in this case, Bathurst's work did form the basis for the jet pump used. A description of the design principles involved is presented.

An important requirement for the simulator was the provision of an independent and accurate means of determining the mean air concentration of the effluent air-water mixture. Once this was measured the mean velocity could be simply obtained by a consideration of mixture discharge and tail-pipe area. It was decided that a method whereby the air concentration was determined by measuring the degree of absorption of gamma radiation was the simplest and most accurate. A description of the theoretical principles involved is presented, together with an account of the design, construction, and operating characteristics of the meter.

2.1.2 Operating Principle

The jet pump is a device which performs its pumping action by the transfer of energy from a high velocity jet to one of low velocity. This is achieved by converting the potential energy of the driving flow into kinetic energy by means of a nozzle. This flow then combines with the low velocity suction stream by turbulent mixing in the mixing

chamber of the pump.

Figure 2.1 depicts a typical jet pump layout, and illustrates some of the notation used in the theoretical analysis.

2.1.3 Theoretical Analysis

Notation:

Symbol	Definition
P_1	Gauge pressure of water supply
P_2	Gauge pressure of air at inlet
P_3	Gauge pressure of air-water mixture at end of throat
P_f	Frictional pressure loss in throat
Q_1	Volume flow rate of water
Q_2	Volume flow rate of air
D_1	Diameter of water nozzle
D_3	Diameter of throat
R_D	Ratio of water nozzle diameter to throat diameter (D_1/D_3)
R_L	Ratio of throat length to diameter
U_1	Water velocity at nozzle
U_2	Air velocity at inlet to pump
U_3	Water velocity at bottom of throat
K	Slip velocity at bottom of throat (defined as difference between velocity of water and velocity of air)
A_1	Area of water nozzle
A_3	Area of throat
ρ_1	Density of water
ρ_2	Density of air
γ_1	Specific weight of water
ρ_*	Average density of air-water mixture

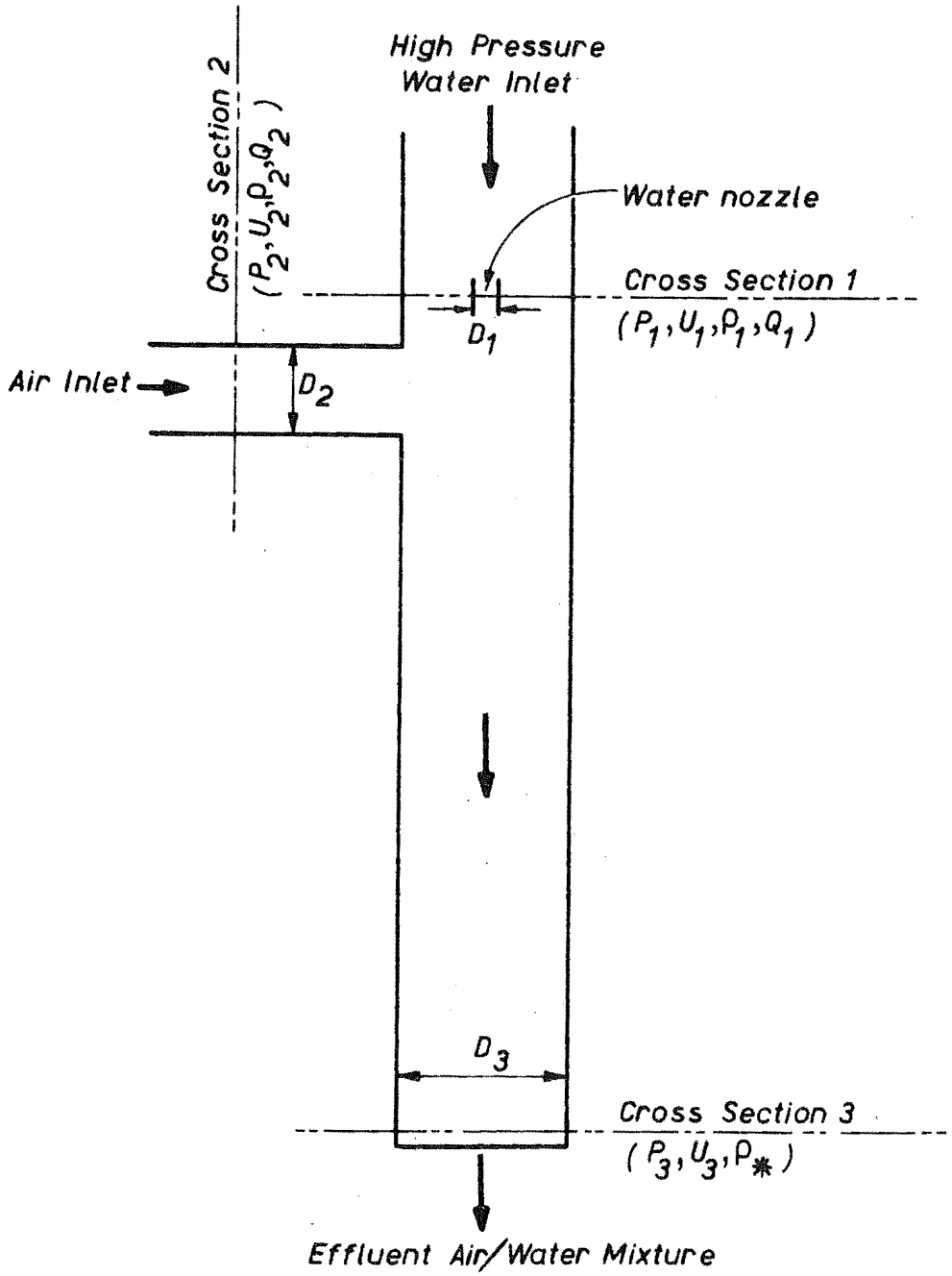

Fig. 2.1: SPILLWAY FLOW SIMULATOR – Schematic showing notation used in theoretical analysis.

R_e Reynolds Number

C_d Discharge coefficient of nozzle

Fundamental Equations (refer to Figure 2.1):

(a) Equation of continuity at cross-section 3

$$\frac{Q_1}{U_3} + \frac{Q_2}{U_3 - K} = A_3 \qquad \ldots 2.1.1$$

(b) Equation of momentum between cross-section 1 and cross-section 3

$$A_3(P_3 - P_2 + P_f) = Q_1\rho_1(U_1 - U_3) + Q_2\,\rho_2(U_2 - U_3 + K)$$

The last function on the right hand side is negligible as the change in momentum of the air is very much less than that of the water.

Thus

$$A_3(P_3 - P_2 + P_f) = Q_1\rho_1(U_1 - U_3)$$

$$\therefore \quad U_3 = U_1 - \frac{A_3}{Q_1\rho_1}(P_3 - P_2 + P_f) \qquad \ldots 2.1.2$$

(c) Energy equation at cross-section 1

$$\frac{(P_1 - P_2)}{\gamma_1} = \frac{1}{C_d^{\,2}} \frac{U_1^{\,2}}{2g}$$

$$\therefore \quad U_1^{\,2} = 2g\, C_d^{\,2} \frac{(P_1 - P_2)}{\gamma_1} \qquad \ldots 2.1.3$$

(d) Continuity equation at cross-section 1

$$Q_1 = A_1 U_1 \qquad \ldots 2.1.4$$

Design Equations:

Substitute Eq. 2.1.4 in Eq. 2.1.2

$$U_3 = U_1 - \frac{(P_3 - P_2 - P_f)}{\rho_1 U_1 (R_D)^2} \qquad \ldots 2.1.5$$

Substitute Eq. 2.1.4 in Eq. 2.1.1 and solve for Q_2

$$Q_2 = A_3(U_3 - K)\left(1 - \frac{(R_D)^2 U_1}{U_3}\right) \qquad \ldots 2.1.6$$

Equations 2.1.3, 2.1.5, and 2.1.6 are the design equations.

Energy Losses:

Energy losses in the pump are accounted for by the terms C_d, P_f, K and some assessment must be made of their values.

The term C_d as used in Eq. 2.1.3 accounts for the water nozzle friction loss.

The loss due to the friction of the air-water mixture against the sides of the throat is represented by the term P_f. In calculating P_f, it is assumed that the air friction against the walls was negligible and only the water friction need be considered. The water velocity decreased from U_1 to U_3 down the throat, thus tending to decrease the loss per foot length; and the average density (defined as the product of the water density and the ratio of cross-sectional area taken up by water to throat area) increased, thus tending to increase the loss per foot length. Thus, as a first approximation, it is assumed that the loss per unit length remained about the same down the throat, and equal to the loss per unit length at the nozzle end of the throat. The friction loss is calculated using the Darcy-Weisbach equation and the Moody diagram. The procedure is detailed in Section 2.1.4c.

The loss due to slipping of the air backwards past the water is described by a slip velocity, K. It was known that K would be small compared with U_3, and hence, as a first approximation, it was reasonable to neglect it.

2.1.4 Simulator Design and Construction

Design Procedure:

(a) Determine a nozzle geometry and a value for C_d.

The shape of the nozzle has a considerable influence on the performance of the pump. Induced turbulence in the water from a rough-walled nozzle is desirable as it aids complete mixing over a short length of throat. However, as the nozzle roughness is increased, the discharge coefficient is reduced because of the increased energy loss across the nozzle.

Several trial designs were considered. Figure 2.2 shows the adopted design. It is similar to one tested by Bathurst which was found to have a discharge coefficient of 0.83. For design purposes, this value for C_d was adopted.

(b) Plot a nozzle characteristic curve of pressure head against discharge, and match this with the corresponding characteristic curve for the high head centrifugal pump (source of the high pressure water in the driving line of the jet pump).

Equation 2.1.3 may be written in the form

$$H = \frac{Q_1^2}{2gC_d^2A_1^2}$$

where H is the head on the water nozzle in ft. of water $\left(= \frac{P_1 - P_2}{\gamma_1} \right)$. The curves are shown in Figure 2.3.

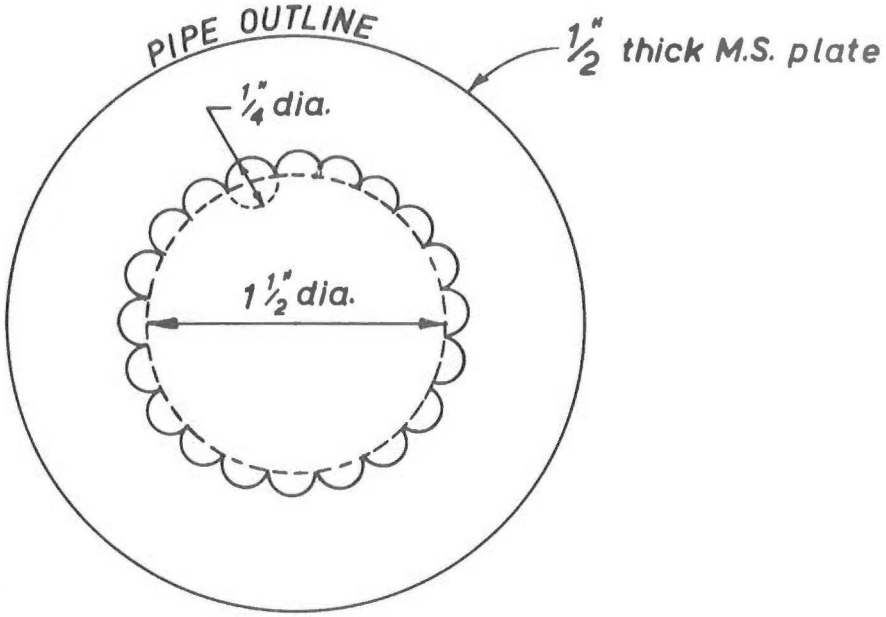

(a) Design sketch (Plan)

(b) Completed nozzle

Fig. 2.2 : SPILLWAY FLOW SIMULATOR-WATER NOZZLE

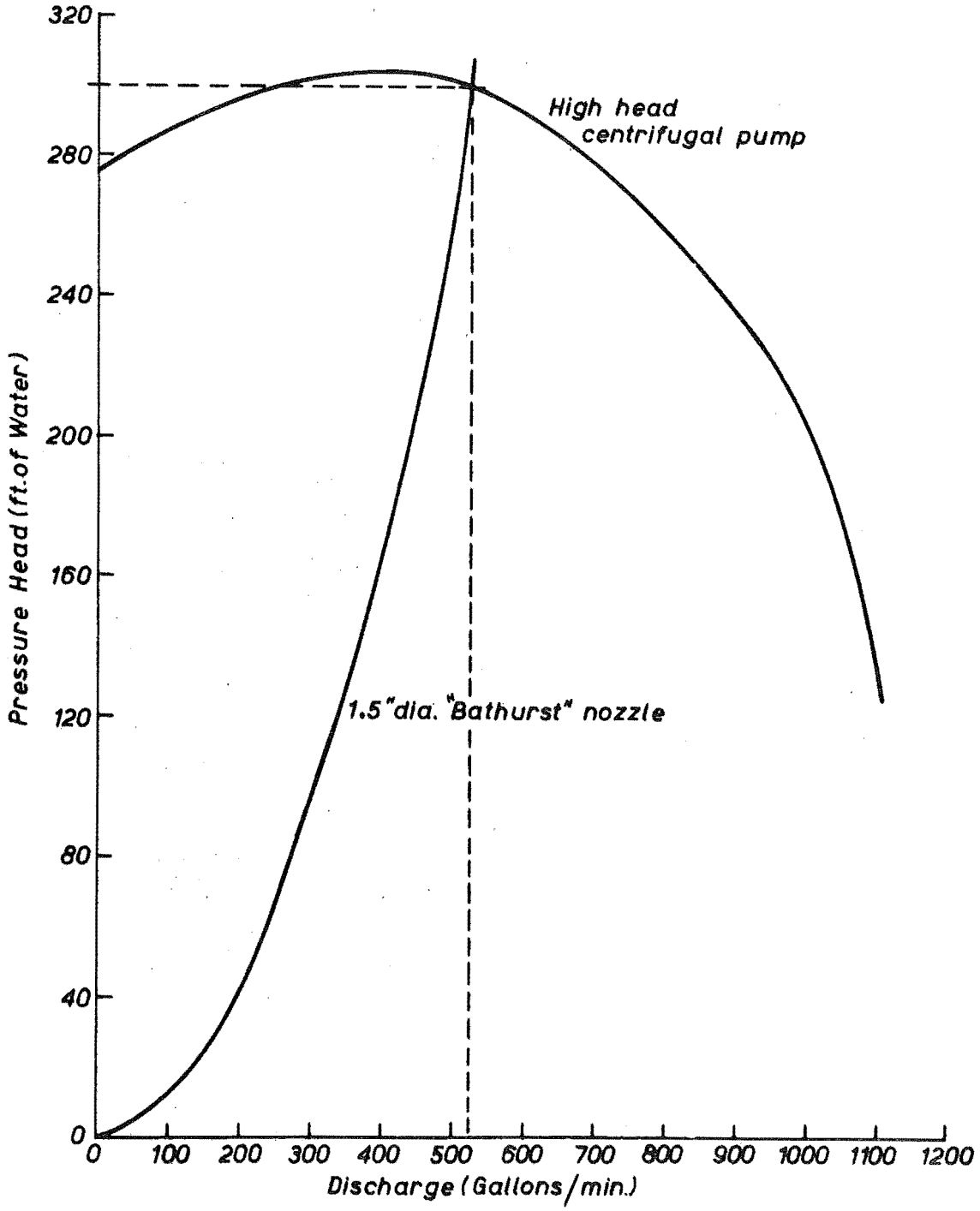

FIG.2.3:SPILLWAY FLOW SIMULATOR—CHARACTERISTIC CURVES FOR NOZZLE & LABORATORY CENTRIFUGAL PUMP.

(c) From Eq. 2.1.3 calculate the value of U_1 , the velocity through the water nozzle, and use this value in Eq. 2.1.5 to calculate U_3 , the effluent mixture velocity.

In Eq. 2.1.3, P_2 was assumed to have a value of -10 psi. Even a large error in this assumption is not significant as P_2 is very much smaller than P_1 .

The friction force, P_f , in Eq. 2.1.5 was estimated by the following procedure:

(1) Calculate the average density, ρ_* , at the top of the throat

$$\rho_* = \rho_1 (R_D)^2$$

(2) Calculate a Reynolds number using the throat diameter, D_3 , initial water velocity, U_1 , the water viscosity, μ , and the average density, ρ_* .

$$R_e = \frac{\rho_* U_1 D_3}{\mu}$$

(3) Use the Moody diagram to obtain the friction factor, f , assuming the tailpipe material, perspex, to be hydraulically smooth.

(4) Calculate P_f from the Darcy-Weisbach equation using an assumed value for the throat length to diameter ratio, R_L , of 15.

$$P_f = f R_L \frac{U_1^2}{2g} \rho_*$$

Substitution in Eq. 2.1.5 gives the value of U_3 . It should be noted that $P_3 = 0$ (as the bottom of the throat is open to the atmosphere).

(d) From Eq. 2.1.6 calculate the volume flow of air, Q_2 , into the pump.

The air concentration, C , of the effluent air-water mixture is then simply obtained from

$$C = \frac{Q_2}{Q_2 + Q_1} \times 100$$

The above design yielded a value for air concentration of 72% and an efflux air-water mixture velocity of 109 ft/sec. It was felt that these values were sufficiently good to justify building the pump and making any necessary adjustments by trial and error under operational conditions.

Construction:

Construction of the simulator was reasonably straightforward.

It was important that pipe friction losses upstream of the jet pump nozzle be kept to a minimum. For this reason six inch diameter pipe was used, only reducing to three inch diameter immediately before the nozzle.

The test section was made from $\frac{1}{4}$ inch perspex sheet, fabricated to a three inch diameter pipe with flanges fitted top and bottom. The top flange attached the test section to the jet pump piping; the bottom flange was drilled to take the supports for the prototype instruments.

General and detailed drawings and photographs of the spillway flow simulator are shown in Figures 2.4 through 2.6.

2.1.5 Simulator Monitor Equipment - Theory, Design, Operating Characteristics

Two methods of determining density (which may be directly related in this case to air concentration) are widely used:

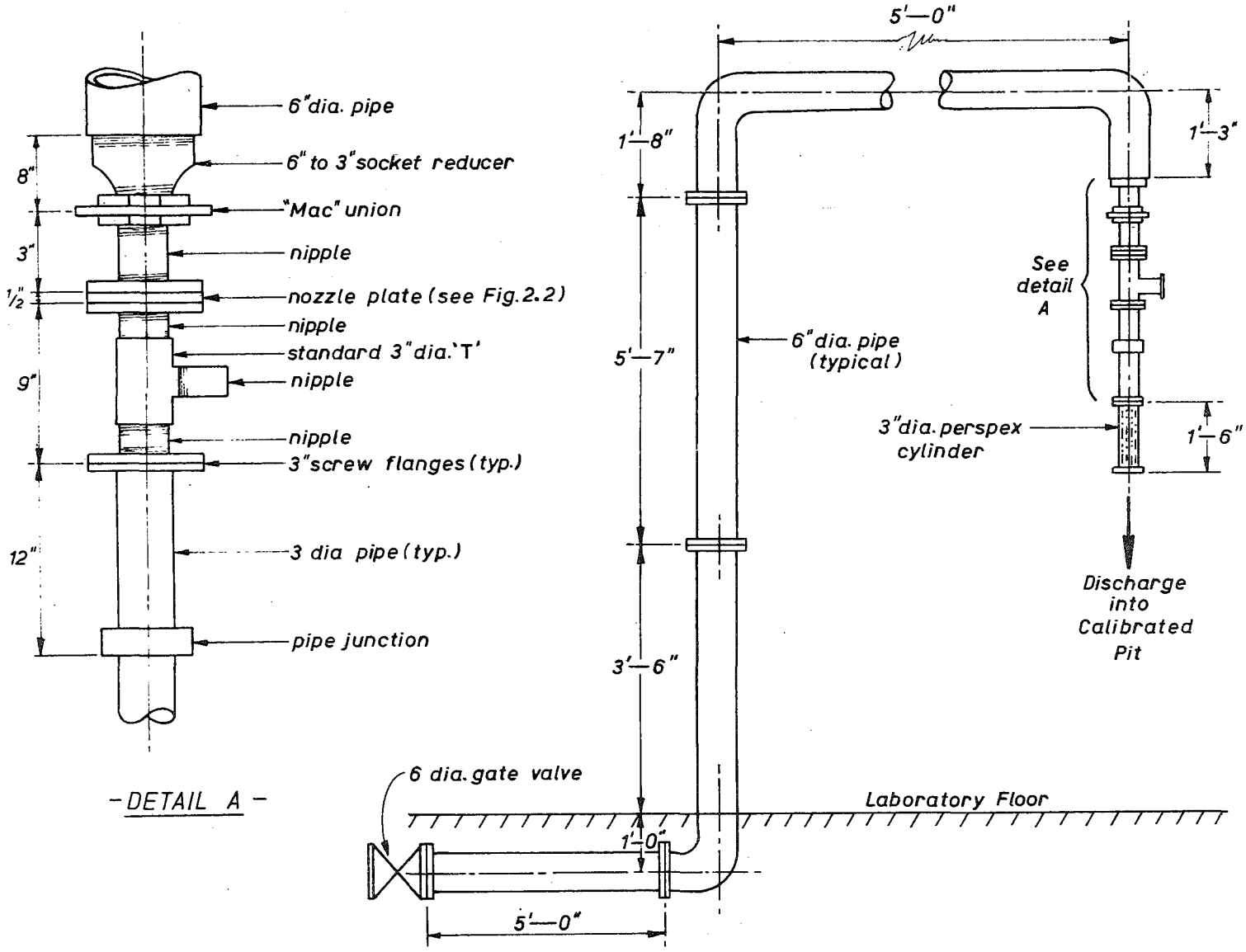

Fig. 2.4 : SPILLWAY FLOW SIMULATOR – BASIC DESIGN

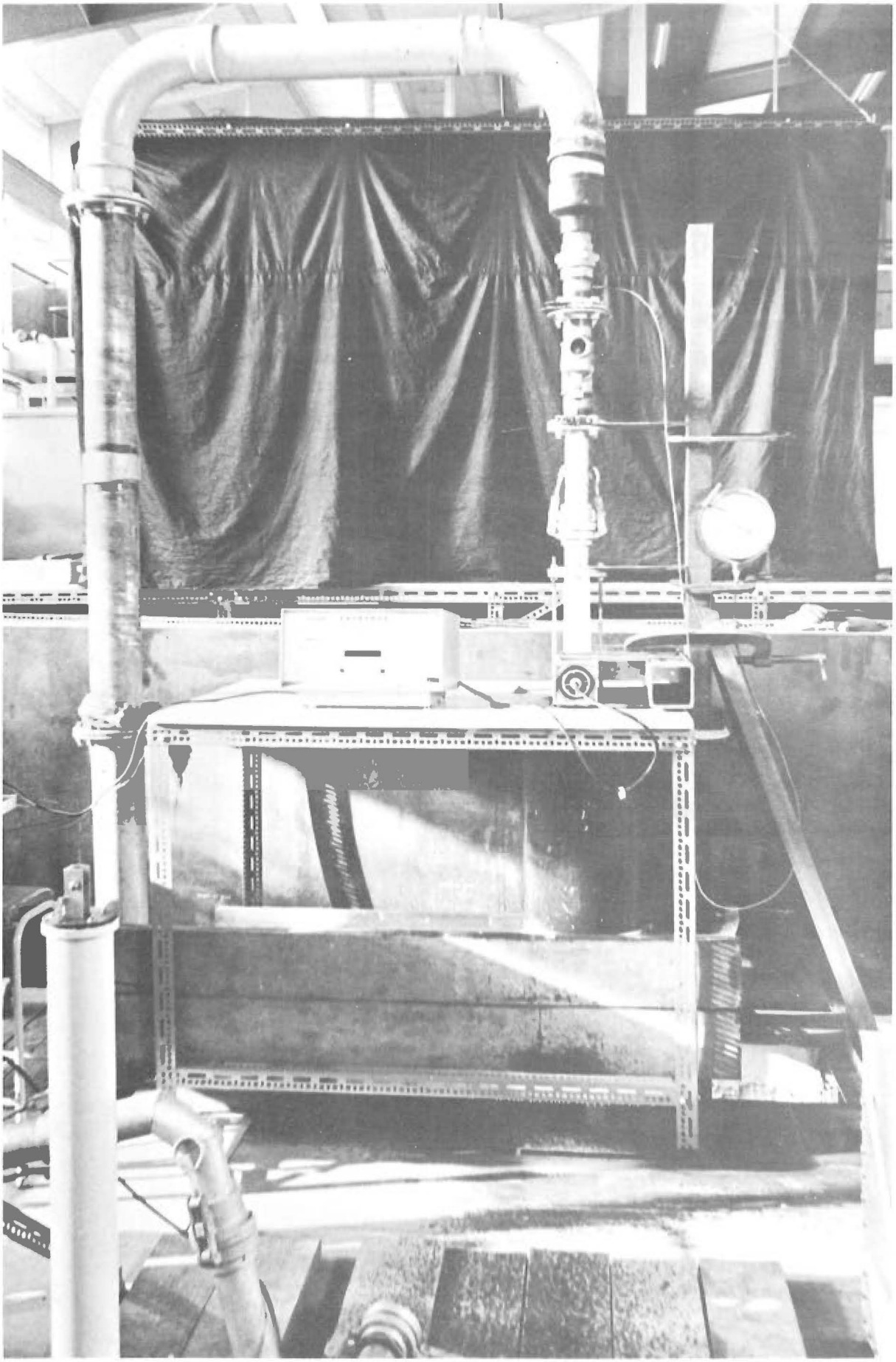

Fig. 2.5 : SPILLWAY FLOW SIMULATOR.

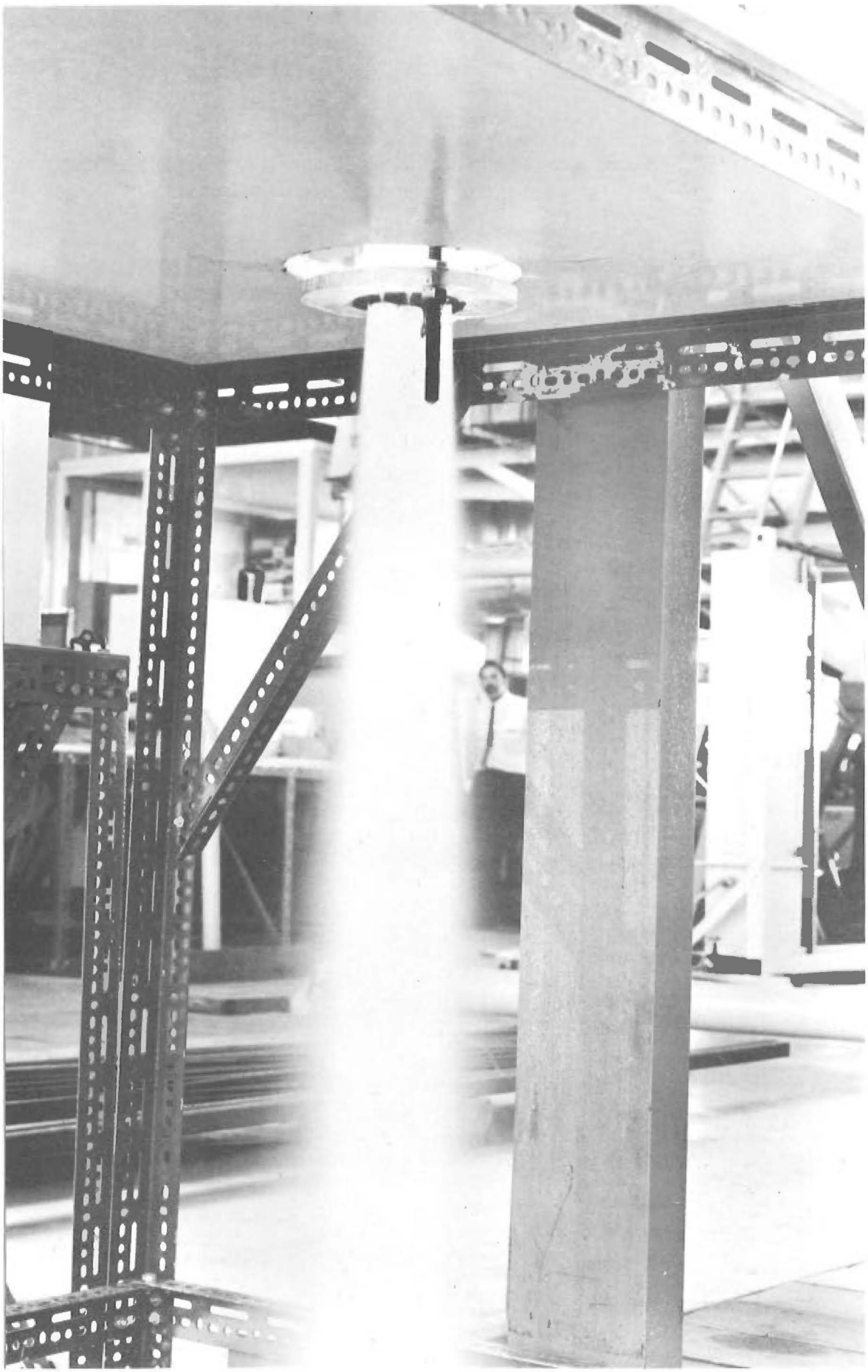

Fig.2.6 : EFFLUX AIR–WATER MIXTURE.

(1) By measurement of back scatter of gamma rays

(2) By measurement of transmitted gamma rays.

The first method gives the mixture density in the region of the radiation source only. The second method gives the average density across the absorber and, hence, is more suitable in this case.

In general, the attenuation of gamma rays obeys an exponential law[14]. This is rigorously true for narrow beams of radiation and good as a first approximation for broad beams. The law may be expressed by the equation

$$I = I_o \, e^{-\mu x} \qquad \ldots 2.1.7$$

where I is the radiation intensity passing through the absorber

I_o is the radiation intensity incident on the absorber

μ is the linear absorption coefficient (which may be considered as the fractional decrease in intensity of the radiation per unit thickness of the absorber)

x is the thickness of the absorber.

The equation may be written in the form

$$I = I_o \, e^{-\mu_m m_a}$$

where μ_m is the mass absorption coefficient, defined as $\mu_m = \frac{\mu}{\rho}$ in which ρ is the absorber density

m_a is the mass of the absorber per unit area i.e. $m_a = x\rho$.

It is known that μ_m varies only slightly from material to material, i.e. $\frac{\mu}{\rho} \simeq$ constant (k) or $\mu = k\rho$.

Equation 2.1.7 may then be rewritten as

$$\log I = \log I_o - k\rho x \qquad \ldots 2.1.8$$

Equation 2.1.8 predicts that, if the incident radiation and the

absorber thickness are constant, a graph of log I against ρ plots as a straight line. Furthermore, in this particular case, the density is linearly proportional to the air concentration of the mixture, C ($\rho = \rho_w(1-C)$ where ρ_w is the water density). Thus, for a particular test, any two points define the calibration plot of transmitted radiation against air concentration.

This immediately suggests a procedure for determining the mean air concentration across a diameter of the test section.

(a) Set up the apparatus such that the radio-active source and the detector are diametrically opposite each other.

(b) Obtain values of transmitted radiation (I) for 0% air (pure water - obtainable by closing the air intake valve on the simulator) and 100% air (no flow of water).

(c) Plot log I against air concentration for each of the two calibration points and join with a straight line.

(d) The mean air concentration of the test mixture is then obtained by measuring the transmitted radiation intensity and interpolating the air concentration from the calibration plot.

It is emphasised that this method depends on the theory of exponential attenuation, which is correct for very narrow beams of radiation. However, the accuracy of the method can be verified with a simple check procedure.

The procedure involves mounting the test section horizontally and blocking both ends. A valve is incorporated such that the section can be filled or emptied in a controlled manner. A sensitive point gauge is fitted such that the ratio of water depth to pipe diameter can be accurately determined. The radiation equipment is mounted on a vertical diameter and readings of transmitted radiation intensity noted for

various water depths. For the purpose of this test the water depth can be directly related to air "concentration" along the diameter by the equation

$$C = \frac{D - d}{D}$$

where D is the test section diameter

d is the water depth.

A graph of log I against C will plot as a straight line if the assumption of exponential attenuation is valid.

The important design considerations were those of source strength and shielding. Use of a 1 curie C_s^{137} sample was first considered due to its ready availability from a previous research project[15]. However, 1 curie represents a high energy source, which means very little radiation attenuation would occur in air; hence little change in the absorption properties of the mixture with change in the air concentration. On the other hand, it was important that the energy of the source be not too low, as this would lead to a high percentage of radiation attenuation in the perspex side walls of the test section.

Therefore, a 100 micro curie C_o^{60} source was decided upon and initially tested with different sized lead plugs between the source and the mixture. It was found that a one inch lead plug reduced the radiation incident on the mixture to a level where an easily measurable change in transmitted gamma radiation corresponded to a comparatively small change in air concentration.

A detailed shield design from the safety point of view was not necessary due to the low energy of the source. However, it was important to eliminate as much scattered radiation as possible from the detector unit, as such radiation, indistinguishable from that transmitted through the mixture, could invalidate the assumption of exponential attenuation. The detector was, therefore, surrounded by a combined

iron and lead shield.

A simple source shield was manufactured by pouring molten lead into an iron mould.

The "narrow beam" characteristics of the combined shielded source-detector unit were checked by the procedure described on page 26. The resulting graph of log I against C is presented in Figure 2.7. The linearity of the plot justified the assumption of exponential attenuation.

The detection unit used was a Philips PW4111 Scintillation Detector. Basically this unit comprises a scintillation crystal which transforms incident gamma radiation into electrical pulses. The unit requires a sensitive high voltage supply and an important operating characteristic is the dependence of the count rate (directly related to the number of emitted electrical pulses) on the magnitude of the voltage. A graph of count rate, in the presence of a constant radio-active source, against voltage, exhibits a "plateau" or levelling in the count rate over a considerable voltage range. The correct operating voltage is in the middle of this plateau where minor unavoidable changes in voltage will not influence the count rate during a particular test. The position of the plateau relative to the applied voltage varies for different radio-active substances. The correct operating voltage for C_o^{60} was found to be 1350 volts.

The electrical pulses from the scintillation detector were "processed" by a Nuclear Chicago Model 183B Count-O-Matic Scalar. The number of pulses counted was indicated by eight interpolation lights and a four digit electro-mechanical register. The time elapsed during a counting period was indicated on a six digit odometer timer. The operation mode used for all testing was "Pre-Count"; by which the time for a pre-set number of counts was obtained. The scalar incorporates a well-regulated high voltage supply which powers the detector unit.

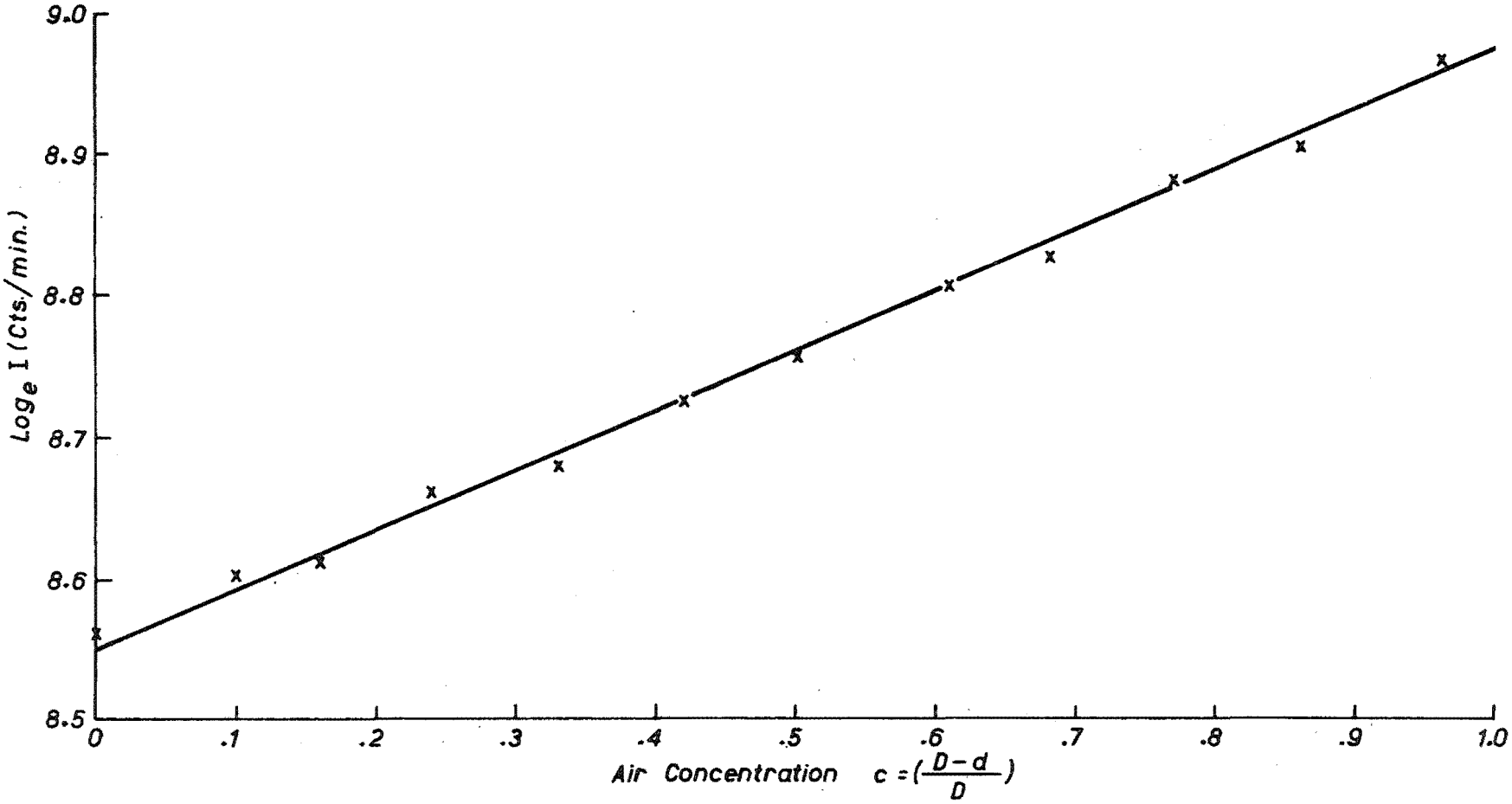

Fig. 2.7 : SIMULATOR AIR CONCENTRATION METER – EXPONENTIAL ATTENUATION TEST.

Figure 2.8 shows a photograph of the radiation detection and counting units.

Operating Characteristics:

Any radiation detector exhibits a certain "background" count rate, caused by cosmic rays. This count rate is measured, in the absence of the radio-active source, in the same way as the sample count rate. It is then subtracted from the apparent count rate measured during testing.

In practice the background radiation was measured before and after a test and a linear variation with time assumed. This procedure was justified as the background radiation was found to be very low compared with the measured source radiation. Thus, any divergence from a linear variation in the background count rate had a negligible effect on the measured sample rate.

In assessing the accuracy of radio-active measurements, attention must be given to the question of statistical errors. Disintegrations of a radio-active material do not occur at evenly spaced time intervals but have a random distribution in time. It can be shown[16] that the number of counts in a given period is distributed according to the Poisson distribution. Probability theory then shows that the error associated with the average value determined from a sample of random counts is inversely proportional to the square root of the total number of counts regardless of the time required; i.e.

$$\text{Error} = \frac{k}{\sqrt{N}} \qquad \ldots 2.1.9$$

where N is the total number of counts recorded

k reflects the "confidence" in the computed error.

A confidence level of 90% is obtained by giving k the value of

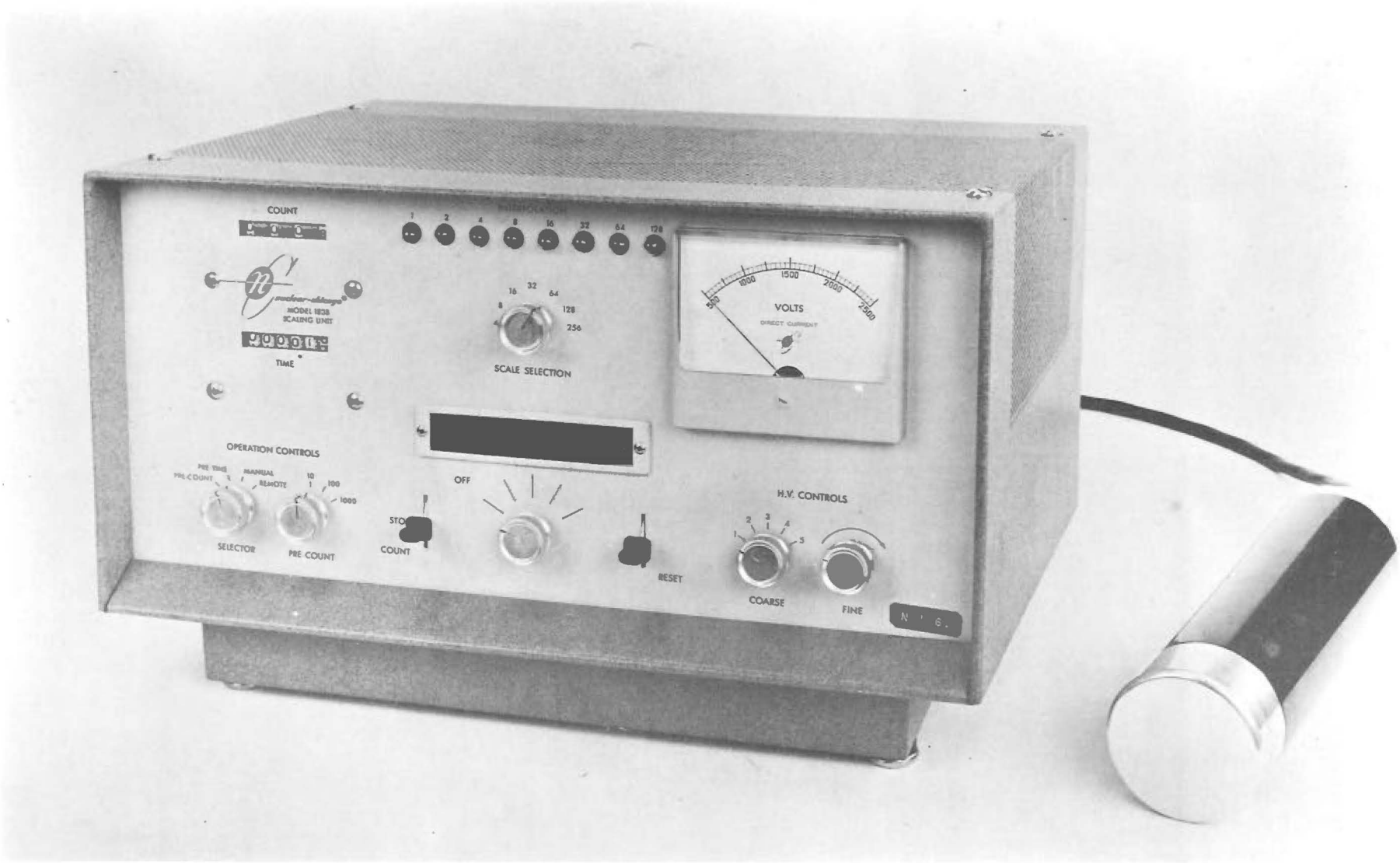

Fig. 2.8 : γ RADIATION DETECTION AND COUNTING UNITS.

1.6449[17]. The error associated with this value of k is called the "reliable error".

From Eq. 2.1.9 the percentage deviation, D , from the observed count rate can be calculated from

$$D = \frac{100\ k}{\sqrt{N}}$$

$$= \frac{164.49}{\sqrt{N}} \qquad \ldots\ 2.1.10$$

As the radiation method was a standard reference measure of air concentration, it was important for it to be of a high degree of accuracy. Initially an arbitrary value of $\pm$ 1% was set for the maximum allowable error, and Eq. 2.1.10 then specified a minimum count of 27,000 to achieve this. In practice it was much more convenient to use a count of 25,600. This gave a maximum error of 1.03% - certainly of sufficient accuracy for this work.

The only other possible sources of error were those due to coincidence losses and register losses.

The coincidence loss is dependent on the resolution time of the counting system; i.e. the minimum time between two disintegrations such that both disintegrations will be counted. Thus, any disintegration occurring less than the resolution time after the preceding disintegration will not be counted, and the coincidence loss is defined as the count loss due to this effect. The counting system used had a very low resolution time (1 micro second) and it could be shown[17] that the error due to coincidence loss was negligible.

Register losses occur when the count rate of random pulses produces a high register speed. It is desirable to use the highest possible scaling factor, to keep the average register speed as low as

possible. In practice the scaling factor of 256 was almost invariably used, and it could be shown[17] that under these conditions, the percentage of lost register counts was also negligible.

2.2 AIR CONCENTRATION PROBE

2.2.1 Introduction

With regard to the measurement of air concentration, an adequate definition of content and distribution of air implies that the portion of the cross-sectional area included in a single measurement (the so-called "point" of measurement) must be small in relation to the entire cross-sectional area. On the other hand, the area of individual measurement must be large enough to accommodate several air bubbles if a condition of full-scale variation of the measuring instrument at every bubble passage is to be avoided. The instrument sensitivity depends upon its ability to detect small shifts in the mean air concentration at a point. It was important that the instrument be relatively independent of external calibration and insensitive to variables other than concentration of air, since there are no absolute standards of comparison that may be used as a control on the field experimental work.

The high velocity of streams where self-aeration occurs requires the use of a rugged and fairly simple element for insertion into the flow. The shape of this element must not unduly disturb the flow filament being measured, as it is evident that any enforced curvature of the flowing mixture would tend to separate the air from the water because of the difference in densities. Simplicity of operation, freedom from observer errors, and conservation of time are obvious advantages.

This section firstly describes the theory, design, and construction of an electrical air concentration probe which satisfies the basic criteria described above. Although basically similar to the St Anthony Falls meter, described in Chapter One, the air concentration probe

incorporates several features which make it unique.

Laboratory testing procedure and performance conclusions make up the remainder of this section.

2.2.2 Electrical Theory

The electrical method of measuring air concentration consists basically of a measurement of the difference between the conductivity of a mixture of air and water and the conductivity of water alone.

The method depends on the fact that the electrical conductivity of a suspension of particles in a fluid medium varies directly with the total volume of the suspended particles. It is known that the conductivity of the suspension also depends upon the shape and orientation of the suspended particles.

Variations of resistance with temperature and ionization are definite problems in all resistance measurements of suspensions and it is important to be able to account for their effects.

An expression for the conductivity of a suspension of homogeneous non-polarizable spheres was derived by Maxwell[18] as

$$\frac{r - r_1}{2r + r_1} = p\frac{r_2 - r_1}{2r_2 + r_1} \qquad \ldots 2.2.1$$

where

r_1 is the specific resistivity of the suspending liquid

r_2 is the specific resistivity of the suspended spheres

r is the specific resistivity of the suspension

p is the volume concentration of the suspended material

(Note that r is the reciprocal of the electrical conductivity).

In his derivation of Eq. 2.2.1, Maxwell assumed that the spheres were spaced at such a distance from each other that their individual effect in disturbing the course of the electrical current was independent

of the disturbance caused by neighbouring particles.

Photographic observations have shown[19] that air entrained flow may be considered as a suspension of spherical air bubbles in water, thus justifying the use of Eq. 2.2.1. An air bubble adheres closely to the spherical shape because, when it is large enough to become appreciably distorted, the forces of motion tend to rupture the bubble which consequently divides into spheroids of smaller size.

In the case of non-conducting spheres, the right hand side of Eq. 2.2.1 becomes equal to $p/2$, since r_2 tends to ∞., and the solution for volume concentration of the suspended material is

$$p = \frac{\frac{r}{r_1} - 1}{\frac{r}{r_1} + \frac{1}{2}} \qquad \ldots 2.2.2$$

If the specific resistivities are taken over the same volume, electrical resistances may be substituted in the ratios for the resistivity values; thus

$$p = \frac{\frac{R}{R_1} - 1}{\frac{R}{R_1} + \frac{1}{2}} \qquad \ldots 2.2.3$$

where

R is the electrical resistance of the mixture

R_1 is the electrical resistance of the suspending liquid.

Equation 2.2.3 is the basis of the electrical method of measuring air concentration.

The equation may be developed further by considering the following equivalent circuit:

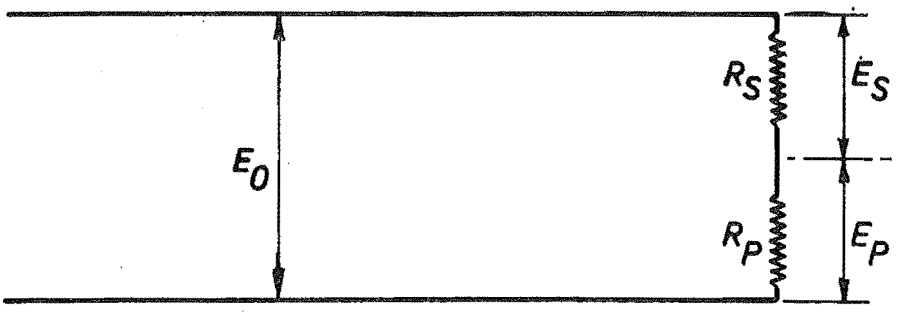

where

E_o is the supply voltage

R_p is the equivalent resistance across the probes in the mixture (= R in Eq. 2.2.3)

R_s is an arbitrary series resistance

E_s is the voltage across R_s

E_p is the voltage across the probes

Then from Ohms Law

$$E_p = I R_p = E_o - E_s = E_o - I R_s \qquad \ldots 2.2.4$$

where

I is the current in the circuit due to E_o . Substitution of Eq. 2.2.4 into Eq. 2.2.3, and of C for p , where C is the volumetric air concentration, yields

$$C = \frac{\frac{E_p}{I} - R_1}{\frac{E_p}{I} + \frac{R_1}{2}}$$

$$= \frac{E_o - I R_s - I R_1}{E_o - I R_s + \frac{I R_1}{2}}$$

i.e. $$C = \frac{E_o - I(R_s + R_1)}{E_o - I(R_s - \frac{R_1}{2})} \qquad \ldots 2.2.5$$

The concept of the field test apparatus incorporated several air concentration probes, each consisting of two electrodes. It was anticipated that the series resistance, R_s , would be common to all probes, but that R_1 , the resistance across the two electrodes of a single probe when placed in de-aerated water, would vary slightly from probe to probe due to slight unavoidable differences in the physical

properties of the probes. A factor, w , which will thus have a unique value for each probe, may be defined by the equation

$$w = \frac{R_1}{R_s} \qquad \ldots 2.2.6$$

Substitution of Eq. 2.2.6 in Eq. 2.2.5 yields

$$C = \frac{E_o - I R_s(1 + w)}{E_o - I R_s(1 - \frac{w}{2})}$$

$$= \frac{E_o - E_s(1 + w)}{E_o - E_s(1 - \frac{w}{2})}$$

$$C = \frac{\frac{E_o}{E_s} - (1 + w)}{\frac{E_o}{E_s} - (1 - \frac{w}{2})} \qquad \ldots 2.2.7$$

Under pure water conditions, C , the air concentration, has a zero value i.e.

$$\frac{E_o}{E_s} = 1 + w = z = \text{ratio of supply voltage to potential}$$

difference across the series resistance when the air concentration probe is placed in de-aerated water.

Equation 2.2.7 may be expressed in the form

$$C = \frac{\frac{E_o}{E_s} - z}{\frac{E_o}{E_s} - \frac{3 - z}{2}} \qquad \ldots 2.2.8$$

It is evident from Eq. 2.2.8 that, if the numerical value of z is 3, the relationship between C and E_s is linear. In practice it was not possible to establish exactly this linear relationship for each probe due to the minor physical differences between them.

The factor z may be obtained experimentally for each probe. For a particular test in aerated water, the supply voltage, E_o, is known, and E_s may be measured. The air concentration is then determined from Eq. 2.2.8.

Photographic observations[7] have shown that above an air concentration of about 60%, the flow can no longer be thought of as a conducting water medium containing non conducting air bubbles. However, Killen and Lamb[7] in the development of the St Anthony Falls meter obtained accurate results at higher air concentrations and sought an explanation. They devised a simple test to obtain a picture of the flow structure, and found that the flow near the surface of an aerated stream is composed of alternate slugs of non-conducting air and conducting air-water mixture. Then, if the indicating instrument of the electrical method follows the rapid concentration changes perfectly, its mean reading over a period of time yields the true value of the mean concentration (except for the small quantity of spray and droplets that might be present in the air pockets and would not be measured.)

2.2.3 Probe Design and Construction

Because the field test apparatus was to incorporate several air concentration probes, some consideration had to be given to the possibility of electrical leakage between probes. This possibility was eliminated by adopting a co-axial probe design, incorporating a centre spike electrode and an outer earthed cylindrical electrode. This concept is shown in Figure 2.9.

The main problem in the hydraulic design of the probes was the prevention of separation of the high speed flow from the conducting surfaces. This was overcome by tapering the centre electrode, so that a small contraction of the flow filament occurred.

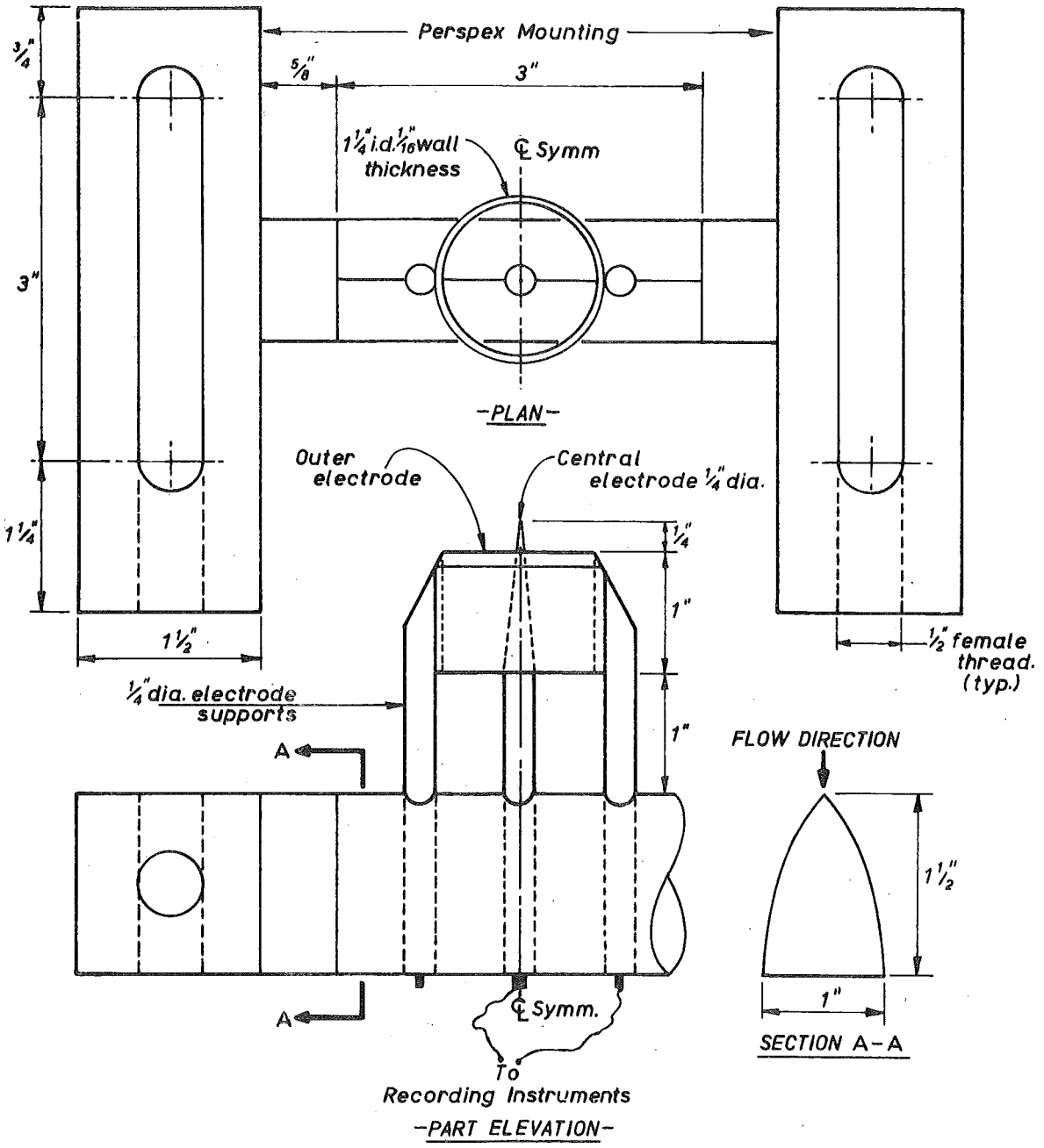

Fig. 2.9 : PROTOTYPE AIR CONCENTRATION METER AND TESTING MOUNT — BASIC DESIGN

The remaining problem was to decide the size of the space between the electrodes. The main considerations were:

(i) The space had to be small enough such that sufficient vertical resolution was obtained with the meter.

(ii) The distance between separate probes on the field test unit had to be small enough, relative to the "area" of the flow incorporated in a single measurement, to adequately define the depth profile of air concentration.

It was known that the minimum possible probe spacing was two inches. (The reasons for this are discussed in Section 2.4.4).

(iii) The space between the electrodes had to be large enough to include several bubble diameters if a condition of full scale variation of the measuring instrument at every bubble passage was to be avoided.

The size of the air bubbles in an aerated stream depends on the balance between the turbulence intensity of the flow and the surface energy of the resultant bubbles.

The St Anthony Falls meter utilized an electrode spacing of $\frac{1}{4}$ inch which proved satisfactory in the model tests subsequently carried out. However, no information could be found regarding the order of bubble size to be expected in full scale aerated flows. Accordingly, to satisfy this condition, a conservative minimum electrode spacing of $\frac{1}{2}$ inch was adopted.

With the above considerations in mind a prototype probe design was adopted as shown in Figure 2.9.

The outer electrode was machined to an inside diameter of $1\frac{1}{4}$ inches, and the inner electrode made from $\frac{1}{4}$ inch brass rod. The outer electrode was held in position with two $\frac{1}{4}$ inch brass rod supports. The supporting

strut was made from perspex and shaped to the streamlined section shown in Figure 2.9.

Subsequent testing of this prototype probe proved completely successful and no further development was necessary.

A photograph of the prototype meter is shown in Figure 2.10. This figure illustrates also the means of traversing the prototype probe across the flow simulator tail pipe.

2.2.4 Testing Procedure

The procedure basically involved obtaining an apparent mean air concentration across a diameter with the electrical probe, and comparing it with the true diametrical mean air concentration obtained with the radiation equipment.

The procedure for determining the true mean air concentration is described in Section 2.1.5.

The apparent mean air concentration was obtained with the electrical probe as follows:

1. The probe was placed in a beaker of clear water, and the secondary resistance adjusted until the value of the factor z (defined in Section 2.2.2) was equal to 3.
2. The probe was traversed across a diameter and at each of five positions, the mean (time average) value of E_s was noted and the air concentration calculated from Eq. 2.2.8.
3. The diametrical mean air concentration was calculated as the average of the five point values across the diameter.

Results from a typical test run are shown in Table 2.1.

2.2.5 Performance Conclusions

Testing was carried out over an air concentration range of 0 - 80%, and a velocity range of 10 - 110 ft/sec. Because of discharge limitations on the centrifugal pump supplying the simulator, it was not possible to

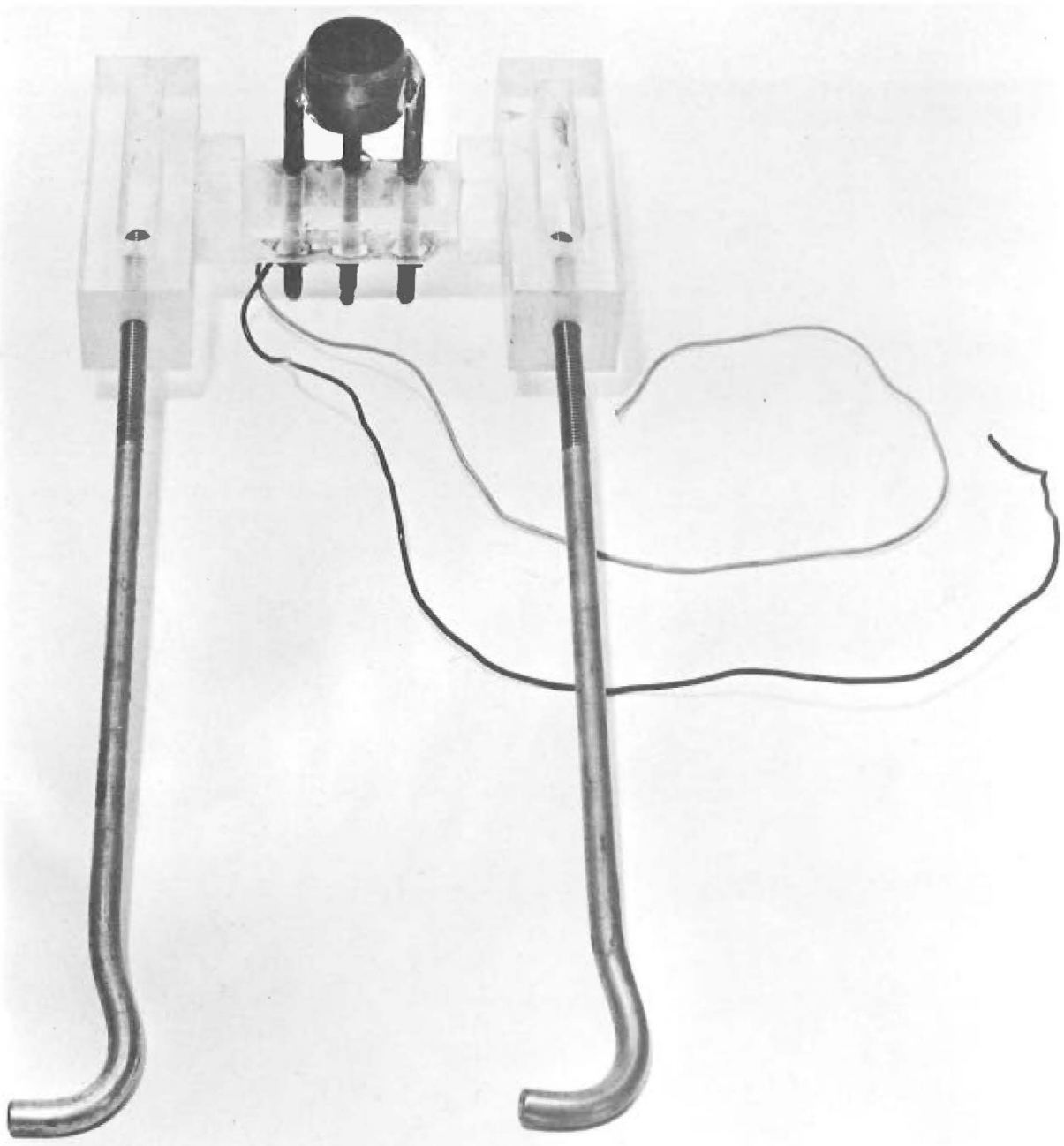

Fig. 2.10 : PROTOTYPE AIR CONCENTRATION PROBE.

Air Concentration measured with rad. meter Gamma Radiation Count Rate (Cts/min.)					True mean Air Concentration
0% air		100% air		Test	
12,277		15,662		14,851	79%
Air Concentration measured with elect. meter Position (across simulator diameter)					**Apparent mean Air Concentration**
1	2	3	4	5	
87%	81%	75%	75%	79%	79.4%

TABLE 2.1: SUMMARY OF RESULTS FROM TYPICAL AIR CONCENTRATION PROBE TEST.

create high speed - low air content flows. However, this limitation was not considered serious as the most arduous test conditions were those that combined high air concentration with high velocity.

Exhaustive testing over this nevertheless wide range of flows showed the probe to be accurate to within 2%.

2.3 VELOCITY METER

2.3.1 Introduction

A satisfactory method of measuring point velocities in high speed air-water mixtures has proved particularly elusive in the past.

Viparelli[20] used a form of Pitot tube incorporating a three way tapping, whereby water at a comparatively high pressure was passed through the tube and into the flow up until the time a reading was taken. In this way air bubbles from the flow were kept out of the manometer lines. The meter, which proved cumbersome even in the laboratory, would have proved impractical under field conditions where remote control was necessary.

A "salt velocity" meter was developed in 1953 at St Anthony Falls by Straub, Killen and Lamb[8] and has been used successfully in model studies. However, it incorporated some features which made it unsuitable for field work. The meter consisted basically of an injection unit and two pairs of electrodes. Small slugs of salt solution, of controllable size and frequency of discharge, were injected into the flow upstream of the first pair of electrodes. The time of travel between the two pairs of electrodes was measured electronically. Absolute control of the size of the salt slug and the frequency of injection were of critical importance and could not be guaranteed under field conditions. Furthermore, the comparatively large size of the injection system and the salt reservoir made the meter unattractive for use in the field, where these parts would

have had to be mounted within a very confined space and all operations carried out by remote control. A further complication was the fact that to obtain a velocity profile, the equipment would have had to have been either duplicated for each probe or arranged such that it could vertically traverse the flow. These factors precluded the use of the meter under field conditions and no attempt was made to duplicate it.

The writer spent considerable time investigating a method which involved measuring the Doppler frequency shift caused by relative motion between fixed transducers and reflecting particles. The method is based on the principle that if ultrasonic energy is radiated into the flow, the air bubbles act as "scatterers" and the frequency difference between the transmitted and the received signals is related to the velocity of the bubbles. A prototype meter was built (see Figure 2.11) but extensive testing in the jet pump showed that reasonably accurate results could be obtained only for velocities less than about 10 ft/sec. and air contents below 5% - impossible limitations for field work. It is thought that at higher velocities and air contents, a "buffer" region, constituting a highly turbulent flow element within which the velocities of the air bubbles were completely non-representative of the true velocity of the main stream, formed in front of the flat surfaces of the transducers. The transmitted signal was not strong enough to penetrate into the main stream from where reflections would have given a true indication of the flow velocity. Instead, reflections from the air bubbles within the buffer region gave a completely false picture.

The next step was the investigation of a method whereby velocities were obtained by measuring stagnation pressures with a strain gauged diaphragm. A meter operating on this principle was developed and proved to be completely suitable for use under the field conditions.

Details of the meter, its development and testing constitute the remainder of this section.

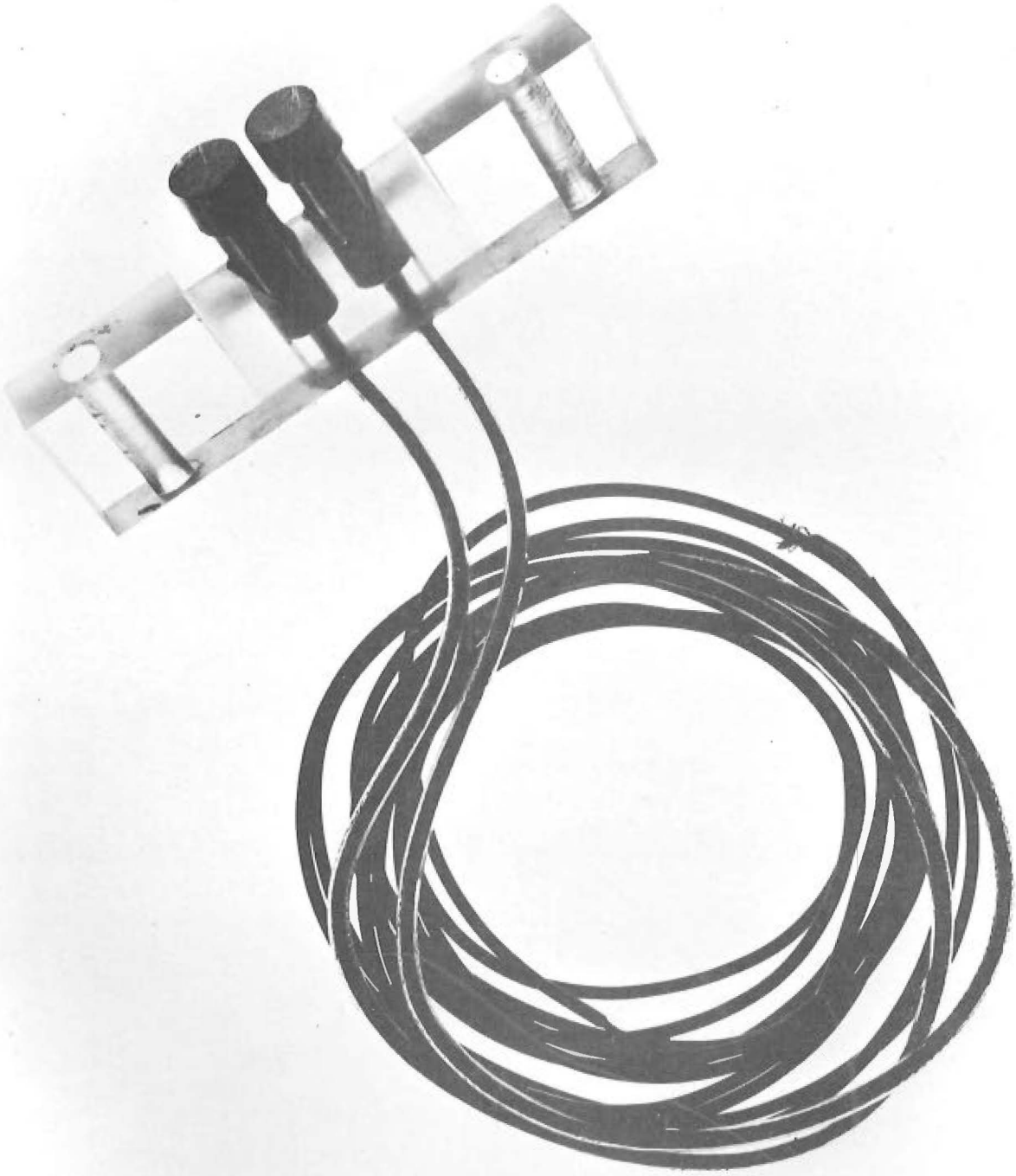

Fig. 2.11 : FIRST PROTOTYPE (ULTRASONIC) VELOCITY METER.

2.3.2 Theoretical Considerations

The basic equation linking stagnation pressure and velocity is simply obtained from the Bernoulli equation and may be expressed in the form

$$P = P_{stat} + \tfrac{1}{2}\rho V^2 \qquad \ldots 2.3.1$$

where (for the point under consideration)

P is the stagnation pressure

P_{stat} is the static pressure due to the weight of overlying fluid

ρ is the density

V is the velocity

Equation 2.3.1 is generally applied to homogeneous fluids. Thus it was important to determine its applicability to a heterogeneous air-water mixture where ρ was considered to be the equivalent mixture density. Viparelli assumed this relationship to be true in the development of his Pitot tube velocity meter and his checks on the meter accuracy validated the assumption.

The mixture density, ρ, may be expressed in terms of the air concentration by the equation

$$\rho = \rho_w (1-\theta C) \qquad \ldots 2.3.2$$

where (for the point under consideration)

ρ_w is the density of non-aerated water

C is the true air concentration

θ the "tapping coefficient", is defined as the ratio of the air concentrations at a point with the velocity meter present and absent.

The inclusion of the tapping coefficient, θ, was apparently necessary because the unavoidable disturbance of the flow by the velocity meter would tend to induce a degree of separation of the air from the

water. However, it has been shown[19] that the value of θ is effectively unity when the ratio of bubble diameter to measuring tube diameter is small, and that in any case θ does not depart significantly from this value for well streamlined shapes.

As a first approximation, therefore, Eq. 2.3.2 was expressed as

$$\rho = \rho_w(1-C) \qquad \ldots 2.3.3$$

Substitution of Eq. 2.3.3 into Eq. 2.3.1 yields

$$P = P_{stat} + \tfrac{1}{2}\rho_w(1-C)V^2$$

or

$$V = \sqrt{\frac{2(P - P_{stat})}{\rho_w(1-C)}} \qquad \ldots 2.3.4$$

Despite the apparent success of Viparelli's meter, it was felt necessary, before embarking on the development of the strain gauged velocity meter, to be completely sure of the applicability of Eq. 2.3.1 to heterogeneous mixtures. Accordingly, a Pitot tube operating on the same principle as Viparelli's was built and tested as a velocity meter in the laboratory simulator.

A photograph of the apparatus is shown in Figure 2.12.

The Pitot tube was tested over a wide range of velocities and air concentrations and was found to be accurate to within 3%, thereby validating the basic assumption of Eq. 2.3.1.

The testing procedure was identical to that for the subsequently developed strain gauge velocity meter and is described in detail in Section 2.3.5.

2.3.3 Meter Design and Construction

The detailed design of the pressure diaphragm was of critical importance as it had to be thick enough to withstand the dynamic shock loading from the highly turbulent flow, yet sensitive enough to respond

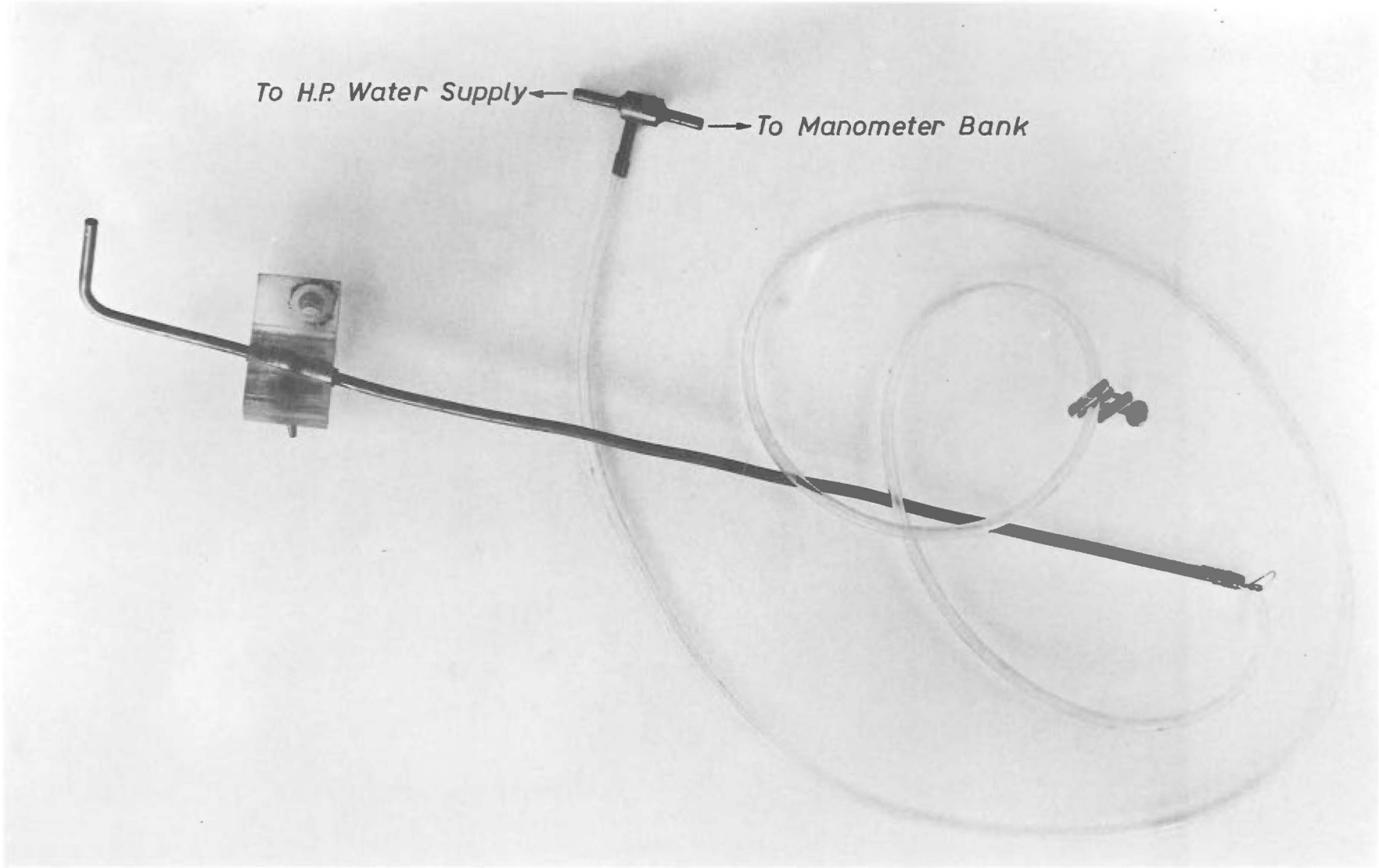

Fig. 2.12 : PITOT TUBE VELOCITY METER.

to small variations in the flow velocity.

The diameter of the diaphragm was dependent on the size of strain gauge used. It was important that this dimension be as small as possible in order that the overall dimensions of the meter be such that a minimum disturbance was created in the flow. The smallest, readily available, suitable gauge was the Shinkoh type FD108 gauge which required a diaphragm diameter of 0.34" for most efficient use.

The diaphragm was designed using the standard theory for circular plates fully built in at the circumference[21]. The design equation for such plates is

$$\sigma_{max} = \frac{3}{4} \times P \times \frac{a^2}{h^2} \qquad \ldots 2.3.5$$

where

σ_{max} is the maximum allowable stress

P is the differential pressure on the diaphragm

a is the diaphragm radius

h is the diaphragm thickness

The diaphragm was designed to be made from brass, reducing the allowable working stress from 20,000 psi to 10,000 psi to allow for dynamic shock loading considerations and the extremely small thickness of the section.

Design Procedure:

(1) Determine a maximum design pressure for the diaphragm.

The difference in elevation between the normal head water operating level at Aviemore and the bottom recording station is 118 ft. and the design pressure for the diaphragm was considered as that due to the velocity of pure water falling through this height. This gave a conservative estimate as, although the velocity at the bottom station approaches this figure, some aeration is present and the pressure is

consequently lower due to the decreased density. The design pressure thus determined was 51 psi.

(2) Determine the diaphragm thickness to withstand this pressure.

From Eq. 2.3.5

$$h^2 = \frac{3}{4} \frac{Pa^2}{\sigma_{max}}$$

which yielded a value of .010" for the minimum thickness of the diaphragm.

(3) Determine the natural frequency of the lowest mode of vibration of the diaphragm.

It has been shown[22] that the natural frequency of vibration can be expressed in terms of the properties of the diaphragm and the surrounding fluid by

$$F = \frac{10.21}{a^2 \sqrt{1 + \beta}} \sqrt{\frac{gD}{\gamma h}} \qquad \ldots 2.3.6$$

in which

$$\beta = 0.6689 \frac{\gamma_1}{\gamma} \frac{a}{h}$$

where

F is the natural frequency of the lowest mode of vibration

D is the flexural rigidity of the diaphragm ($= \frac{Eh^3}{12(1 - \mu^2)}$ where E is the elastic modulus and μ the Poissons ratio for the diaphragm material)

γ_1 is the specific weight of the surrounding fluid

γ is the specific weight of the diaphragm material.

A conservative estimate of the frequency was obtained by considering the diaphragm as being completely surrounded by water. Eq. 2.3.6 then

gave a value of 92,400 cycles/second.

As this was a very high natural frequency, far higher than the expected frequencies of turbulent fluctuations in the spillway flow, the dynamic properties of the diaphragm were satisfactory.

(4) Determine the strain characteristics of the diaphragm and, hence, determine the sensitivity of readings from the strain gauge bonded to the diaphragm.

The strain equations for circular plates are as follows

$$\epsilon_r = \frac{\sigma}{Eh^2} \frac{P}{16} [a^2 (1 + \mu) - r^2 (3 + \mu)] \quad \ldots 2.3.7$$

and

$$\epsilon_t = \frac{\sigma}{Eh^2} \frac{P}{16} [a^2 (1 + \mu) - r^2 (1 + 3\mu)] \quad \ldots 2.3.8$$

where

ϵ_r is the radial strain

ϵ_t is the circumferential strain

r is the radial distance of the point under consideration from the centre of the diaphragm.

The strains were then calculated in terms of P and r from Eq. 2.3.7 and Eq. 2.3.8 and gave

$$\epsilon_r = 2.68 \times 10^{-4} P(.0376 - 3.3r^2) \quad \ldots 2.3.9$$

$$\epsilon_t = 2.68 \times 10^{-4} P(.0376 - 1.9r^2) \quad \ldots 2.3.10$$

Equations 2.3.9 and 2.3.10 were plotted for unit applied pressure (psi) to give profiles of radial and circumferential strain. These are shown in Figure 2.13.

Because of the approximately linear strain-radius relationship over both the radial and the circumferential arms of the strain gauge, the net strain output from each arm could be considered as the actual strain at the middle of each arm. Thus, from Figure 2.13, the values of

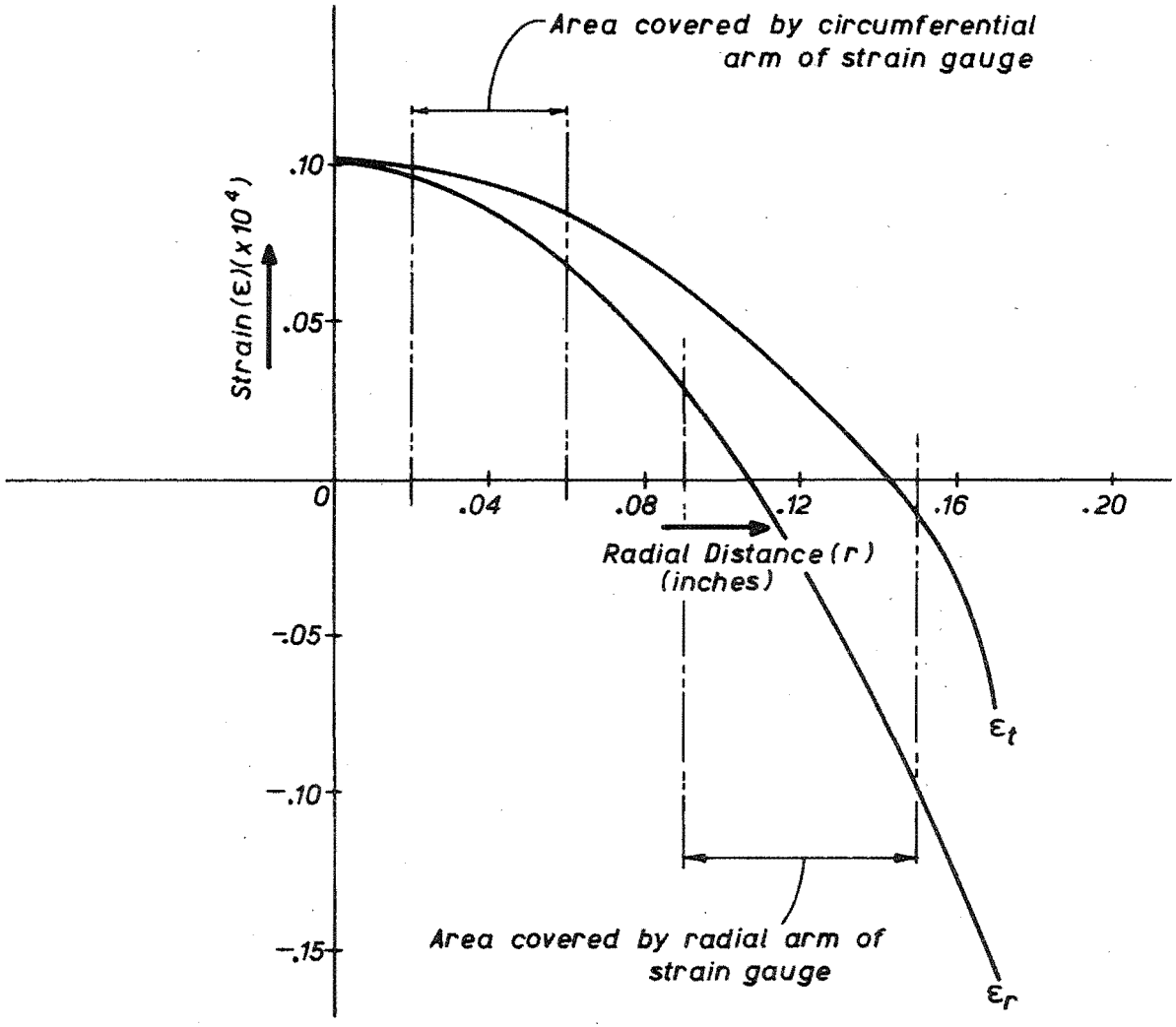

FIG.2.13: VELOCITY METER DIAPHRAGM
(Strain profiles for unit applied load)

radial and circumferential strain output are shown to be $-2.68 \times 10^{-6}P$ and $9.27 \times 10^{-6}P$ respectively.

The total measured strain output from a diaphragm gauge is the arithmetic sum of the radial and circumferential components, with allowance made for the thickness of the backing material between the gauge and the diaphragm.

The influence of the backing material on the magnitude of the measured output is shown in Figure 2.14. This figure shows that, for a diaphragm thickness of .010" and a backing thickness of .001", the measured strain output, ϵ , is given by

$$\epsilon = (|\epsilon_t| + |\epsilon_r|) \times \frac{6}{5}$$

or

$$\epsilon = 14.3 \times 10^{-6}P \qquad \ldots 2.3.11$$

Substitution of Eq. 2.3.1 in Eq. 2.3.11 yields

$$\epsilon = .096 \times 10^{-6} V^2 \qquad \ldots 2.3.12$$

where P_{stat} is assumed to be negligible and the fluid density is assumed to be that of water (i.e. $\rho = 1.94$).

The sensitivity of the velocity meter was then calculated by differentiating Eq. 2.3.12 to give

$$V\Delta V = 5.2\, \Delta\epsilon \qquad \ldots 2.3.13$$

where $\Delta\epsilon$ is expressed in microstrains and $\frac{d\epsilon}{dv}$ is considered equal to $\frac{\Delta\epsilon}{\Delta v}$.

The available strain measuring equipment was capable of measuring strains to an absolute accuracy of 1 microstrain. With $\Delta\epsilon$ restricted to this value, Eq. 2.3.13 predicts Δv to be less than 1 ft./sec. for all velocities greater than 5.2 ft./sec.

If the above analysis were applied to a mixture of air and water, the factor 5.2 in Eq. 2.3.13 would be considerably higher because of the decreased density. For example, the same analysis applied to a mixture

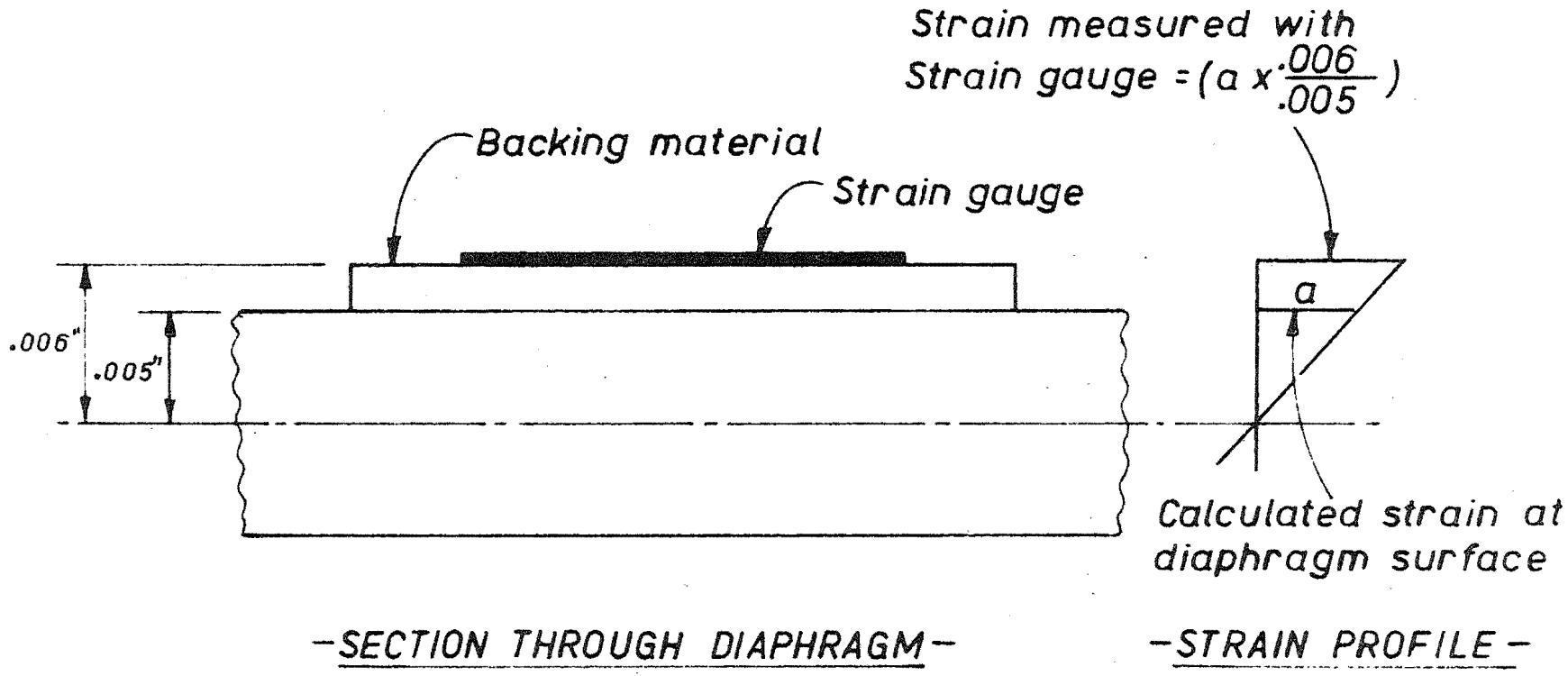

Fig. 2.14 : VELOCITY METER – Influence of Gauge Backing Material on Strain Output.

of 80% air concentration shows that Δv would be less than 1 ft./sec. for all velocities above 26 ft./sec. Even this is not constricting, as it was most unlikely that field conditions would be encountered where velocities of high air concentration mixtures were less than this figure.

The above analysis showed that the sensitivity was sufficiently good to justify building a prototype velocity meter to this design and testing its various characteristics.

(5) Determine the velocity meter overall dimensions and the incorporation of the strain-gauged diaphragm.

It was important that the sides of the stagnation pressure cell be very stiff compared to the diaphragm to prevent rotation at the edge of the diaphragm. As such a thin diaphragm could not be brazed or fixed satisfactorily in any way to a cell wall, the entire section had to be machined from a single piece of brass. To facilitate manufacture a minimum thickness for the walls was set at $\frac{1}{8}$".

These considerations determined a minimum diameter for the meter of 0.59" (diameter of the diaphragm plus twice the wall thickness. The conditions governing the diametrical measurement of the diaphragm are described on page 50). The adopted value for the external diameter of the meter was $\frac{5}{8}$" (0.625") which proved completely satisfactory in subsequent testing.

The preliminary configuration of the meter is shown in Figure 2.15. A prototype was constructed but was abandoned when it was found that its geometry made it extremely difficult to bond the strain gauges on to the back of the diaphragm section. Furthermore such a configuration allowed very little latitude for experimenting with different shaped head sections under test conditions.

Figure 2.16 shows an improved version of the meter design, and it

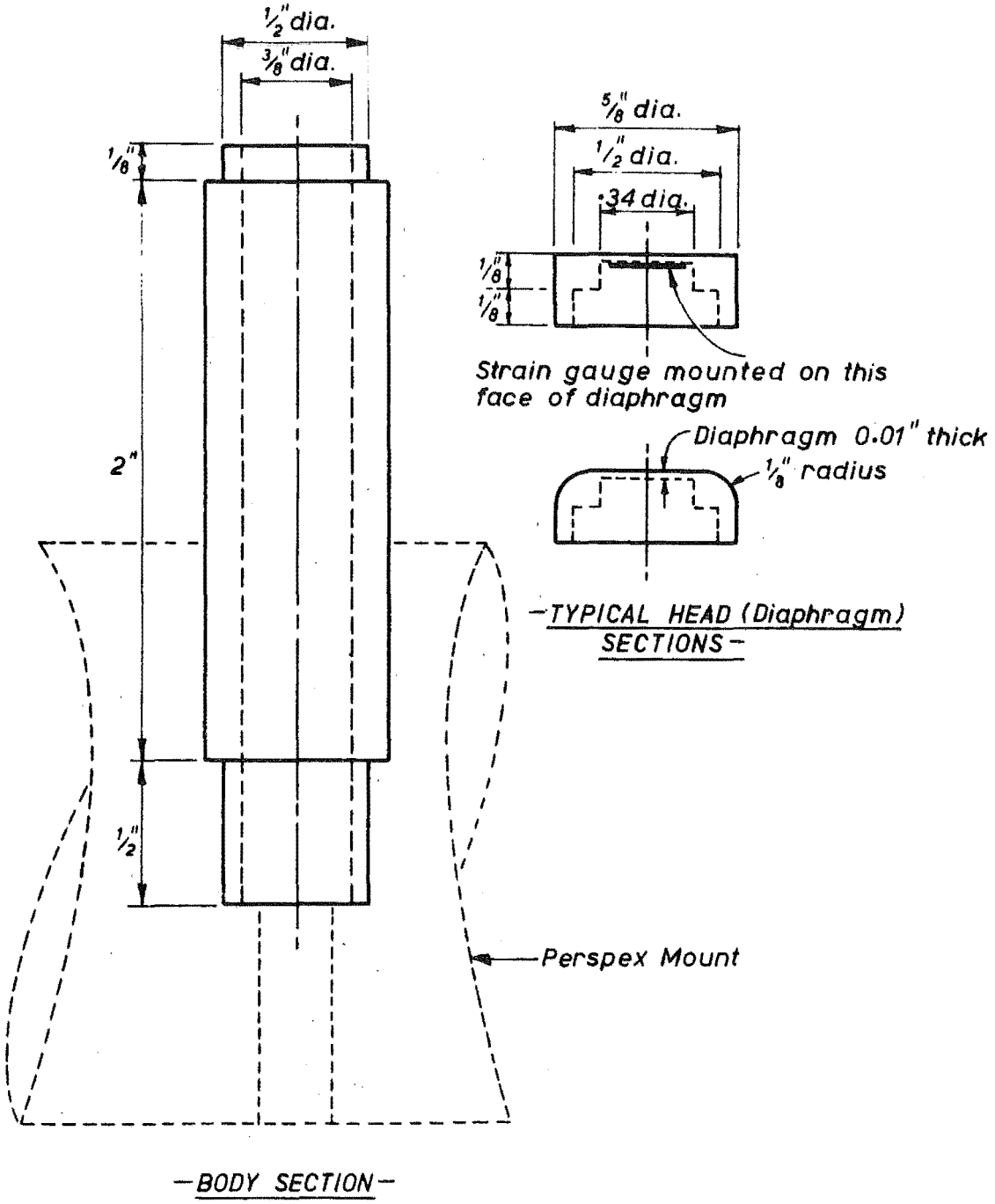

Fig. 2.15 : FIRST PROTOTYPE (STAG. PRESS.) VELOCITY METER — BASIC DESIGN.

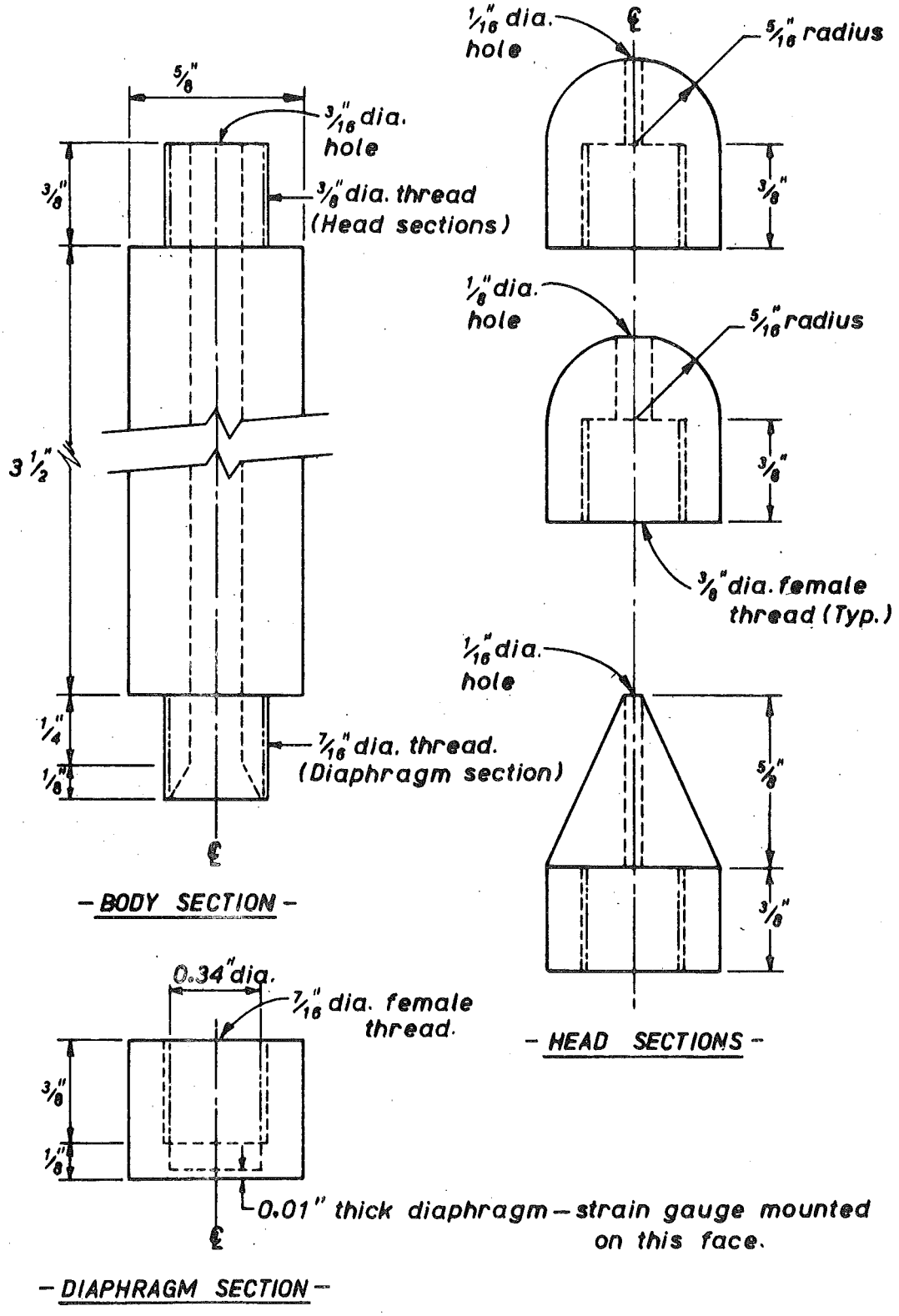

Fig. 2.16 : FINAL PROTOTYPE VELOCITY METER-BASIC DESIGN.

was a prototype of this particular meter which was successfully tested in the jet pump. Several different shaped head sections were manufactured such that they could be screwed on the body section.

Construction:

The body section, head sections, and diaphragm section were turned down from brass rod to the dimensions shown in Figure 2.16. The prototype meter was mounted in a perspex mount, which incorporated two slots at right angles at each end such that the meter could be traversed along two mutually perpendicular diameters without the necessity of adjusting the flow or tailpipe orientation.

The mounting of the strain gauge was a delicate and painstaking task, as was the soldering of the wires to the gauge. Particular care was taken in mounting the gauge centrally on the diaphragm as the maximum sensitivity could be obtained only with the gauge in this position.

Figure 2.17(a) shows a photograph of the prototype velocity meter. A magnified view of a mounted strain gauge is shown in Figure 2.17(b).

2.3.4 Calibration

Before testing could be carried out, a relationship had to be established between the measured output from the strain gauge and the corresponding applied pressure on the diaphragm. Equation 2.3.11 implies that this relationship will be linear (strain = (constant) x pressure).

The strain gauge output was measured as a voltage change across the gauge where the current was kept constant and the resistance altered by the applied pressure.

A calibration unit was constructed incorporating a sensitive pressure measuring device, a pressurisation cell and a monitor pressure gauge.

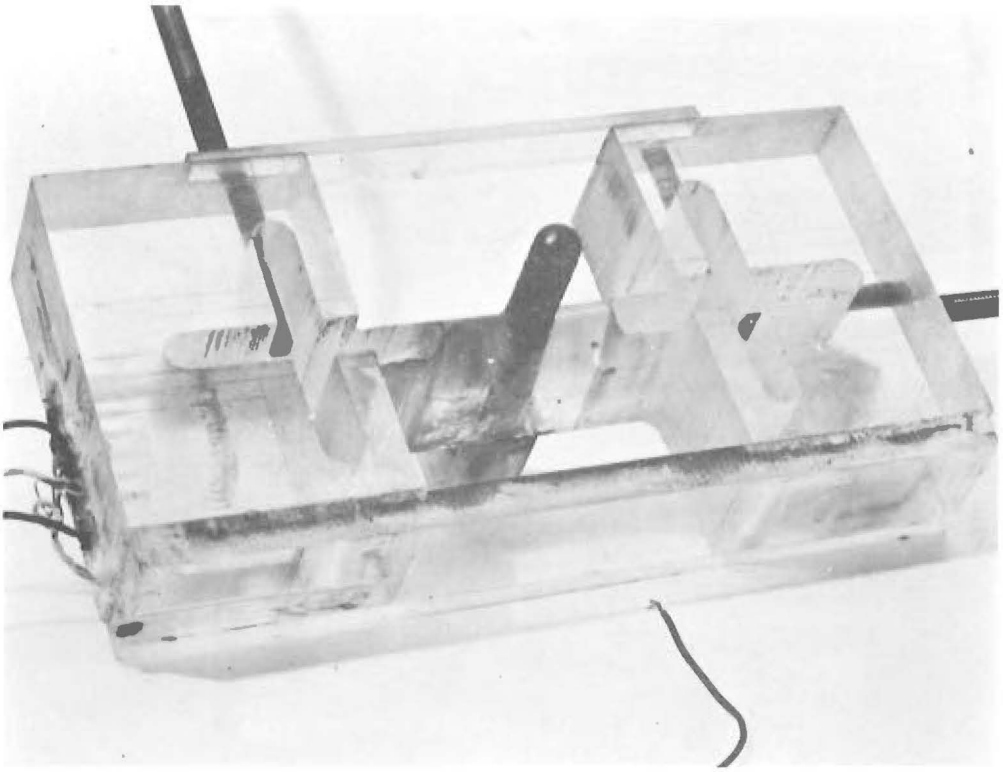

(a)

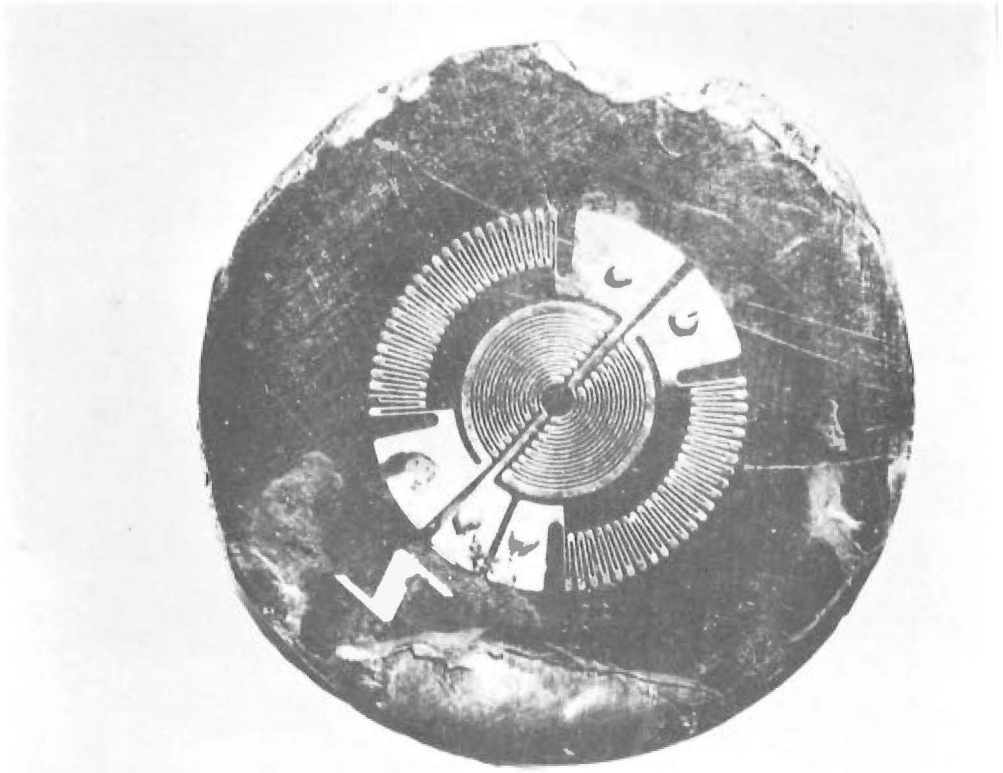

(b)

Fig. 2.17(a): FINAL PROTOTYPE VELOCITY METER.
(b): PRESSURE SENSING STRAIN GAUGE.

Mercury-water manometers were used to accurately measure the pressure. To keep the unit as compact as possible for the 50 psi pressure range for static calibration, 2 manometers connected in series were used.

The equation for the calculation of pressure from the manometer bank is

$$H = 12.6\,[(A_1 - A_2) - (B_1 - B_2) + (C_1 - C_2)] - 13.6\,(D_1 - D_2) \quad \ldots 2.3.14$$

where

H is the pressure on the diaphragm in feet of water

A and B are the mercury elevations in the two arms of the first manometer

C and D are the mercury elevations in the two arms of the second manometer

Subscript 1 represents a condition of zero pressure on the diaphragm

Subscript 2 represents a condition of the pressure being measured on the diaphragm.

The derivation of Eq. 2.3.14 is presented in Appendix I .

Figure 2.18 shows a photograph of the calibration equipment.

The output from the strain gauge was monitored with an "Edac" data logger. This instrument automatically recorded the output from the strain gauge on paper tape at a sample rate of 40 readings/minute.

The calibration procedure consisted of obtaining a series of data logger readings at pressure intervals of 5 or 10 psi. The monitor gauge gave the approximate pressure on the diaphragm and served as a check on the computed results from Eq. 2.3.14.

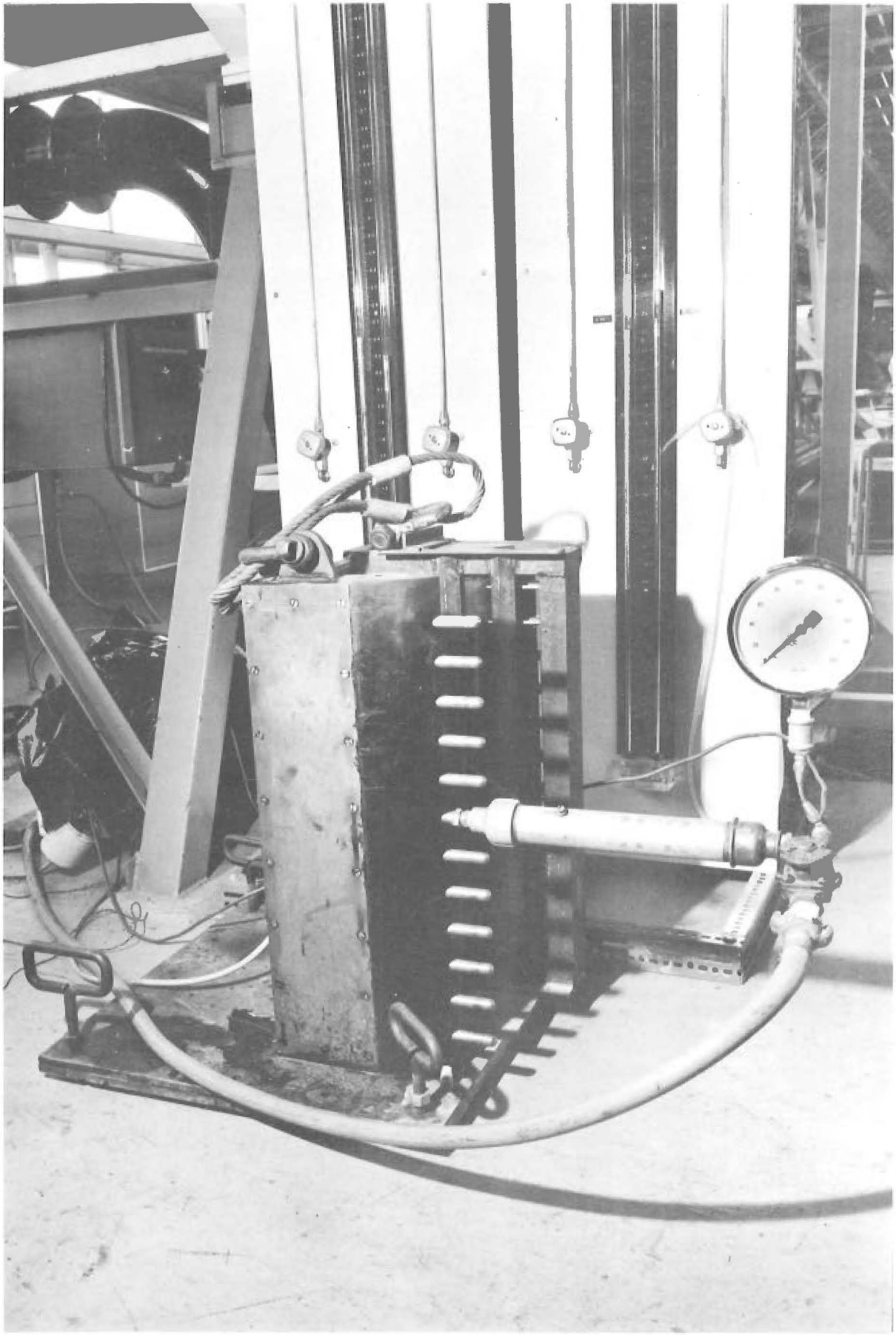

Fig.2.18 : VELOCITY METER CALIBRATION.

A computer programme was developed to solve Eq. 2.3.14 and to produce a mean data logger reading from the series obtained at each pressure. The programme is detailed in Appendix II .

A typical calibration plot is shown in Figure 2.19.

The dynamic calibration characteristic of concern was the response time of the strain gauged diaphragm to a sudden change in the stagnation pressure at the head of the velocity meter. This was of importance because, for the velocity meter to follow closely the turbulent pressure fluctuations, it was necessary for the response time to be considerably less than the period of the pressure fluctuations.

The response time was determined by incorporating a quick acting valve with the static calibration cell. By means of the valve a virtually instantaneous pressure could be applied to the velocity meter. An extremely sensitive (300 cps) ultraviolet chart recorder was used to monitor the output from the strain gauge.

The response curve for a sudden pressure increase of 17 psi is shown in Figure 2.20. This curve shows a response time of the order of 1/100 second which is many times faster than the period of the expected turbulence fluctuations. The low frequency fluctuations following the sharp increase are due to pressure surges in the static calibration cell.

It is concluded that, for the anticipated field conditions, the dynamic response characteristics of the velocity meter are entirely satisfactory.

2.3.5 Velocity Meter Testing - Theoretical Considerations and Procedure

The testing procedure basically involved the comparison of an apparent mean (area average) velocity from the velocity meter with the true mean velocity of the flow as independently measured.

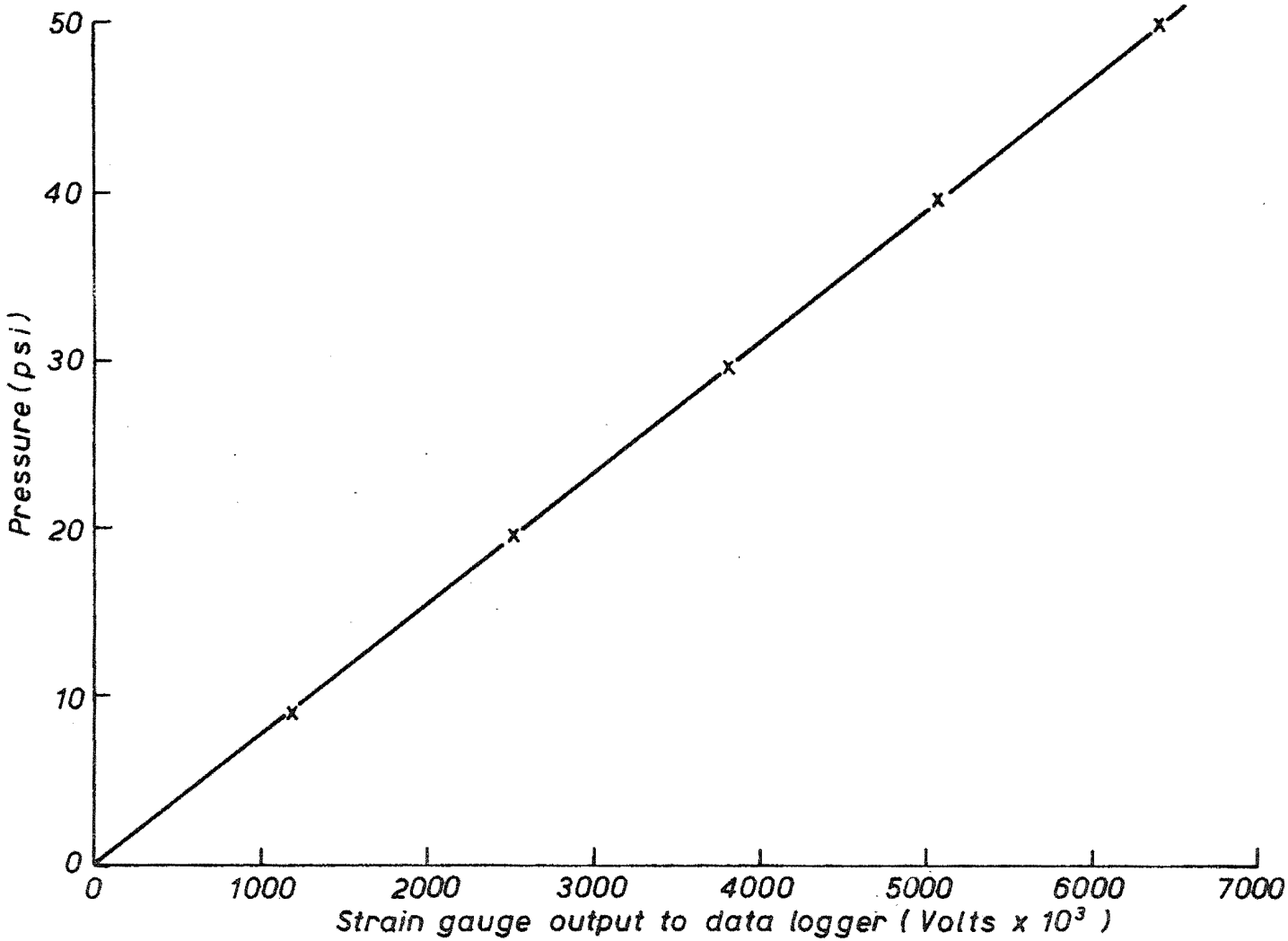

Fig. 2.19 : VELOCITY METER-Typical Calibration Plot

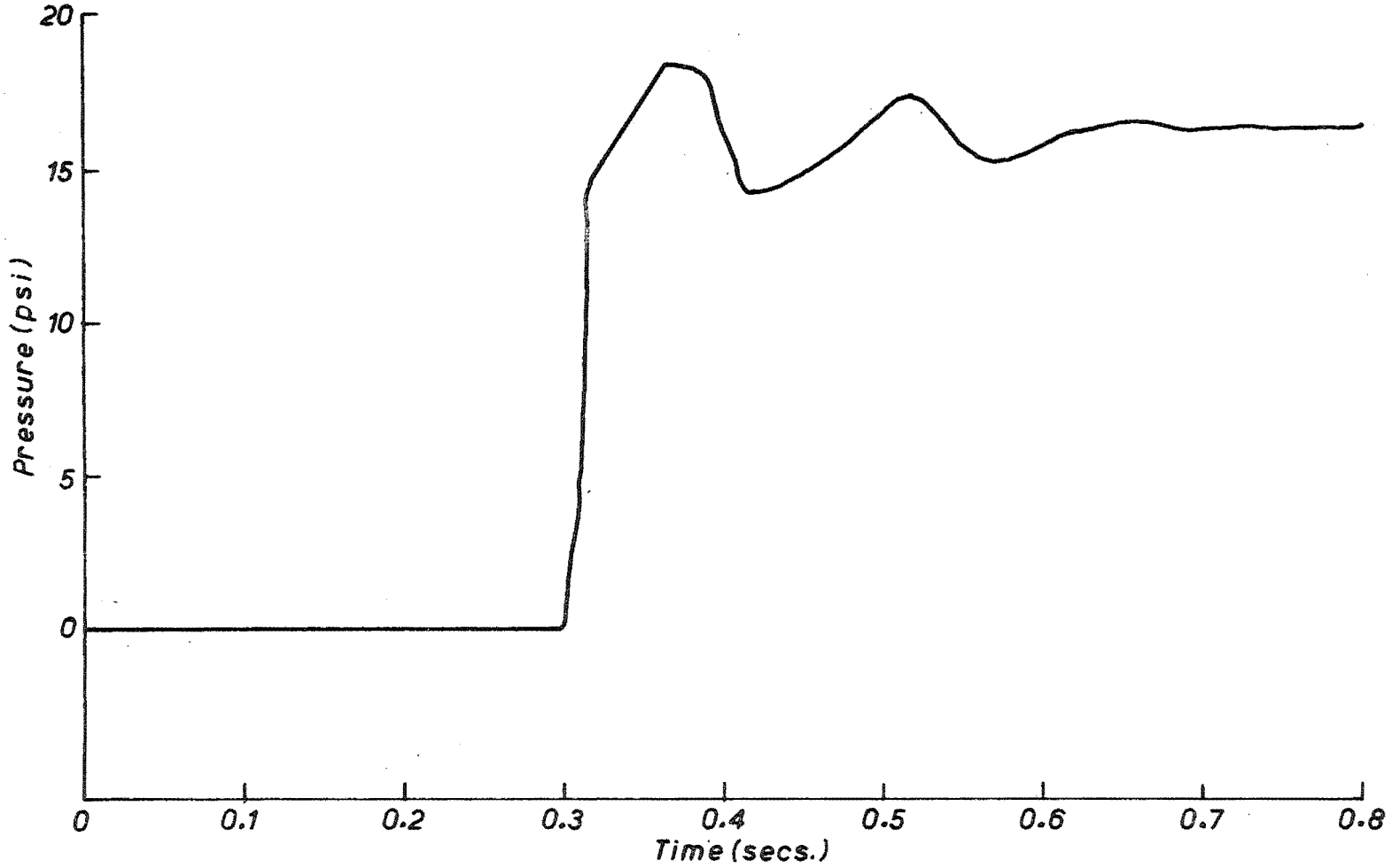

Fig. 2.20 : VELOCITY METER–DYNAMIC RESPONSE TO RAPID INCREASE IN PRESSURE

Theoretical Considerations:

The true mean velocity over the cross-section of the simulator tailpipe may be obtained indirectly by continuity from measurements of water discharge and mean air concentration.

The apparent mean velocity of the flow may be obtained from a developed form of Eq. 2.3.4.

Because the static pressure at the downstream end of the perspex tailpipe was zero (as the pipe was open to the atmosphere) Eq. 2.3.4 reduces to

$$V = \sqrt{\frac{2P}{\rho_w (1 - C)}} \qquad \ldots 2.3.15$$

Equation 2.3.15 is strictly only applicable to the case of a point velocity obtained from measurements of air concentration and stagnation pressure at the same point.

It was not possible to fulfil this requirement in the laboratory simulator, because such a method would require the simulator to be switched off while the velocity meter (which measures stagnation pressure) was substituted for the air concentration probe. Further, it was not possible to accurately reset the simulator to the same flow conditions after substitution.

However, it was possible to measure a diametrical mean air concentration with the radiation equipment (as described in Section 2.1.5). Several such means taken along different diameters could be used to give an accurate measure of the average air concentration over the cross-section of the simulator tailpipe. Simultaneously, the pressure distribution, and hence the mean (area average) pressure, over the tail-pipe area could be obtained by traversing the velocity meter along several diameters.

The following analysis of Eq. 2.3.15 shows that it is applicable to mean values of velocity, stagnation pressure, and air concentration

provided certain conditions are met.

Equation 2.3.15 may be expressed as

$$V = \sqrt{\frac{2P}{\rho}} \qquad \ldots 2.3.16$$

where ρ is the air-water density.

Notation:

Symbol	Definition
$\bar{\bar{P}}$	Mean pressure over cross-section of pipe
$\bar{\bar{\rho}}$	Mean density over cross-section of pipe
$\bar{\bar{V}}$	Mean velocity over cross-section of pipe
$\bar{P}$	Mean (time average) pressure at a point
$\bar{\rho}$	Mean (time average) density at a point
$\bar{V}$	Mean (time average) velocity at a point
P''	Variation of $\bar{P}$ from $\bar{\bar{P}}$ $(= \bar{P}-\bar{\bar{P}})$
ρ''	Variation of $\bar{\rho}$ from $\bar{\bar{\rho}}$ $(= \bar{\rho}-\bar{\bar{\rho}})$
V''	Variation of $\bar{V}$ from $\bar{\bar{V}}$ $(= \bar{V}-\bar{\bar{V}})$
P'	Turbulent pressure fluctuation at a point
ρ'	Turbulent density fluctuation at a point
V'	Turbulent velocity fluctuation at a point

In the following analysis, terms higher than second order are assumed negligible. It will be shown that this assumption is valid.

At a particular point on the cross-section of the simulator tail-pipe, for a particular instant in time, Eq. 2.3.16 may be expressed in terms of the above notation as

$$\bar{V} + V' = \sqrt{\frac{2\,(\bar{\bar{P}} + P')}{\bar{\bar{\rho}} + \rho'}}$$

$$= \sqrt{\frac{2\bar{\bar{P}}}{\bar{\bar{\rho}}}} \left(1 + \frac{P'}{\bar{\bar{P}}}\right)^{\frac{1}{2}} \left(1 + \frac{\rho'}{\bar{\bar{\rho}}}\right)^{-\frac{1}{2}}$$

$$= \sqrt{\frac{2\bar{P}}{\bar{\rho}}}\left[1 + \tfrac{1}{2}\left(\frac{P'}{\bar{P}}\right) - \tfrac{1}{8}\left(\frac{P'}{\bar{P}}\right)^2 + \ldots\right]\left[1 - \tfrac{1}{2}\left(\frac{\rho'}{\bar{\rho}}\right) + \tfrac{3}{8}\left(\frac{\rho'}{\bar{\rho}}\right)^2 + \ldots\right]$$

or

$$\bar{V} + V' = \sqrt{\frac{2\bar{P}}{\bar{\rho}}}\left[1 - \tfrac{1}{2}\left(\frac{\rho'}{\bar{\rho}}\right) + \tfrac{3}{8}\left(\frac{\rho'}{\bar{\rho}}\right)^2 + \tfrac{1}{2}\left(\frac{P'}{\bar{P}}\right) - \tfrac{1}{4}\left(\frac{P'}{\bar{P}}\right)\left(\frac{\rho'}{\bar{\rho}}\right) - \tfrac{1}{8}\left(\frac{P'}{\bar{P}}\right)^2\right] \quad \ldots 2.3.17$$

A time average of Eq. 2.3.17 gives

$$\bar{\bar{V}} = \sqrt{\frac{2\bar{P}}{\bar{\rho}}}\left[1 + \tfrac{3}{8}\left(\frac{\rho'}{\bar{\rho}}\right)^2 - \tfrac{1}{4}\left(\frac{P'}{\bar{P}}\right)\left(\frac{\rho'}{\bar{\rho}}\right) - \tfrac{1}{8}\left(\frac{P'}{\bar{P}}\right)^2\right]$$

(Terms of first order in V' , P' , ρ' disappear because the time averages of turbulent fluctuations about a time average mean are zero.)

i.e. $$\bar{V} = \sqrt{\frac{2\bar{P}}{\bar{\rho}}}\left[1 + B_1 + B_2 + B_3\right] \quad \ldots 2.3.18$$

where

$$B_1 = \overline{\tfrac{3}{8}\left(\frac{\rho'}{\bar{\rho}}\right)^2} = \frac{1}{T}\int_T \tfrac{3}{8}\left(\frac{\rho'}{\bar{\rho}}\right)^2 dt$$

$$B_2 = \overline{-\tfrac{1}{4}\left(\frac{P'}{\bar{P}}\right)\left(\frac{\rho'}{\bar{\rho}}\right)} = -\frac{1}{T}\int_T \tfrac{1}{4}\left(\frac{P'}{\bar{P}}\right)\left(\frac{\rho'}{\bar{\rho}}\right) dt$$

$$B_3 = \overline{-\tfrac{1}{8}\left(\frac{P'}{\bar{P}}\right)^2} = \frac{1}{T}\int_T \tfrac{1}{8}\left(\frac{P'}{\bar{P}}\right)^2 dt$$

T = time over which average is taken

Equation 2.3.18 may be expressed in terms of area averages of velocity, pressure, and density, because (from the notation)

$$\bar{V} = \bar{\bar{V}} + V'' \ , \quad \bar{P} = \bar{\bar{P}} + P'' \ , \quad \bar{\rho} = \bar{\bar{\rho}} + \rho''$$

i.e.

$$\bar{\bar{V}} + V'' = \sqrt{\frac{2(\bar{\bar{P}} + P'')}{\bar{\bar{\rho}} + \rho''}}\left[1 + B_1 + B_2 + B_3\right]$$

$$= \sqrt{\frac{2\bar{\bar{P}}}{\bar{\bar{\rho}}}} \left(1 + \frac{P''}{\bar{\bar{P}}}\right)^{\frac{1}{2}} \left(1 + \frac{\rho''}{\bar{\bar{\rho}}}\right)^{-\frac{1}{2}} \left[1 + B_1 + B_2 + B_3\right)$$

$$= \sqrt{\frac{2\bar{\bar{P}}}{\bar{\bar{\rho}}}} \left[1 + \tfrac{1}{2}\left(\frac{P''}{\bar{\bar{P}}}\right) - \tfrac{1}{8}\left(\frac{P'}{\bar{\bar{P}}}\right)^2 + \ldots\right] \left[1 - \tfrac{1}{2}\left(\frac{\rho''}{\bar{\bar{\rho}}}\right) + \tfrac{3}{8}\left(\frac{\rho''}{\bar{\bar{\rho}}}\right)^2 + \ldots\right]$$

$$\left[1 + B_1 + B_2 + B_3\right]$$

or

$$\bar{\bar{V}} + V'' = \sqrt{\frac{2\bar{\bar{P}}}{\bar{\bar{\rho}}}} \left[1 - \tfrac{1}{2}\left(\frac{\rho''}{\bar{\bar{\rho}}}\right) + \tfrac{3}{8}\left(\frac{\rho''}{\bar{\bar{\rho}}}\right)^2 + \tfrac{1}{2}\left(\frac{P''}{\bar{\bar{P}}}\right) - \tfrac{1}{4}\left(\frac{P''}{\bar{\bar{P}}}\right)\left(\frac{\rho''}{\bar{\bar{\rho}}}\right) - \tfrac{1}{8}\left(\frac{P''}{\bar{\bar{P}}}\right)^2\right]$$

$$\left[1 + B_1 + B_2 + B_3\right]$$

$$= \sqrt{\frac{2\bar{\bar{P}}}{\bar{\bar{\rho}}}} \left[1 + B_4 + B_5 + B_6 + B_7 + B_8\right] \left[1 + B_1 + B_2 + B_3\right]$$

... 2.3.19

where

$$B_4 = -\tfrac{1}{2}\left(\frac{\rho''}{\bar{\bar{\rho}}}\right)$$

$$B_5 = \tfrac{3}{8}\left(\frac{\rho''}{\bar{\bar{\rho}}}\right)^2$$

$$B_6 = \tfrac{1}{2}\left(\frac{P''}{\bar{\bar{P}}}\right)$$

$$B_7 = -\tfrac{1}{4}\left(\frac{P''}{\bar{\bar{P}}}\right)\left(\frac{\rho''}{\bar{\bar{\rho}}}\right)$$

$$B_8 = -\tfrac{1}{8}\left(\frac{P''}{\bar{\bar{P}}}\right)^2$$

Equation 2.3.19 may be expressed as

$$\bar{\bar{V}} + V'' = \sqrt{\frac{2\bar{\bar{P}}}{\bar{\bar{\rho}}}}\left[1 + B_1 + B_2 + B_3 + B_4 + B_5 + B_6 + B_7 + B_8\right] \quad \ldots 2.3.20$$

where terms higher than second order are neglected.

An area average of Eq. 2.3.20 (over the cross-section of the pipe) gives

$$\bar{\bar{V}} = \sqrt{\frac{2\bar{\bar{P}}}{\bar{\bar{\rho}}}}\left[1 + \bar{B}_1 + \bar{B}_2 + \bar{B}_3 + \bar{B}_5 + \bar{B}_7 + \bar{B}_8\right] \quad \ldots 2.3.21$$

where

$$\bar{B}_n = \frac{1}{A}\int_A B_n \, da$$

A = area over which average is taken.

(Terms in V'' , P'' , ρ'' disappear because the area average of variations from an area average mean are zero.)

If it can be shown that the terms $\bar{B}_1$, $\bar{B}_2$, $\bar{B}_3$, $\bar{B}_5$, $\bar{B}_7$, $\bar{B}_8$ in Eq. 2.3.21 are negligible then terms higher than second order, which are very much less in value, may also be considered negligible.

If this condition is met then

$$\bar{\bar{V}} = \sqrt{\frac{2\bar{\bar{P}}}{\bar{\bar{\rho}}}} \quad \ldots 2.3.22$$

Procedure:

The true mean (area average) velocity through the simulator was obtained as follows:

(1) The water flow through the simulator was measured by discharging into a calibrated pit.

(2) The average air concentration across a cross-section of the perspex tail-pipe was obtained from measurements of the diametrical mean concentration along several diameters with the radiation equipment. (The method of measuring the diametrical mean air concentration is

described in Section 2.1.5).

(3) The air-water mixture discharge was then obtained from

$$Q = \frac{Q_w}{1 - \bar{\bar{C}}} \qquad \ldots 2.3.23$$

where

Q is the mixture discharge

Q_w is the water discharge

$\bar{\bar{C}}$ is the mean (area average) air concentration.

(4) The tail-pipe diameter was then accurately measured with a micrometer and the true mean velocity in the tail-pipe calculated from

$$\bar{\bar{V}}_T = \frac{Q}{\pi \frac{D^2}{4}} \qquad \ldots 2.3.24$$

Substitution of Eq. 2.3.23 in Eq. 2.3.24 yields

$$\bar{\bar{V}}_T = \frac{4\, Q_w}{(1 - \bar{\bar{C}})\, \pi D^2} \qquad \ldots 2.3.25$$

where

$\bar{\bar{V}}_T$ is the true mean velocity

D is the tail-pipe diameter.

Prior to the measurement of the apparent mean velocity, the simulator was set as accurately as possible to the test flow conditions and traverses made along several representative diameters with the electrical air concentration probe. For each point on the traverse, the output from the probe was monitored with the "Edac" data logger which automatically recorded the output on paper tape at a sample rate of 40 readings/minute. These traverses enabled representative values

of the dimensionless density parameters $\frac{\rho''}{\bar{\bar{\rho}}}$ and $\frac{\rho'}{\bar{\rho}}$ to be obtained for the particular test conditions.

It was found that dynamic "working" of the velocity meter diaphragm was necessary before the zero pressure output reading stabilised. Accordingly, prior to the test, the velocity meter was placed in the spillway flow simulator which was then turned on to its position of maximum flow. Two or three minutes of this treatment was sufficient to stabilise the zero pressure output.

The apparent mean velocity was then obtained as follows:

(1) Simultaneously with the measurements of diametrical mean air concentration (described in (2) above), traverses of pressure along each of the same diameters were obtained. Sets of readings were recorded at nine points on each diameter with the data logger, and values of the mean (time average) pressure ($\bar{P}$) and turbulent pressure fluctuations (P') were calculated for each point.

(2) Pressures equidistant from the centre of the simulator tail-pipe were averaged linearly and a graph of radius versus $\bar{P}$ was plotted.

(3) The mean (area average) pressure ($\bar{\bar{P}}$) was calculated from

$$\bar{\bar{P}} = \frac{1}{A} \int_A \bar{P} dA$$

or

$$\bar{\bar{P}} = \frac{1}{\pi R^2} \int_R \bar{P}\, 2\pi\, r dr$$

where

R is the tail-pipe radius.

(4) The apparent mean velocity was then calculated from Eq. 2.3.22 where $\bar{\bar{\rho}} = \rho_w (1 - \bar{\bar{C}})$.

(5) The mean pressure obtained in (3) above was combined with the information obtained in (1) above and values obtained of the dimensionless pressure parameters $\frac{\bar{P}''}{\bar{P}}$ and $\frac{\bar{P}'}{\bar{P}}$.

(6) The values of the terms $\bar{B}_1$, $\bar{B}_2$, $\bar{B}_3$, $\bar{B}_5$, $\bar{B}_7$, $\bar{B}_8$ in Eq. 2.3.21 were then calculated and an assessment made of the inherent error in the testing procedure.

Two computer programmes were developed to process the raw data from the velocity meter tests. The first accepted card data containing velocity meter calibration factors and relevant information for the radiation calculations, also tape data from the "Edac" data logger comprising the output from the velocity meter. The programme calculated the true mean (area average) velocity, mean density and linearly averaged pressures at progressively increasing radial distances from the centre of the simulator tail-pipe.

The second programme accepted card data comprising co-ordinates of pressure for different values of radius, interpolated from a graph of radius versus pressure. The programme calculated the apparent mean (area average) velocity from Eq. 2.3.22.

The two programmes are listed in Appendix II .

A summary of results from a typical test run is shown in Table 2.2.

2.3.6 Performance Conclusions

Tests of the velocity meter were carried out for a range of velocities from 10-110 ft/sec. and air concentrations from 0-85%. As explained in the performance conclusions for the air concentration probe (Section 2.2.5), it was not possible with the simulator to achieve high velocity - low air concentration flows. Again, however, this limitation was not serious as the most arduous test conditions

PRELIMINARY TRAVERSE ACROSS DIAMETER WITH A/C PROBE

Dist. from Pipe δ	$\bar{C}$	C'	C''	$\bar{\rho}$	ρ'	ρ''	$(\frac{\rho''}{\bar{\rho}})$	$(\frac{\rho''}{\bar{\rho}})^2$	$(\frac{\rho'}{\bar{\rho}})$	$(\frac{\rho'}{\bar{\rho}})^2$	
0	.66	.05	-.02	.660	.097	.040	.064	.004	.147	.022	
0.37	.66	.05	-.02	.660	.097	.040	.064	.004	.147	.022	$\bar{\bar{C}} = 0.68$
0.75	.66	.04	-.02	.660	.078	.040	.064	.004	.118	.014	$\therefore \bar{\bar{\rho}} = 0.620$
1.12	.67	.05	-.01	.640	.097	.020	.032	.001	.151	.023	
1.31	.70	.06	.02	.582	.116	-.038	-.061	.004	.199	.040	

MAIN TEST - A/C READINGS OBTAINED WITH RADIATION EQUIPMENT

Dist. from Pipe δ	$\bar{P}$	P'	P''	$(\frac{P'}{\bar{P}})$	$(\frac{P'}{\bar{P}})^2$	$(\frac{P''}{\bar{P}})$	$(\frac{P''}{\bar{P}})^2$	$(\frac{\rho'}{\bar{\rho}})$	$(\frac{\rho'}{\bar{\rho}})^2$	$(\frac{P'}{\bar{P}})(\frac{\rho'}{\bar{\rho}})$	$(\frac{\rho''}{\bar{\rho}})$	$(\frac{\rho''}{\bar{\rho}})^2$	$(\frac{P''}{\bar{P}})(\frac{\rho''}{\bar{\rho}})$
0	11.46	2.89	2.46	.252	.063	.273	.075	.147	.022	.037	.064	.004	.017
0.37	10.69	2.93	1.69	.274	.075	.188	.035	.147	.022	.040	.064	.004	.012
0.75	9.66	3.16	0.66	.327	.107	.073	.005	.118	.014	.039	.064	.004	.005
1.12	9.82	3.72	0.82	.379	.144	.091	.008	.151	.023	.057	.032	.001	.003
1.31	8.47	3.26	-0.53	.386	.149	-.059	.003	.199	.040	.077	-.061	.004	.004

A/C = 0.67 MIXTURE DISCHARGE = 2.853 CUSECS TAILPIPE AREA = 0.046 sq.ft. TRUE MEAN VELOCITY = 62.02 ft/sec.

DENSITY = 0.640 = $\bar{\bar{\rho}}$ MEAN PRESSURE = 9.00 psi = $\bar{\bar{P}}$

MEAN VELOCITY FROM VELOCITY METER = $(\bar{\bar{V}}) = \sqrt{2\bar{\bar{P}}/\bar{\bar{\rho}}}$ = 63.70 ft/sec.

Error = +2.71%

ISMENT OF TESTING FORMULA $\bar{\bar{V}} = \sqrt{\frac{2\bar{\bar{P}}}{\bar{\bar{\rho}}}}\,[1 + \bar{B}_1 + \bar{B}_2 + \bar{B}_3 + \bar{B}_5 + \bar{B}_7 + \bar{B}_8 + \text{terms of higher order}]$

where

$\bar{B}_1 = \frac{1}{A}\int \frac{3}{8}(\frac{\rho'}{\bar{\rho}})^2\,dA$ which is the order of .011 = 1.1%

$\bar{B}_2 = -\frac{1}{A}\int \frac{1}{4}(\frac{P'}{\bar{P}})(\frac{\rho'}{\bar{\rho}})\,dA$ " " " " " -.012 = -1.2%

$\bar{B}_3 = -\frac{1}{A}\int \frac{1}{8}(\frac{P'}{\bar{P}})^2\,dA$ " " " " " -.014 = -1.4%

$\bar{B}_5 = \frac{1}{A}\int \frac{3}{8}(\frac{\rho''}{\bar{\rho}})^2\,dA$ " " " " " .001 = .1%

$\bar{B}_7 = -\frac{1}{A}\int \frac{1}{4}(\frac{P''}{\bar{P}})(\frac{\rho''}{\bar{\rho}})\,dA$ " " " " " -.002 = -.2%

$\bar{B}_8 = -\frac{1}{A}\int \frac{1}{8}(\frac{P''}{\bar{P}})^2\,dA$ " " " " " -.001 = -.1%

; OF HIGHER ORDER WILL HAVE VALUES VERY MUCH LESS THAN THESE

$\therefore$ APPROXIMATE TESTING ERROR = 1.7%

MEAN VELOCITY FROM VELOCITY METER IS ESTIMATED APPROXIMATELY 1.7% TOO HIGH

TABLE 2.2: SUMMARY OF RESULTS FROM TYPICAL VELOCITY METER TEST.

were those that combined high air concentration with high velocity.

The inherent error in the testing procedure was never greater than 2% for any of the tests carried out. This was considered a sufficiently good approximation for an accurate comparison to be made of the two values of mean velocity.

Because the measurement of velocity is made indirectly, via an external measurement of air concentration, the accuracy of the meter is dependent on the accuracy of the air concentration probe. Despite this drawback, which results in the compounding of experimental errors, the velocity meter proved to be extremely accurate, and gave readings to within 3% over the entire test range of flow conditions.

2.4 FIELD TEST APPARATUS

2.4.1 Introduction

The original aim of the project called for the measurement of depth profiles of air concentration and velocity at different points on the Aviemore spillway. The field system to achieve this utilised one moveable field unit which could be mounted at any one of a series of test stations on the spillway face.

The unit was designed to incorporate fixed measuring probes mounted at different depths in the flow. It was necessary for the unit to be readily portable, yet strong enough to hold the probes under the very demanding high speed flow conditions.

It was further necessary to be able to select the output from any probe by a remote switching system.

This section first describes the overall instrumentation system and the special cable design necessary to implement it. The electronic features of the system are described generally only - detailed circuit diagrams are included in Appendix III.

A description of the test station design and layout on the spillway face is then presented.

The concept of the field test unit is discussed together with its design and construction.

The adaption of the laboratory air concentration and velocity meters to field use and a description of the field recording equipment constitute the remainder of the section.

2.4.2 Instrumentation System and Cable Requirements

A remote sampling system was used by which (for a particular station on the spillway) the output from each probe on the test unit was sampled in turn.

The system had the disadvantage that it was not possible to record, simultaneously, readings from each probe. However, the system was designed in this manner in the interests of economy since only one processing unit for each flow parameter was required at the test unit, and only one screened output wire was required to transfer the signals to the recording station.

The remote switching at the test unit was achieved by incorporating three switch control wires in the system. By using three switching states (+ , o , -) on each wire and assigning a unique combination of states to each probe on the test unit, it was possible to sample to a maximum of twenty seven probes.

A block diagram of the instrumentation system is shown in Figure 2.21.

A matrix of reed relays was used as the switching system, controlled directly by signals from the recording station. Reed relays offered the advantages of small size, reliability (10^8 operations), economy, low contact resistance, and a high "noise" imunity.

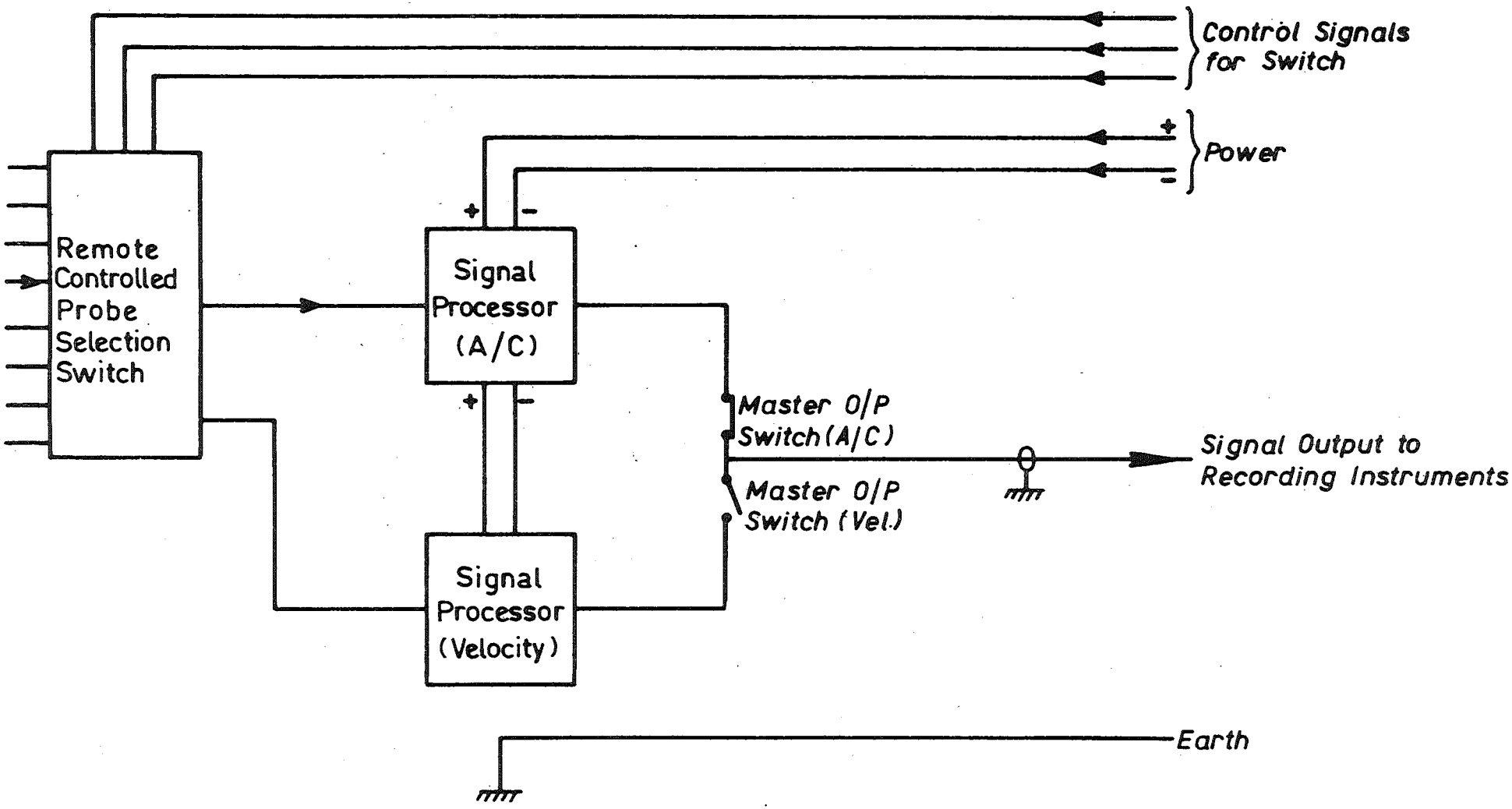

FIG.2.21 : BLOCK DIAGRAM OF FIELD TEST UNIT INSTRUMENTATION SYSTEM

The instrumentation system described above required a cable with seven conductors - two for power, three for switch control, one earth, and one shielded signal output wire. As large ground currents at the fundamental mains frequency and high order harmonics were expected because of the proximity of the power station, it was further necessary to screen the whole cable to prevent pick up. The additional screen also had the effect of adding mechanical strength to the cable.

A detailed description of the electronics of the instrumentation system, complete with circuit diagrams and cable specification, is presented in Appendix III.

2.4.3 Spillway Test Stations - Construction and Layout

Ten test stations for the field unit were established on the spillway face above tail-water level.

Each station consisted of a steel sided box, 1'-6" x 1'-6" x 1'-6" deep, let into the face of the spillway. When not in use each station could be blanked off with a 2'-0" x 2'-0" x 1" thick steel plate, held in position with stainless steel countersunk screws. The plate was recessed flush with the spillway face to minimise flow disturbances.

The stations were located in two longitudinal lines of five stations each. One line was situated well away from the sidewalls of the spillway in a region where the flow could be considered two dimensional. The other line was located near one spillway wall where the influence of the wall-induced boundary layer on the flow could be examined. In each case the stations were longitudinally spaced at intervals of twenty feet.

The test stations were inter-connected with 6" diameter pipe ducting embedded one foot below the spillway surface.

Each station was served, via the ducting, by a separate cable. The cables from all test stations terminated at a recording station situated in the spillway side wall.

Location drawings of the anchorage stations and cable ducting are shown in Figures 2.22 and 2.23.

2.4.4 Field Test Unit

(a) Concept: The unit consisted basically of two piers mounted side by side, twelve inches apart, on a single base plate. One pier incorporated the air concentration probes, the other incorporated the velocity meters. Velocity values were calculated from the stagnation pressure readings, making the very reasonable assumption that the time average air concentration at the velocity meter was the same as the measured time average air concentration at the same height on the air concentration pier.

Thus, it was assumed that, over the width of the field test unit, the flow was essentially two-dimensional in character.

(b) Design and Construction: The main design criteria were that the test unit be high enough to meter the full depth of the test flows, that sufficient space be provided in the piers to accommodate the electronic circuitry and calibration equipment necessary for field testing, and that the unit be strong enough to withstand the severe buffeting from the high speed test flows.

From photographs taken during a previous series of spillway trials, it was found that self-aeration was not evident in flows greater than two feet in depth. This, then, represented the maximum depth for which profiles of air concentration and velocity were required, and was, hence, set as the metered height of the field test unit.

As discussed in Section 2.4.2, twenty seven switching states were available. Three of these were required for monitoring the electronics within the test unit. Thus, the maximum number of switching states available for each pier was twelve. As the maximum spillway flow depth for which profiles were required was two feet, this dictated a minimum

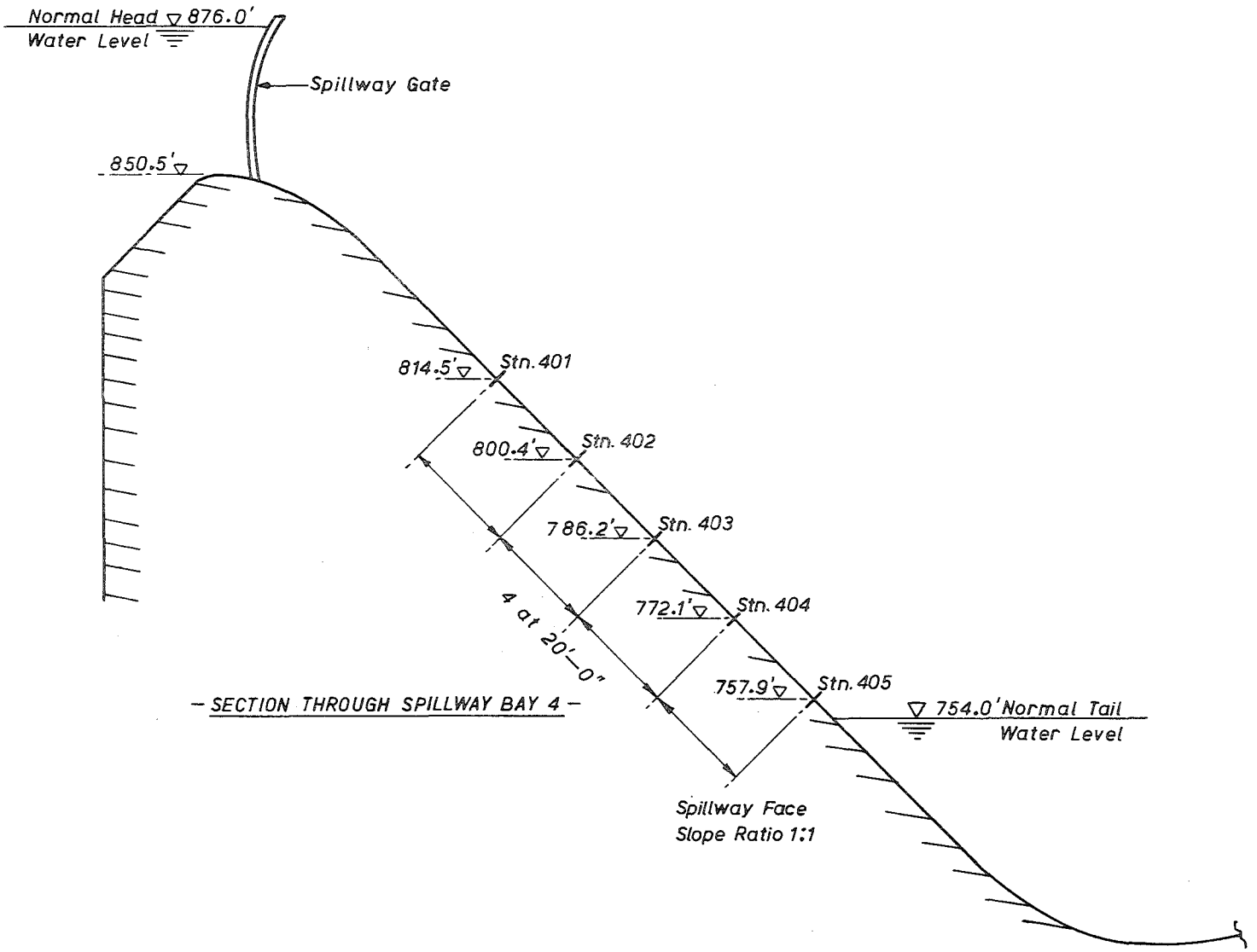

Fig. 2.22 : LOCATION OF FIELD TEST UNIT ANCHORAGE STATIONS ON SPILLWAY

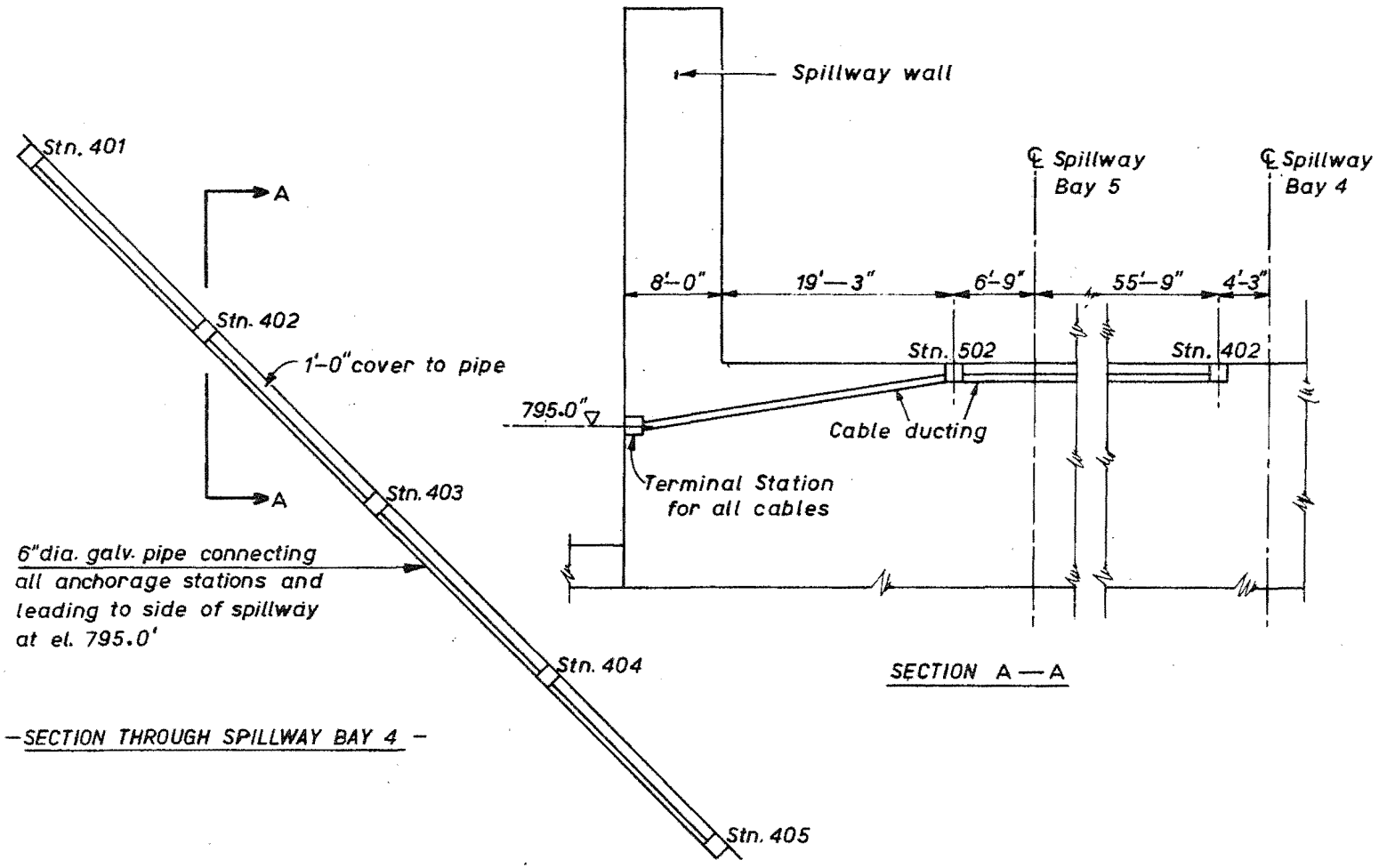

Fig. 2.23 : CABLE DUCTING LAYOUT ON SPILLWAY

probe spacing of two inches. Ideally, as discussed in Chapter Five. a smaller probe spacing would have been preferable. However, the spacing set by this cable limitation had to be adopted.

Space requirements for the electronic circuitry and calibration equipment were easily determined. The electronics were mounted on small circuit boards as described in Appendix III. Calibration equipment was required only for the air concentration pier and consisted essentially of two probes, of the same cross-sectional dimensions as the air concentration probes, mounted in tandem in a calibration compartment inside the pier. (The calibration equipment is described in detail in Section 2.4.5).

Minimum internal dimensions for each pier of 5" x $2\frac{1}{2}$" x 1'-6" high were dictated by the above requirements.

The structural design of the field test unit is detailed in Appendix IV.

One design factor remained - the provision of mounts for the air concentration probes and velocity meters. These were designed as two separate nose cones, one for each pier. It was necessary that they be streamlined, mechanically strong, and made from an insulating material to prevent stray electrical leakage between probes.

Originally they were made from cast Araldite, but preliminary field trials indicated that, because of its brittle nature, this material was unsatisfactory.

The field test unit, in its finally developed form, incorporated nose cones made from Tufnol; a mechanically strong, easily worked material which has excellent insulation properties.

Construction drawings and a photograph of the complete field test unit are shown in Figures 2.24 and 2.25.

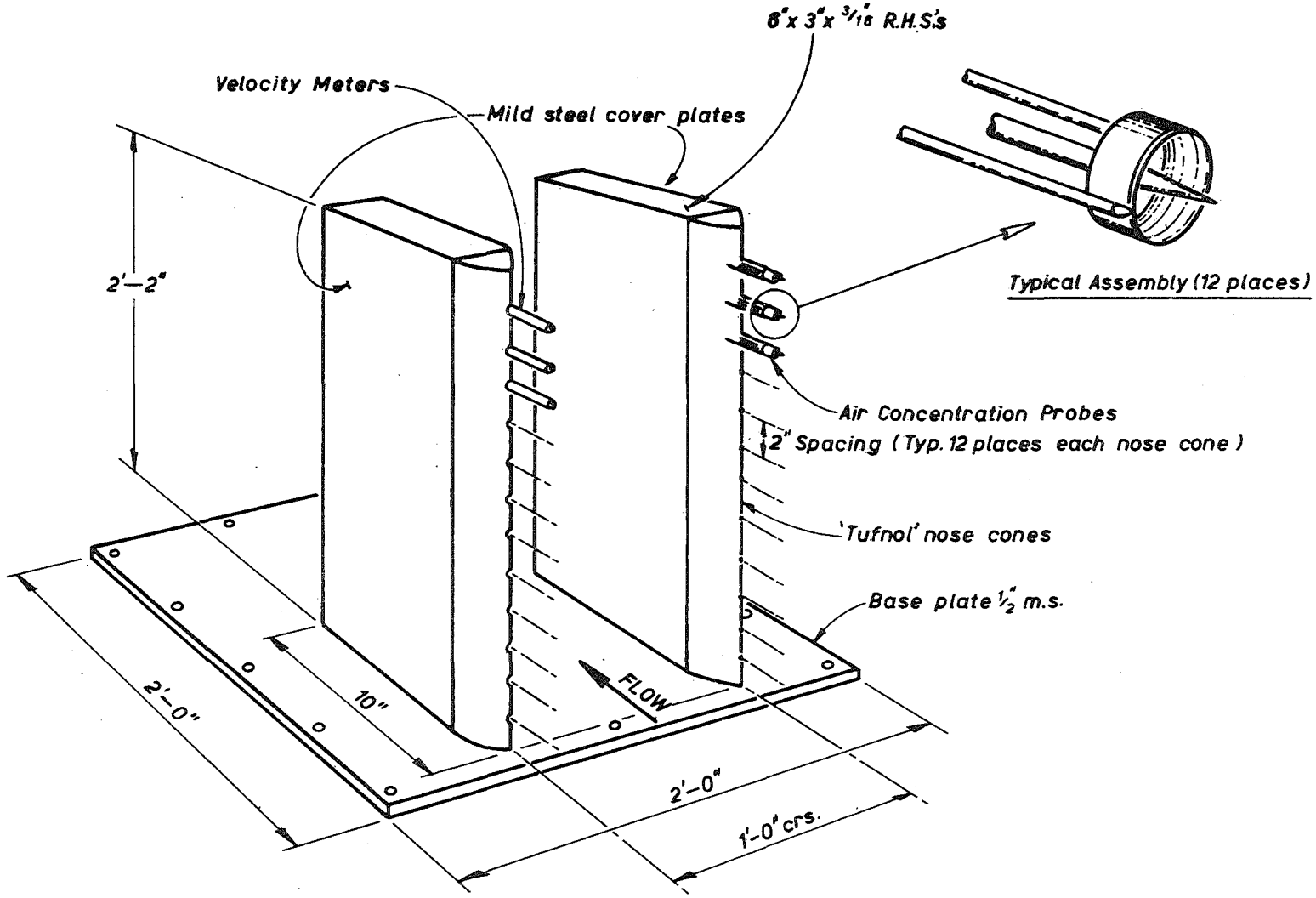

Fig. 2.24 : Aviemore Spillway Field Test Unit

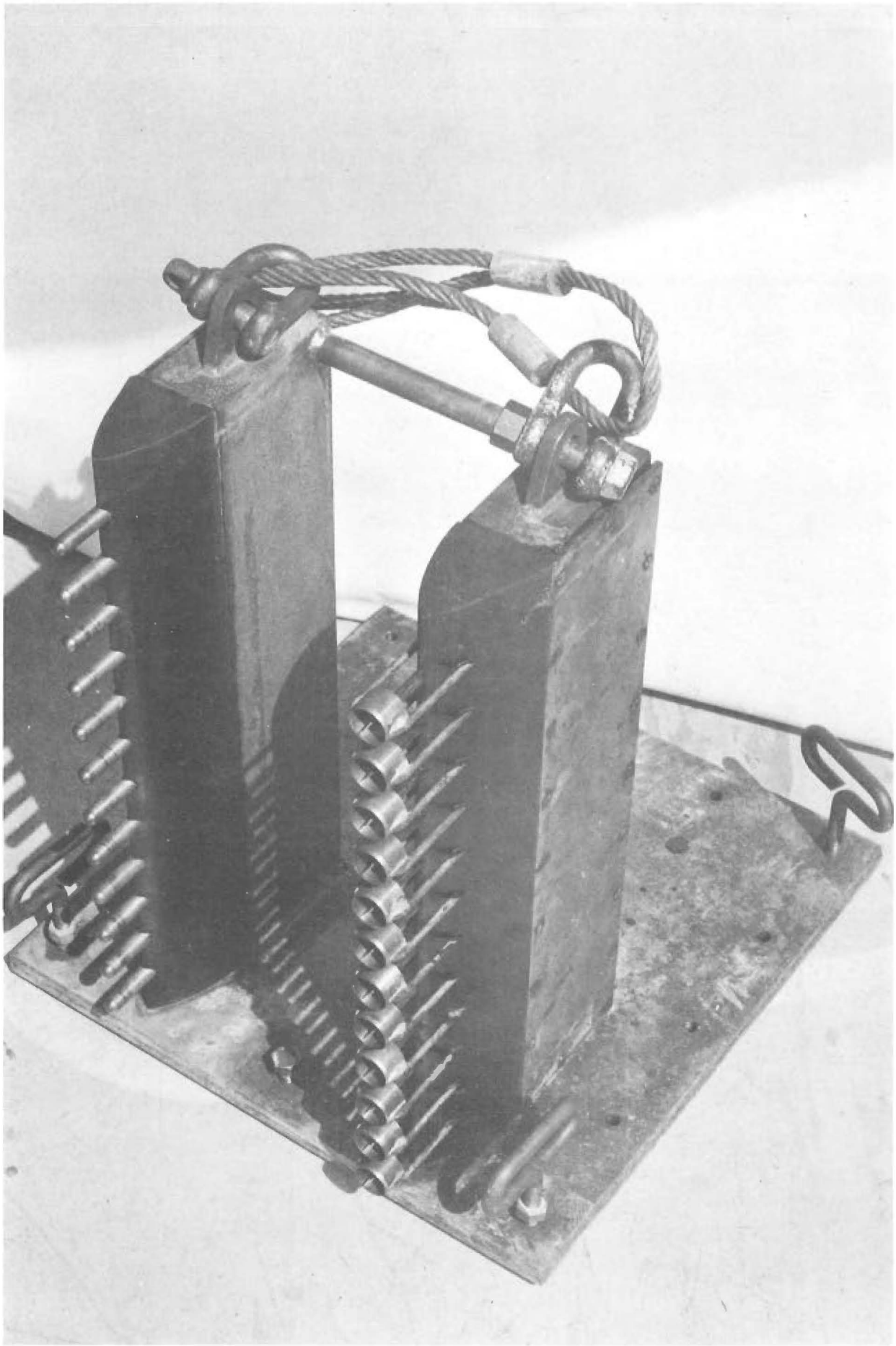

Fig. 2.25 : FIELD TEST UNIT.

2.4.5 Adaption of Laboratory Instruments to Field Use

(a) Air Concentration Probe: As described in Section 2.2.2, the method of measuring air concentration consisted basically of a measurement of the electrical conductivity of the air-water mixture relative to the conductivity of water alone.

The two main considerations in the adaption of the laboratory probe to field use were:

(1) The prevention of electrical leakage between probes.

(2) The provision of a continuous relative measurement of the conductivity of de-aerated water. (A continuous measurement was necessary because the conductivity of the de-aerated water could change with time due to changes in the concentrations of dissolved minerals and other impurities.)

Leakage was no problem as, due to the co-axial nature of the probes, the electrical field of each one was fully contained within its own confines. Further, by earthing the outer electrodes of all the probes, the possibility of electrical leakage between them was eliminated.

The second requirement was satisfied by the design and construction of a de-aeration/calibration unit which was incorporated in the air concentration pier.

The unit consisted of a de-aeration tank and a calibration compartment. A mixture of air and water was continuously tapped from the spillway flow and passed into the de-aeration tank. The resulting de-aerated water passed through the calibration compartment and discharged back into the spillway flow.

The calibration compartment was divided into two parts. In one part the secondary probe, which monitored the water conductivity, was mounted. The other part contained a dummy probe, having the same physical dimensions as the main air concentration probes, which could be used to check the performance of the de-aeration/calibration unit.

Figure 2.26 shows a photograph of the unit mounted inside the air concentration pier.

A block diagram of the electronic system for the measurement of air concentration is shown in Figure 2.27.

(b) Velocity Meter: As described in Section 2.3.2, the basic principle of the velocity meter involved a measurement of the stagnation pressure of the flow with a strain gauged diaphragm.

The only problem encountered in the adaption of the laboratory meter to field use was associated with the relative differences in the diaphragm gauges used.

A general discussion only is presented in this section - the electronic details are presented in Appendix III.

With reference to Figure 2.28, the "zero pressure" reading from the strain gauge is dependent on the ratio of the resistance values of the two gauge arms (R_A/R_B). Due to the high signal amplification used, even very small differences in the "zero pressure" values of the ratio R_A/R_B would tend to give vastly different zero readings for each velocity meter.

As this was not acceptable, due to the comparatively small measuring range of the data logger (described in Section 2.4.6), some form of adjustment on the zero signal was required.

This was achieved by overlaying the zero signal with a separate, variable voltage using a differential amplifier. The output from the amplifier was the difference between the zero signal and the overlaid voltage. Each probe had its own potentiometer circuit and the "zero pressure" output from the differential amplifier could thus be adjusted to a unique value for each probe.

A block diagram of the electronic system for the measurement of velocity is shown in Figure 2.29.

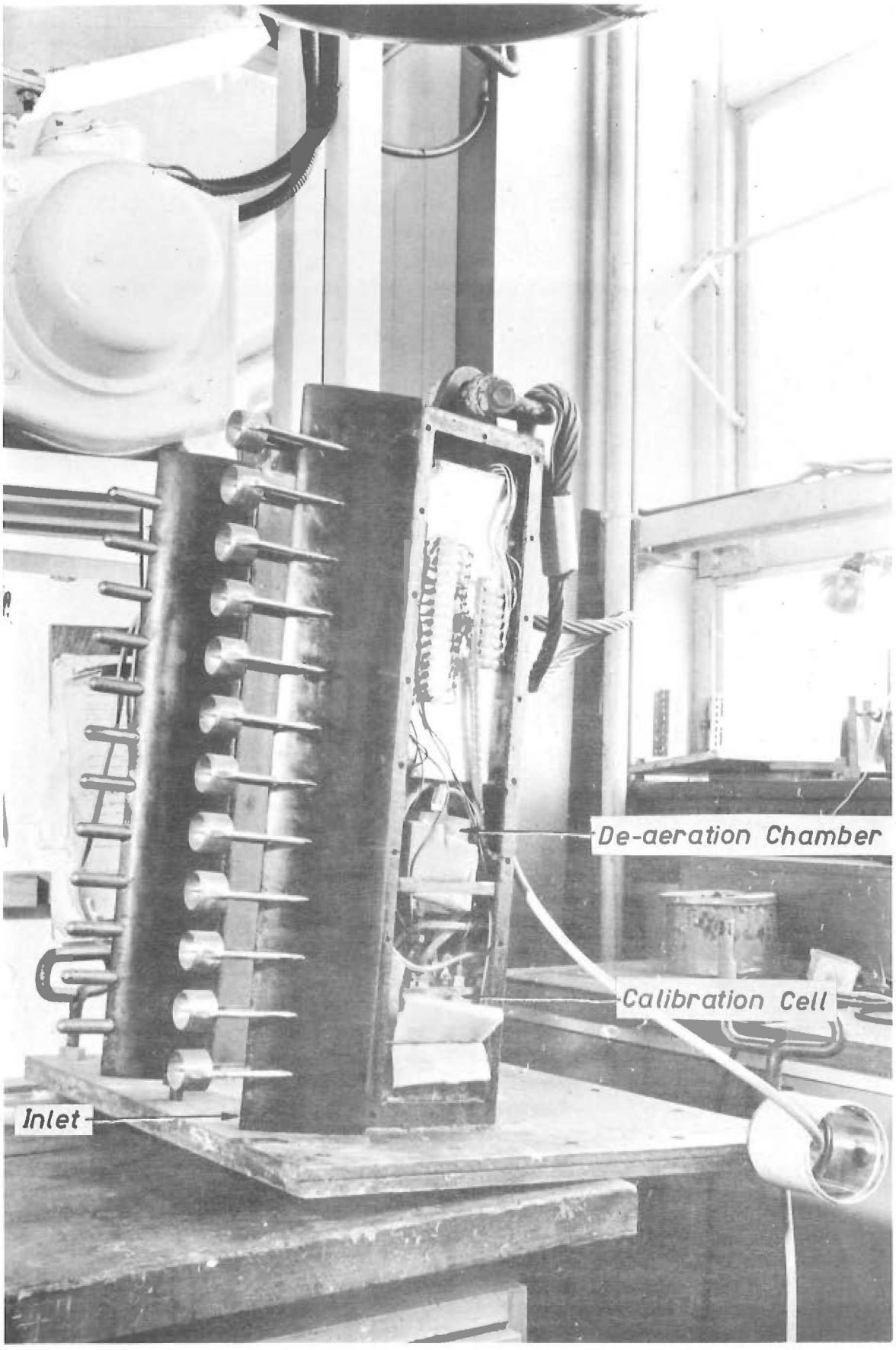

Fig.2.26 : AIR CONCENTRATION CALIBRATION UNIT.

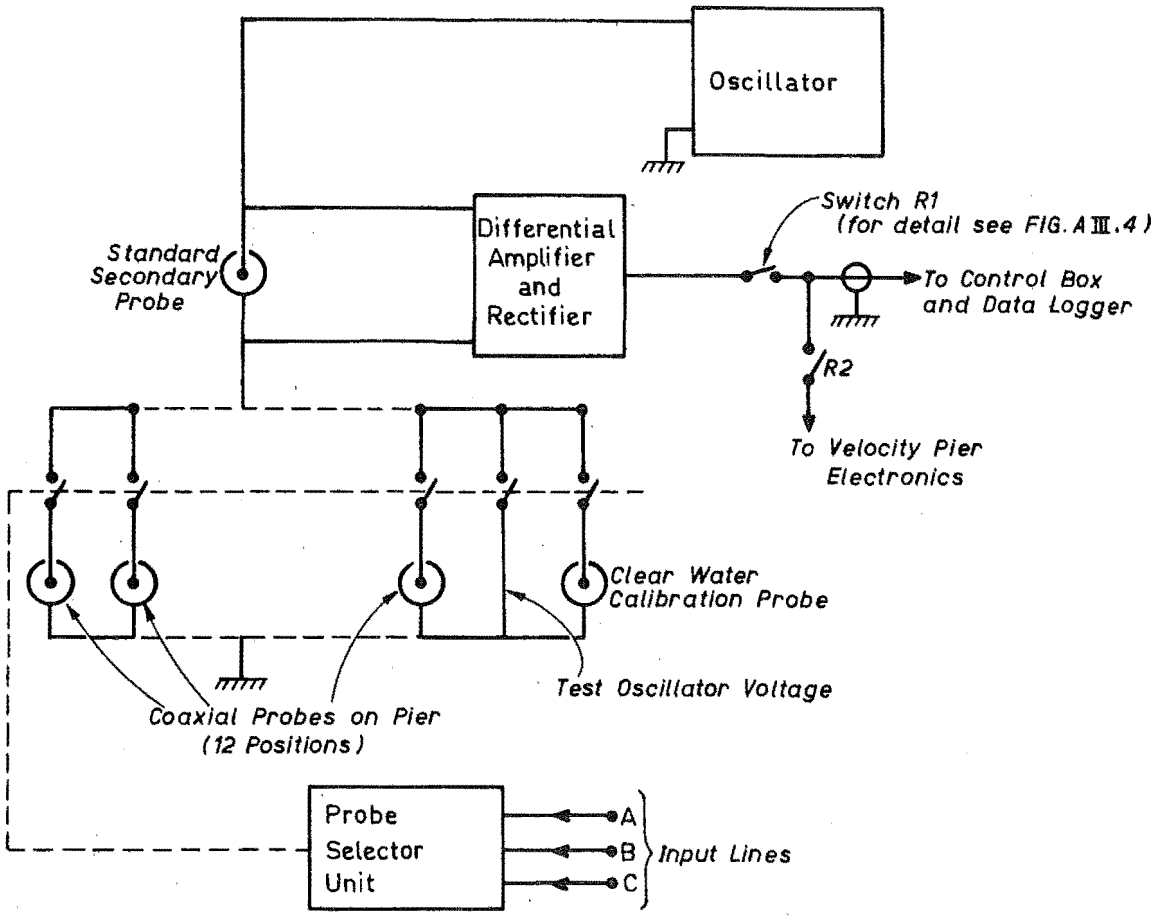

FIG.2.27:BLOCK DIAGRAM OF AIR CONTENT PIER ELECTRONICS

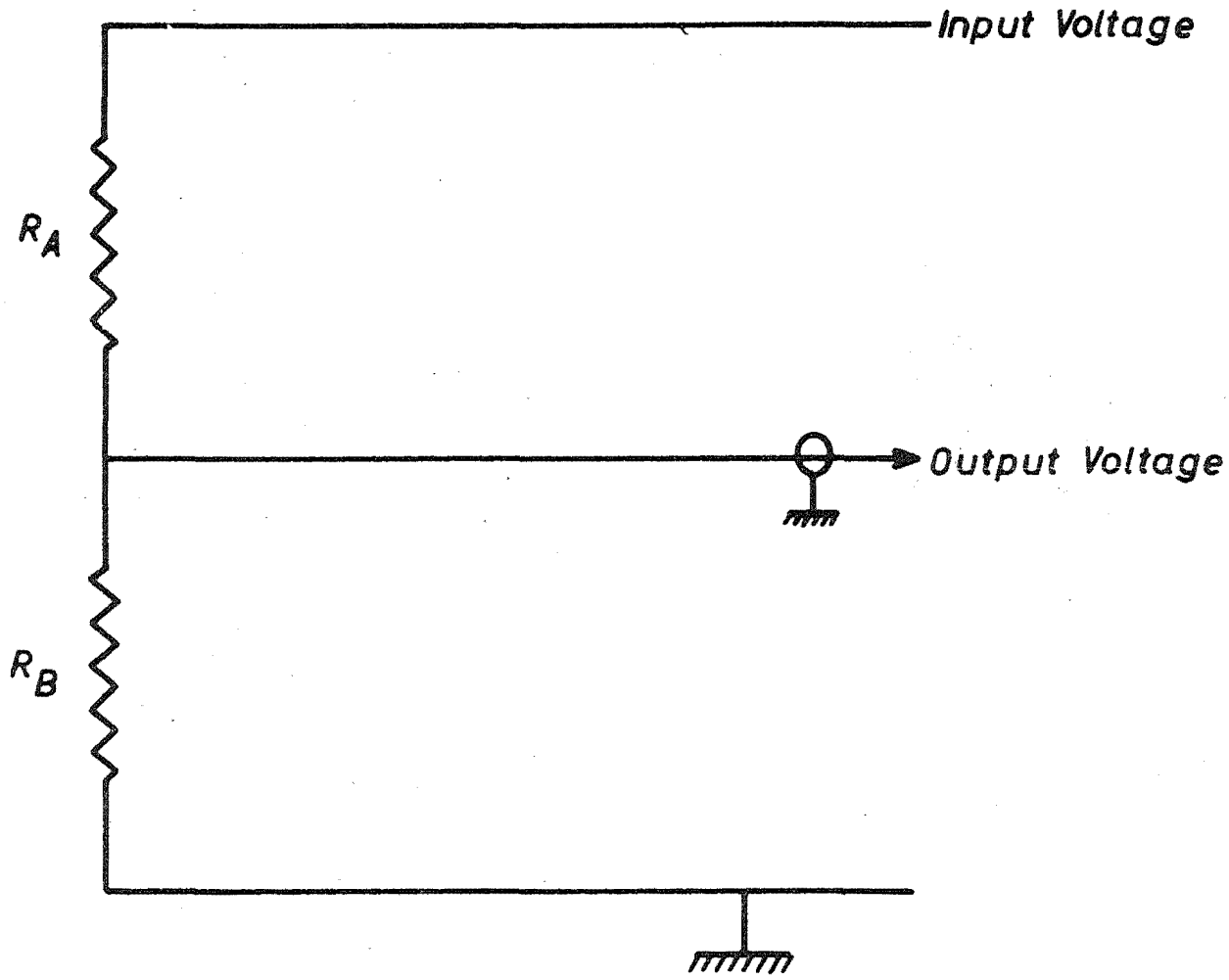

Fig. 2.28 : SCHEMATIC OF SINGLE DIAPHRAGM STRAIN GAUGE.

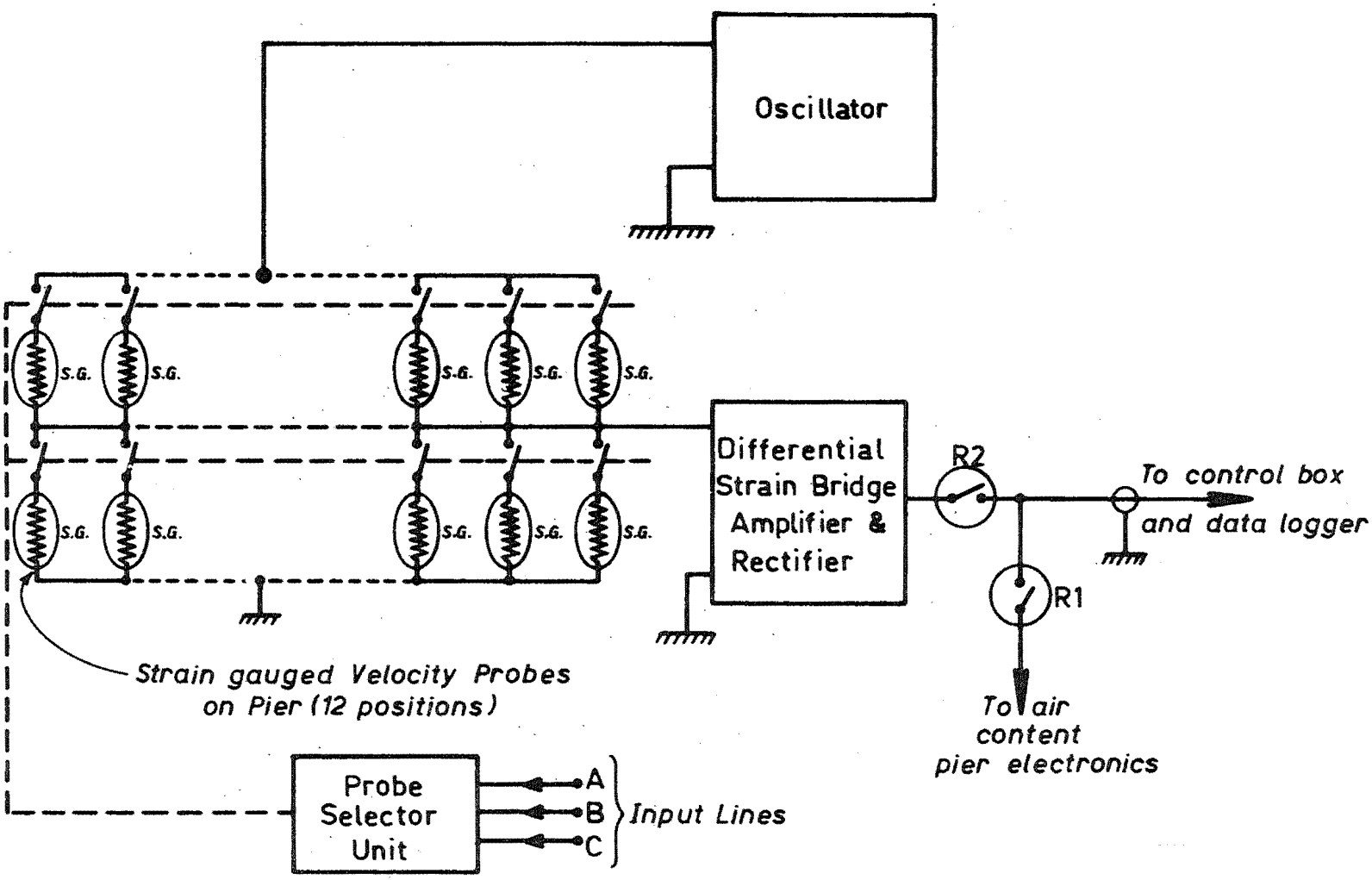

FIG.2.29:BLOCK DIAGRAM OF VELOCITY PIER ELECTRONICS

Each velocity meter was calibrated by the procedure described in Section 2.3.4. It was found in all cases that the graph of pressure against strain gauge output plotted as a straight line. This linear relationship was expressed by the equation

$$P = E_s \times CF \qquad \ldots 2.4.1$$

where

P is the diaphragm pressure in psi

E_s is the output reading

CF is a constant which has a unique value for each velocity meter.

2.4.6 Field Recording Equipment

The output from the field test unit on the spillway consisted of a voltage which subsequently required decoding into either a stagnation pressure or an air concentration according to the relevant calibration formula.

A Solartron data logger was used to record voltage.

The basic measuring unit of the data logger was a digital voltmeter which, by means of various peripheral units, could be made to sample the voltage on the output line at a maximum speed of two readings per second and record it automatically on paper tape.

The mean (time average) value of the flow parameter being measured was simply calculated by averaging several hundred values of the parameter obtained at consecutive half second intervals. Additionally, by plotting the variations of the separate sampled readings from the mean against time, a measure of the turbulent fluctuation of the particular flow parameter could be obtained.

Figure 2.30 shows a photograph of the Solartron data logger and tape punch unit.

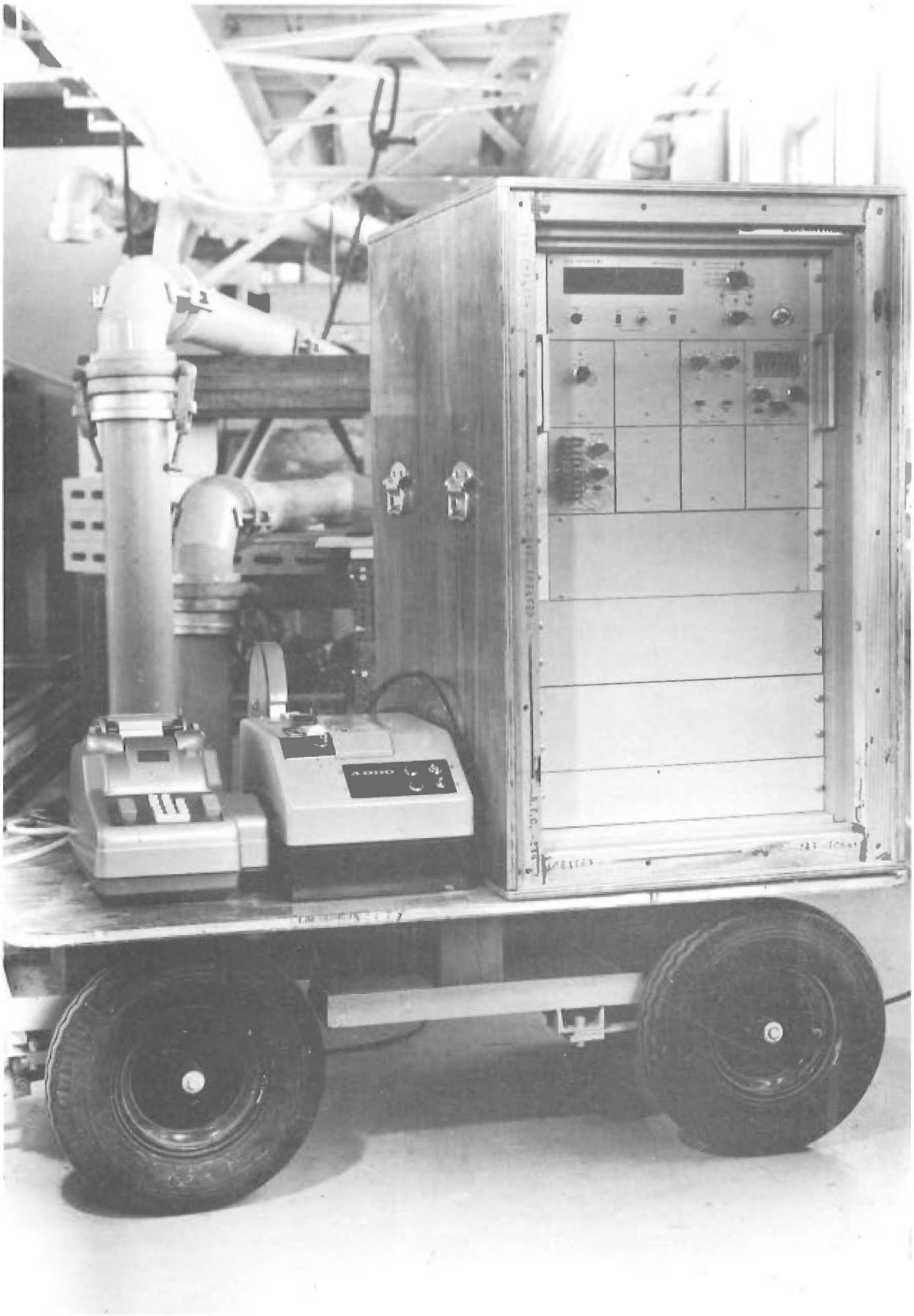

Fig. 2.30 : FIELD RECORDING EQUIPMENT.

CHAPTER THREE

EXPERIMENTAL PROGRAMME

SYNOPSIS

This chapter describes the experimental programme carried out on the spillway of the Aviemore Dam.

The chapter is sub-divided into three broad sections detailing the aims of the experimental programme, the experimental procedure, and the overall work programme carried out to attain the experimental aims.

Details of the apparatus used are given in Chapter Two and the results from the experimental programme are presented in Chapter Four.

3.1 AIMS

It is generally accepted that self-aeration does not commence on a spillway until a "critical point" is reached at which the boundary layer thickness is equal to the flow depth.

In Chapter One, an empirical equation, deduced from experiments carried out by Bauer[6], for locating the "critical point" on an overflow spillway, is presented. The aims of the experimental programme were:

1. To use the developed instrumentation to obtain depth profiles of air concentration and velocity at different points on the Aviemore spillway.

2. To observe the flow profile and "critical point" for each of several flow discharges and to compare them with those predicted

from Bauer's equation adapted to the case of a gated spillway.

3. To investigate the time dependence of the turbulent fluctuations of the flow parameters measured with the field test unit.

3.2 EXPERIMENTAL PROCEDURE

3.2.1 Introduction

In general, water at the Aviemore Dam is available for spilling only during the summer months October to March. During this period, the comparatively low electricity demand coincides with an abundance of water due to the seasonally high rainfall in the upper catchment area of the Waitaki River which feeds Aviemore Lake. Field tests on the spillway could, thus, be carried out only at this time.

The full testing programme, which was carried out during the period 27 September to 8 October 1970, involved close liaison with personnel of the New Zealand Electricity Department, to assist with the operation of the spillway gates, and with personnel of the Ministry of Works from the nearby construction town of Otematata, who assisted with the installation of the field test unit on the spillway.

Testing was carried out using steady non-uniform flows on the spillway of the Aviemore Dam. Measurements of air concentration and stagnation pressure as functions of time were obtained at various depths in the flow at each of five test stations situated in a longitudinal line in Spillway Bay 4. Using these measurements, depth profiles of mean (time average) air concentration and velocity were obtained at each of the test stations.

For all stations, three different gate openings (one, two, and three feet) were used. Additionally, a gate opening of four feet was used at the highest station on the spillway. Thus, a total of sixteen sets of results were obtained.

This section comprises detailed descriptions of the installation procedure for the field test unit and of the experimental testing procedure.

3.2.2 Field Test Unit Installation Procedure

The field test unit was installed on the spillway from a specially designed skip, which could be raised or lowered by crane. The skip was designed with sloping runners such that it provided a stable, horizontal working platform on the spillway surface.

Three persons were required on the skip - two to carry out the actual installation and a third to liase with the crane operator.

The skip was first positioned immediately below a particular test station and the blanking plate covering the station removed. The end of the cable below the blanking plate was then stripped and screwed into a terminal strip on the back of the field test unit. A waterproof cover was screwed into place to protect the terminal strip. The unit was then carefully manouvered into place on the anchorage station and securely bolted down. Finally, before the skip was hoisted off the spillway, the protective guards were removed from the nose cones of the two piers.

Various stages in the installation procedure are shown in Figure 3.1.

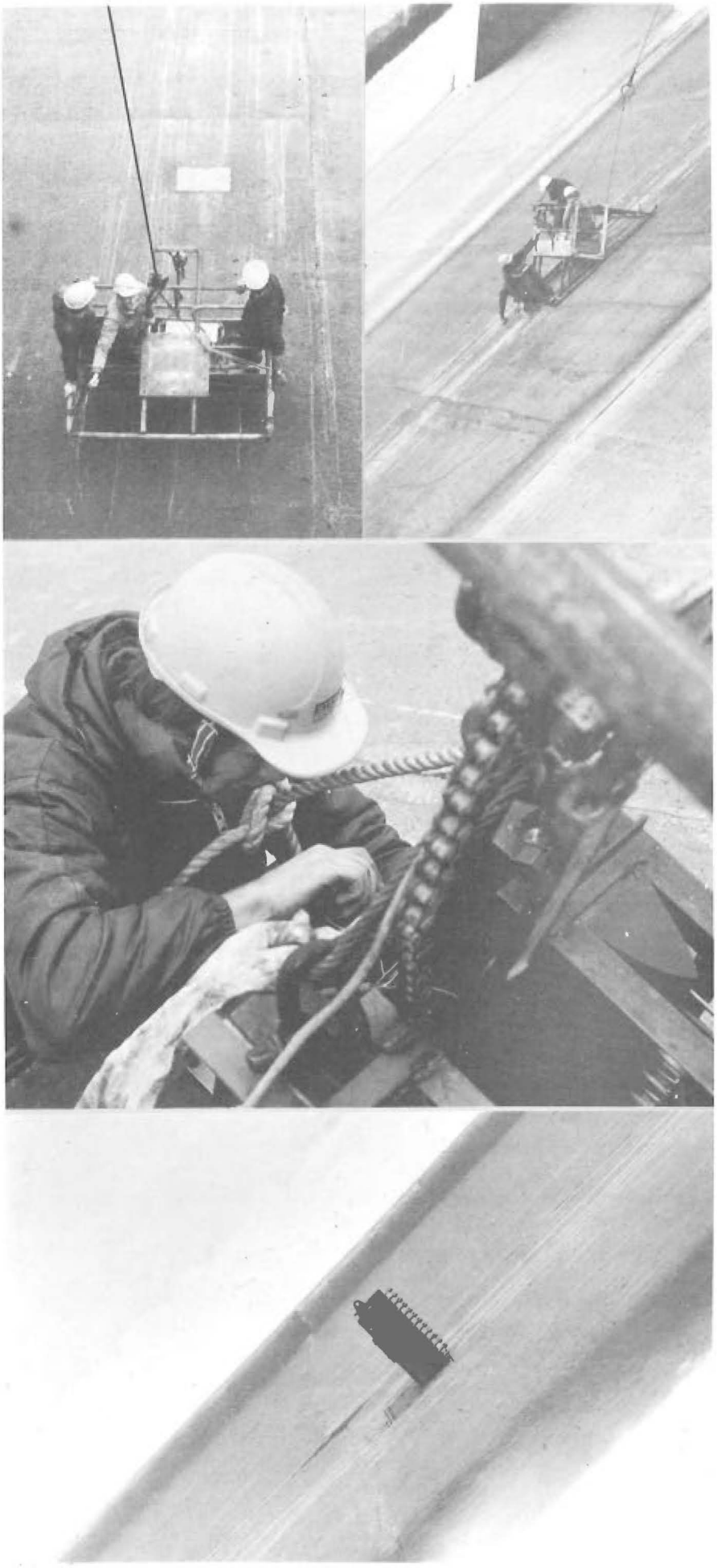

Fig. 3.1 : FIELD TEST UNIT – INSTALLATION ON SPILLWAY.

3.2.3 Testing Procedure

For each test run, and for each of the various switch positions, the complete data block, required for subsequent analysis, consisted of three data sets - an initial set of zero readings, a set of test readings, and a final set of zero readings. Each data set consisted of up to three hundred readings, automatically recorded at consecutive half second intervals.

The corresponding data sets for all switch positions were recorded consecutively. Figure 3.2 shows the switching order followed.

Test Procedure:

1. The recording instrumentation was connected to the field test unit, via the previously installed spillway cable, and all electrical circuits checked. The instrumentation was left switched on for at least twelve hours prior to testing, to enable any electronic drift to stabilise.

2. A data set of zero readings was recorded for each switch position.

3. The spillway gate was opened to three feet, held at this for five minutes, and reclosed.

This step was to allow dynamic "working" of the velocity meter diaphragms, as was found to be necessary before the zero pressure readings would stabilise, and is described in Section 2.3.5 (page 72).

4. A second series of zero data sets was recorded.

5. The spillway gate was then opened to the first test opening and the series of test data sets recorded.

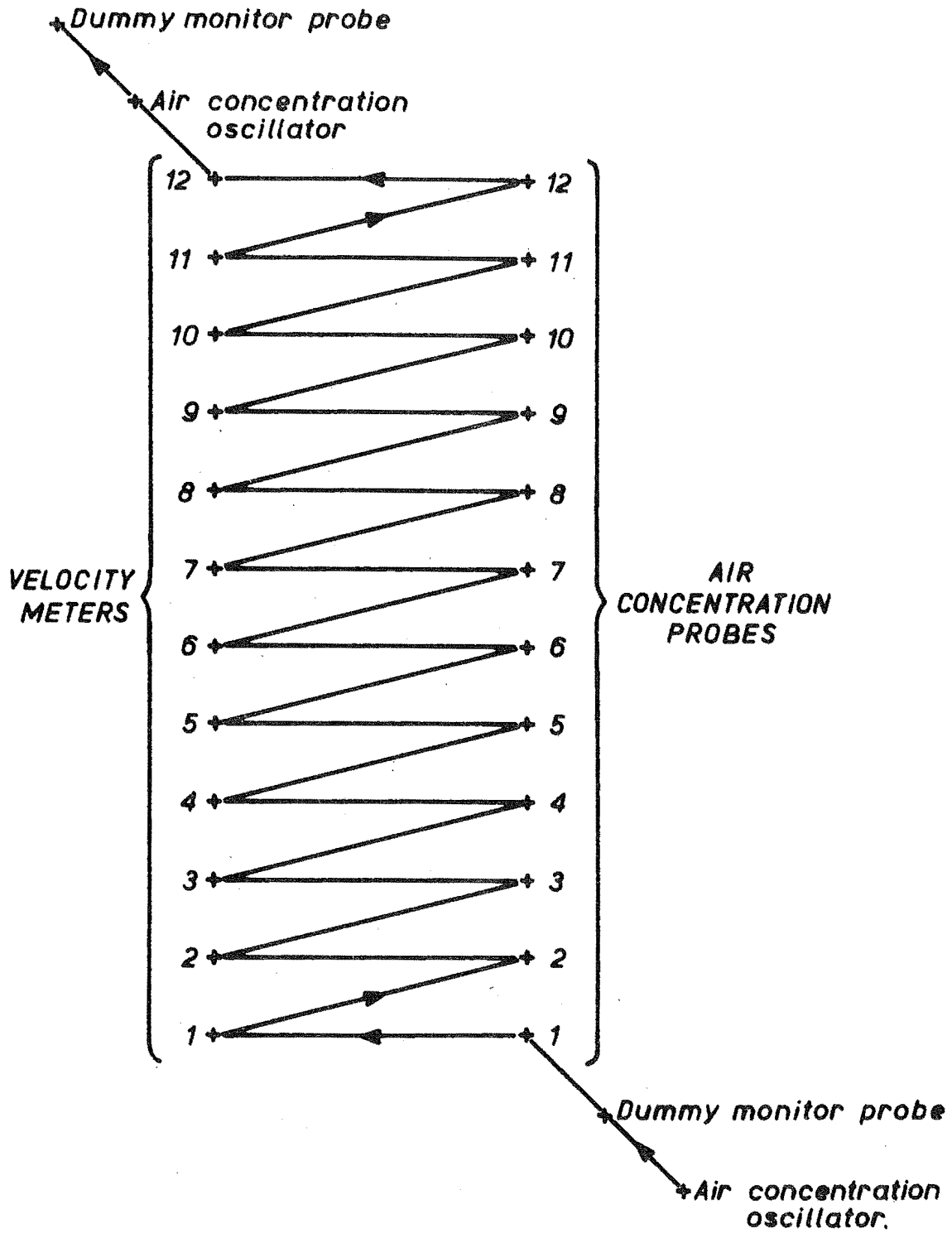

Fig.3.2: FIELD TESTING SWITCHING ORDER FOR TYPICAL TEST RUN.

6. The spillway gate was closed and a further series of zero data sets recorded.

These readings were compared with those obtained in step 4., above. If a zero drift, within a data block, greater than 5% was observed, the test readings were repeated. Furthermore, these data sets represented the initial series of zero data sets for the next test gate opening.

7. Steps 5. and 6. were then repeated for each of the test openings of the spillway gate.

Spillway Gate Control:

During testing, the spillway gates were electrically operated, by personnel of the New Zealand Electricity Department, from the roadway on top of the dam. Radio communication was maintained with the recording instrument hut set up at the side of the spillway.

3.3 WORK PROGRAMME

Tests were carried out for the five anchorage stations, in Spillway Bay 4, commencing at the bottom of the spillway and working towards the top.

The testing procedure (described in Section 3.2.3) called for the field test unit to be installed at least twelve hours before testing. This was achieved by installing the unit on the spillway in the afternoon of the day before testing. The instrumentation was left switched on overnight and the test carried out next morning. The test unit was then moved in the afternoon to the next test anchorage station and the test procedure repeated.

It was not always possible to follow the work programme as described above because occasional high winds on Aviemore Lake caused water to be thrown over the top of the closed gate, creating

hazardous working conditions on the spillway. This effect is shown in Figure 3.3.

Because of this problem, some delays were experienced in the execution of the work programme. Nevertheless, the stipulation that the instrumentation be left switched on for at least twelve hours prior to testing was rigidly adhered to.

Fig.3.3 : WATER THROWN OVER CLOSED GATE BY HIGH WIND VELOCITY.

CHAPTER FOUR

EXPERIMENTAL RESULTS

SYNOPSIS

This chapter presents and discusses representative results from the experimental programme described in Chapter Three.

The chapter is subdivided into three sections.

In the first section the data processing techniques are described and the depth profiles of air concentration and velocity, obtained at each spillway anchorage station for the test discharges, are presented and discussed.

Bauer's method for determining the critical point is tested in the second section with reference to the observations made at Aviemore.

The third section presents and discusses representative time variation curves of air concentration and stagnation pressure.

INTRODUCTION

Preliminary observations of the spillway flow showed the surface to be highly turbulent and unstable with relation to the surface aeration pattern. Figure 4.1 shows two photographs, taken during the same test, of the spillway flow for a gate opening of two feet, with the field test unit mounted at Station 402. The unstable nature of the flow surface is evident from the vastly dissimilar surface aeration patterns, implying that the assumption

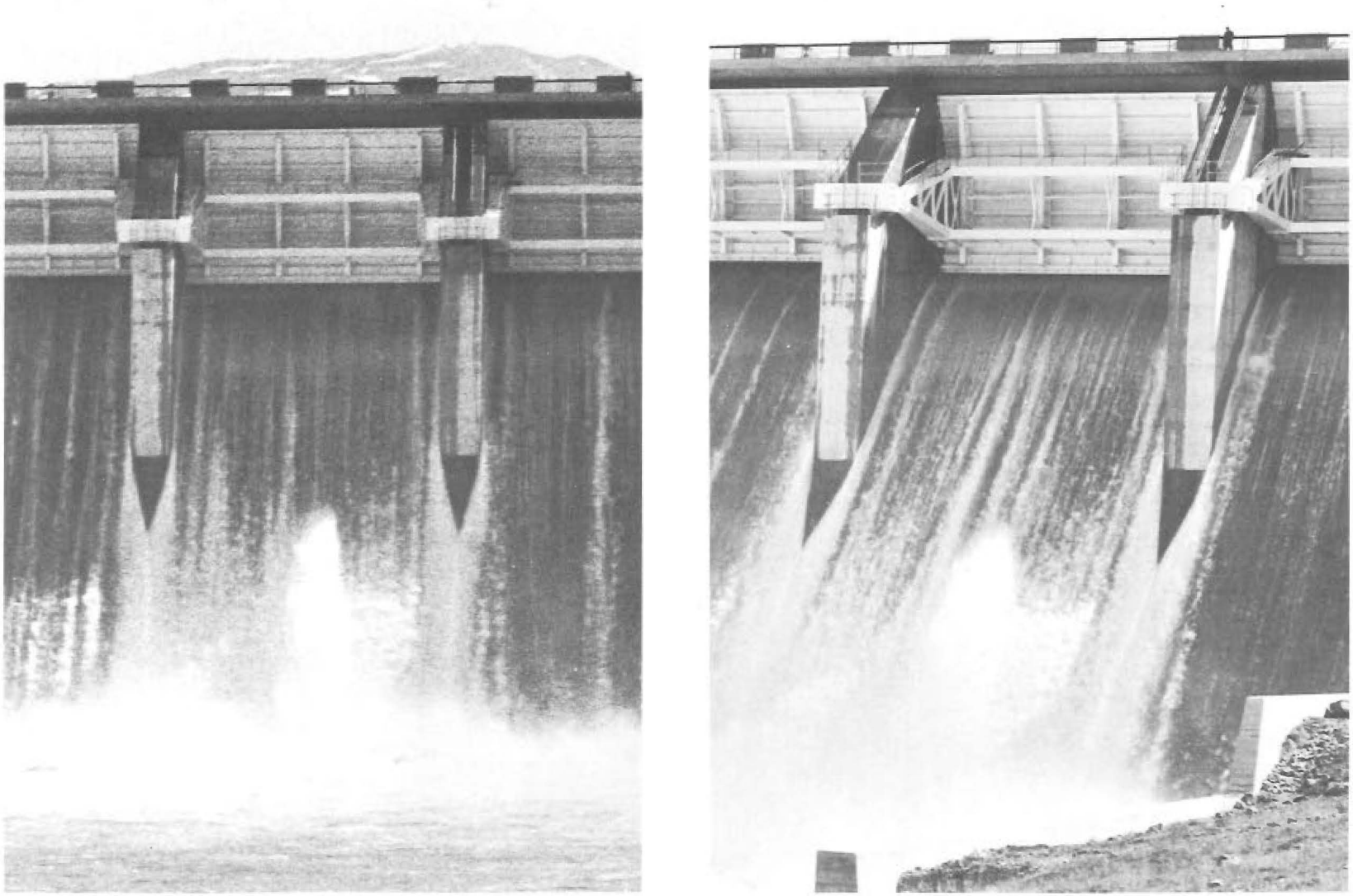

Fig. 4.1 : INSTABILITY OF FLOW SURFACE PATTERN.

of two-dimensional flow is not altogether justifiable near the surface. Thus, it was obvious that considerable care would have to be exercised in the interpretation of results near the flow surface.

Preliminary trials to test the suitability of the developed instruments were first attempted in April 1969. At this time the air concentration pier was installed on the spillway, but, owing to a breakdown in liaison, water could not be made available.

The field test unit was then left on the spillway until the following September. However, in the intervening months, the unit had been extensively damaged, thought to be the result of a large log going over the spillway. The damaged unit is shown in Figure 4.2.

Extensive rebuilding was required and preliminary trials were finally carried out in March 1970.

These trials have been reported elsewhere[23]. This chapter is concerned only with the results of the main experimental programme which, nevertheless, included also the test conditions covered during the preliminary trials.

4.1 DATA PROCESSING AND DEPTH PROFILES OF AIR CONCENTRATION AND VELOCITY

4.1.1 Data Processing Techniques:

The data output from the field test unit consisted of a large number of voltage readings which subsequently required decoding into either air concentrations or stagnation pressures by use of particular calibration formulae.

As explained in Section 3.2.3, the field data for each test opening of the spillway gate consisted of a block of three data

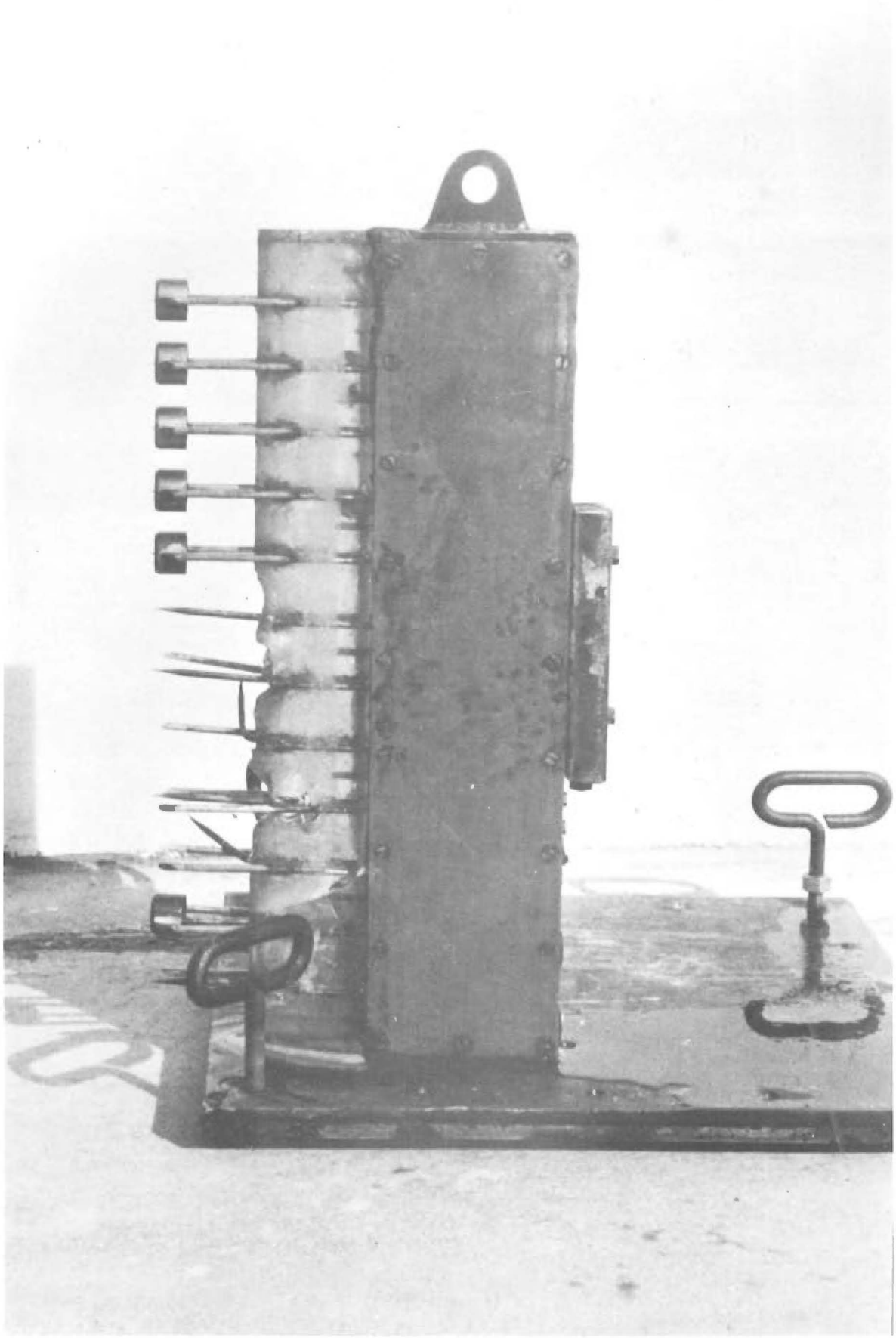

Fig. 4.2 : DAMAGED FIELD TEST UNIT.

sets for each of the air concentration probes and velocity meters. Each block comprised an initial set of zero readings, a set of test gate opening readings, and a final set of zero readings. An acceptability limit of 5% was imposed on the drift between initial and final zero data sets.

Within each zero data set, the mean value of the readings was obtained, which was then assumed to vary linearly with time between zero data sets in the same block. Thus, zero output values for the air concentration probes and velocity meters at the time of the test readings could be interpolated.

Using these interpolated zero values, the relative voltage on the output line due to the test flow was obtained for each individually recorded reading.

The relative readings were then decoded differently, depending on which flow parameter they represented. The processing techniques (for air concentration, stagnation pressure, and velocity) are detailed below.

(a) Air Concentration:

For each of the relative readings, the air concentration was obtained from Eq. 2.2.8 (page 37)

$$C = \frac{\frac{E_o}{E_s} - z}{\frac{E_o}{E_s} - \frac{3 - z}{2}} \qquad \ldots 2.2.8$$

where

E_o is the air concentration oscillator output

E_s is the relative output reading

z is the ratio of E_o to E_s for zero air concentration.

(The ratio z for each air concentration probe was calculated from

readings obtained at the highest station on the spillway for a test gate opening of four feet. At this gate opening, it was readily observed that there was no air in the water).

For each air concentration probe the mean (time average) value of the air concentration was obtained by averaging all the calculated values.

(b) Stagnation Pressure:

For each of the relative readings, the stagnation pressure was obtained from Eq. 2.4.1 (page 91)

$$P = E_s \times CF \qquad \ldots \quad 2.4.1$$

where

E_s is the relative output reading

CF is the calibration factor for the velocity meter. The procedure for obtaining the factor CF for each velocity meter is detailed in Section 2.3.4).

For each velocity meter the mean (time average) value of the stagnation pressure was obtained by averaging all the calculated values.

(c) Velocity:

The mean (time average) velocity at each velocity meter was calculated from the mean values of stagnation pressure and air concentration using the equation

$$\overline{V} = \sqrt{\frac{2\,(\overline{P} - P_{stat})}{\rho_w\,(1 - \overline{C})}} \qquad \ldots \quad 4.1.1$$

where

ρ_w is the density of water

P_{stat} is the static pressure at the velocity meter due to the weight of overlying fluid.

With reference to Figure 4.3 the static pressure was expressed by the equation

$$P_{stat} = \left[\int_Y (1 - \bar{C}_y)\, dy\right] \gamma \cos\alpha \qquad \ldots 4.1.2$$

where

Y is the distance, normal to the spillway, from the point under consideration (A) to the flow surface

$\bar{C}_y$ is the mean (time average) air concentration at a normal distance y from point A

γ is the specific weight of water

α is the spillway slope

Due to the high velocities on the spillway and the comparatively small depths of flow, P_{stat} was very much smaller in value than $\bar{P}$. Thus, even large errors in the value of $\bar{C}_y$ in Eq. 4.1.2 would not have substantially affected the accuracy of Eq. 4.1.1.

Equation 4.1.1 was developed in exactly the same way as Eq. 2.3.18, the only difference being the inclusion of the static pressure term.

It should be noted that in the derivation of Eq. 4.1.1, the second order turbulent fluctuation terms, analogous to B_1, B_2, B_3 in Eq. 2.3.18, are functions of the ratios $\frac{\rho'}{\bar{\rho}}$ and $\frac{P'}{\bar{P} - P_{stat}}$. Equation 4.1.1 is correct only when these terms are negligible.

Computing:

A single computer programme was developed to handle all the raw data from tests carried out at each anchorage station on the spillway face.

The input consisted of raw tape data, from the data logger tape punch, and card control data.

The main printed output consisted of mean (time average) values of air concentration, stagnation pressure, and velocity for each probe position on the field test unit and for each gate opening

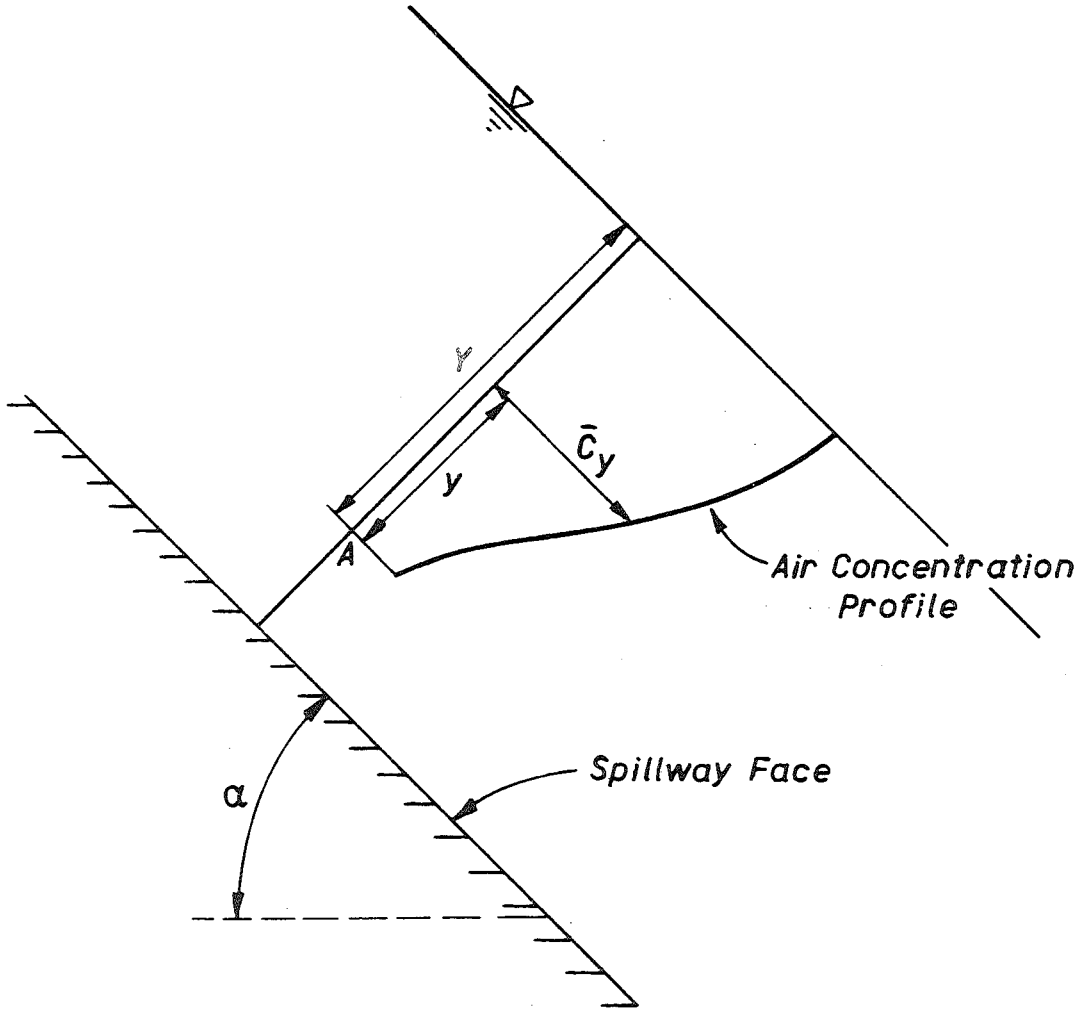

Fig. 4.3 : DEFINITION SKETCH FOR DERIVATION OF EQUATION 4.1.2.

tested.

Punched card output was also produced which was later used to automatically plot the fluctuations with time of air concentration and stagnation pressure.

The programme is listed in Appendix II.

4.1.2 Depth Profiles of Air Concentration and Velocity

The profiles of air concentration, obtained at each spillway anchorage station for gate openings of one and two feet, and of velocity for gate openings of one, two, and three foot are presented in Figures 4.4 to 4.8.

The parts of the profiles shown as dashed lines are inaccurate. The reasons for this are discussed in Section 4.1.3.

The theoretical maximum velocities shown on the velocity graphs were computed from

$$V = \sqrt{2gh} \qquad \ldots 4.1.3$$

where

h is the vertical distance from the spillway station to the head water level behind the dam.

Figure 4.9 shows a series of representative photographs of the field test unit on the spillway during testing.

4.1.3 Accuracy of Results

The reliability of results from an experimental study can only be assessed by reference to an error analysis. Such an analysis is especially important in this study, where, for each air concentration probe and velocity meter, a single mean value is obtained from a mass of statistical data.

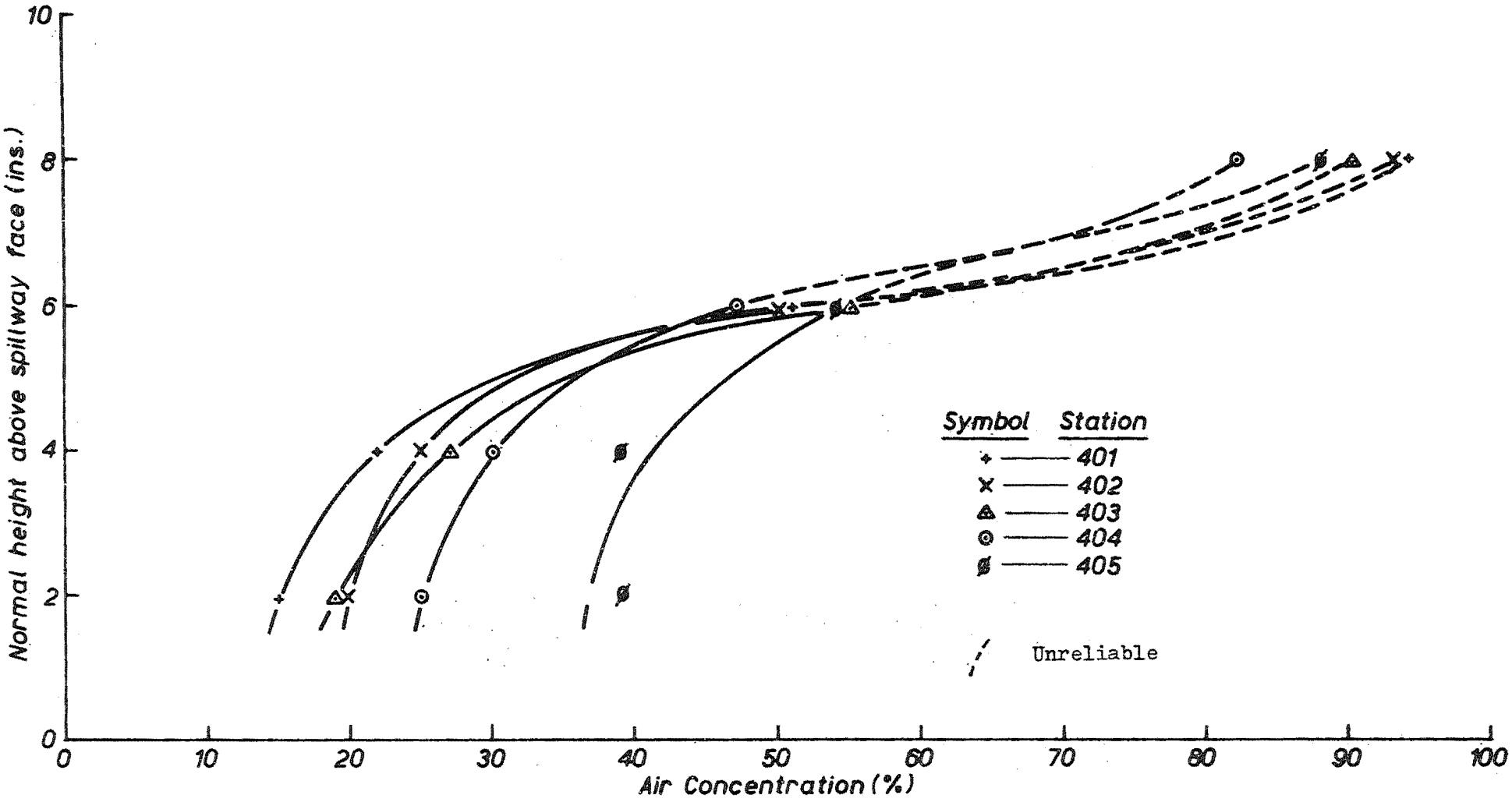

Fig. 4.4 : AIR CONCENTRATION PROFILES FOR GATE OPENING OF 1 FOOT

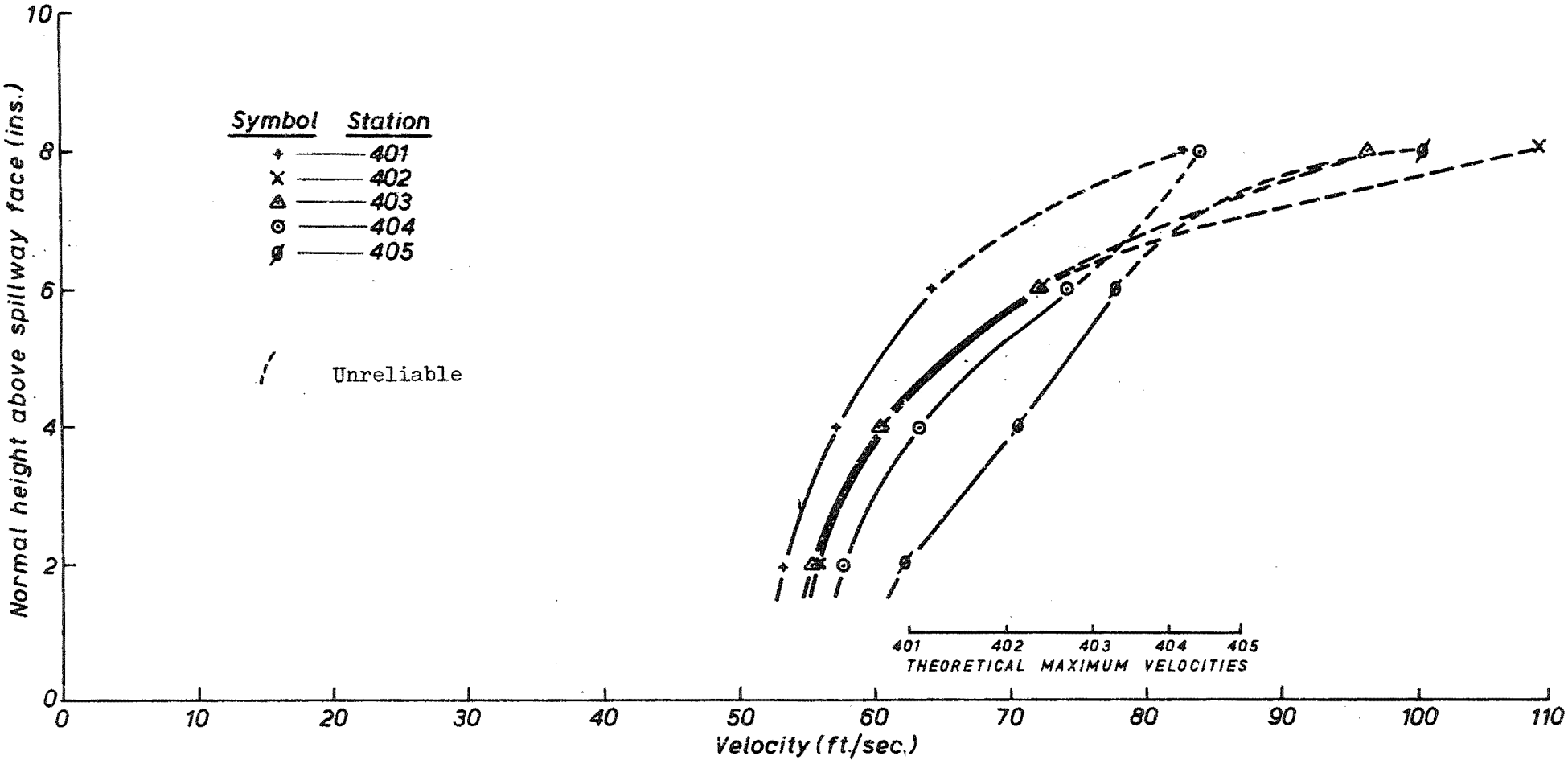

Fig. 4.5 : VELOCITY PROFILES FOR GATE OPENING OF 1 FOOT

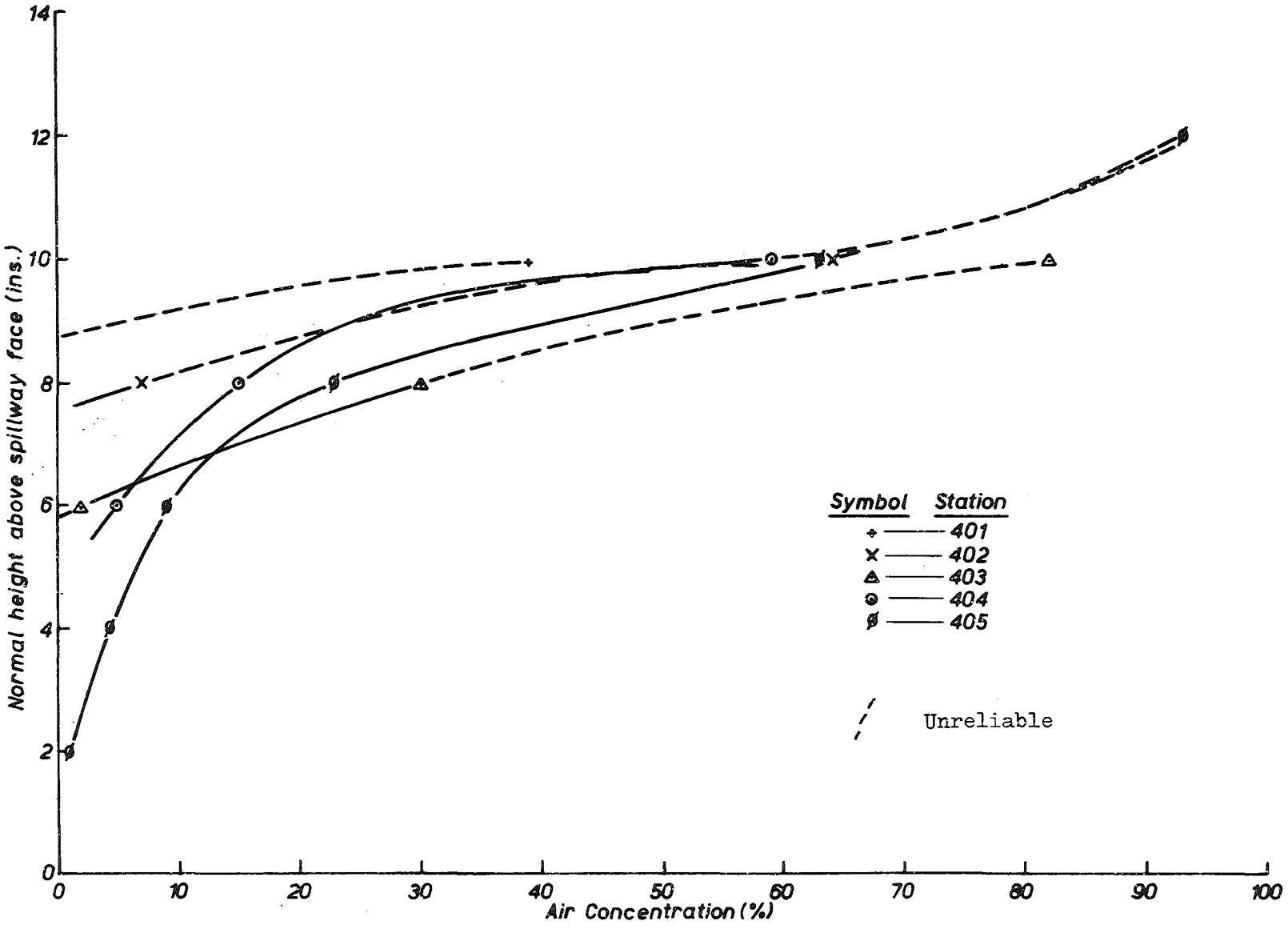

Fig. 4.6 : AIR CONCENTRATION PROFILES FOR GATE OPENING OF 2 FOOT

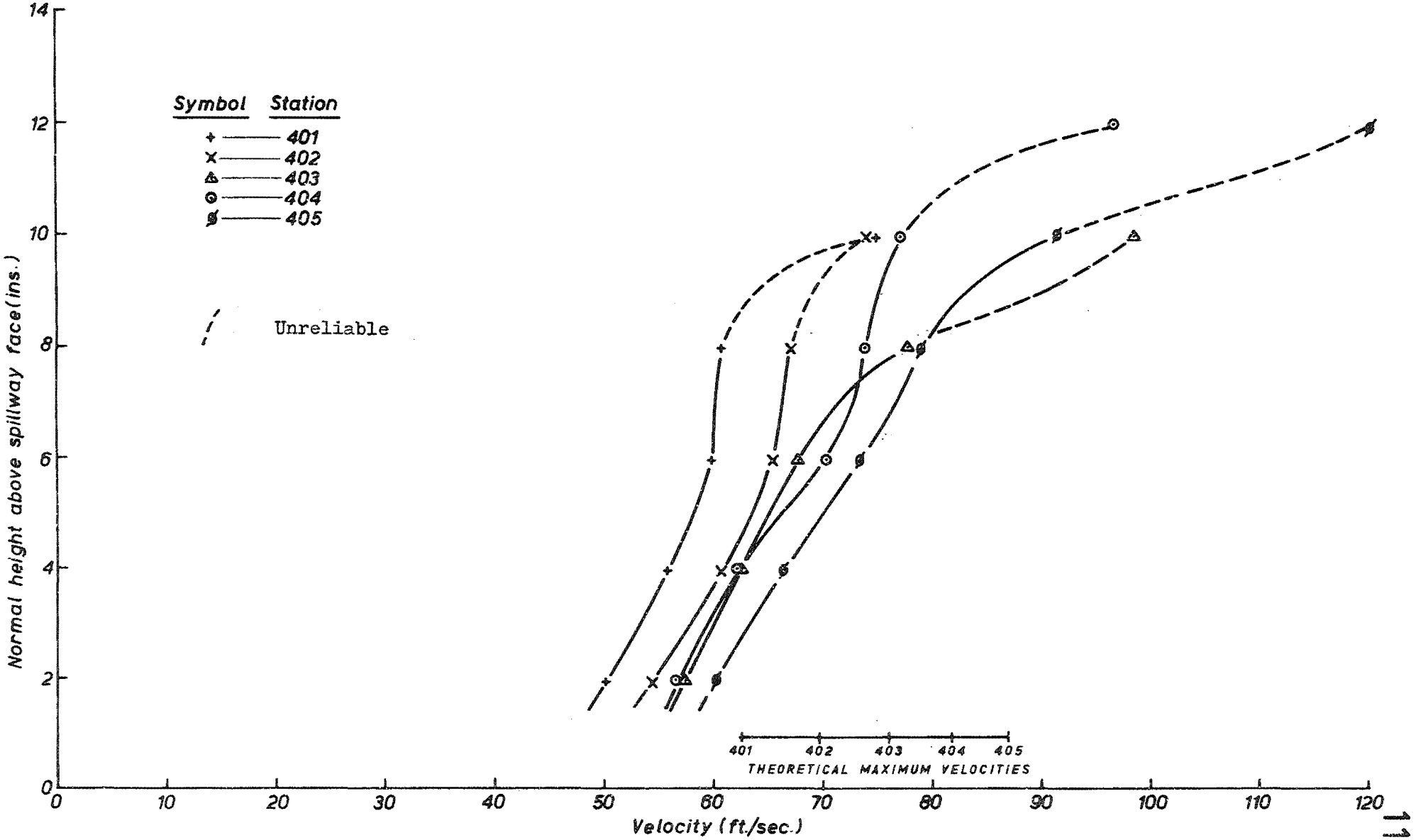

Fig.4.7 : VELOCITY PROFILES FOR GATE OPENING OF 2 FOOT

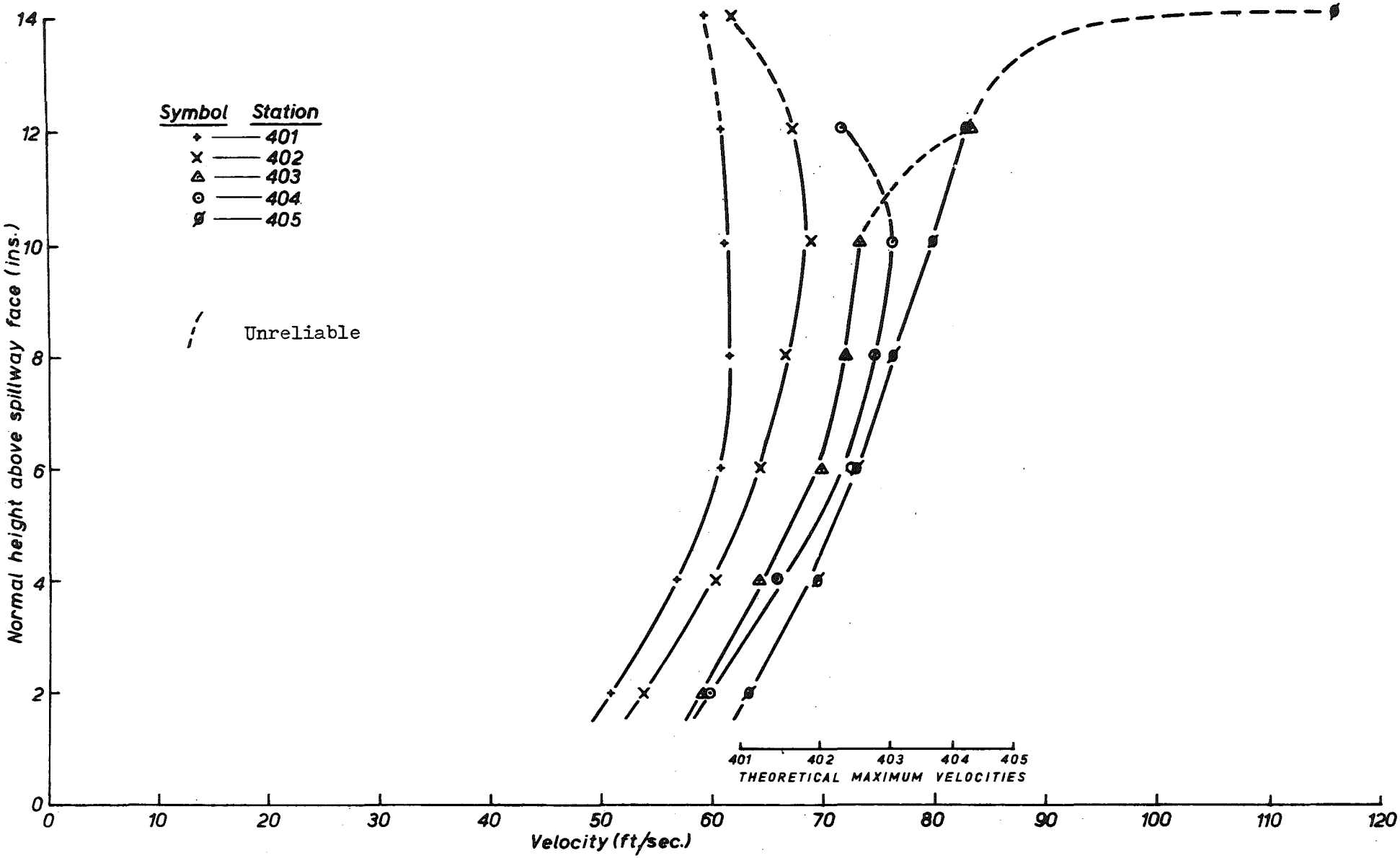

Fig. 4.8 : VELOCITY PROFILES FOR GATE OPENING OF 3 FOOT

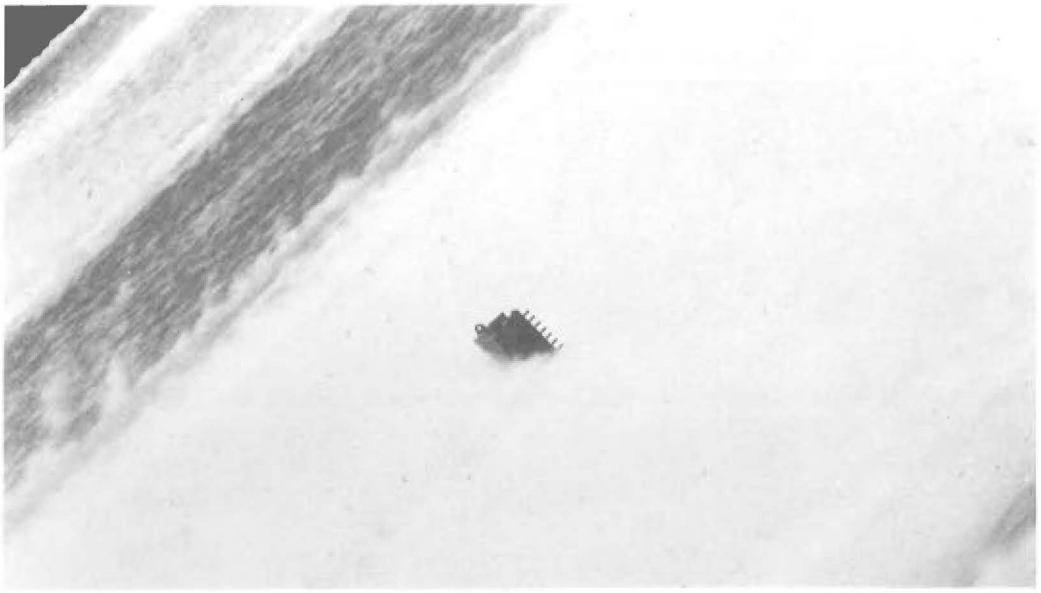

(a)

(b)

(c)

Fig. 4.9 : FIELD TEST UNIT ON SPILLWAY FOR GATE OPENINGS (a) 1ft. Stn. 403, (b) 2ft. Stn. 405 AND (c) 3ft. Stn. 404.

The techniques for assessing the reliability of the various results are described below.

(a) Air Concentration and Stagnation Pressure:

The accuracy of these results proved relatively easy to assess.

The mean value at a particular point was simply calculated as the time average of all the readings obtained at the point. The accuracy of this value was assessed by calculating the "root mean square" error, E, defined by the equation

$$E = \frac{\sigma}{\sqrt{n}} \qquad \ldots 4.1.4$$

where

σ is the statistical standard deviation of the data block

n is the number of readings in the data block

It can be shown[24] that Eq. 4.1.4 implies a 68% probability that the true value of the mean will lie in the range $m \pm E$, where m is the calculated value of the mean.

In accordance with accepted mathematical practice, the term E is referred to as the "expected error" in accepting m as the true value of the mean.

Magnitudes of the "expected errors" in the mean values of air concentration and stagnation pressure, expressed as percentages of the mean values, are presented in Tables 4.1, 4.2, and 4.3 for the results from spillway gate openings of one, two, and three feet respectively. The error values are distinguished between by using the subscripts C, and P for air concentration and stagnation pressure respectively.

The tables show that, with the exception of some results annotated separately, the largest error was 6.5% and that most of the errors were substantially lower.

(b) Velocity:

The mean velocity of the air-water mixture at a particular depth in the flow was calculated from the mean air concentration and stagnation pressure at the same depth using Eq. 4.1.1.

As explained in Section 4.1.1, Eq. 4.1.1 is applicable only where second order terms of the ratios $\left(\frac{\rho'}{\overline{\rho}}\right)$ and $\left(\frac{P'}{\overline{P} - P_{stat}}\right)$ are assumed to be negligible.

A check on the accuracy of the mean velocity calculated from Eq. 4.1.1 was maintained by calculating the order of magnitude of these second order terms and, hence, the order of magnitude of their cumulative sum.

As orders of magnitude only were required, the values of ρ' and P' were estimated by relating them directly to the standard deviations of the data block. The ratio $\frac{\rho'}{\overline{\rho}}$ was expressed in terms of the mean air concentration, $\overline{C}$, and its standard deviation, C', by the equation $\frac{\rho'}{\overline{\rho}} = \frac{C'}{(1 - \overline{C})}$. Furthermore, the static pressure, P_{stat}, was known to be very much smaller than the mean pressure, $\overline{P}$, and the calculations of the second order terms could, thus, be simplified by using the approximation that $\frac{P'}{\overline{P} - P_{stat}} = \frac{P'}{\overline{P}}$.

Magnitudes of the computed velocity errors, E_V, expressed as percentages of the mean values, are included in Tables 4.1, 4.2, and 4.3.

The tables show that large errors, up to 39%, occur in the velocity profiles near the flow surface. To some extent, this accounts for the sharp increase in the apparent velocities in this region.

However, a further factor must be taken into consideration where air concentration and stagnation pressure readings are recorded near

STATION	PROBE	AIR CONCENTRATION				STAGNATION PRESSURE				VELOCITY				
		$\bar{C}$(%)	C'(%)	n	E_c(%)	$\bar{P}$(psi)	P'(psi)	n	E_p(%)	$\bar{V}$(fps)	B_1(1)	B_2(1)	B_3(1)	E_v(%)
401	1	15	3.1	152	1.7	16.25	2.32	154	1.2	53.30	0	.001	.003	.4
	2	22	4.6	152	1.7	17.40	2.60	212	1.0	57.35	.001	.002	.003	.6
	3	51	12.2	260	1.5	13.52	2.81	203	1.5	64.24	.024	.013	.005	4.2
	4(3)	94	4.0	105	.4	2.96	1.75	200	4.2	82.65	.143	.091	.044	27.8
402	1	20	2.7	203	1.0	17.00	2.17	214	.9	55.94	0	.001	.002	.3
	2	25	4.5	253	1.1	18.64	2.51	259	.8	60.71	.001	.002	.002	.5
	3	50	10.1	263	1.2	17.43	2.43	203	1.0	72.23	.016	.007	.002	2.5
	4(3)	93	3.8	125	.4	5.61	2.92	264	3.2	108.58	.110	.070	.034	21.4
403	1	19	2.8	151	1.2	16.64	2.10	155	1.0	55.22	0	.001	.002	.3
	2	27	5.8	164	1.7	17.90	2.05	218	.8	60.27	.002	.002	.002	.6
	3	55	9.4	219	1.2	15.62	2.66	206	1.2	71.83	.017	.009	.004	3.0
	4(3)	90	3.8	130	.4	6.46	2.47	207	2.7	96.21	.050	.035	.018	10.3
404	1	25	4.5	152	1.5	16.94	2.62	154	1.2	57.67	.001	.002	.003	.6
	2	30	6.4	152	1.7	18.88	2.17	156	.9	63.25	.003	.003	.002	.8
	3	47	9.4	164	1.6	19.50	2.24	154	.9	74.20	.012	.005	.002	1.9
	4(3)	82	7.7	102	.9	8.67	3.32	155	3.1	83.89	.067	.020	.018	10.5
405	1	39	4.3	153	.9	16.03	2.92	154	1.5	62.32	.002	.003	.004	.8
	2	39	6.6	153	1.4	20.41	3.08	204	1.1	70.38	.004	.004	.003	1.1
	3	54	9.2	153	1.4	18.55	2.68	152	1.2	77.65	.015	.007	.003	2.5
	4(3)	88	4.2	93	.5	8.23	3.25	152	3.2	100.04	.044	.034	.019	9.7

Notes:

(1) $B_1 = \int_T \frac{1}{8} \left(\frac{\rho'}{\bar{\rho}}\right)^2 dt$, $B_2 = \int_T \frac{1}{4} \left(\frac{P'}{\bar{P}}\right)\left(\frac{\rho'}{\bar{\rho}}\right) dt$, $B_3 = \int_T \frac{1}{8} \left(\frac{P'}{\bar{P}}\right)^2 dt$

where $\int_T f(P,\rho)dt$ represents a time average

$\frac{\rho'}{\bar{\rho}} = \frac{C'}{(1-\bar{C})}$ (see page 118)

(2) These error values indicate that the air concentration probe is not accurate when measuring air concentrations of the order of 1 or 2%. However, at these very low air concentrations, the error is insignificant as it represents an absolute magnitude of less than 1 in the value of $\bar{C}$.

(3) Indicated values for these probes are unreliable (see page 118).

TABLE 4.1: CALCULATION OF ERRORS IN THE MEAN (TIME AVERAGE) VALUES OF AIR CONCENTRATIONS, STAGNATION PRESSURE, AND VELOCITY FOR FLOW FROM SPILLWAY GATE OPENING OF 1 FOOT.

STATION	PROBE	AIR CONCENTRATION				STAGNATION PRESSURE				VELOCITY				
		$\bar{C}$(%)	C'(%)	n	E_c(%)	$\bar{P}$(psi)	P'(psi)	n	E_p(%)	$\bar{V}$(fps)	B_1(1)	B_2(1)	B_3(1)	E_v(%)
401	1	0	0	25	-	16.92	1.57	136	.8	50.32	0	0	.001	.1
	2	0	0	36	-	20.68	1.28	122	.6	55.78	0	0	0	0
	3	0	.1	36	-	23.85	1.23	151	.4	59.96	0	0	0	0
	4	0	.3	98	-	24.51	.64	146	.2	60.78	0	0	0	0
	5(3)	39	24.6	154	5.0	22.87	3.30	193	1.0	74.88	.062	.015	.003	8
402	1	0	.2	58	-	19.96	2.34	204	.8	54.52	0	0	.002	.2
	2	0	.3	99	-	24.66	2.06	252	.5	60.77	0	0	.001	.1
	3	0	.8	137	-	28.25	1.53	253	.3	65.26	0	0	0	0
	4	7	5.4	246	4.9	28.25	1.77	248	.4	67.04	.001	.001	0	.2
	5(3)	64	19.1	249	1.9	13.15	7.74	270	3.5	73.78	.106	.078	.043	22.7
403	1	0	.6	73	-	22.37	2.17	222	.7	57.43	0	0	.001	.1
	2	0	1.3	153	-	26.44	2.48	205	.7	62.53	0	0	.001	.1
	3	2	3.3	201	11.5(2)	30.42	1.65	205	.4	67.67	0	0	0	0
	4	30	12.9	256	2.7	28.34	2.78	251	.6	77.57	.013	.005	.001	1.9
	5(3)	82	7.6	121	.8	11.51	4.32	255	2.4	98.08	.069	.040	.018	12.7
404	1	0	1.3	101	-	21.78	2.53	202	.8	56.64	0	0	.002	.2
	2	0	1.6	148	-	26.13	2.78	205	.7	62.15	0	0	.001	.1
	3	5	3.4	202	4.8	31.71	2.38	205	.5	70.15	0	.001	.001	.2
	4	15	5.9	200	2.8	30.88	2.86	202	.7	73.57	.002	.002	.001	.5
	5	59	12.0	238	1.3	16.36	5.14	237	2.0	76.95	.032	.023	.012	6.7
	6(3)	93	4.1	155	.3	4.16	2.49	205	4.2	96.22	.140	.091	.045	27.6
405	1	1	2.2	151	18(2)	23.98	3.40	204	1.0	60.01	0	.001	.003	.4
	2	4	2.6	101	6.5	28.61	3.61	204	.9	66.31	0	.001	.002	.3
	3	9	5.2	152	4.7	32.89	3.95	204	.8	73.27	.001	.002	.002	.5
	4	23	9.6	203	2.9	32.38	3.58	202	.8	78.79	.006	.003	.002	1.1
	5	63	13.4	211	1.5	20.87	4.80	204	1.6	91.15	.049	.021	.007	7.7
	6(3)	93	4.2	151	.4	7.30	3.48	204	3.3	120.83	.120	.067	.028	21.5

(1)
(2)
(3) } See Notes Table 4.1

TABLE 4.2: CALCULATION OF ERRORS IN THE MEAN (TIME AVERAGE) VALUES OF AIR CONCENTRATION, STAGNATION PRESSURE, AND VELOCITY FOR FLOW FROM SPILLWAY GATE OPENING OF 2 FOOT.

STATION	PROBE	AIR CONCENTRATION				STAGNATION PRESSURE				VELOCITY				
		$\bar{C}$(%)	C'(%)	n	E_c(%)	$\bar{P}$(psi)	P'(psi)	n	E_p(%)	$\bar{V}$(fps)	B_1(1)	B_2(1)	B_3(1)	E_v(%)
401	1	0	0	26	-	17.53	1.64	178	.7	50.77	0	0	.001	.1
	2	0	0	35	-	21.84	1.65	163	.6	56.82	0	0	.001	.1
	3	0	.1	66	-	24.81	1.19	161	.4	60.66	0	0	0	0
	4	0	.1	45	-	25.49	.32	146	.1	61.54	0	0	0	0
	5	0	.1	51	-	25.12	.22	87	.1	61.08	0	0	0	0
	6	0	.4	67	-	24.93	.64	131	.2	60.95	0	0	0	0
	7(3)	8	6.6	188	6.0	21.66	.97	116	.4	59.16	.002	.001	0	.3
402	1	0	0	50	-	19.83	1.96	233	.6	53.88	0	0	.001	.1
	2	0	0	69	-	24.74	2.02	254	.5	60.32	0	0	.001	.1
	3	0	.1	59	-	28.13	1.58	206	.4	64.43	0	0	0	0
	4	0	.1	92	-	29.97	1.23	199	.3	66.57	0	0	0	0
	5	0	.3	106	-	32.03	.83	169	.2	68.89	0	0	0	0
	6	0	.9	152	-	30.26	.69	200	.2	67.07	0	0	0	0
	7(3)	57	29.8	191	3.8	10.96	8.48	256	4.8	61.63	.182	.135	.075	39.2
403	1	0	0	50	-	23.71	2.46	195	.7	59.02	0	0	.001	.1
	2	0	0	50	-	27.95	2.05	203	.5	64.20	0	0	.001	.1
	3	0	0	49	-	33.04	1.63	180	.4	69.89	0	0	0	0
	4	0	.1	73	-	34.08	1.28	203	.3	71.04	0	0	0	0
	5	0	.9	122	-	36.27	.91	181	.2	73.35	0	0	0	0
	6(3)	29	16.9	265	3.6	33.20	3.42	260	.6	83.29	.021	.006	.001	2.8
404	1	0	.1	68	-	24.29	2.67	204	.8	59.75	0	0	.002	.2
	2	0	.2	52	-	29.41	2.48	204	.6	65.87	0	0	.001	.1
	3	0	.1	66	-	35.52	2.19	205	.4	72.48	0	0	0	0
	4	0	1.0	101	-	36.11	1.90	204	.4	75.00	0	0	0	0
	5	0	3.1	197	-	39.68	1.99	199	.4	76.73	0	0	0	0
	6(3)	34	15.4	256	2.8	22.59	6.86	257	1.9	71.52	.021	.018	.012	5.1
405	1	0	.4	44	-	27.18	3.25	204	.8	63.25	0	0	.002	.2
	2	0	.4	49	-	32.71	2.91	204	.6	69.49	0	0	.001	.1
	3	0	1.3	150	-	35.93	4.00	204	.8	72.91	0	0	.002	.2
	4	0	2.4	95	-	39.20	2.76	212	.5	76.21	0	0	.001	.1
	5	5	6.9	151	11.2(2)	40.62	3.43	214	.6	79.81	.002	.001	.001	.4
	6	43	15.3	305	2.0	26.35	7.16	305	1.6	83.00	.027	.018	.009	5.4
	7(3)	91	4.6	115	.5	7.91	4.30	300	3.1	116.69	.108	.073	.037	21.8

(1)
(2)
(3) } See Notes Table 4.1

TABLE 4.3: CALCULATION OF ERRORS IN THE MEAN (TIME AVERAGE) VALUES OF AIR CONCENTRATION, STAGNATION PRESSURE, AND VELOCITY FOR FLOW FROM SPILLWAY GATE OPENING OF 3 FOOT.

the flow surface. If the surface fluctuates in a vertical direction, then, due to the relatively large diameter of the air concentration probe, a number of the readings in a test data set are recorded with the probe only partially in the flow. This gives rise to an air concentration profile, over the vertical diameter of the probe, of the form shown in Figure 4.10.

As explained in Section 2.2.1, the output reading from the air concentration probe represents the mean air concentration over the area of the probe, which in this case is considerably greater than the actual instantaneous air concentration at the centre of the probe. Several such recordings in a test data set will thus result in an apparent mean (time average) air concentration considerably greater than the true mean air concentration at the centre of the probe.

The values of stagnation pressure recorded with the velocity meter are not subject to the same errors, because of the very much smaller size of the pitot hole at the head of the meter.

Use of the apparent mean air concentration in Eq. 4.1.1 will, thus, result in an over-estimate of the true mean velocity. This effect is shown by the dashed lines in Figures 4.4 to 4.8, where apparent large air concentrations and velocities occur near the flow surface.

Thus, considerable care had to be exercised in interpreting results obtained near the flow surface. The extremely broken, unsteady nature of the surface of an aerated flow is illustrated by Figure 4.11. For such flows values of air concentration and velocity recorded within two inches of the flow surface were disregarded. Figure 4.12 shows the much steadier nature of the surface of a non - or partially - aerated flow. For these flows

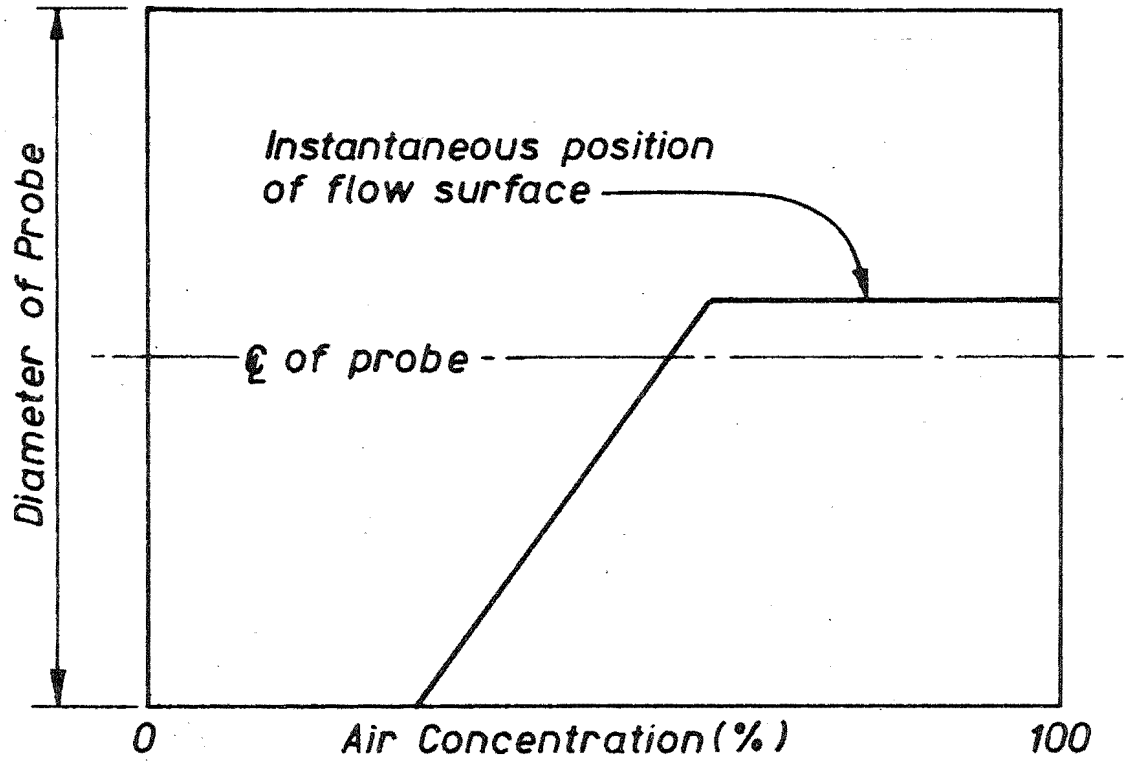

Fig.4.10 : INSTANTANEOUS VERTICAL AIR CONCENTRATION PROFILE ACROSS PROBE WHERE PROBE IS PARTIALLY IMMERSED IN FLOW.

Fig. 4.11 : AERATED FLOW SURFACE.

Fig. 4.12 : NON-AERATED FLOW SURFACE.

values were considered accurate to within one inch of the surface.

For the remaining portions of the flow profiles, shown in Figures 4.4 to 4.8 by solid lines, the error limits specified in Tables 4.1, 4.2, and 4.3 are reliable.

Overall Accuracy of Results:

An assessment of the overall accuracy of the profiles of air concentration and velocity with depth was obtained by a comparison of discharges.

The apparent water discharge on the spillway, at a particular station and for a particular gate opening, was calculated using the relevant air concentration and velocity profiles. From the Continuity principle

$$Q_W = B \int_Y \overline{V}_y \, (1 - \overline{C}_y) \, dy \qquad \ldots 4.1.5$$

where

Q_W is the calculated water discharge

B is the width of the spillway bay

$\overline{V}_y$ and $\overline{C}_y$ are the mean (time average) velocity and air concentration respectively at a height y above the spillway face.

Y is the depth of the air-water flow.

Tables for the Aviemore Spillway[25], giving water discharge in terms of upstream lake level and spillway gate opening, were prepared by the Ministry of Works (M.O.W.) from model studies.

A comparison of the discharges, obtained from these tables, with those calculated from Eq. 4.1.5 gave an assessment of the overall accuracy of the depth profiles of air concentration and velocity. The use of Eq. 4 1.5 is not invalidated by the large errors in the air concentration and velocity profiles near the flow surface, because these errors occur in a region of high air concentration.

Thus, the volume of water affected is very small.

A computer programme, written to solve Eq. 4.1.5 for each of the tests, is listed in Appendix II.

In Table 4.4 the computed values of discharge are compared with those obtained from the M.O.W. tables. The table shows that the largest discrepancy in the values is 7%. In view of the assumption that the flow is two dimensional and the known inaccuracies of the profiles near the flow surface, this represents a high degree of accuracy.

It is notable that nearly all the values of computed discharge in Table 4.4 are lower than the corresponding M.O.W. values. The reason for this becomes apparent when the function $\overline{V}_y$ is eliminated from Eq. 4.1.5. Substituting Eq. 4.1.1 into Eq. 4.1.5

$$Q_W = B \int_Y \sqrt{\frac{2[(\overline{P} - P_{stat})_y]}{\rho_w (1 - \overline{C}_y)}} \; (1 - \overline{C}_y) \; dy \quad \ldots 4.1.6$$

where

$(\overline{P} - P_{stat})_y$ is the mean (time average) velocity head (in lbs/sq.ft) at a height y above the spillway face.

Equation 4.1.6 simplifies to

$$Q_W = B \sqrt{\frac{2}{\rho_w}} \int_Y [(\overline{P} - P_{stat})_y \; (1 - \overline{C}_y)]^{\frac{1}{2}} \; dy \quad \ldots 4.1.7$$

It is evident from Eq. 4.1.7 that if the measured value of $\overline{C}_y$ is larger than the true value, as occurs near the flow surface, then the computed value of Q_W is lower than the true water discharge.

Gate Opening (ft)	Discharge from M.O.W. Tables (cusecs)	Station No.	Computed Discharge (cusecs)	Error (%)
1	1375	401	1278	-7.0
		402	1334	-3.0
		403	1326	-3.6
		404	1399	1.7
		405	1287	-6.4
2	2585	401	2517	-2.6
		402	2514	-2.8
		403	2461	-4.8
		404	2671	3.3
		405	2743	6.1
3	3742	401	3625	-3.1
		402	3680	-1.7
		403	3539	-5.4
		404	3638	-2.8
		405	3746	0.0
4	4884	401	4674	-4.3

TABLE 4.4: COMPARISON OF DISCHARGES COMPUTED FROM PROFILES WITH THOSE FROM M.O.W. TABLES

4.1.4 Result Discussion

Air Concentration Profiles:

Figures 4.4 and 4.6 show the air concentration profiles at all spillway anchorage stations for spillway gate openings of one feet and two foot respectively.

In Figure 4.4 (1ft opening), aeration is apparent at all of the stations, although it becomes more substantial with distance down the spillway. It can be seen that the profile gradient, $\frac{dc}{dy}$, increases from the spillway face until a maximum is reached. Beyond this point the dashed lines indicate that $\frac{dc}{dy}$ decreases towards the surface.

This conclusion is valid, despite the inaccuracy of the dashed parts of the profiles, because, as was shown in Section 4.1.3, the measured values of air concentration near the flow surface were greater than the true values. Thus, with an accurate air concentration profile, the tendency for $\frac{dc}{dy}$ to decrease towards the surface would be even more marked.

Straub and Anderson[9] noted the same tendencies in their experimental profiles.

In Figure 4.6 (2ft opening), the profiles for Stations 401 and 402 indicate that the entrained air at these stations does not penetrate deeply into the flow and a bottom layer of pure water exists.

The subsequent profiles show that the point of zero air concentration is closer to the spillway face with distance downstream, indicating the deeper penetration of the air bubbles.

Velocity Profiles:

Depth profiles of velocity at all spillway anchorage stations, and for gate openings of one foot, two feet, and three feet, are presented in Figures 4.5, 4.7, and 4.8 respectively.

In Figure 4.5 (1ft opening), for which aerated flow existed at all spillway stations, a characteristic of the profiles is a reverse curvature; i.e. the profile gradient $\frac{dv}{dy}$ increases with distance from the bed instead of decreasing as would be expected in a non-aerated flow.

The profiles for Stations 402 and 403 are very similar, suggesting that a uniform flow condition had been reached. However, the progressive increase in velocities for Stations 404 and 405 contradict this suggestion. The reason for the paradox is not apparent from the results, but is possibly due to a breakdown of the assumption that the flow is two dimensional.

The maximum velocity observed on each profile approaches the theoretical maximum calculated from $\sqrt{2gh}$. It is probable that above the point of maximum velocity, a sharp velocity decrease occurs towards the surface due to atmospheric resistance at the highly turbulent flow surface. Such a tendency was noted by K.K. Lai[26] who carried out a model experimental study in 1970. A typical velocity profile from his results is shown in Figure 4.13.

The flow at Stations 401 and 402 for a spillway gate opening of two feet (Figure 4.7) was non-aerated and the velocity profiles have the shape characteristic of this condition. At Station 403 air was present in the flow above a height of about six inches from the spillway face (see Figure 4.6) and a sharp velocity increase is evident in this region. This tendency is evident also in the profiles for Stations 404 and 405.

Figure 4.7 shows also the apparent anomaly evident in Figure 4.5 (1ft opening), - the velocity profiles for Stations 403 and 404 are similar, yet a further velocity increase is evident at Station 405.

For a gate opening of three feet (Figure 4.8), the flow was non-aerated for all stations except for a thin air-water layer at the

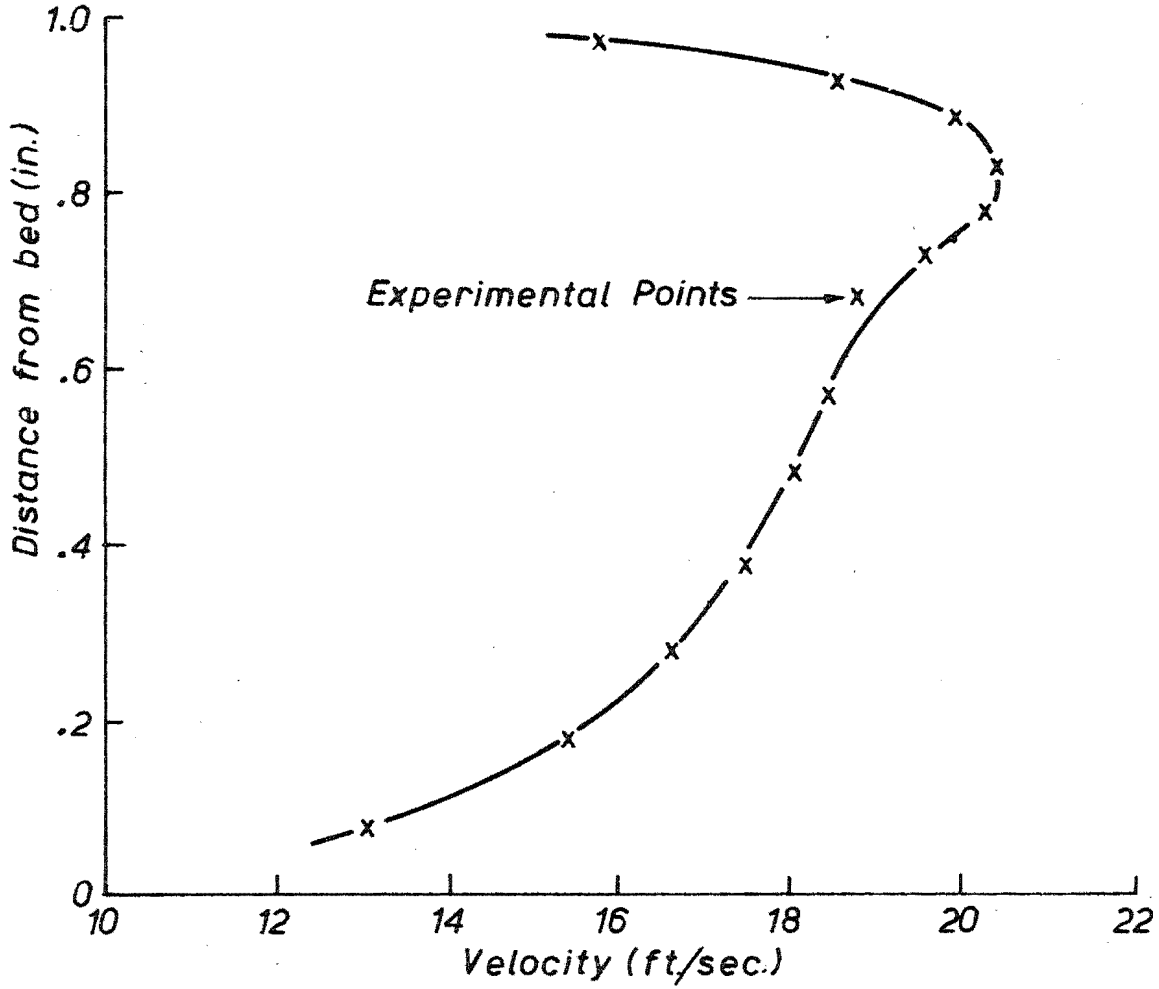

Fig. 4.13 : TYPICAL VELOCITY PROFILE IN AERATED FLOW (after K K Lai[26])

surface at Station 405. The profiles for the other four stations follow the expected shape for non-aerated flows.

The observations described indicate that aeration has the effect of increasing the velocity of the flow. To investigate this effect further, the velocity profiles for all three gate openings were plotted station by station as shown in Figure 4.14. In this way aerated and non-aerated flows at each station could be directly compared.

Figure 4.14 contains only the accurate portions of each velocity profile.

It is notable from Figure 4.14 that, for the lower six inches of the flows, the maximum velocity at each station occurs for a gate opening of one foot. This effect is most marked for Stations 401 and 402 where air is present only for a gate opening of one foot. The effect is masked to some degree at Stations 403, 404, and 405, where air is present also for a gate opening of two foot.

However, if the whole of each profile is considered, it appears unlikely, from the results obtained, that the mean (depth average) velocity of an aerated flow is substantially greater than that for a corresponding non-aerated flow.

4.2 PREDICTION OF THE CRITICAL POINT

In Chapter One, the boundary layer equation

$$\delta = 0.0447\, k_s^{0.154} x^{0.845} \qquad \ldots 1.2$$

deduced from experiments carried out by Bauer[32], was presented. Bauer's experiments were restricted to overflow spillways but the equation may be simply adapted to the case of a gated spillway.

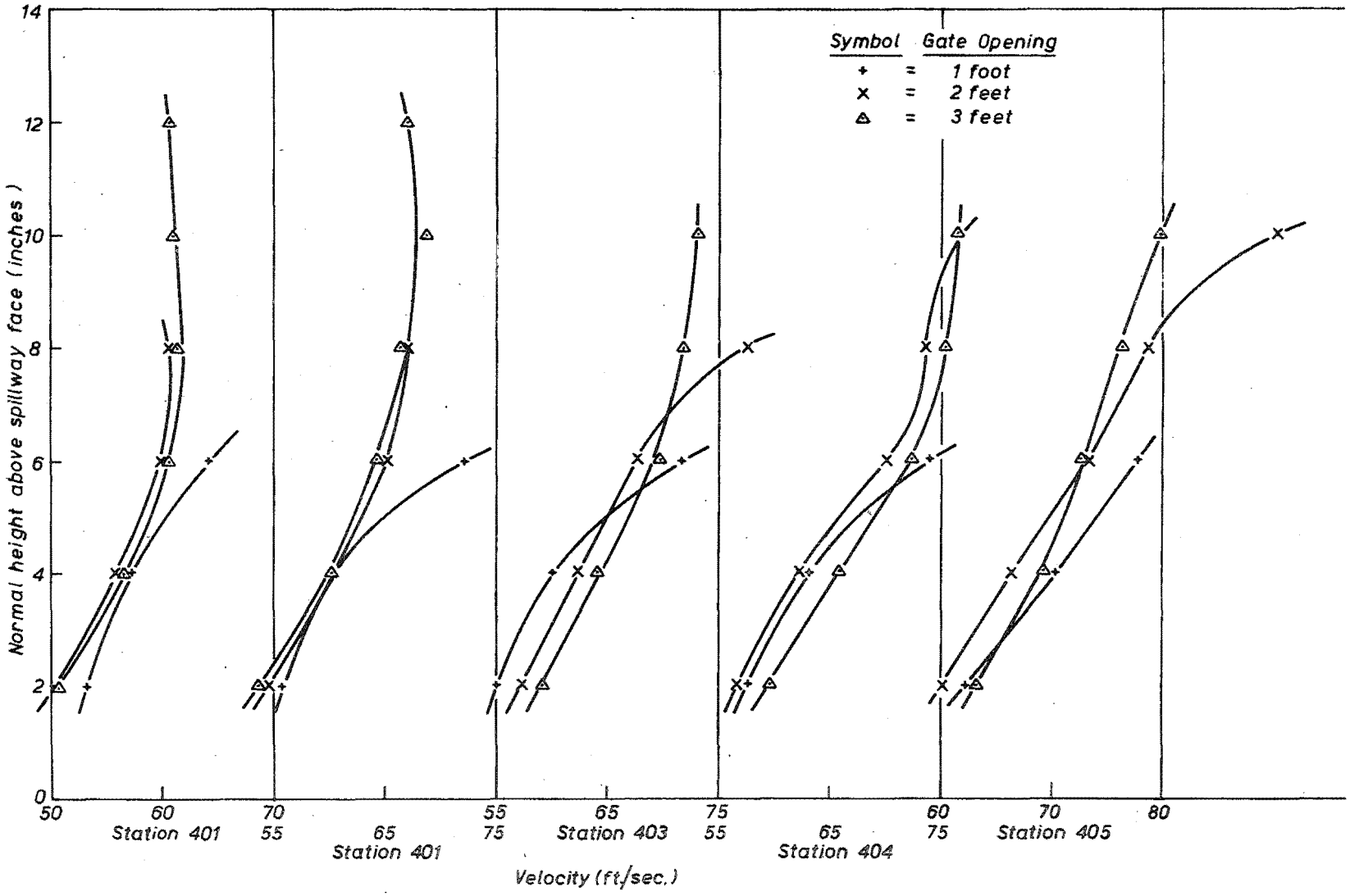

Fig. 4.14 : VELOCITY PROFILES (STATION BY STATION FOR ALL TEST GATE OPENINGS)

Bauer further proposed an approximate but practical method of locating the "critical point", the intersection of the boundary layer and water surface profiles, for a particular discharge. He calculated the flow depth as the sum of the potential flow thickness and the displacement thickness. The potential flow thickness is given by $\frac{q}{U}$ where q is the discharge per unit width and U the free stream velocity computed from the velocity head $\frac{U^2}{2g}$. The displacement thickness is defined as the distance from the boundary that the potential flow has been displaced by the presence of the boundary layer, and, for turbulent flow, where the velocity distribution is assumed to obey a power law [27], can be shown to be approximately ten percent of the boundary layer thickness (see Appendix V). Equation 1.2 is used to plot the boundary layer profile where, for a gate spillway, x is considered as the distance down the slope from the upstream lake level.

The above method was applied to spillway gate openings of one, two, three, and four feet. In the application of Eq. 1.2, the value of the absolute roughness (k_s) of the concrete spillway was assumed to be 0.01 ft. It is unimportant if this value is in even substantial error as a simple differentiation of Eq. 1.2 shows that the value of δ is relatively insensitive to large changes in k_s.

The computed boundary layer and flow profiles are shown in Figure 4.15. The location of the consequently predicted critical points for gate openings of one, two and three feet are superimposed on photographs of the flows in Figure 4.16.

From this figure it is seen that the locations agree well with the observed area on the spillway where white water becomes fairly general.

Superimposed on Figure 4.15 are the observed flow depths at each test station, assessed from photographs of the flow. In most cases the

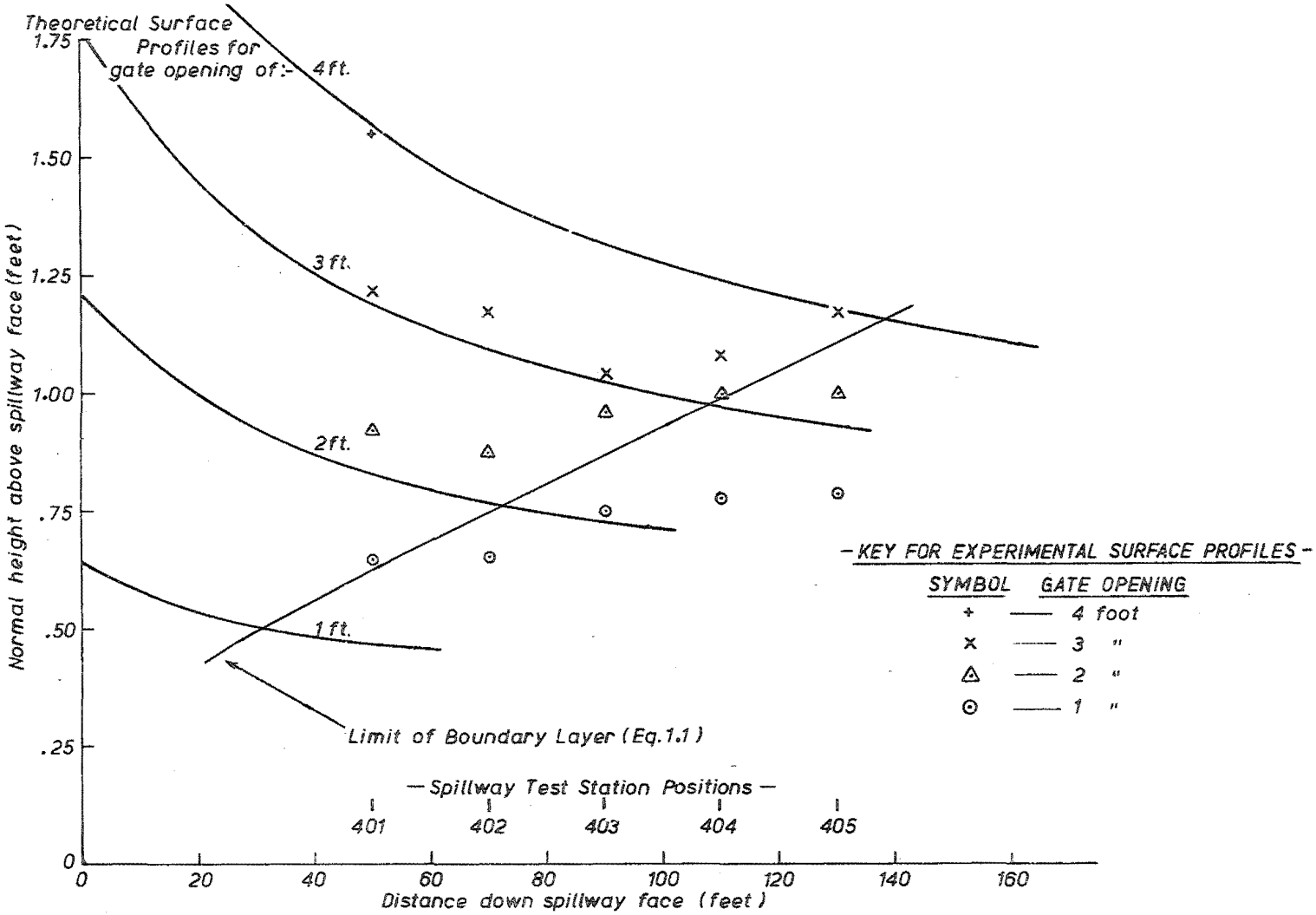

Fig. 4.15 : DETERMINATION OF "CRITICAL POINTS" FOR SPILLWAY GATE OPENINGS OF 1, 2, 3 & 4 foot.

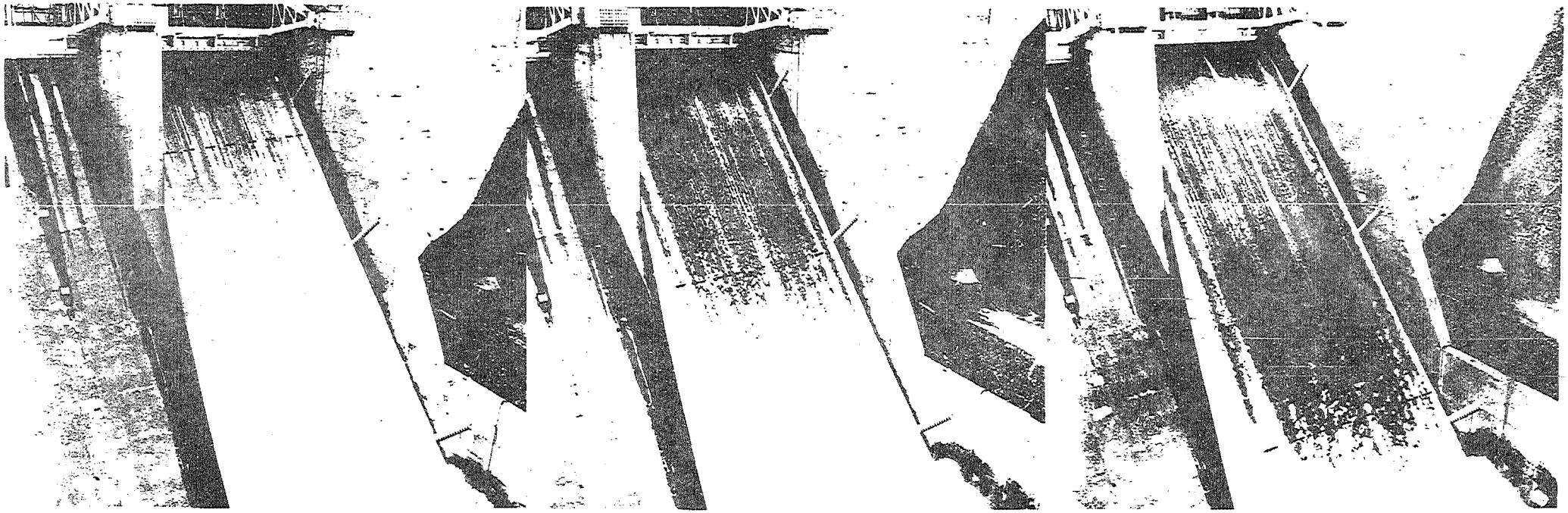

Fig. 4.16 : PREDICTED CRITICAL POINT FOR GATE OPENINGS OF (a) 1 ft., (b) 2 ft., & (c) 3 ft.

observed depth is greater than that predicted. This is thought to be due to the turbulent nature of the flow surface, which results in surface "humps" obscuring the true flow surface at the field test unit.

The photographs also show streaks of surface aeration occurring over the full length of the spillway upstream of the critical point. These are thought to be the result of the shedding of vortices from irregularities on the lip of the gate. The vortices are thought to stretch down the spillway and entrain air when they eventually reach the flow surface.

The observations indicate that Eq. 1.2 is suitable for predicting the occurrence of bottom induced flow aeration. However, Figure 4.17 shows fairly extensive air bulking at the spillway wall due to the growth of the wall boundary layer. Thus, although, for a particular spillway, Eq. 1.2 may predict no bottom induced aeration for the maximum design discharge, this fact alone is not sufficient for spillway design as the governing criterion in setting the wall heights under these circumstances may be the extent of wall-induced aeration.

4.3 TIME FLUCTUATION CURVES

4.3.1 Introduction

Representative time fluctuation curves of air concentration and stagnation pressure are presented in Figures 4.18 to 4.24. The curves were obtained by joining the values of points sampled at consecutive time intervals of $\frac{1}{2}$ second, and were plotted relative to the mean value of the data set containing the points.

The curves presented in this section comprise those obtained for a gate opening of 1 foot at each spillway test station, for a gate opening of 2 foot at Station 403, and for a gate opening of 4 foot at Station 401. The remaining curves obtained are filed at the Civil Engineering Department, University of Canterbury.

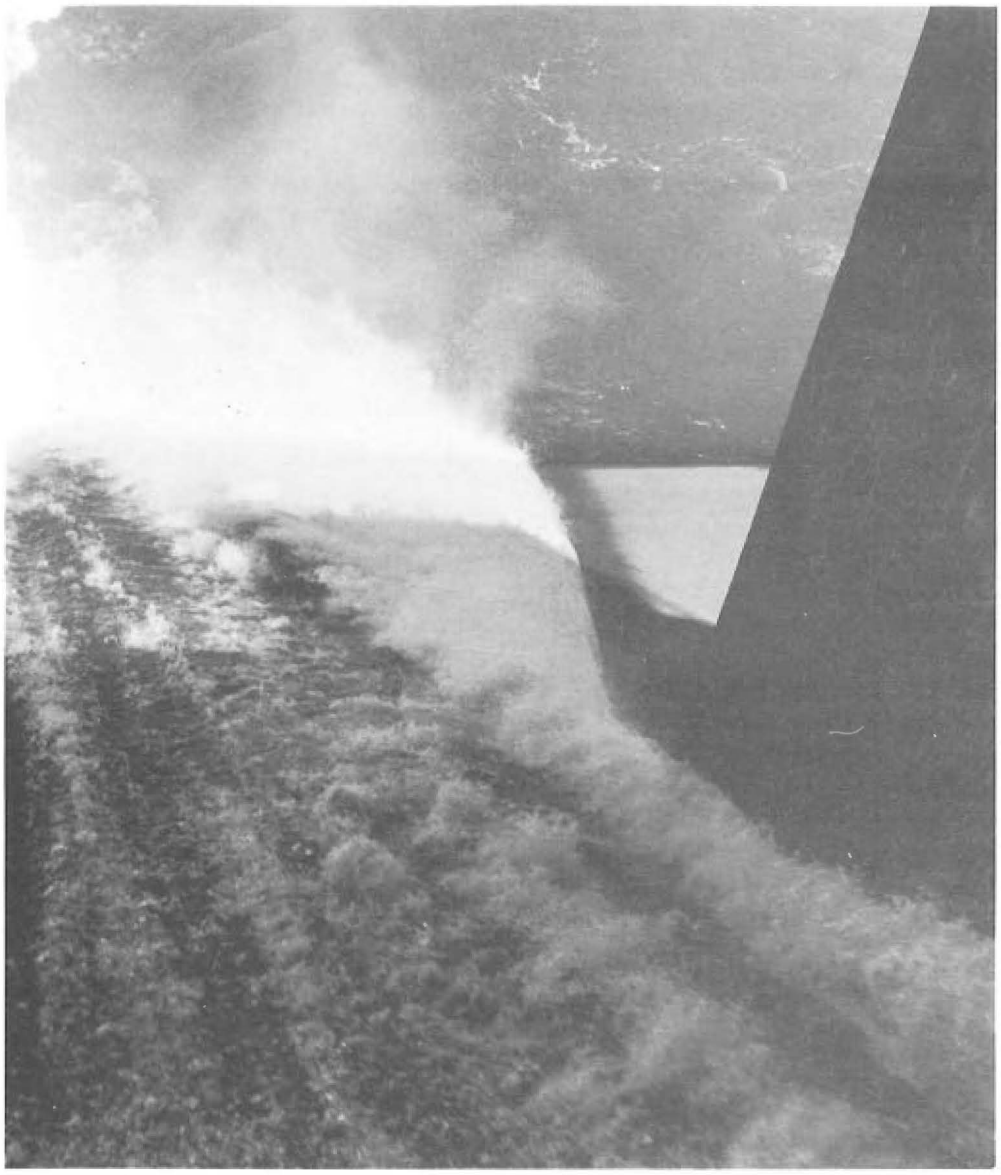

Fig. 4.17 : SIDE WALL INDUCED AIR BULKING.

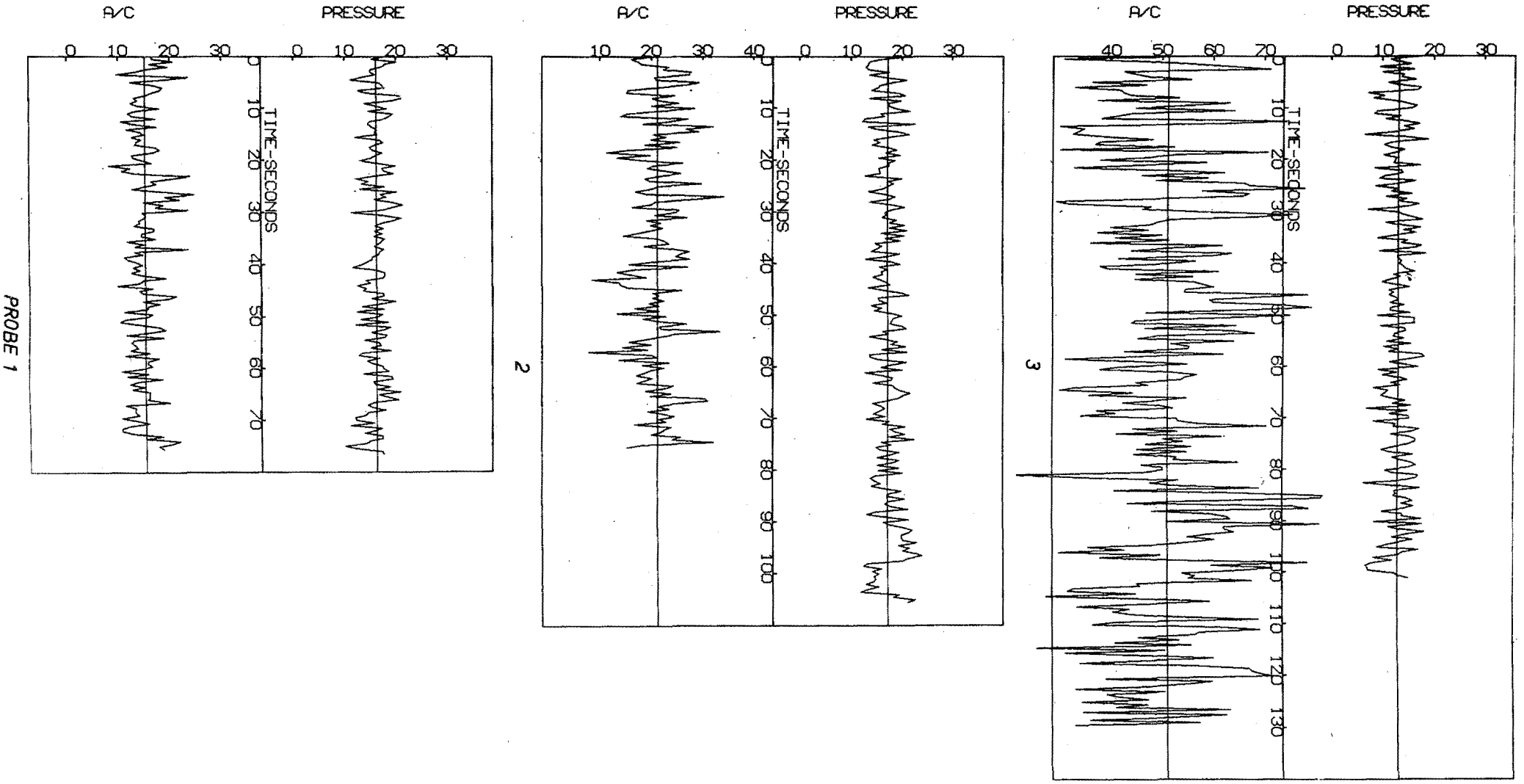

Fig. 4.18 : TIME VARIATION OF AIR CONCENTRATION AND STAGNATION PRESSURE – GATE OPENING 1ft. – STATION 401

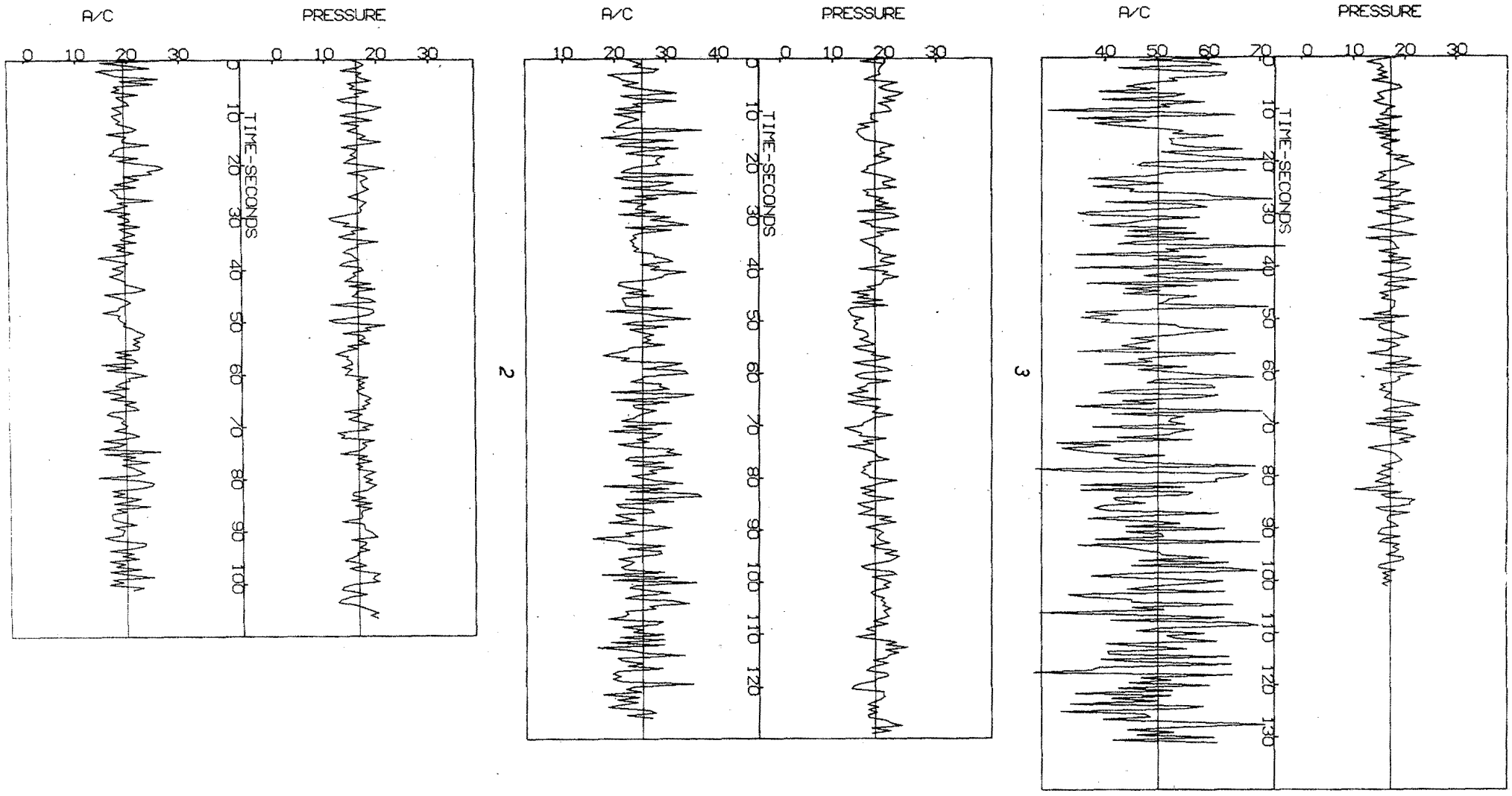

Fig. 4.19 :TIME VARIATION OF AIR CONCENTRATION AND STAGNATION PRESSURE – GATE OPENING 1ft. – STATION 402

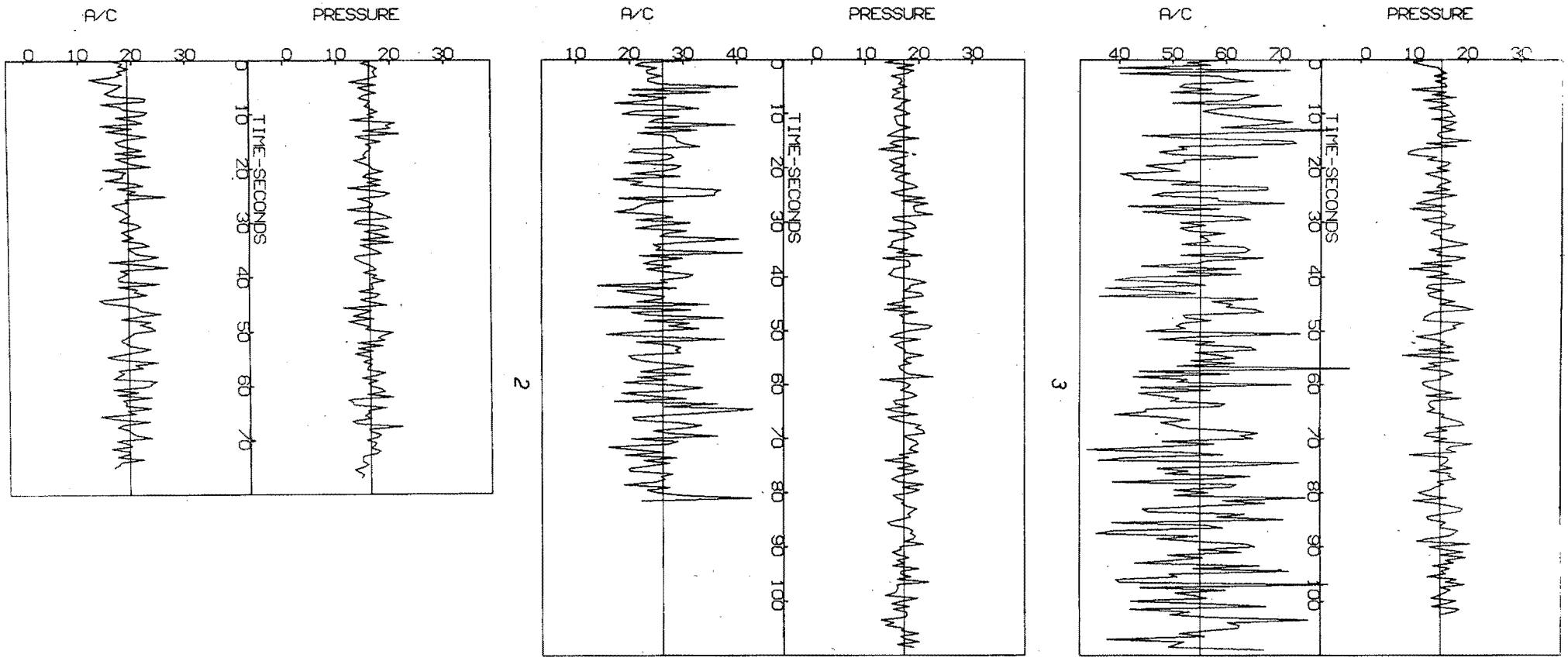

Fig. 4.20 : TIME VARIATION OF AIR CONCENTRATION AND STAGNATION PRESSURE – GATE OPENING 1ft. – STATION 403

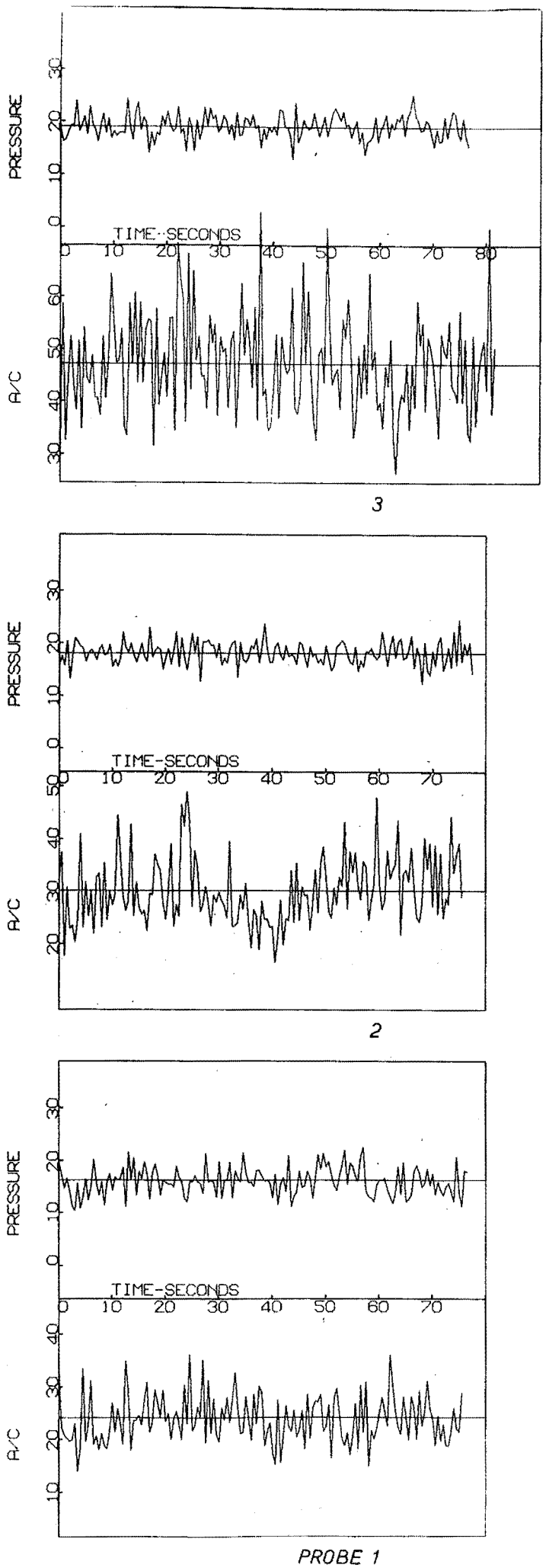

Fig. 4.21 :TIME VARIATION OF AIR CONCENTRATION AND STAGNATION PRESSURE – GATE OPENING 1ft. – STATION 404

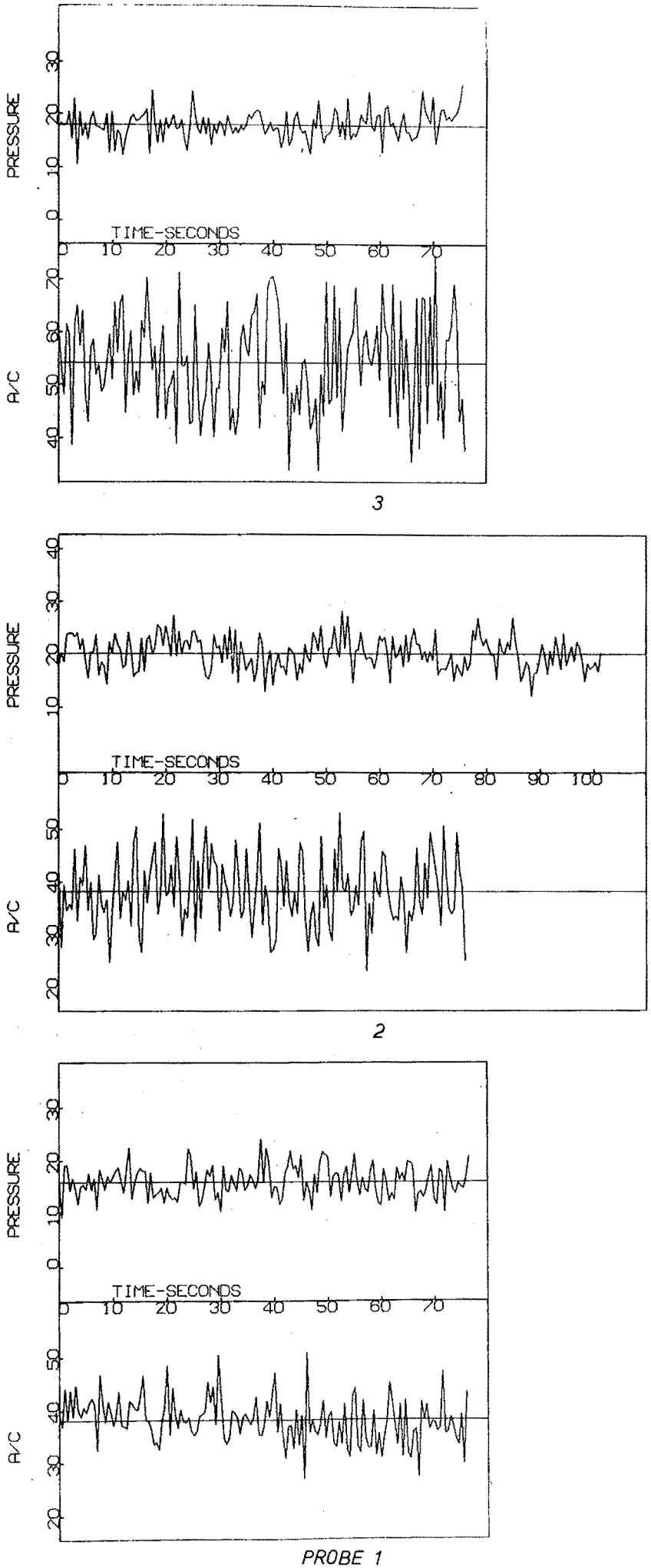

Fig. 4.22 :TIME VARIATION OF AIR CONCENTRATION AND STAGNATION PRESSURE – GATE OPENING 1ft. – STATION 405

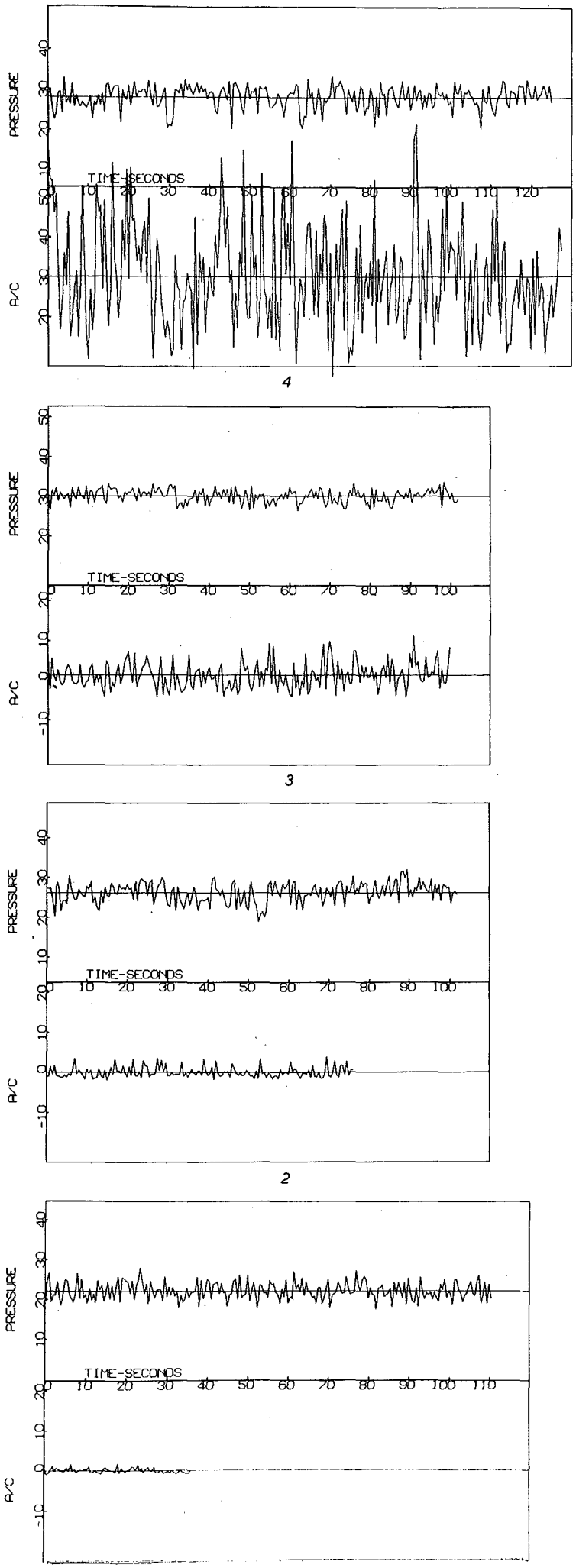

Fig.4.23 :TIME VARIATION OF AIR CONCENTRATION AND STAGNATION PRESSURE – GATE OPENING 2ft.–STATION 403

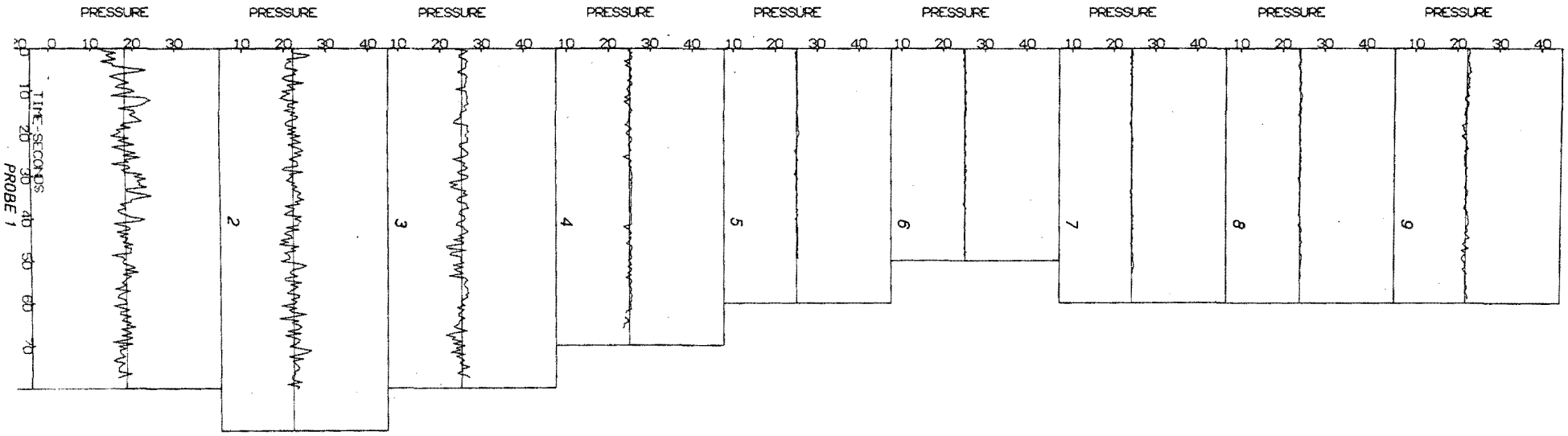

Fig. 4.24 : TIME VARIATION OF STAGNATION PRESSURE – GATE OPENING 4 ft. – STATION 401

A general observation, from the curves, is that the period of the turbulent fluctuations in both the air concentration and the stagnation pressure curves is about $2\frac{1}{2}$ seconds. Thus, the sampling time is about one fifth of the turbulence period - too large to allow any accurate quantitative results to be obtained by (for example) a spectrum analysis of each curve.

Nevertheless, some qualitative and semi-quantitative observations can be made from the curves and these are presented in the following discussions.

4.3.2 Curves for Gate Opening of 1 Foot

Figures 4.18 to 4.22 show the fluctuation curves at each station for a gate opening of 1 foot. At this gate opening air was evident in the flow at all stations and for all probes below the flow surface.

At each station the amplitude of the air concentration fluctuations, at the probe nearest the surface, is very large compared with that for the probes deeper in the flow. This large comparative amplitude is not as noticeable in the pressure fluctuation curves. However, the effect is much less pronounced when the fluctuations are tabulated in a non-dimensional form.

Table 4.5 shows a comparison of the values of $\frac{P'}{\overline{P}}$ and $\frac{C'}{\overline{C}}$ for each probe and at each station. The comparatively small variation in the values from probe to probe indicates that, to some extent, the amplitude of the parameter fluctuation is dependent on the value of the parameter.

The air concentration curves for probe 3 (nearest the surface) at each station apparently show an overlaid wave function, with a period of approximately 60 seconds. This phenomenon is also evident in the air concentration curves for the lower probes at Stations 404

Station	Probe	$\overline{C}$	C'	$\overline{P}$ (psi)	P' (psi)	C'/$\overline{C}$	P'/$\overline{P}$
401	1	.15	.031	16.25	2.32	.207	.143
	2	.22	.046	17.40	2.60	.209	.149
	3	.51	.122	13.52	2.81	.239	.208
402	1	.20	.027	17.00	2.17	.135	.128
	2	.25	.045	18.64	2.51	.180	.135
	3	.50	.101	17.43	2.43	.202	.139
403	1	.19	.028	16.64	2.10	.147	.126
	2	.27	.058	17.90	2.05	.211	.114
	3	.55	.094	15.62	2.66	.171	.170
404	1	.25	.045	16.94	2.62	.180	.155
	2	.30	.064	18.88	2.17	.213	.115
	3	.47	.094	19.50	2.24	.200	.115
405	1	.39	.043	16.03	2.92	.113	.182
	2	.39	.066	20.41	3.08	.169	.151
	3	.54	.092	18.55	2.68	.170	.144

TABLE 4.5: NON-DIMENSIONAL FLUCTUATION VALUES FOR SPILLWAY GATE OPENING 1 FOOT.

and 405. It appears to be primarily a surface phenomenon and is possibly caused by the movement of the stretched vortices mentioned in Section 4.2. Corroboration of this hypothesis must await a comprehensive series of movie photographs.

4.3.3 Curves for Gate Opening of 2 Feet

Figure 4.23 shows the fluctuation curves at Station 403 for a gate opening of two feet. The curves are interesting in that significant aeration is apparent only near the surface. The air concentration curve for the top-most probe shows the same overlaid wave function described in Section 4.3.2.

The air concentration curve for probe 3 shows that some of the readings obtained in the data set were apparently sub-zero. This anomaly is thought to be due to a minor change in the electrical properties of the secondary probe inside the air concentration pier. After testing was completed, it was noticed that a number of air bubbles had adhered to the conducting surfaces of the secondary probe, thereby slightly increasing the electrical resistance across the electrodes. It can be shown (Appendix VI) that such an increase gives rise to a decrease in the subsequently computed value of air concentration. However, it is evident from the fluctuation curve for probe 3, that the value of the error is of the order of 3% - sufficiently low to be neglected.

4.3.4 Curves for Gate Opening of 4 Feet

Figure 4.24 shows the stagnation pressure fluctuation curves at Station 401 for a gate opening of four feet. At this gate opening, the air concentration was zero for all immersed probes.

The curves are notable in that they show the presence of three distinct flow regions. The comparatively large pressure fluctuations

for probes 1, 2, and 3 indicate the presence of a spillway face induced boundary layer. The pressure fluctuations are very much smaller for probes 4 to 8, characteristic of an inviscid flow region. At probe 9, the slight increase in the magnitude of the pressure fluctuations indicates the presence of a surface boundary layer induced by atmospheric drag.

CHAPTER FIVE

MODEL DATA ANALYSIS AND DESIGN PROCEDURE

SYNOPSIS

In this chapter an analysis, of the data obtained by K.K. Lai[26] is presented.

Lai's experimental measurements were carried out in the region of partially aerated developing flow, which enabled a comparison to be made with prototype data obtained on the spillway of the Aviemore Dam.

Using the analysis as a basis, the chapter concludes by proposing a design procedure whereby the full velocity profile, and air concentration profile, within the region of partially-aerated, developing flow, may be derived.

This region is not necessarily the most important because the aerated flow may attain a fully developed state, and, hence, a maximum degree of air bulking, before reaching the foot of the channel. Nevertheless, the analysis represents a first step toward a complete design procedure.

5.1 INTRODUCTION

Lai's data was obtained from experiments conducted in a glass-bottomed flume with smooth perspex side walls to minimise wall boundary effects. The length of the flume was 27 feet and the width 18 inches.

The data consisted of measurements of local air concentrations and velocities for several discharges and slopes.

Velocity was measured with a pitot tube operating on the same principle as Viparelli's[20], described in Section 2.3.1 . Values of air concentration were obtained by using the pitot tube as a sampler, similar in principle to the closed sampler used by Viparelli.

Experiments were carried out using flow discharges of 1.2, 1.7 and 2.2 cusecs on each of the flume gradients 18^{o} and 24^{o}. The data was presented by Lai in the form of profiles of air concentration and velocity, normal to the channel

bed, obtained at five stations along the centre-line of the flume, for each of the six flow conditions.

Apart from an experimental verification of his measuring instruments, Lai's thesis does not include an error analysis of the data obtained. Nevertheless, the fact that the experimental values of air concentration and velocity fit the smoothed experimental curves with only negligible scatter indicates a high degree of accuracy.

The writer did not have access to Lai's original data. The parameters used in the analysis were measured from the small scale profiles presented in Lai's thesis. Great care was taken and it is felt that the errors associated with the parameter values are less than $\pm$ 4 percent.

The essential feature which distinguishes the writer's analysis from Lai's is that the writer considered the aerated region as a separate phenomenon, quite independent of the underlying water layer and the physical conditions upstream of the critical point. The analysis is carried out treating the flow conditions at the critical point as initial conditions and defining all measurements in the flow direction with reference to the critical point as origin.

5.2 DATA ANALYSIS

In Lai's work, the position of the critical point was obtained experimentally by determining where air first became evident in the flow. This position agreed well with the point predicted by Bauers method. (P.133).

The growth of the aerated region downstream of the critical point is, in many ways, analagous to the development of a boundary layer. In the boundary layer, the velocity distribution is self-similar. It is not unreasonable, therefore, to test for self-similarity of the air concentration and velocity profiles in the aerated region.

This hypothesis was tested by plotting the data in a non-dimensional form. Figure 5.1 shows a plot of C against $\frac{y}{y_d}$, where C is the air concentratio at an elevation y above the bottom of the aerated layer, and

y_d is the thickness of the layer. The nominal upper and lower limits

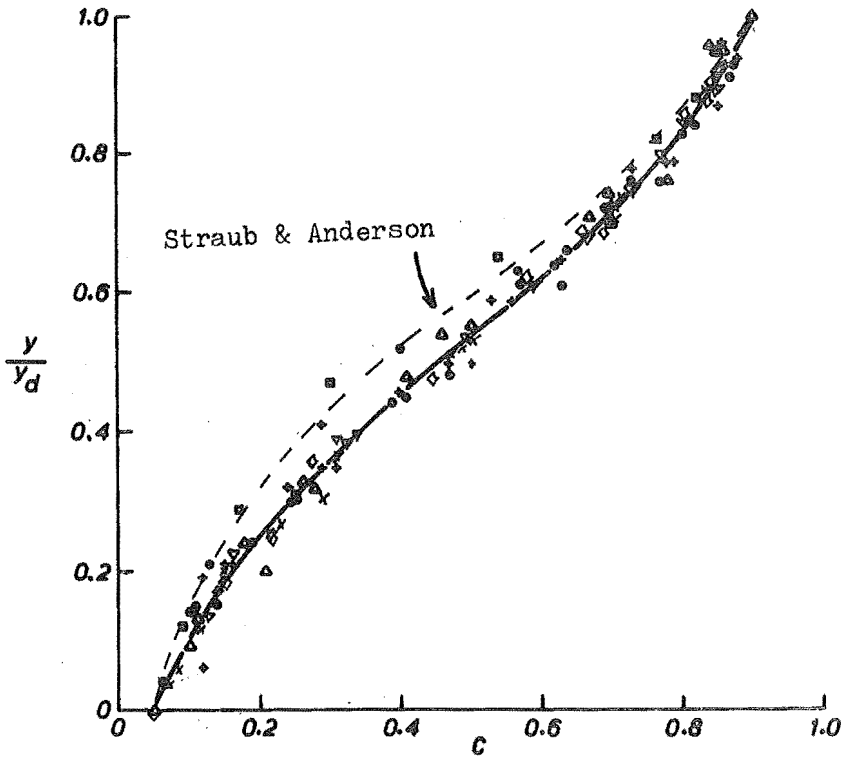

FIG. 5.1: NON-DIMENSIONAL AIR CONCENTRATION PROFILE

DATA KEY

△	α = 18°, q = 0·8 cusecs/ft	LAI
×	" " " " 1·13 " "	LAI
▽	" " " " 1·47 " "	LAI
◇	α = 24°, q = 0·8 cusecs/ft	LAI
○	" " " " 1·13 " "	LAI
+	" " " " 1·47 " "	LAI
•	" " 7·5°, " 4·27 " "	STRAUB & ANDERSON
□	" " 15°, " 6·4 " "	STRAUB & ANDERSON

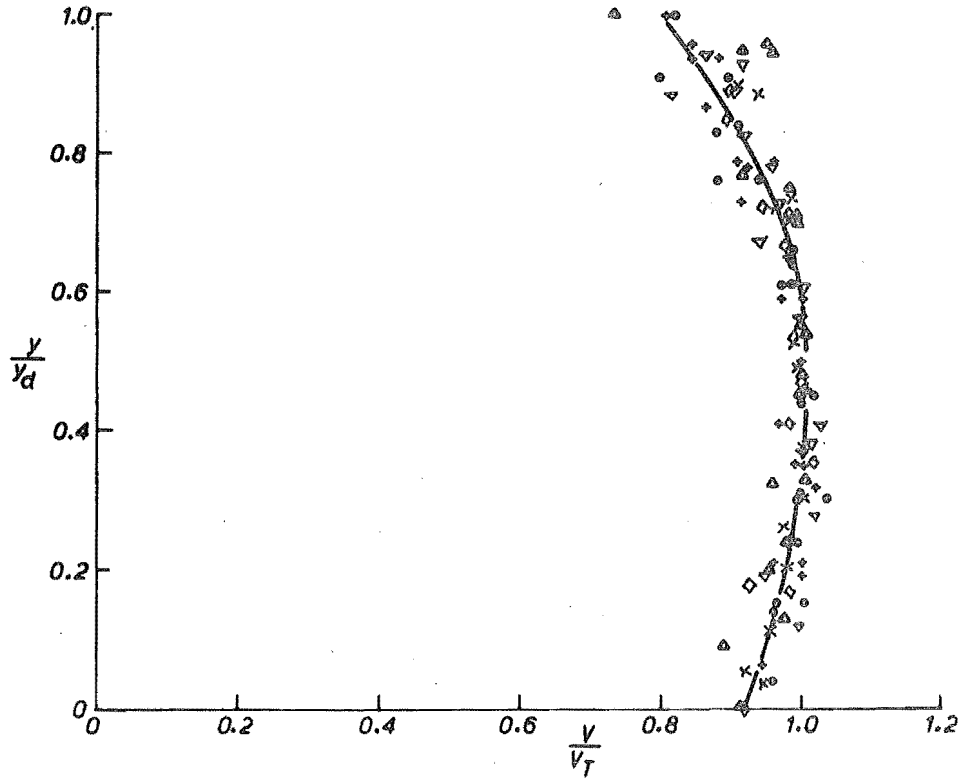

FIG. 5.2: NON-DIMENSIONAL VELOCITY PROFILE

were arbitarily defined as the elevations where $C = 0.90$ and 0.05 respectively. These limits were chosen because they could be reliably measured and because they represented boundaries which contained effectively all the air entrained in the flow.

It can be seen from Figure 5.1 that the air concentration at the transition surface (where the concentration gradient is a maximum[9]) is 50 percent.

Also plotted on Figure 5.1 are representative results from experiments carried out by Straub and Anderson[9] in the fully developed aerated region of flows on slopes below 15°. For such fully developed flows, the air concentrations at the bed and at the transition surface were observed to be of the order of 0.05 and 0.50 respectively. The results plot consistently above the curve of best fit of Lai's data. The reason appears to be concerned with the influence of the channel bed on the aerated flow parameters and is discussed in Section 5.3.

In Figure 5.2, the velocity data is presented in a non-dimensional form. The velocity, V, at an elevation, y, above the bottom of the aerated layer is non-dimensionalized using the velocity at the transition surface, V_T.

The self-similarity of the profiles in Figures 5.1 and 5.2 is indicated by the comparatively small scatter of the data about the curves of best fit.

Figures 5.1 and 5.2 may be used to compute the water discharge within the aerated layer in terms of V_T and y_d. This discharge may be expressed as

$$q_w = \int_{y_d} V\,(1 - C)\,dy$$

or, in terms of a small incremental depth, as

$$q_w = \sum_{y_d} V\,(1 - C)\,\Delta y \qquad \ldots 5.2.1$$

Equation 5.2.1 may be expressed as

$$q_w = V_T\ y_d \sum_{\frac{y}{y_d}} \frac{V}{V_T}\ (1 - C)\ \Delta\left(\frac{y}{y_d}\right) \qquad \ldots 5.2.2$$

The summation in Equation 5.2.2 simply represents the combined integration of the plots of Figures 5.1 and 5.2 and is found to equal 0.519.

$$\text{i.e.} \quad q_w = 0.519\ V_T\ y_d \qquad \ldots 5.2.3$$

Before Equation 5.2.3 can be used as a design equation, it is necessary to be able to predict the values of V_T and y_d for a given position in the channel.

The significant parameters determining the magnitude of V_T can be expressed in a functional relationship as

$$V_T = f(x,\ \nu,\ S,\ g,\ V_I,\ y_I) \qquad \ldots 5.2.4$$

where

- x is distance downstream from critical point
- ν is kinematic viscosity of water
- S is channel slope
- g is gravitational constant.

V_I is the surface velocity (also the transition velocity) at the critical point. (In the calculation of V_I, the effect of the surface boundary layer is neglected i.e. $V_I = \sqrt{2g\ S\ x_{cr}}$ where x_{cr} is the distance along the spillway from the total energy line to the critical point.)

y_I is the depth at the critical point (V_I and y_I represent the initial conditions.)

Dimensionless combinations of these variables can be formed to give

$$\frac{V_T}{V_I} = \phi\left(\frac{V_I x}{\nu},\ S,\ \frac{V_I}{\sqrt{g\ S\ y_I}},\ \frac{V_I y_I}{\nu}\right) \qquad \ldots 5.2.5$$

The first parameter represents a Reynolds number, R_x.

The third parameter represents a Froude number. It's value, computed

for all model and prototype data, was found to vary only slightly compared with the other parameters in Equation 5.2.5. The Froude numbers are tabulated in Table 5.1.

The reason for this becomes apparent upon examination of Halbronn's equations (obtained from Bauers data), Equations 1.2 and 1.3

$$\delta = 0.0447\ k_s^{0.154}\ x^{0.846} \qquad \ldots 1.2$$

$$\delta = \frac{0.0104}{0.0485}\ x^{0.8515} \qquad \ldots 1.3$$

Noting that, at the critical point, y_I may be substituted for and $V_I^2 = 2\,g\,S\,x_{cr}$ (Figure 1.3), Equation 1.2 may be written as

$$y_I = 0.0447\ k_s^{0.154}\ \left(\frac{V_I^2}{2gS}\right)^{0.846} \qquad \ldots 5.2.6$$

or

$$\frac{V_I}{\sqrt{gSy_I}} = F_r = 8.9\ \left(\frac{y_I}{k_s}\right)^{0.091} \qquad \ldots 5.2.7$$

It is evident from Equation 5.2.7 that the value of the Froude number on a rough bed is relatively insensitive to even very large variations in the value of $\frac{y_I}{k_s}$.

The same substitution in Equation 1.3 yields

$$\frac{V_I}{\sqrt{gSy_I}} = F_r = 20.5\ S^{.0285}\ y_I^{.087} \qquad \ldots 5.2.8$$

Equation 5.2.8 shows that F_r is relatively insensitive to variations in S and y_I.

For the same value of Froude number on a smooth and rough slope

$$20.5\ S^{.0285}\ y_{IS}^{.087} = \frac{8.9}{k_s^{.091}}\ y_{IR}^{.091} \qquad \ldots 5.2.9$$

Slope	Discharge (cusecs)	y_I (ft.)	V_I (ft/sec)	F_r
	Lai (smooth model)			
18°	1.2	.0685	13.0	15.8
	1.7	.0855	14.9	16.2
	2.2	.0990	16.2	16.3
24°	1.2	.0620	14.3	15.9
	1.7	.0770	16.3	16.2
	2.2	.0917	18.0	16.4
	Keller (rough prototype)			
45°	2585	.75	68.0	16.4

TABLE 5.1: COMPARISON OF INCEPTION FROUDE NUMBERS.

where

subscripts S and R refer to smooth and rough respectively.

For all practical flow cases, $S^{.0285}$ and $\left(\frac{y_{IR}}{y_{IS}}\right)^{.09}$ are approximately unity.

$$\text{i.e.} \quad 20.5 = \frac{8.9}{k_s^{.091}}$$

or $k_s = .0001$ ft , which represents the roughness height on a slope giving the same Froude number as on a smooth slope.

Equation 5.2.9 shows further, that for $0.0001 < k_s < .01$, which covers most practical rough surfaces, the ratio of Froude numbers on a rough and smooth slope lies in the range

$$1 > \frac{F_{rR}}{F_{rs}} > 0.66$$

The aerated flow region is highly turbulent and unlikely to pose stability problems. This means that a small change in the magnitude of the Froude number is unlikely to have a large effect on the aerated flow.

It has been shown that the Froude number varies only slightly for vastly different flow properties in both rough and smooth channels, and it is reasonable, therefore, to neglect it.

The fourth parameter in Equation 5.2.5 is a dimensionless expression for the total water discharge per unit width, q .

In general, therefore, the ratio $\frac{V_T}{V_I}$ may be expressed as a function of the Reynolds number, the channel gradient, and the discharge.

$$\text{i.e.} \quad \frac{V_T}{V_I} = \phi \left(R_x , S , \frac{q}{\nu}\right) \qquad \ldots 5.2.10$$

The significant parameters determining the magnitude of y_d can be expressed in a functional relationship as

$$y_d = f(x , \nu , S, g , V_I , y_I) \qquad ...5.2.11$$

Using the same argument as above, the ratio $\frac{y_d}{y_I}$ may be expressed also as a function of the Reynolds number, the channel gradient, and the flow discharge per unit width.

$$\text{i.e.} \quad \frac{y_d}{y_I} = \phi (R_x , S , \frac{q}{\nu}) \qquad ...5.2.12$$

Equations 5.2.10 and 5.2.12 furnish a basis for plotting Lai's data.

In Figure 5.3 , the values of $\frac{V_T}{V_I}$ are plotted against the Reynolds number, R_x . The data for both slopes and all discharges plot about a single curve of best fit.

Figure 5.4 shows the values of the parameter $\frac{y_d}{y_I}$ plotted against Reynolds number. On inspection it can be seen that points corresponding to the same slope but different discharges fall along the same line, within the limits of experimental scatter. A curve of best fit for all the data was obtained empirically by plotting $\frac{y_d}{y_I\sqrt{S}}$ against Reynolds number (Figure 5.5)

The negligible role of the discharge, apparent from the graphs in Figures 5.3 and 5.5 , may be explained by an examination of the discharge parameter, $\frac{V_I\, y_I}{\nu}$, in Equations 5.2.10 and 5.2.12 .

Equations 5.2.7 and 5.2.8 show that the value of the Froude number is approximately constant for both smooth and rough channels, i.e.

$$V_I \propto \sqrt{y_I\, S}$$

Thus, for a constant slope and water viscosity, the discharge parameter is proportional to $y_I^{\frac{3}{2}}$.

Expressed in this form, the parameter represents the influence of the flow depth on the aerated layer. The resistance at the channel bed is transferred to the aerated layer by turbulent shear, which can exist only if there is a vertical velocity gradient.

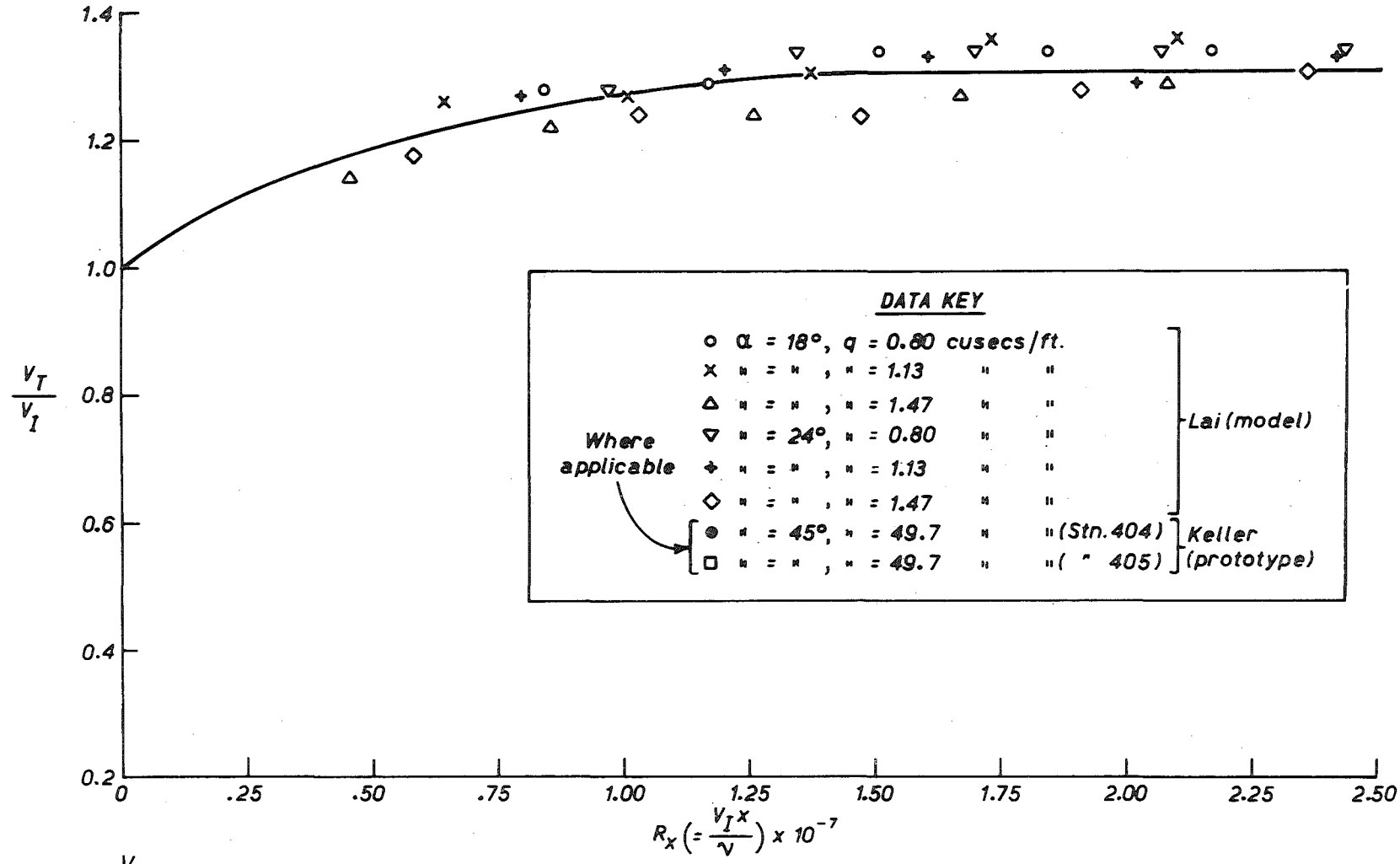

FIG. 5.3: $\frac{V_T}{V_I}$ AS FUNCTION OF REYNOLDS Nº

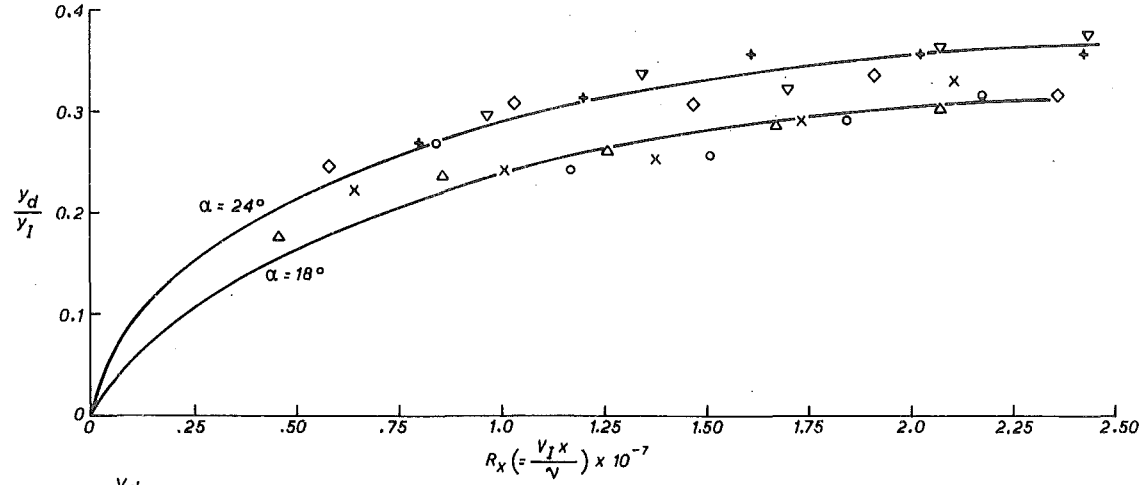

FIG.5.4: $\frac{y_d}{y_I}$ AS FUNCTION OF REYNOLDS Nº

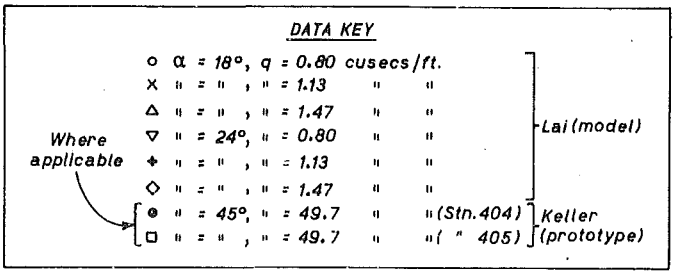

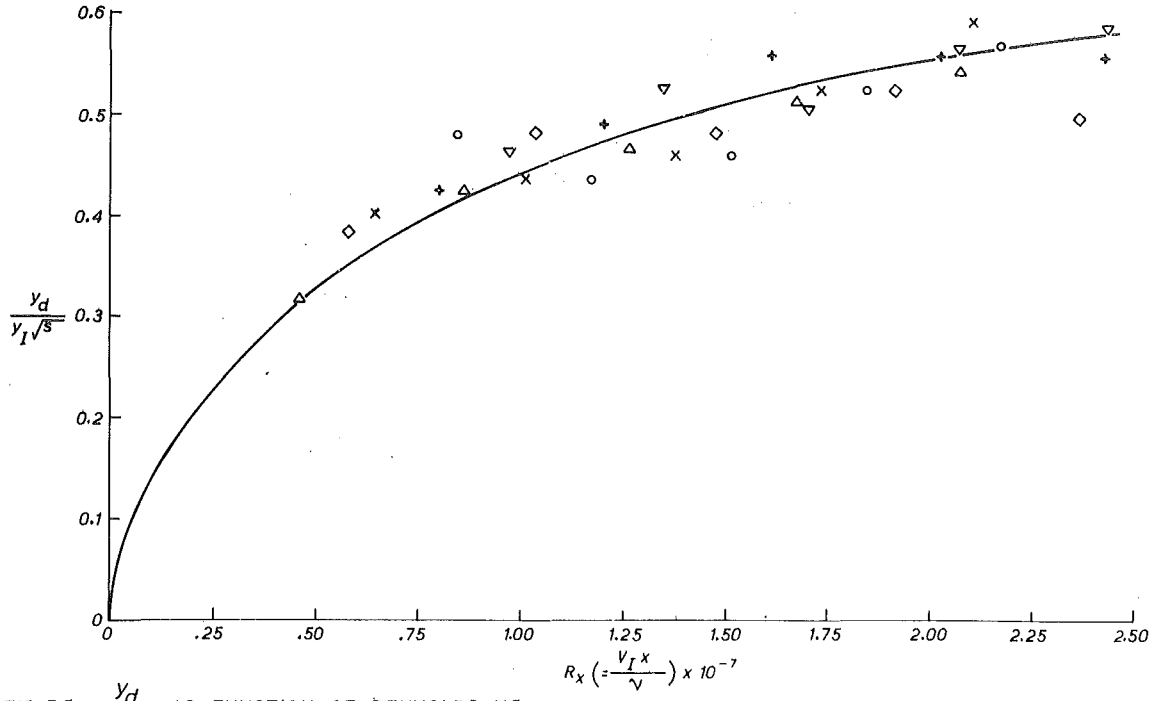

FIG.5.5: $\frac{y_d}{y_I\sqrt{s}}$ AS FUNCTION OF REYNOLDS Nº

If the velocity distribution was constant over the flow depth; y_I , and hence the discharge, would have no influence on the properties of the aerated layer.

For a logarithmic velocity distribution, the velocity variation over a considerable depth from the surface is small compared to that near the channel bed. It follows that the aerated layer must penetrate close to the channel bed before the diffusion of the air bubbles is appreciably affected by the velocity gradient.

The velocity profiles obtained by Lai for a discharge of 1.7 cusecs and a slope of 24 degrees, typical of all his profiles, are plotted in Figure 5.6 . The bottom of the aerated layer is marked on each profile.

It is apparent that the aerated region never constitutes more than half the total flow depth. Furthermore, the velocity gradient at the interface between the water and air-water layers is small compared with that near the channel bed.

It follows that, for the range of Lai's data, the influence of the channel bed, and, hence, of the discharge, is comparatively small.

5.3 COMPARISON WITH PROTOTYPE DATA AND DISCUSSION

Prototype data in the partially aerated, developing region was obtained at Aviemore for a spillway gate opening of 2 feet. The air concentration and velocity profiles are presented on pages 113 and 114 respectively.

The position of the critical point was calculated using Bauers method (P.133) Profiles obtained at Stations 403, 404, and 405 were within the partially aerated region. Information from the profiles obtained at Station 403 was inconclusive due to the comparative thinness, relative to the instrument spacing and size, of the aerated layer at this point. Consequently, results from the other two stations only are presented.

Reynolds numbers on the prototype spillway were of the order of ten times

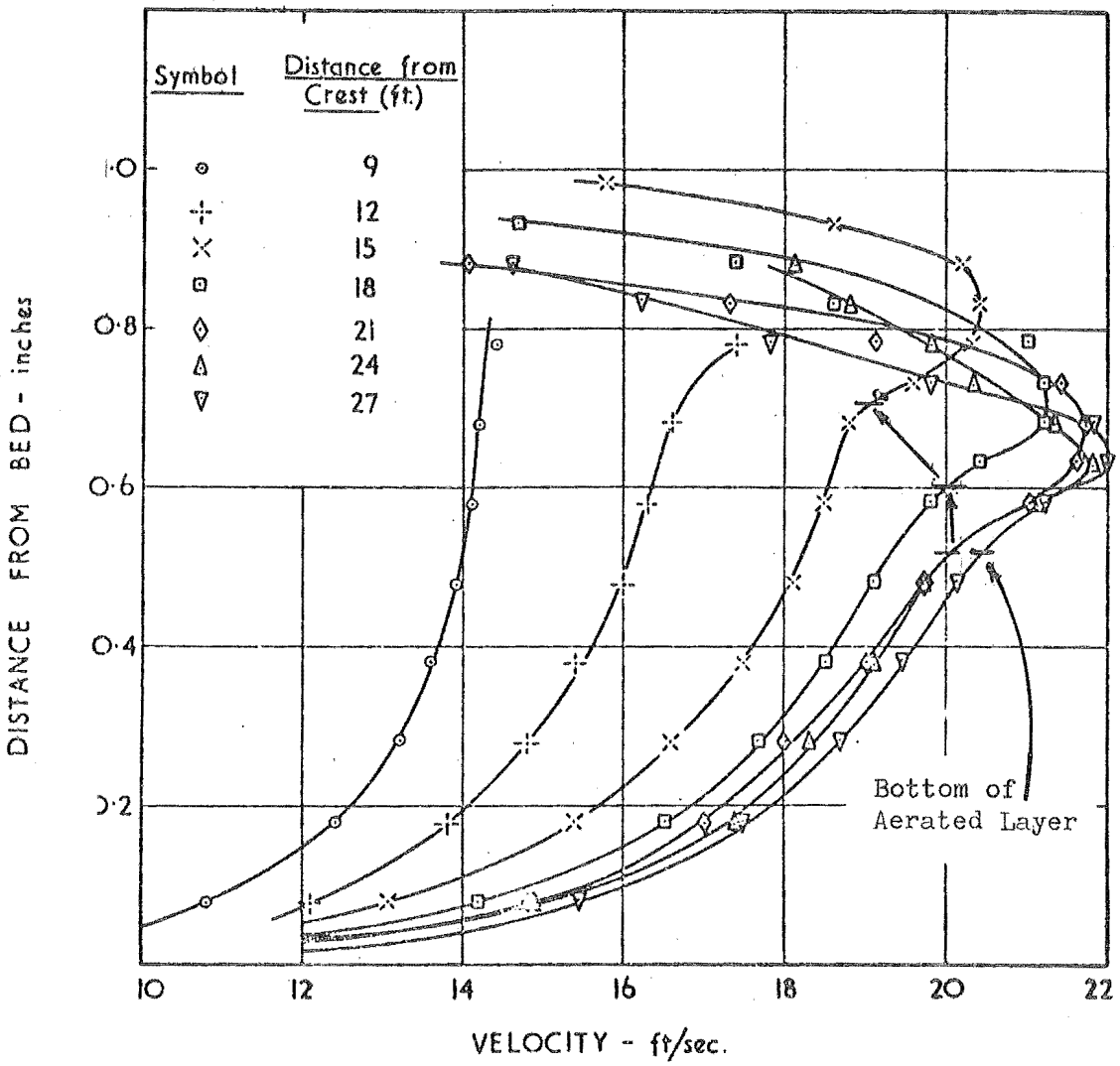

FIG. 5.6: MODEL VELOCITY PROFILES FOR SLOPE 24°, DISCHARGE 1.70 cfs.

those in Lai's model so a data comparison involves extrapolating the curves of Figures 5.3 and 5.5 . Accordingly, these curves are reproduced, using a log scale for Reynolds number, in Figures 5.7 and 5.8 with prototype data from Stations 404 and 405 superimposed. The poor vertical resolution of the profiles on pages 113 and 114 necessitated the adoption of rather coarse accuracy limits (± 8%) shown in Figures 5.7 and 5.8 .

The curve of best fit in Figure 5.7 indicates that the ratio $\frac{V_T}{V_I}$ becomes constant beyond a Reynolds number of about 2×10^7 . However, the flow beyond this Reynolds number cannot be uniform because Figure 5.8 indicates that the thickness of the aerated layer is still increasing.

This kind of flow phenomenon, where the characteristic velocity is constant while the characteristic length changes, has its counterparts in other fluid flow situations. For example, when two parallel streams, flowing at different velocities, are suddenly brought together, the velocity at the interface remains constant while the mutually induced shear results in a thickening diffusion zone with distance downstream[28].

The data in Figure 5.8 falls on a straight line which has the equation

$$\frac{y_d}{y_I \sqrt{S}} = 0.275 \log_{10} R_x - 1.47 \qquad \ldots 5.3.1$$

Apparently, it should now be possible to use Figures 5.7 and 5.8 to predict the point where the aerated region reaches the channel bed, i.e. where q_w is equal to q (the total water discharge/unit width.)

Now,

$$\frac{q_w}{q \sqrt{S}} = \frac{0.519 \, V_T y_d}{0.9 \, V_I y_I \, S} \qquad \ldots 5.3.2$$

(The factor 0.9 is introduced in Equation 5.3.2 because the depth at the critical point is the theoretical depth $(\frac{q}{V_I})$ plus the boundary layer

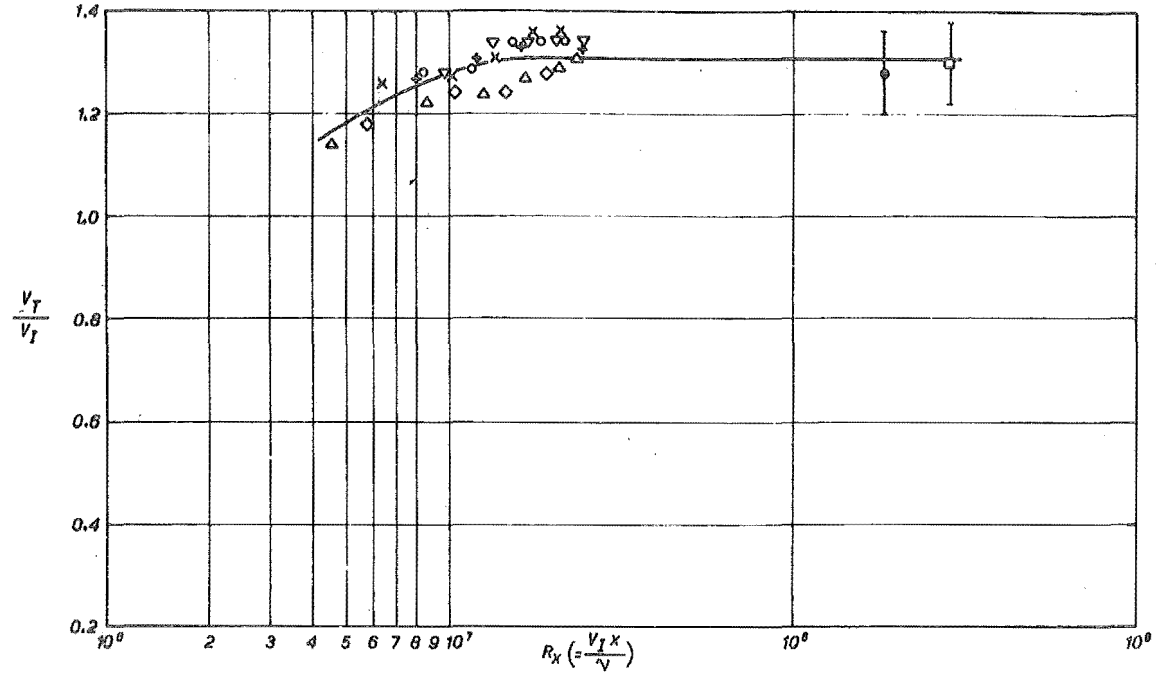

FIG 5.7: $\frac{V_T}{V_I}$ AS FUNCTION OF REYNOLDS Nº

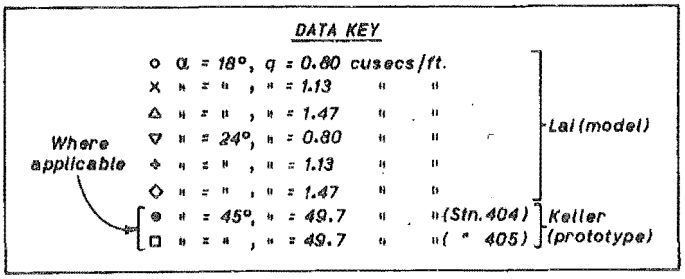

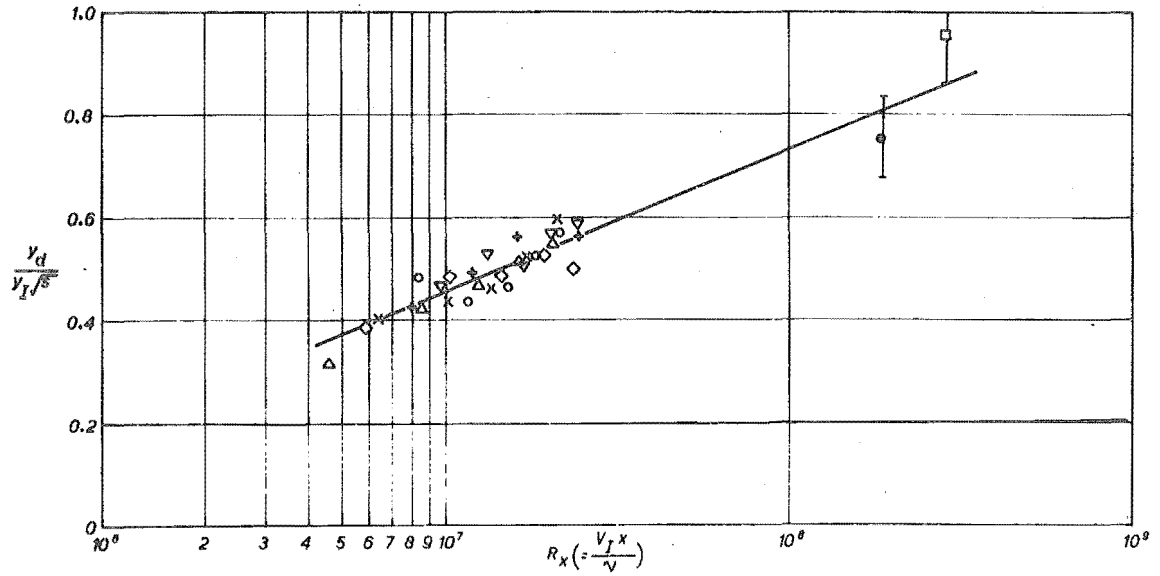

FIG 5.8: $\frac{y_d}{y_I\sqrt{s}}$ AS FUNCTION OF REYNOLDS Nº

displacement thickness ($0.1\ y_I$ - see Appendix V)).

$$\text{i.e.} \quad \frac{q_w}{q\sqrt{S}} = 0.576\ \frac{V_T}{V_I} \cdot \frac{y_d}{Y_I\ S} \qquad \ldots 5.3.3$$

However, the use of Figures 5.7 and 5.8 and Equation 5.3.3 to determine where the aerated layer reaches the channel bed is invalid. The reason for this may be explained by the argument on P 157 concerning the influence of the channel bed. The experimental points plotted in Figures 5.7 and 5.8 were obtained for flows where this influence was negligible. It is invalid to extrapolate the graphs without taking account of the increasing effect of the channel bed as the aerated layer penetrates deeper into the flow.

The experimental results of Straub and Anderson, plotted in Figure 5.1 , were obtained for flows where the aerated layer had penetrated to the channel bed. The consistent deviation from the curve of best fit through Lai's data appears to be due to the relative importance of the influence of the channel bed on the two sets of results.

This influence is probably manifested in the different distributions of the air-bubble mixing parameter, ε_b , for the two cases. Straub and Anderson assumed a parabolic distribution with values of zero at the transition surface and the bed (the lower limit of the air-water mixture). The assumption is not valid for Lai's profiles where the lower boundary of the air-water mixture is a moving water interface.

Before Figures 5.7 and 5.8 may be used for design purposes, it is necessary to know the general form of the velocity profiles in the water region underlying the aerated layer.

In Figures 5.9 and 5.10 representative velocity profiles for both model and prototype are plotted semi-logarithmically. The straight-line character in the water region indicates a semi-logarithmic distribution law,

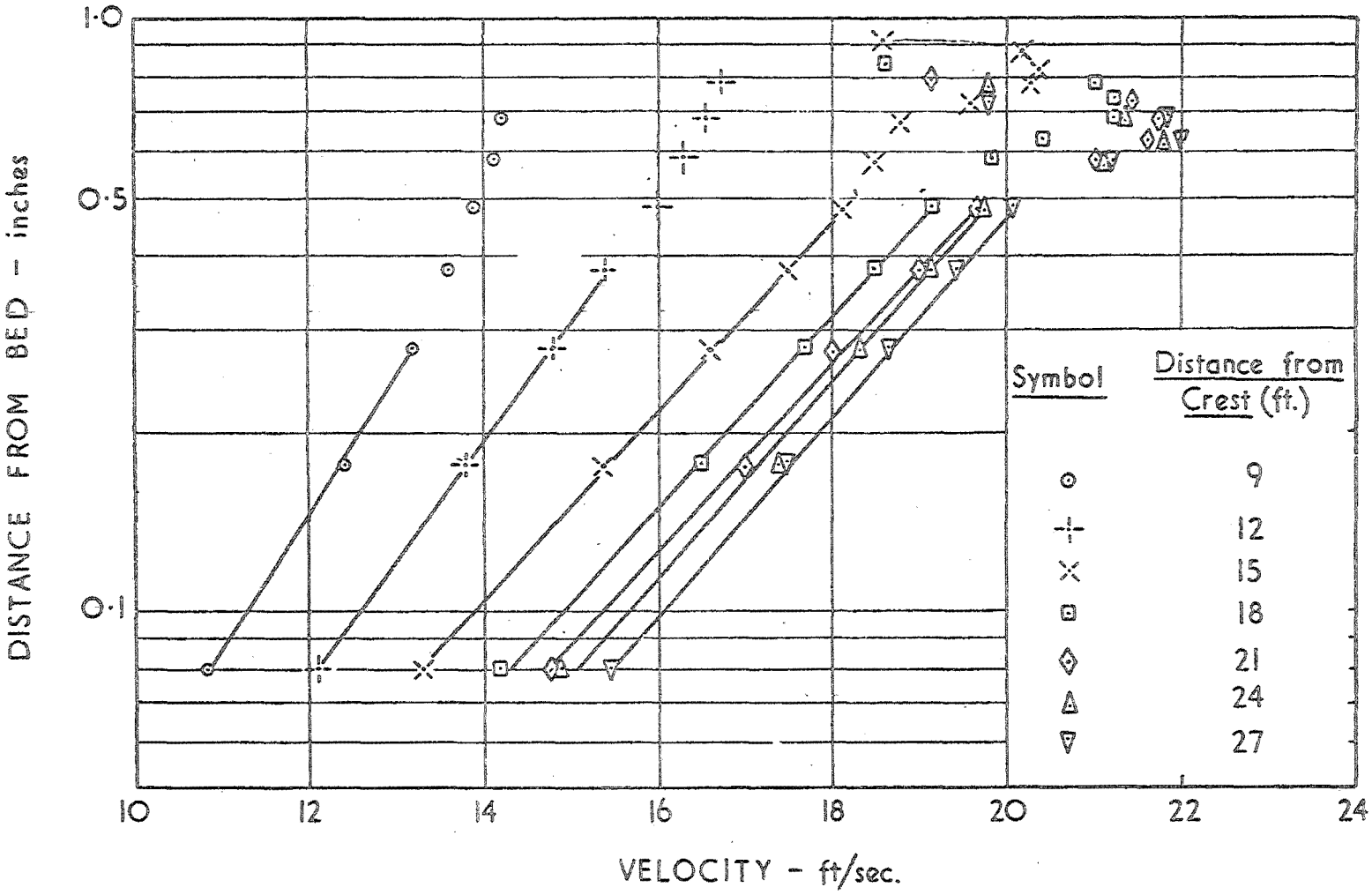

FIG. 5.9: VELOCITY PROFILES (SEMI-LOG PLOT) - LAI

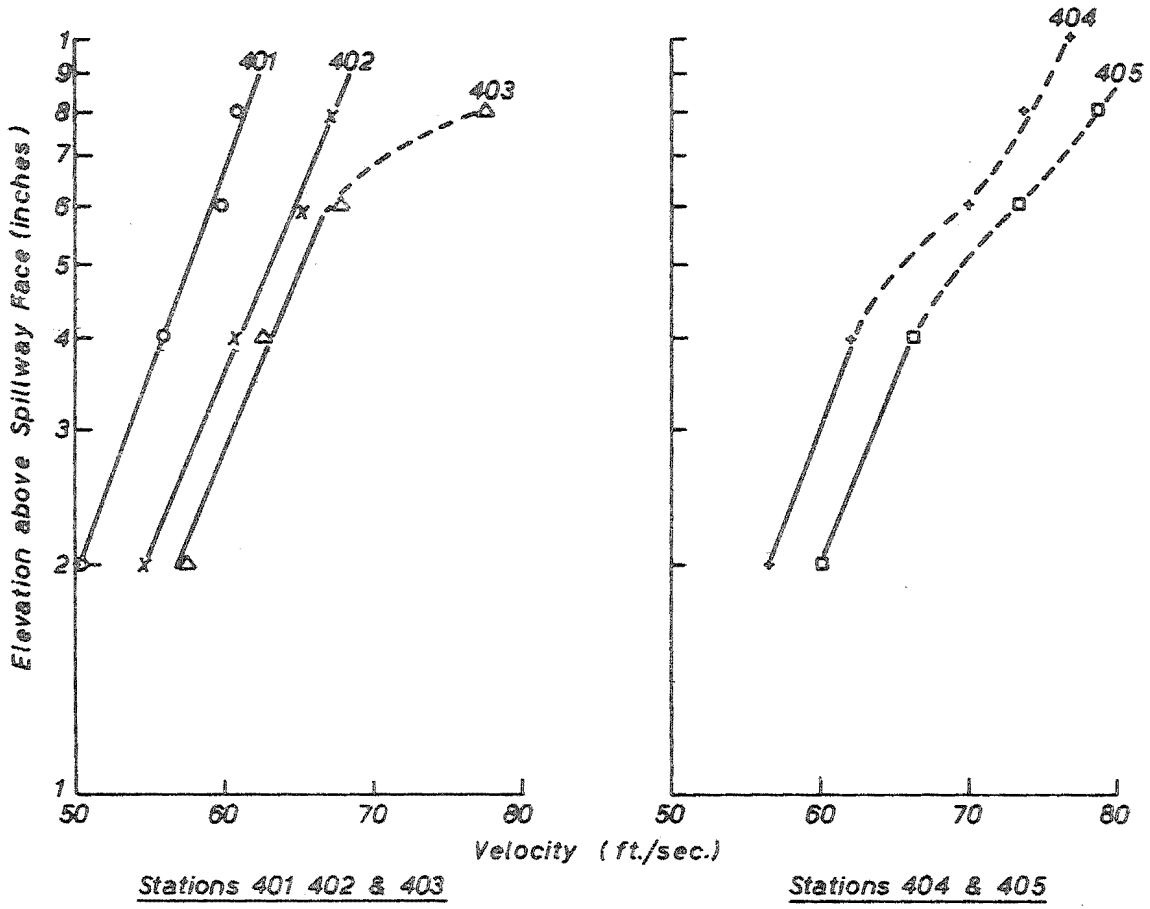

FIG.5.10: VERIFICATION OF SEMI-LOG FORM OF VELOCITY PROFILE IN NON-AERATED REGION OF FLOW (Aviemore Dam Gate opening 2ft.)

which may be expressed as[34]

$$v = 2.5\ V_s \log_e \frac{9V_s y}{\nu} \qquad \ldots 5.3.4$$

where V_s is the shear velocity.

5.4 DESIGN PROCEDURE

On the basis of the data analysis of Sections 5.2 and 5.3, a design procedure, for determining the complete velocity and air concentration profiles within the partially-aerated developing region, may be formalised.

The assumption is made that the non-dimensional profiles in Figures 5.1 and 5.2 are applicable to full-scale aerated flows. This assumption allows the use of Equation 5.2.3 to compute the water discharge in the aerated layer.

The procedure is valid only in that part of the region where the thickness of the aerated layer constitutes less than two thirds of the total flow depth.

This procedure follows:

1) Compute the position of the critical point (from Bauers method P. 133) and the inception properties V_I and y_I.
2) Compute the Reynolds number ($R_x = \frac{V_I x}{\nu}$)
3) Obtain the values of V_T and y_d from Figures 5.7 and 5.8 .
4) Compute the water discharge within the aerated layer from Equation 5.2.3 .

$$q_w = 0.519\ V_T\ y_d \qquad \ldots 5.2.3.$$

5) Use Equation 5.3.4 and the continuity principle to compute the elevation of the bottom of the aerated layer, $y_{0.05}$, and the shear velocity, V_s .

$$v = 2.5\ V_s \log_e \frac{9V_s y}{\nu} \qquad \ldots 5.3.4$$

or

$$v_{0.05} = 2.5\ V_s \log_e \frac{9V_s\ y_{0.05}}{\nu} \qquad \ldots 5.4.1$$

where

$V_{0.05}$ is the velocity at the bottom of the aerated layer, and may be determined from Figure 5.2 .

By continuity

$$q = q_w + \int_{y_{0.05}} v \, dy \qquad \ldots 5.4.2$$

Substitution of Equation 5.3.4 into Equation 5.4.2 yields

$$q = q_w + \int_{y_{0.05}} 2.5 \, V_s \log_e \frac{9 V_s \, y}{\nu} \, dy \qquad \ldots 5.4.3$$

Equations 5.4.1 and 5.4.3 yield two relationships between $y_{0.05}$ and V_s, allowing the evaluation of both parameters.

6) The air concentration and velocity profiles may now be plotted.

The origin of the air concentration profile is given by the value of $y_{0.05}$. The profile is plotted using Figure 5.1 with the value of y_d predicted from Figure 5.8 .

The velocity profile is plotted using Equation 5.3.4 for the underlying water layer, and Figure 5.2 for the aerated layer.

This procedure was used to confirm Lai's experimental profiles and those obtained on the Aviemore spillway. A typical comparison for Lai's data is shown in Figure 5.11 . Typical prototype comparisons are shown in Figures 5.12 and 5.13 .

Figure 5.11 shows that the experimental velocity profile deviates from a logarithmic distribution at a lower elevation than is indicated by the predicted profile. This is thought to be due to the influence of the air in the flow below the arbitrarily defined lower limit of the aerated layer.

The close comparison evident in Figure 5.11 is to be expected because the graphs used to predict the velocity profile were obtained from Lai's data.

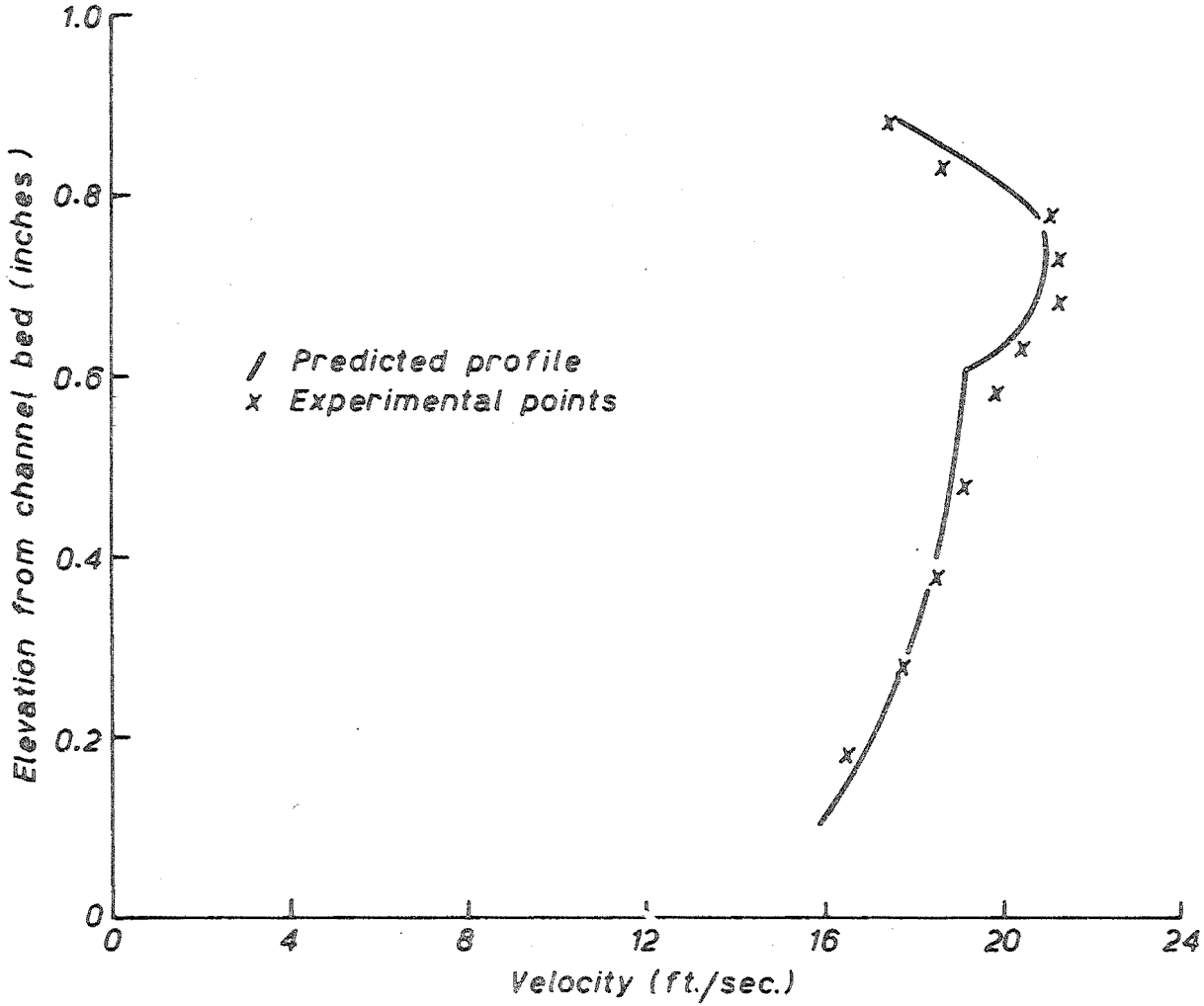

Fig. 5.11 : COMPARISON OF PREDICTED AND EXPERIMENTAL PROFILES FOR:— Discharge = 1.7 cusecs, Channel slope = 24°, Channel stn. = 18 ft. from crest.

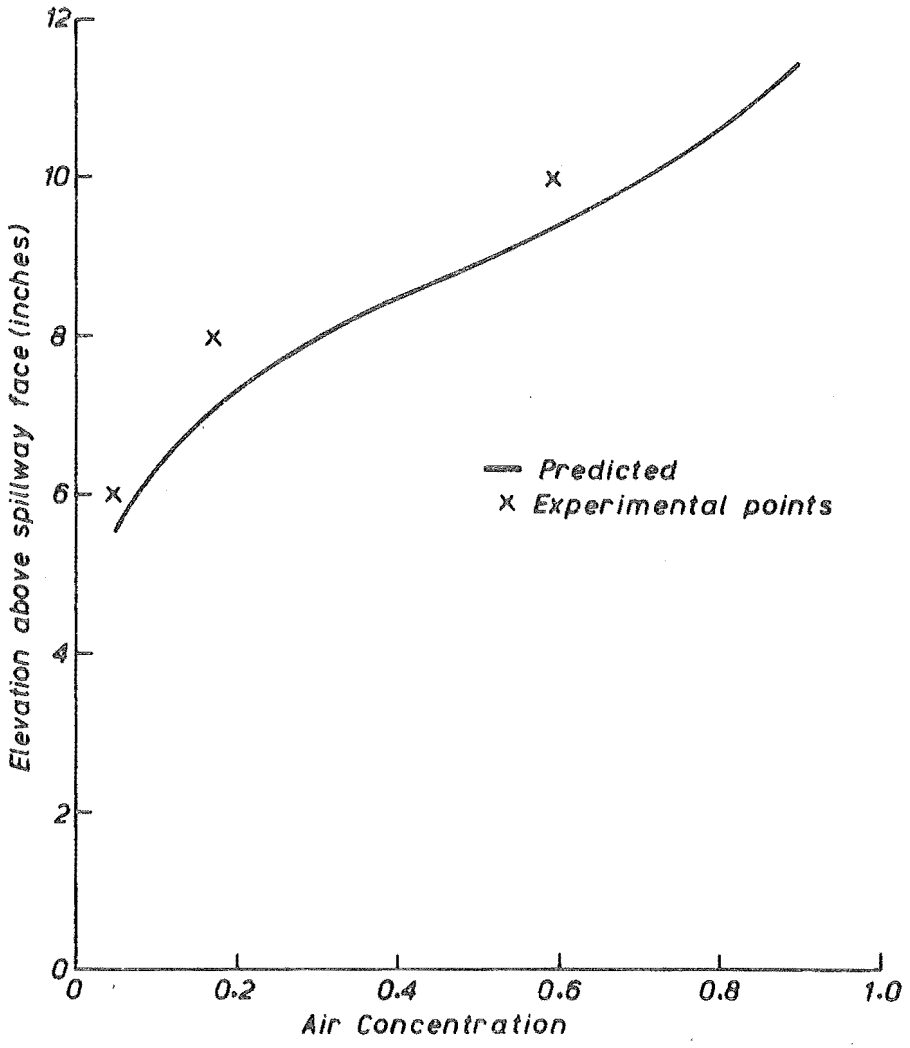

Fig. 5.12: Comparison of Predicted and Experimental Air Concentration Profiles for Aviemore Spillway — Gate opening 2ft. — Station 404

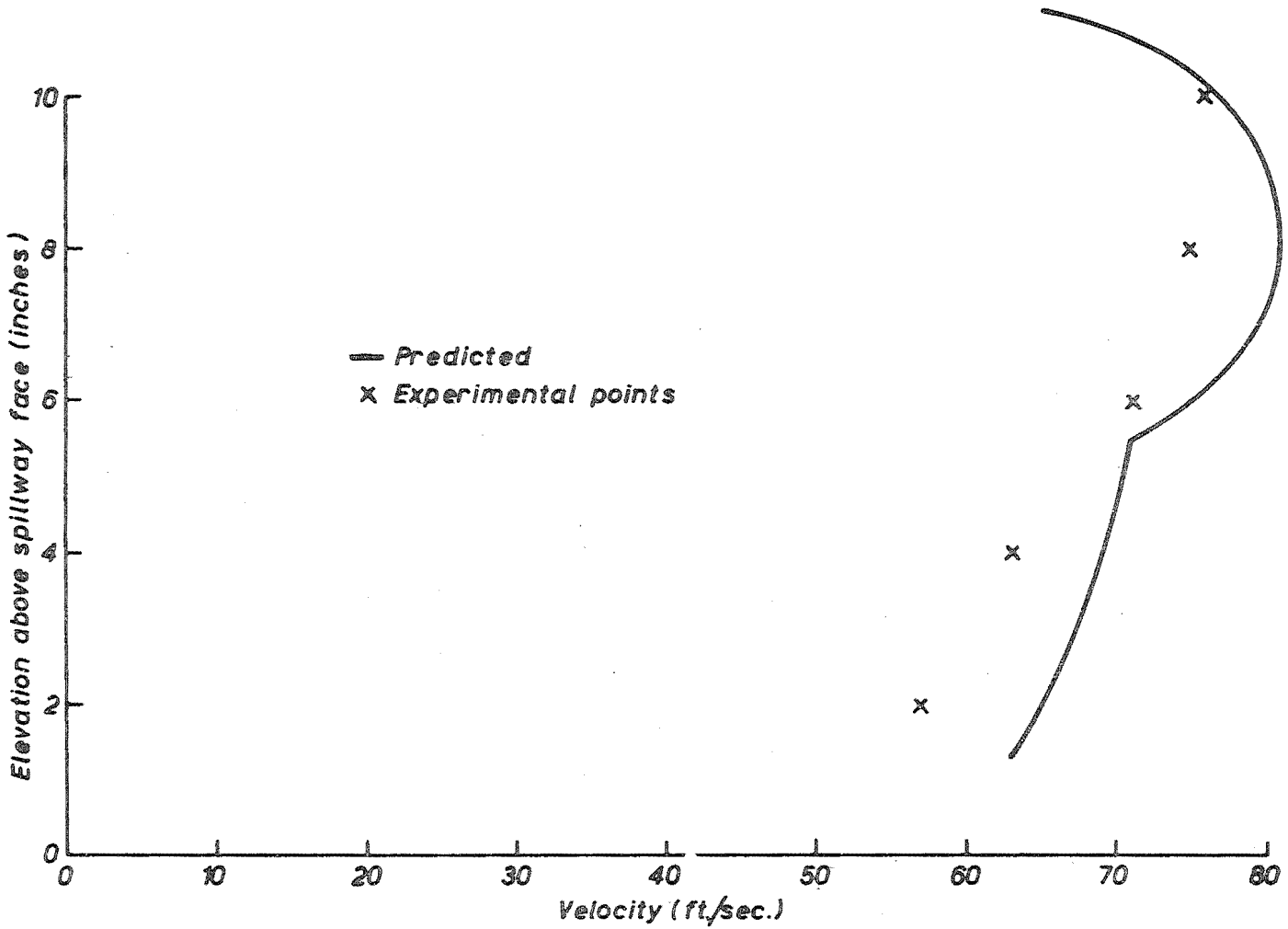

Fig. 5.13 : Comparison of Predicted and Experimental Velocity Profiles for Aviemore Spillway — Gate opening 2ft.—Station 404

Nevertheless, the figure demonstrates the negligible effect of the data scatter in Figures 5.1 to 5.10 .

Figure 5.12 shows that the experimental measurements of air concentration follow the shape of the predicted profile but are somewhat lower in magnitude. This discrepancy occurs because the elevation of the bottom of the aerated layer has been predicted about 10 percent too low. The discrepancy has the effect of lowering the predicted profile towards the channel bed without altering its shape.

Figure 5.13 shows that the computed velocity profile predicts values of velocity greater than those experimentally measured, by up to 10 percent.

The water discharge within the aerated layer may be expressed (Equation 5.2.1) as

$$q_w = \sum_{y_d} (1 - C)\, V\, \Delta y \qquad \ldots 5.2.1$$

This equation shows that, for a common water discharge within the aerated layer, an increase in air concentration must be balanced by an increased velocity. Thus, the discrepancy between the experimental and computed plots within the aerated layer in Figure 5.13 is consistent with the corresponding discrepancy in Figure 5.12 .

The correlation between the predicted and the experimental prototype profiles is reasonably good considering the assumptions made.

In particular, the values of V_s and $y_{0.05}$, computed in step 5 of the design procedure, are dependent on the calculated water discharge in the aerated layer. This discharge was calculated assuming self-similarity of the non-dimensional air concentration and velocity profiles (Figures 5.1 and 5.2) between Lai's model and the Aviemore spillway.

If, for example, in the prototype, the air concentration at the transition surface is greater than 50% , the value of the constant in Equation 5.2.3 will be less than 0.519 . Use of Equation 5.2.3 will, thus, result in an overestimate of the water discharge in the aerated layer, and consequent inaccuracies in the predicted air concentration and velocity profiles.

The experimental data incorporated in the design procedure was obtained in flows where the aerated layer constituted less than two thirds of the flow depth. It has been shown in Section 5.3 that the properties of the layer, when it penetrates deep into the flow, are profoundly affected by the influence of the channel bed. Thus, in the absence of further information, it is concluded that the design method is valid only for developing aerated flows up to the point where the aerated layer constitutes two thirds of the total flow depth.

CHAPTER SIX

CONCLUSIONS AND FUTURE CONSIDERATIONS

A. Conclusions on the Behaviour of, and Proposed Modifications to, the Field Apparatus.

After carrying out the experimental programme, the following conclusions on the behaviour of the field apparatus were reached:

1. The methods used to measure air concentration and stagnation pressure were satisfactory. Furthermore the results show that, except near the flow surface, the errors associated with the computed values of mean (time average) air concentration, stagnation pressure, and velocity were small.

2. Measured values of air concentration could not be relied on near the wildly fluctuating surface, where there was the possibility that readings were taken with the probe only partially immersed in the flow. Under such circumstances, the computed value of mean (time average) air concentration was higher than the true mean air concentration at the centre of the probe.

3. Computed values of velocity near the flow surface could not be relied on due to two factors:

   (a) The inaccuracy of the air concentration reading as discussed in 2. above.

   (b) The high degree of turbulence which meant that the turbulent fluctuation terms associated with Eq. 4.1.1 (page 107) could no longer be disregarded.

4. The probes mounted on the field test unit were too far apart to enable the obtaining of accurate depth profiles of air concentration and velocity in the comparatively shallow test flows.
5. The sampling rate of the Solartron Data logger was too slow to enable comprehensive time profiles of air concentration and stagnation pressure to be obtained. This was due to the slow speed of the only available tape punch, used to automatically record the data, and could not be avoided.

Proposed Modifications:

Problems of accuracy in the use of Eq. 4.1.1 would be eliminated if instantaneous readings of air concentration and stagnation pressure were obtained simultaneously. Under such circumstances, Eq. 2.3.4 (page 48) could be used to obtain instantaneous values of velocity whose accuracy would be independent of the extent of the turbulent fluctuations. Furthermore, the mean (time average) velocity could be more directly obtained than is possible from mean values of air concentration and stagnation pressure.

The restriction that the flow be two-dimensional could be overcome by making a composite air concentration-stagnation pressure meter. Such an instrument would enable measurements to be made near a spillway side wall, where the extent of air induced bulking may be the criterion for spillway design.

Figure 5.1 shows a meter which would satisfy the above criterion.

The critical factor in the design of the meter would be the gap size necessary for the air concentration measurements. The important consideration is the size of the air bubbles. This aspect could be investigated by photographing full-scale flows using a very high speed or stroboscopic camera.

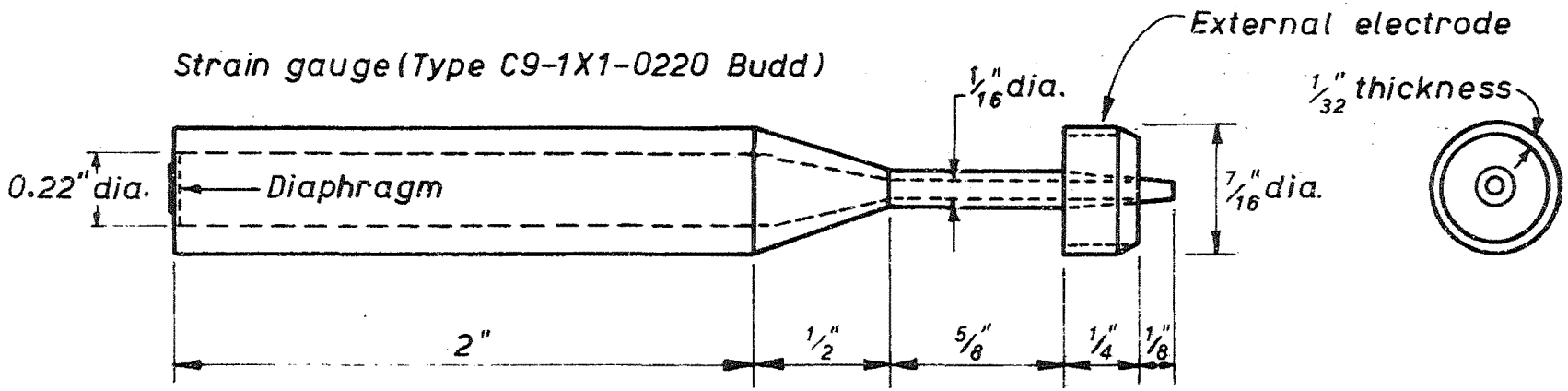

Fig. 6.1 : PROPOSED DESIGN FOR COMPOSITE AIR CONCENTRATION-VELOCITY METER

One of the failings of the present experimental setup is the poor vertical resolution of the air concentration and velocity profiles. This could be improved by using a single meter mounted on a vertical screw thread. The meter could then be set at any desired elevation in the flow by use of a remote controlled electric motor inside the pier assembly.

A considerable improvement in the present data recording system would be the use of a multi-track magnetic tape unit. Such a unit would enable the continuous measurement of air concentration and stagnation pressure simultaneously. The tape could subsequently be decoded and digital readings of the two parameters obtained at any desired time interval.

B. Conclusions from the Experimental Results and Proposed Future Research.

After carrying out the experimental programme and analysis described in this thesis, the following conclusions were reached:

1. The flow down a steep open channel of sufficient length consists of two regions - a region of pure water flow followed by a region of air-water mixture.
2. Downstream of the critical point, where aeration commences, the flow consists initially of two layers - water against the spillway face, overlaid by an air-water mixture. The quantity of entrained air and the penetration of the air bubbles into the flow increase with distance downstream, resulting in an increasing thickness of the air-water layer.

Conclusions 1 and 2 confirm, for a prototype structure, observations made in a previous model study[26].

3. Halbronn's equation (Equation 1.2) for predicting the critical point, deduced from experiments on model overflow spillways, is applicable to a prototype gate spillway where the distance to the critical point is measured from the lake level upstream of the gate. The equation may, thus, be used to predict whether or not bottom-induced aeration will occur in a given length of spillway.

4. The period of the most predominant turbulence function is approximately $2\frac{1}{2}$ seconds. No attempt was made to carry out a spectrum analysis on the fluctuation curves obtained due to the slow sampling rate of the recording data logger.

5. The analysis of model data obtained by K.K. Lai[26] (Chapter Five) provided a good correlation with prototype data obtained on the Aviemore spillway.

The experimental data was obtained in flows where the aerated layer constituted less than two thirds of the flow depth. For these data it was shown that the influence of the channel bed was negligible. However, this influence was shown to be significant when the aerated layer penetrated close to the bed.

On the basis of the analysis a design method is proposed whereby the air concentration and velocity profiles may be predicted. The method was used to confirm model and prototype profiles and showed reasonably close agreement with the experimental measurements.

Because of the limitations on the region from which the data was obtained, the method is considered valid only for developing aerated flows up to the point where the aerated layer constitutes two thirds of the total flow depth.

Proposed Future Research:

The most immediate requirement for the extension of the field tests described in this thesis is the further development of the instrumentation as described in part A of this chapter.

The tests carried out at Aviemore should be repeated with the improved instruments. Unfortunately, aerated flow occurs on the Aviemore spillway for a comparatively small range of discharges. A comprehensive experimental programme should include tests on a number of spillways of different hydraulic characteristics.

The improved instrumentation should incorporate a magnetic tape recording unit. A spectrum analysis of the fluctuation curves thus obtained would yield valuable data on the turbulence structure of prototype aerated and non-aerated flows.

It is evident that flow bulking due to aeration is extensive close to the spillway side-wall and future testing should include the measurement of air concentration and velocity profiles in this region. For such testing, a composite air concentration-velocity meter would be essential because the flow cannot be assumed to be two-dimensional in character. It is important that further prototype measurements be obtained to confirm the model and prototype correlation in Figures 5.7 and 5.8 and to extend the procedure to include comparatively deeper aerated flows.

In conclusion, it is apparent, from this work, that the most serious drawback to the satisfactory explanation and analysis of aerated flows is the lack of reliable experimental data from prototype structures.

The writer believes that the experimental methods, developed as part of the investigation described in this thesis, are satisfactory for the obtaining of such data. Further development along the lines suggested in this chapter, and the execution of a comprehensive experimental programme would constitute a valuable contribution towards the development of a rational design method for prototype spillways.

REFERENCES

1. ELLISON, T.H. (1960): A Note on the Velocity Profile and Longitudinal Mixing in a Broad Open Channel. Jnl. of Fluid Mechanics, Vol. 8, Part 1, pp. 33-40.
2. HINZE, J.O. (1959): Turbulence. An Introduction to its Mechanism and Theory. McGraw-Hill Book Company, Inc., New York, U.S.A.
3. PRANDTL, L. (1952): Essentials of Fluid Dynamics. Blackie and Son Ltd., London, U.K.
4. BIRD, R.B. STEWART, W.E., LIGHTFOOT, E.N. (1960): Transport Phenomena. John Wiley and Sons, Inc., New York, U.S.A.
5. EHRENBERGER, R. (1926): Wasserbewegung in steilen Rinnen (Schusstennen) mit besonder Berücksichtigung der Selbstbelüftung. (Flow in Steep Chutes with Special Reference to Self-aeration). Osterreichischer Ingenieur - und Architektverein, No. 15/16 and 17/18.
6. LANE, E.W. (1939): Entrainment of Air in Swiftly Flowing Water. Civil Engineering, Vol. 9, No. 2, pp. 88-91.
7. LAMB, O.P., KILLEN, J.M. (1952): An Electrical Method for Measuring Air Concentration in Flowing Air-Water Mixtures. Technical Paper No. 10, Series B, St Anthony Falls Hydraulic Laboratory, University of Minnesota.
8. STRAUB, L.G., KILLEN, J.M., LAMB, O.P. (1954): Velocity Measurement of Air-Water Mixtures. Trans. A.S.C.E., Vol. 119, pp. 207-220.
9. STRAUB, L.G., ANDERSON, A.G. (1958): Experiments on Self-aerated Flow in Open Channels. Journal of Hydraulics Division Proc. A.S.C.E., Vol. 84, No. HY7.
10. VANONI, V.A. (1946): Transportation of Suspended Sediment by Water. Trans. A.S.C.E., Vol. 111, pp 67-102.

11. GANGADHARAIAH, T., RAO, N.S.L., SEETHARAMIAH, K. (1970): Inception and Entrainment in Self-aerated Flows. Journal of Hydraulics Division, Proc. A.S.C.E., Vol. 96, No. HY7.

12. HINO, M. (1961): On the Mechanism of Self-aerated Flow on Steep Slope Channels. Application of the Statistical Theory of Turbulence. Proc. 9th Convention, International Association for Hydraulic Research.

13. BATHURST, C.F. (1969): The Flow of Gas through a Choked Nozzle. Ph.D. Thesis, University of Canterbury, Christchurch, New Zealand.

14. PRICE, B.T., HORTON, C.C., SPINNEY, K.T. (1957): Radiation Shielding. International Series of Monographs on Nuclear Energy, Pergamon Press, London.

15. HILL, I.K. (1967): Fluvial Sediment Transport at a Large Bed Shear Stress. Ph.D. Thesis, University of Canterbury, Christchurch, New Zealand.

16. FRY, T.C. (1965): Probability and its Engineering Uses. D. Van Nostrand Company, Inc., New York, U.S.A.

17. Model 183B Count-O-Matic Scaler, Operation and Maintenance Manual. Nuclear Chicago Corp., Illinois, U.S.A.

18. MAXWELL, J.C. (1873): A Treatise on Electricity and Magnetism. Oxford: Clarendon Press, U.K.

19. HALBRONN, G., DURAND, R., COHEN DE LARA, G. (1953): Air Entrainment in Steeply Sloping Flumes. Proc. 5th Meeting, International Association for Hydraulic Research, pp. 455-466.

20. VIPARELLI, M. (1953): The Flow in a Flume with 1:1 Slope. Proc. 5th Meeting, International Association for Hydraulic Research, pp. 415-423.

21. TIMOSHENKO, S., WOINOWSKY-KRIEGER, S. (1959): Theory of Plates and Shells. McGraw-Hill Book Company, Inc., New York, U.S.A.

22. TIMOSHENKO, S. (1955): Vibration Problems in Engineering. D. Van Nostrand Company, Inc., New York, U.S.A.

23. HINCE, R.F., KELLER, R.J. (1971): Field Measurement of Self-aerated High Speed Open Channel Flow. New Zealand Engineering, Vol. 26, No. 1, pp. 20-24.

24. PARADINE, C.G., RIVETT, B.H.P. (1960): Statistical Methods for Technologists. English Universities Press Ltd, London, U.K.

25. NEW ZEALAND MINISTRY OF WORKS (1968): Discharge Tables for the Aviemore Spillway.

26. LAI, K.K. (1971): Studies of Air Entrainment in Steep Open Channels. M.E. thesis, University of New South Wales, Sydney, Australia.

27. HENDERSON, F.M. (1966): Open Channel Flow. Macmillan Co., New York, U.S.A.

28. ROUSE, HUNTER (1959): Advanced Mechanics of Fluids. John Wiley and Sons, Inc., New York, U.S.A.

29. HICKOX, G.H. (1945): Air Entrainment on Spillway Faces. Civil Engineering, Vol. 15, No. 12, pp. 562-563.

30. HALBRONN, G. (1952): Etude de la mise en regime des ecoulements sur les ouvrages a forte pente. La Houille Blanche, No. 1, pp. 21-40.

31. HALL, L.S. (1943): Entrainment of Air in Flowing Water: Open Channel Flow at High Velocities. Trans. A.S.C.E., Vol. 108, pp. 1394-1434.

32. BAUER, W.J. (1954): Turbulent Boundary Layer on Steep Slopes. Trans. A.S.C.E., Vol. 119, pp. 1212-1232.

33. HALBRONN, G. (1954): Discussion of Reference 32.

34. STREETER, V.L. (1966): Fluid Mechanics. McGraw-Hill Book Company, Inc., New York, U.S.A.

APPENDIX I

DERIVATION OF VELOCITY METER CALIBRATION FORMULA

The equation for the calculation of pressure from the manometer bank readings can be derived with reference to Figure AI.1.

The manometer bank measures the pressure difference between some initial condition (denoted by subscript 1) and a final condition (denoted by subscript 2).

Initially

$$H_{x1} = 13.6\,[(B_1 - A_1) + (D_1 - C_1) + [(C_1 - B_1)] + (A_1 - X) \quad \ldots \text{AI.1}$$

where

H_{x1} is the initial pressure on the diaphragm in ft. of water.

Finally

$$H_{x2} = 13.6\,[(B_2 - A_2) + (D_2 - C_2)] + [(C_2 - B_2) + (A_2 - X) \quad \ldots \text{AI.2}$$

where

H_{x2} is the final pressure on the diaphragm in ft. of water.

Subtract AI.2 from AI.1

$$H_{x2} - H_{x1} = 12.6\,[(A_1 - A_2) - (B_1 - B_2) + (C_1 - C_2)] - 13.6\,(D_1 - D_2) \quad \ldots \text{AI.3}$$

For an initial condition of atmospheric pressure, $H_{x1} = 0$ thus

$$H = 12.6\,[(A_1 - A_2) - (B_1 - B_2) + (C_1 - C_2)] - 13.6\,(D_1 - D_2) \quad \ldots \text{AI.4}$$

where

H is the pressure on the diaphragm in ft. of water.

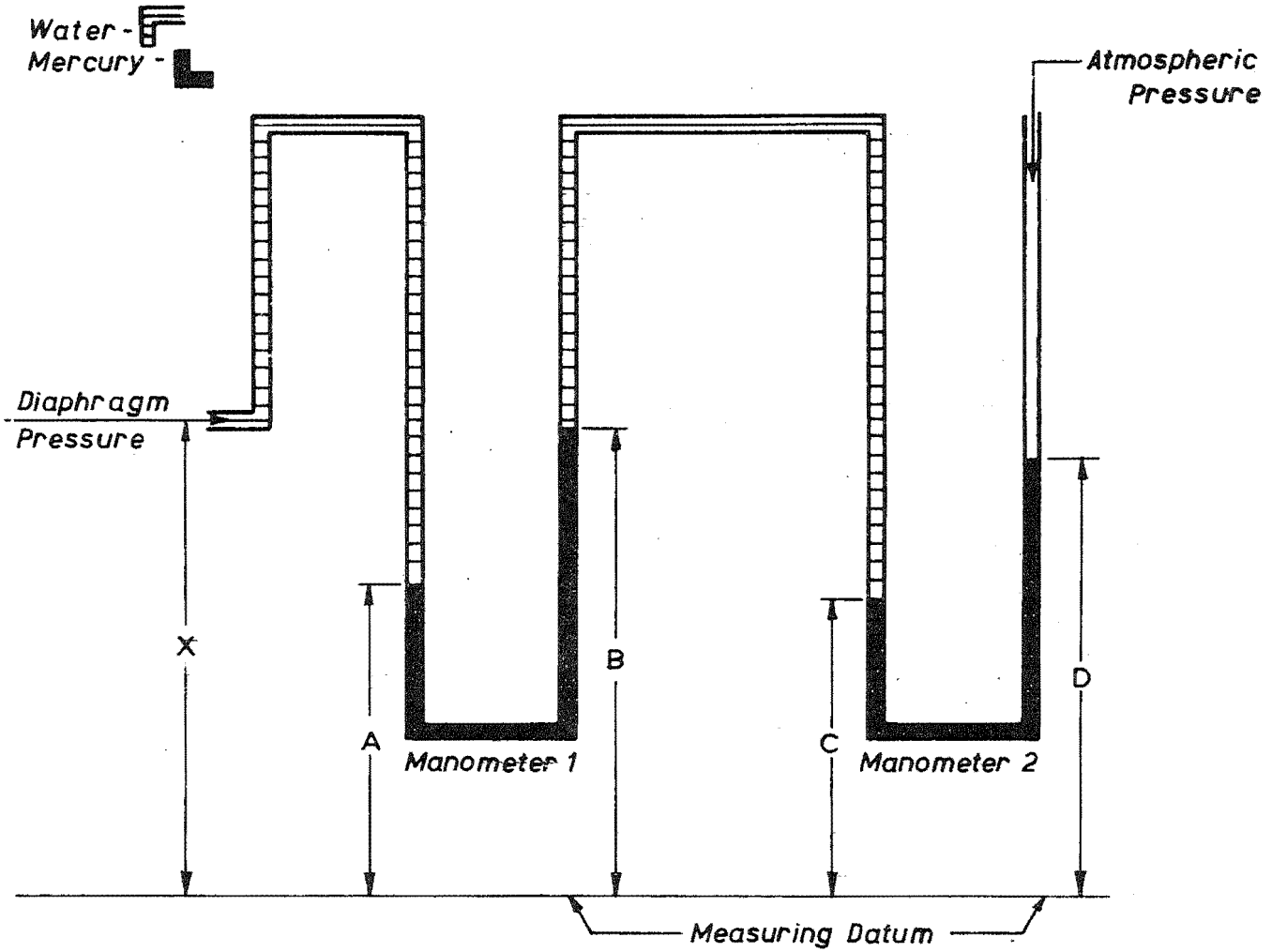

Fig. AI.1: VELOCITY METER STATIC CALIBRATION — SCHEMATIC OF MANOMETER BANK

APPENDIX II

COMPUTER PROGRAMMES

1. Velocity Meter Static Calibration Programme

Purpose:

To provide co-ordinates for plotting (pressure) v (strain gauge output) curves for each of the twelve velocity meters.

Comments:

The programme is designed for use with a mercury-water two manometer system.

In its present form the programme will accept tape data sets of up to 50 readings each. However, this capacity could be extended by altering the appropriate dimension statements.

Card Input Data:

	Card	Data	Format
Repeat for each probe	1	Probe number	I2
Repeat for each press. incr.	2	Data control factor, manometer arm readings (ft), approximate pressure (psi)	I1,4F7.3,I4

Data Control Factor Values:

1	First (zero) tape data set
4	All subsequent tape data sets except last
2	Last tape data set
3	Additional data card after last tape data set

5	Additional data card after all probe tape data sets.

Tape Input Data:

Data sets of individual strain gauge output readings. Format is machine dependent. For the University of Canterbury computer installation it is designated KELLEY.

Output Data:

(a) Manometer arm readings and raw tape data for each pressure increment.

(b) Co-ordinates of pressure and strain gauge output for each probe.

```
      ********************************************

      PROGRAM TO PROCESS STATIC CALIBRATION DATA

      ********************************************


      EXTERNAL KELLEY
      INTEGER Z,AMAX,AMIN,PN,RMAX,RMIN,RRAN,BLIST
      INTEGER*2 NDATA(300)
      REAL*4 L
      DIMENSION ZERO(4),A(4),L(4),K(50),Y(50),PLIST(25),AVLIST(25),
     1BLIST(25),M(50)
C     READ PROBE NUMBER
   32 READ(5,35) PN
   35 FORMAT(I2)
      KOUNT=0
      PZERO=0.0
      DO 55 I=1,4
   55 ZERO(I)=0.0
C     READ CONTROL FACTOR,MANOMETER ARM READINGS,APPROX.PRESSURE
   24 READ(5,1) NPLS,(A(I),I=1,4),KP
    1 FORMAT(I1,4F7.3,I4)
      IF(NPLS.EQ.3) GO TO 25
      IF(NPLS.EQ.5) CALL EXIT
      KOUNT=KOUNT+1
      DO 2 I=1,4
    2 L(I)=ZERO(I)-A(I)
C     CALCULATE PRESSURE
      P=(12.6*(L(1)-L(2)+L(3))-13.6*L(4))*62.4/144
      IF(NPLS.EQ.4) GO TO 26
      P=0.
      DO 53 I=1,4
   53 ZERO(I)=A(I)
C     READ TAPE DATA
   26 CALL PTAPE(NDATA,1800,N,KELLEY)
C     WRITE MANOMETER ARM READINGS AND RAW TAPE DATA
      WRITE(6,33)
   33 FORMAT('1',4(4X,'MANO.ARM'),/)
      WRITE(6,34) (A(I),I=1,4)
   34 FORMAT('0',4F12.3,/)
      DO 54 J=1,N
   54 K(J)=NDATA(J)
      WRITE(6,3) (K(J),J=1,N)
    3 FORMAT('0',5(10X,I6),/)
C     CALCULATE AVERAGE
   70 TOTAL=0.
      DO 13 J=1,N
      Y(J)=K(J)
   13 TOTAL=TOTAL+Y(J)
      AN=N
      AVE=TOTAL/AN
C     CALCULATE STANDARD DEVIATION
      TOTAL=0.
      DO 14 J=1,N
   14 TOTAL=TOTAL+(Y(J)-AVE)**2
      SD=SQRT(TOTAL/AN)
      KMAX=-10000
      KMIN=10000
      DO 15 J=1,N
      IF(K(J).GT.KMAX) KMAX=K(J)
      IF(K(J).EQ.KMAX) L1=J
      IF(K(J).LT.KMIN) KMIN=K(J)
      IF(K(J).EQ.KMIN) L2=J
   15 CONTINUE
      KRAN=KMAX-KMIN
C     ELIMINATE SPURIOUS TAPE READINGS
      AMAX=KMAX
      AMIN=KMIN
      AGAX=AMAX-AVE
      AGAN=AVE-AMIN
      TD=3*SD
      IF(AGAX.GT.TD) GO TO 60
  101 IF(AGAN.GT.TD) GO TO 100
      GO TO 80
   60 DO 61 J=L1,N
   61 K(J)=K(J&1)
      N=N-1
      GO TO 70
  100 DO 102 J=L2,N
  102 K(J)=K(J&1)
      N=N-1
      GO TO 70
   80 IF(NPLS.EQ.1) PZERO=AVE
C     CALCULATE REDUCED AVERAGE
      SAVE=AVE-PZERO
      RMAX=KMAX-PZERO
      RRAN=KRAN
      IF(PZERO.EQ.0.0) RMAX=KMAX-AVE
      RMIN=RMAX-RRAN
      WRITE(6,18)
   18 FORMAT('0',4X,'READINGS ACCEPTED IN RANGE KMAX TO KMIN')
      WRITE(6,19)
   19 FORMAT('0',4X,'KMAX',6X,'KMIN',6X,'KRAN',3X,'STD.DEV.',3X,'NRUNS')
      WRITE(6,20) KMAX,KMIN,KRAN,SD,N
   20 FORMAT('0',I8,2I10,F10.2,I8///)
      WRITE(6,21)
   21 FORMAT('0',4X,'REDUCED READINGS')
      WRITE(6,22)
   22 FORMAT('0',4X,'RMAX',6X,'RMIN',6X,'RRAN')
      WRITE(6,23) RMAX,RMIN,RRAN
   23 FORMAT('0',I8,2I10///)
      PLIST(KOUNT)=P
      AVLIST(KOUNT)=SAVE
      BLIST(KOUNT)=KP
      IF(NPLS.EQ.2) PZERO=AVE
      GO TO 24
   25 WRITE(6,50)
   50 FORMAT('1',4X'PROBE NUMBER')
      WRITE(6,51) PN
   51 FORMAT('+',I26)
      WRITE(6,52)
   52 FORMAT('0',10X,'PRES',6X,'MSTRAIN',6X,'BGAGE'/)
      DO 27 I=1,KOUNT
   27 WRITE(6,28) PLIST(I),AVLIST(I),BLIST(I)
   28 FORMAT('0',2F14.2,I10///)
      GO TO 32
      END
```

2. Velocity Meter Test Data Processing Programme

Purpose:

To process the raw data from the velocity meter tests.

Comments:

This programme is machine dependent due to the incorporation of the tape translation routine HOPKIN. Furthermore it is only suitable for test results obtained in the same fashion as from the writer's tests. It is included here for the benefit of those continuing the writer's work using the University of Canterbury computer installation.

The various input data parameters are explained at the beginning of the program listing.

```
C**********************************************
C
C VELOCITY METER TEST PROCESSING PROGRAMME
C
C**********************************************

C**************************************************************************
C**************************************************************************
C**************************************************************************
C RAIR=SP.WT.OF AIR(LB/CUB.FT.)
C BCOUNT=BACKGROUND COUNTS
C NCOUNT=TEST COUNTS
C KDISH=TEST VOLUME OF WATER
C TDISH=AVERAGE MIXTURE VOLUME OVER TRIAL
C TBI=TIME FOR INITIAL BACKGROUND COUNT
C TBF=TIME FOR FINAL BACKGROUND COUNT
C X=TIME FOR 100( AIR COUNT
C H=TIME FOR 0( AIR COUNT
C TTI=TIME OF DAY OF INITIAL BACKGROUND COUNT
C TTF=TIME OF DAY OF FINAL BACKGROUND COUNT
C TZI=TIME OF DAY OF ZERO DLOGGER READING BEFORE DIAMETER TESTS
C TZF=TIME OF DAY OF ZERO DLOGGER READING AFTER DIAMETER TESTS
C TYA=TIME OF DAY OF 100( AIR COUNT
C TYW=TIME OF DAY OF 0( AIR COUNT
C NPLS=CONTROL FOR VALUES OF KZERO1,KZEROF
C ZZ=TIME FOR TEST COUNT
C TD=TIME FOR WATER DISCHARGE
C TT=TIME OF DAY OF TEST
C ***COUNT FACTORS***
C COUNT=DIAMETER NUMBER
C KOUNT=TOTAL NUMBER OF TESTS WITHIN SINGLE TRAVERSE
C KINT=TOTAL NUMBER OF NONZERO READINGS IN TRIAL
C KENT=NUMBER OF NONZERO READINGS WITHIN SINGLE TRAVERSE
C KONT=NUMBER OF ZERO READINGS WITHIN A SINGLE TRAVERSE ON TAPE
C WHICH FOLLOW NONZERO READINGS WITHIN THE TRAVERSE
C KANT=NUMBER OF ZERO OR NEGATIVE REDUCED READINGS WITHIN A
C SINGLE TEST
C**************************************************************************
      EXTERNAL HOPKIN
      REAL M
      INTEGER Y,BCOUNT,COUNT,RMAX,RMIN,RRAN,TLIST,E
      DIMENSION NDATA(900),K(300),M(300),Y(300),AVLIST(4,20),
     1PLIST(4,20),TLIST(4,20),ACLIST(4,20),DLIST(4,20),FLIST(4),AV(6),
     1TOTEL(9),PR(6),STOT(9),SAV(6),SP(6)
      KZERO1=0
      KZEROF=0
      KOUNT=0
      COUNT=1
      KINT=0
      KENT=0
      KONT=0
      READ(5,1) CONFAC,RAIR,BCOUNT,NCOUNT,KDISH,AREA
    1 FORMAT(2F7.4,I5,I7,I4,F8.4)
   32 READ(5,31) TBI,TBF,X,H,TTI,TTF,TZI,TZF,TYA,TYW
   31 FORMAT(2F8.3,2F7.3,6F7.2)
      BI=BCOUNT/TBI
      BF=BCOUNT/TBF
      U=ALOG(NCOUNT/X-BI-(BI-BF)*(TTI-TYA)/(TTI-TTF))
      V=ALOG(NCOUNT/H-BI-(BI-BF)*(TTI-TYW)/(TTI-TTF))
   13 READ(5,33) NPLS,KTEST,ZZ,TD,TT
   33 FORMAT(I3,I4,F7.3,F6.1,F7.2)
      KOUNT=KOUNT+1
      IF(NPLS.EQ.1.OR.NPLS.EQ.2.OR.NPLS.EQ.5) KZERO1=0
      IF(NPLS.EQ.1.OR.NPLS.EQ.2.OR.NPLS.EQ.5) KZEROF=0
      IF(KTEST.NE.0) KENT=KENT+1
      IF(KTEST.NE.0) KINT=KINT+1
      IF(KTEST.EQ.0.AND.KENT.NE.0) KONT=KONT+1
      CALL PTAPE(NDATA,4000,KRESID,HOPKIN)
      N=(4000-KRESID)/11
      DO 2 J=1,N
      L=J+J
    2 K(J)=NDATA(L)
      KZERO=KZERO1-(KZERO1-KZEROF)*(TZI-TT)/(TZI-TZF)
      DO 3 J=1,N
      Y(J)=K(J)-KZERO
      IF(NPLS.EQ.3) Y(J)=K(J)
      IF(NPLS.EQ.4) Y(J)=K(J)
    3 CONTINUE
      KANT=0
      DO 4 J=1,N
      Z=Y(J)
      IF(Y(J)) 16,16,17
   17 M(J)=SQRT(Z)
      GO TO 4
   16 M(J)=0
      KANT=KANT+1
      CONTINUE
      TOTAL=0
      DO 5 J=1,N
      TOTAL=TOTAL+M(J)
      AN=N
      Q=AN-KANT
      AVE=(TOTAL/Q)**2
      TOTAL=0
      DO 6 J=1,N
      SK=Y(J)
      TOTAL=TOTAL+(SK-AVE)**2
      SD=SQRT(TOTAL/AN)
      KMAX=-10000
      KMIN=10000
      DO 7 J=1,N
      IF(K(J).GT.KMAX) KMAX=K(J)
      IF(K(J).LT.KMIN) KMIN=K(J)
      KRAN=KMAX-KMIN
      RMAX=KMAX-KZERO
      RRAN=KRAN
      IF(KZEROF.EQ.0) RMAX=KMAX-AVE
      RMIN=RMAX-RRAN
      P=AVE*CONFAC
      IF(KZERO1.EQ.0.OR.KZEROF.EQ.0) P=0.
      IF(NPLS.EQ.5) AC=0.
      IF(NPLS.EQ.1.OR.NPLS.EQ.2) AC=0.
      IF(NPLS.NE.0) GO TO 39
      M=ALOG(NCOUNT/ZZ-BI-(BI-BF)*(TTI-TT)/(TTI-TTF))
      AC=(M-V)/(U-V)
      DISH=KDISH/TD
      WRITE(6,8) (K(J),J=1,N)
    8 FORMAT('0',9(10X,I6)/)
      WRITE(6,9)
    9 FORMAT('0',6X,'KMAX',6X,'KMIN',6X,'KRAN',3X,'STD.DEV.',3X,'NRUNS',
     3X,'N(NEG.OR ZERO READ.)')
      WRITE(6,10) KMAX,KMIN,KRAN,SD,N,KANT
   10 FORMAT('0',3I10,F10.2,I9,I13)
      WRITE(6,11)
   11 FORMAT('0',6X,'RMAX',6X,'RMIN',6X,'RRAN')
      WRITE(6,12) RMAX,RMIN,RRAN
   12 FORMAT('0',3I10/'1')
```

```
      IF(NPLS.EQ.3) KZERO1=AVE
      IF(NPLS.EQ.4) KZEROF=AVE
      PLIST(COUNT,KOUNT)=P
      AVLIST(COUNT,KOUNT)=AVE
      TLIST(COUNT,KOUNT)=KTEST
      ACLIST(COUNT,KOUNT)=AC
      DLIST(COUNT,KOUNT)=DISH
      IF(NPLS.EQ.1) GO TO 14
      IF(NPLS.EQ.2) GO TO 14
      GO TO 13
   14 WRITE(6,15)
   15 FORMAT('1',10X,'*****DIAMETER*****')
      WRITE(6,18) COUNT
   18 FORMAT('0',I19)
      WRITE(6,19)
   19 FORMAT('0',10X,'POSITION',6X,'AVE',6X'PRES',6X'AIR CONTENT')
      DO 20 I=1,KOUNT
   20 WRITE(6,21) TLIST(COUNT,I),AVLIST(COUNT,I),PLIST(COUNT,I),
     1ACLIST(COUNT,I)
   21 FORMAT('0',I15,F12.2,F10.2,F14.2)
      WRITE(6,41)
   41 FORMAT('1')
      F=KOUNT-KENT-KONT+1
      FLIST(COUNT)=F
      IF(NPLS.EQ.2) GO TO 22
      COUNT=COUNT+1
      KENT=0
      KONT=0
      KOUNT=0
      GO TO 32
   22 DO 99 I=1,9
      TOTEL(I)=0.
   99 STOT(I)=0.
      DO 100 E=1,COUNT
      DO 100 I=1,9
      I1=I-1
      TOTEL(I)=TOTEL(I)+AVLIST(E,FLIST(E)+I1)
      STOT(I)=STOT(I)+SQRT(AVLIST(E,FLIST(E)+I1))
  100 CONTINUE
      DO 101 J=1,5
      AV(J)=(TOTEL(J)+TOTEL(10-J))/(COUNT*2)
      SAV(J)=(STOT(J)+STOT(10-J))/(COUNT*2)
  101 CONTINUE
      AV(6)=0.
      SAV(6)=0.
      DO 102 J=1,6
      PR(J)=AV(J)*CONFAC
      SP(J)=SAV(J)*SQRT(CONFAC)
  102 CONTINUE
      TOTAL=0
      DO 23 E=1,COUNT
      DO 23 I=1,KOUNT
   23 TOTAL=TOTAL+ACLIST(E,I)
      AVAC=TOTAL/KINT
      RHO=(62.4-(62.4-RAIR)*AVAC)/32.2
      PAVAC=AVAC*100.
      TOTAL=0
      DO 34 E=1,COUNT
      DO 34 I=1,KOUNT
   34 TOTAL=TOTAL+DLIST(E,I)
      AVDISH=TOTAL/KINT
      TDISH=AVDISH*(1+AVAC/(1-AVAC))
      VEL=TDISH/AREA
      WRITE(6,35)
   35 FORMAT('1',10X,'AVERAGE DISCHARGE=',11X,'CUSECS')
      WRITE(6,36) TDISH
   36 FORMAT('+',F36.3///)
      WRITE(6,37)
   37 FORMAT('0',10X,'AVERAGE AIR CONTENT=',11X,'(')
      WRITE(6,38) PAVAC
   38 FORMAT('+',F38.2///)
      WRITE(6,24)
   24 FORMAT('0',10X,'MIXTURE DENSITY =')
      WRITE(6,25) RHO
   25 FORMAT('+',F34.2///)
      WRITE(6,42)
   42 FORMAT('0',10X,'AVERAGE VELOCITY=',8X,'FT/SEC')
      WRITE(6,43) VEL
   43 FORMAT('+',F34.2///)
      WRITE(6,26)
   26 FORMAT('0',10X,'RADIUS',10X,'0',9X,'3/8',9X'3/4',9X,'9/8',8X,
     1'21/16',8X,'23/16'//)
      WRITE(6,27)
   27 FORMAT('0',9X,'HSTRAIN')
      WRITE(6,28) (AV(6-J),J=1,5),AV(6)
   28 FORMAT('+',F28.2,3F12.2,2F13.2//)
      WRITE(6,29)
   29 FORMAT('0',8X,'PRESSURE')
      WRITE(6,30) (PR(6-J),J=1,5),PR(6)
   30 FORMAT('+',F28.2,3F12.2,2F13.2//)
      WRITE(6,50)
   50 FORMAT('0',8X,'SPRESSURE')
      WRITE(6,51) (SP(6-J),J=1,5),SP(6)
   51 FORMAT('+',F28.2,3F12.2,2F13.2//)
      END
```

3. Velocity Meter Test Analysis Programme

Purpose:

To calculate the mean (area average) velocity at the outlet of the spillway flow simulator from the pressure-radius curve.

Input Data:

	Card	Data	Format
	1	Pressure at simulator centre (psi), mean (area average) density, tail-pipe area (sq.ft)	F7.2,F6.2,F7.3
Repeat for each pressure increment	2	Pressure at radius increment from centre, radius increment, data control factor	F7.2,F7.3,I3

Data Control Factor Values:

0	All cards except that incorporating pressure at side wall of simulator
1	Card incorporating side wall pressure

Output Data:

(a) Graph properties and mean (area average) velocity.

```
C**************************************

C VELOCITY METER TEST ANALYSIS PROGRAMME

C**************************************

      REAL M,K1,K2,MTOT,MLIST,MPRES
      DIMENSION ALIST(20),MLIST(20)
      Q=0.
      KOUNT=0
      READ(5,8) K1,RHO,AREA
    8 FORMAT(F7.2,F6.2,F7.3)
    3 READ(5,1) K2,B,JOK
    1 FORMAT(F7.2,F7.3,I3)
      KOUNT=KOUNT+1
      Q=Q+B
      A=(K1+K2)*B/2
      M=A*(Q*2-B)/2
      ALIST(KOUNT)=A
      MLIST(KOUNT)=M
      IF(JOK.EQ.1) GO TO 2
      K1=K2
      GO TO 3
    2 TOTAL=0.
      DO 4 I=1,KOUNT
    4 TOTAL=TOTAL+ALIST(I)
      ATOT=TOTAL
      TOTAL=0.
      DO 5 I=1,KOUNT
    5 TOTAL=TOTAL+MLIST(I)
      MTOT=TOTAL
      X=MTOT/ATOT
      VOL=MTOT*6.284
      MPRES=VOL/AREA
      V=SQRT(MPRES*2/RHO)
      WRITE(6,6)
    6 FORMAT('1',4X,'TOTAL AREA',4X,'DIST.FROM C.L.TO C.OF G.',4X,
     1'MEAN PRESSURE',4X,'MEAN VELOCITY')
      WRITE(6,7) ATOT,X,MPRES,V
    7 FORMAT('0',F14.3,F27.3,F16.3,F17.2)
      END
```

4. Field Test Data Processing Programme

Purpose:

To process the raw data from the field experiments.

Comments:

The programme in its present form is suitable for use with results from the field test unit developed at the University of Canterbury. It is designed to handle up to 4 flow discharges and data sets of up to 310 individual readings from each of 28 measurement points (12 air concentration, 12 velocity, 4 electronics monitors). However, this capacity could be extended by altering the appropriate dimension statements.

It should be noted that subroutine BPLOT and the tape translation routine are machine dependent, and are compatible only with the University of Canterbury computer installation.

Card Input Data:

	Card	Data	Format
Repeated for each complete test discharge	1	Zero readings for air concentration oscillator and calibration probe	2I4
	2	Calibration factors for velocity meters	12F5.5
	3	Clear water calibration factors for air conc. probes	12F4.3
	4	Gate opening	I1
Repeated for each run of data sets	5 and 6	Time of day (24 hour format) of data sets	14I4
Repeated for each data set	7	Pier, probe number, data control factor	2A3,I2

Data Control Factor Values:

1	Initial series of zero data sets, except last.
11	Last zero data set of initial series.
2	Series of test data sets, except last.
22	Last test data set of series.
3	Final series of zero data sets, except last.
33	Last zero data set of final series.

Tape Input Data:

Data sets of individual readings, obtained in the order shown in Figure 3.2. Format is machine dependent. For the University of Canterbury computer installation it is designated KELLEY.

Output Data:

(a) Mean (time dependent) air concentration, stagnation pressure, and velocity ($\overline{C}$, $\overline{P}$, and $\overline{V}$) for each probe.

(b) Standard deviations (C', P') of test data sets for all probes.

(c) Ratios $C'/(1-\overline{C})$, $P'/\overline{P}$ for all probes.

(d) Punched cards for automatic plotting of time variation curves of air concentration and stagnation pressure.

```
      ****************************************

      FIELD TEST DATA PROCESSING PROGRAMME

      ****************************************


      DIMENSION K(400),        PRLIST(4,12),ACLIST(4,12),VLIST(4,12),TLI
     1ST(3,28),CF(12)
      DIMENSION SD(4,28),PCD(4,28)
      INTEGER*2 NDATA(1000)
      INTEGER TIM(3,28),CZ,GOP,Z1LIST(28),Z2LIST(4,28),Z3LIST(28),PLIST(
     128),RPLIST(28),EO(4,12),OZ
      DIMENSION AK(28,310),NR(4,28)
      DIMENSION R(12)
      DIMENSION AELIST(4,12),PSLIST(4,12)
  900 FORMAT('0',7G13.6)
C     READ ZEROS FOR CALIBRATION CELL AND OSCILLATOR.
C
      READ(5,1) CZ,OZ
    1 FORMAT(2I4)
C     READ CALIBRATION FACTORS FOR VELOCITY PROBES.
C
      READ(5,2) (CF(J),J=1,12)
    2 FORMAT(12F5.5)
C     READ CLEAR WATER CALIBRATION FACTORS FOR A/C PROBES.
C
      READ(5,200) (R(J),J=1,12)
  200 FORMAT(12F4.3)
C     INITIALIZE COUNY FACTORS
C     KONT-GATE OPENING
C     KENT-RUN OF DATA SETS
C     KOUNT-DATA SET
  120 KONT=1
  110 KENT=0
    8 KOUNT=0
      GO TO 19
C     RE-INITIALIZE INITIAL ZERO FROM FINAL ZERO OF PRECEDING GATE OPENI
C     NG
C
   16 KONT=KONT+1
      IF(NPLS.EQ.6) GO TO 110
      DO 18 J=1,28
      TIM(1,J)=TIM(3,J)
      Z1LIST(J)=Z3LIST(J)
   18 CONTINUE
      KENT=1
      GO TO 8
C     READ GATE OPENING
C
   19 READ(5,3) GOP
    3 FORMAT(I1)
      KENT=KENT&1
C     READ TIME OF DAY OF DATA SETS IN 24 HOUR
C     FORMAT
C
      READ(5,4) (TIM(KENT,J),J=1,28)
    4 FORMAT(14I4)
    9 KOUNT=KOUNT&1
C     READ PIER,PROBE NUMBER,DATA CONTROL FACTOR.
C
      READ(5,5) PIER,PN,NPLS
    5 FORMAT(2A3,I2)
C     WRITE GATE OPENING,PIER,PROBE NUMBER
C
      GO TO 1001
 1000 WRITE(6,6)
    6 FORMAT('1',4X,'GATE OPEN(FT.)',4X,'PIER',4X,'PROBE NO.')
      WRITE(6,7) GOP,PIER,PN
    7 FORMAT('0',I10,A8,A13)
 1001 CONTINUE
C     CALL TAPE PROCESS SUBROUTINE
C
      CALL TDATA(NDATA,Z1LIST,Z3LIST,NPLS,K,KOUNT,N)
      IF(NPLS.NE.2.AND.NPLS.NE.22) GO TO 1510
      DO 1511 J=1,N
      AK(KOUNT,J)=K(J)
 1511 CONTINUE
      NR(KONT,KOUNT)=N
C     EXERT CONDITIONAL CONTROL FOR FINAL SET OF RUN OF DATA SETS
C
 1510 IF(NPLS.EQ.7) GO TO 120
      IF(NPLS.EQ.11.OR.NPLS.EQ.22) GO TO 8
      IF(NPLS.NE.33.AND.NPLS.NE.6) GO TO 9
C     CONVERT TIMES OF ALL DATA SETS FOR COMPLETE DEFINITION OF GATE
C     OPENING TO DECIMAL FORMAT.
C
      DO 10 I=1,3
      DO 10 J=1,28
      TLIST(I,J)=(TIM(I,J)/100.-TIM(I,J)/100)*100./60.+TIM(I,J)/100
   10 CONTINUE
C     COMPUTE GATE OPENING DATA SET ZEROS
C     ASSUMING LINEAR ZERO DRIFT WITH TIME
C
      DO 11 J=1,28
      Z2LIST(KONT,J)=Z1LIST(J)+(Z3LIST(J)-Z1LIST(J))*(TLIST(2,J)-TLIST(1
     1,J))/(TLIST(3,J)-TLIST(1,J))
   11 CONTINUE
C     INSERT CALIBRATION ZEROS AND OSCILLATOR ZEROS.
C
      Z2LIST(KONT,2)=CZ
      Z2LIST(KONT,28)=CZ
      Z2LIST(KONT,1)=OZ
      Z2LIST(KONT,27)=OZ
C     COMPUTE REDUCED DATA LOGGER READINGS
C
      DO 13 J=1,28
      NRJ=NR(KONT,J)
      DO 13 L=1,NRJ
      AK(J,L)=AK(J,L)-Z2LIST(KONT,J)
   13 CONTINUE
C     COMPUTE DATA AVERAGES FOR CALCULATION OF OSC. VOLTAGE
      TOTAL=0.
      NRJ=NR(KONT,1)
      DO 1550 L=1,NRJ
 1550 TOTAL=TOTAL+AK(1,L)
      EINIT=TOTAL/NRJ
      TOTAL=0.
      NRJ=NR(KONT,27)
      DO 1551 L=1,NRJ
 1551 TOTAL=TOTAL+AK(27,L)
      EFINL=TOTAL/NRJ
C     COMPUTE OSC. VOLTAGE FOR CALC OF A/C'S.
      DO 14 J=3,26,2
      I=(J-1)/2
      EO(KONT,I)=3*(EINIT+(EFINL-EINIT)*(TLIST(2,J)-TLIST(2,1))/(TLIST(2
     1,27)-TLIST(2,1)))
   14 CONTINUE
```

```
      DO 1545 J=3,26,2
      NRJ=NR(KONT,J)
      DO 1545 L=1,NRJ
      IF(AK(J,L).LT.1) AK(J,L)=1.
 1545 CONTINUE
      DO 1546 J=4,26,2
      NRJ=NR(KONT,J)
      DO 1546 L=1,NRJ
      IF(AK(J,L).LT.1) AK(J,L)=0.
 1546 CONTINUE
C     CALCULATE PRESSURES FOR VELOCITY PROBES
C
C     COMPUTE A/C'S & PRESSURES.
      DO 1540 J=3,26
      NRJ=NR(KONT,J)
      KJ=J
      IJ=(J-1)/2
      JJ=(J-2)/2
      DO 1540 L=1,NRJ
      IF(KJ/2*2.EQ.KJ) AK(J,L)=AK(J,L)*CF(JJ)
      IF(KJ/2*2.NE.KJ) AK(J,L)=FLOAT(EQ(KONT,IJ))/AK(J,L)
      IF(KJ/2*2.NE.KJ) AK(J,L)=(AK(J,L)-R(IJ))/(AK(J,L)-(3-R(IJ))/2.)
 1540 CONTINUE
C     COMPUTE AVERAGES & STANDARD DEVIATIONS.
      DO 1541 J=3,26
      KJ=J
      IJ=(J-1)/2
      JJ=(J-2)/2
      NRJ=NR(KONT,J)
      TOTAL=0.
      DO 1542 L=1,NRJ
 1542 TOTAL=TOTAL+AK(J,L)
      IF(KJ/2*2.EQ.KJ) PRLIST(KONT,JJ)=TOTAL/NRJ
      IF(KJ/2*2.NE.KJ) ACLIST(KONT,IJ)=TOTAL/NRJ
 1541 CONTINUE
      DO 1543 J=3,26
      KJ=J
      IJ=(J-1)/2
      JJ=(J-2)/2
      NRJ=NR(KONT,J)
      TOTAL=0.
      DO 1544 L=1,NRJ
      IF(KJ/2*2.EQ.KJ) TOTAL=TOTAL+(AK(J,L)-PRLIST(KONT,JJ))**2
      IF(KJ/2*2.NE.KJ) TOTAL=TOTAL+(AK(J,L)-ACLIST(KONT,IJ))**2
 1544 CONTINUE
      SD(KONT,J)=SQRT(TOTAL/NRJ)
 1543 CONTINUE
      DO 1565 J=3,26,2
      I=(J-1)/2
      IF(ACLIST(KONT,I).LT.0.) GO TO 1566
      GO TO 1565
 1566 NRJ=NR(KONT,J)
      DO 1567 L=1,NRJ
 1567 AK(J,L)=AK(J,L)-ACLIST(KONT,I)
      ACLIST(KONT,I)=0.
 1565 CONTINUE
      CALL BPLOT(NR,AK,ACLIST,PRLIST,KONT)
C     EXERT CONTROL FOR END OF STATION DATA
C
      IF(KONT.LT.4) GO TO 16
      PRINT900,Z2LIST
      PRINT900,NR
C     CALCULATE AIR CONTENTS FOR ALL GATE OPENINGS AND APPLY BOUNDARY
C     RESTRAINTS
C
      DO 1560 I=1,4
      DO 1560 J=1,12
      IF(ACLIST(I,J).GT.0.98) ACLIST(I,J)=0.99
 1560 CONTINUE
      DO 9500 J=1,4
      DO 9500 I=1,11
      AELIST(J,I)=(ACLIST(J,I)+ACLIST(J,I+1))/2.
      IF(AELIST(J,I).GE.0.98) AELIST(J,I)=1.
 9500 CONTINUE
      DO 9501 J=1,4
      DO 9501 I=1,11
      TOTAL=0.
      DO 9502 M=I,11
 9502 TOTAL=TOTAL+(1-AELIST(J,M))
      PSLIST(J,I)=0.0511*TOTAL
 9501 CONTINUE
      DO 9503 J=1,4
 9503 PSLIST(J,12)=0.
C     CALCULATE VELOCITIES FOR ALL GATE OPENINGS
C
      PRINT900,ACLIST
      DO 23 J=1,4
      DO 23 I=1,12
      IF(PSLIST(J,I).GT.PRLIST(J,I)) PSLIST(J,I)=PRLIST(J,I)
      VLIST(J,I)=SQRT(148.6*(PRLIST(J,I)-PSLIST(J,I))/(1-ACLIST(J,I)))
      IF(ACLIST(J,I).EQ.0.99) VLIST(J,I)=0.0
   23 CONTINUE
      PRINT900,ACLIST
      DO 1568 I=1,4
      DO 1568 J=1,12
      IJ=2*J+1
      JJ=2*J+2
      IF(PRLIST(I,J).EQ.0.) PRLIST(I,J)=1.
      PCD(I,JJ)=SD(I,JJ)/PRLIST(I,J)
      PCD(I,IJ)=SD(I,IJ)/(1-ACLIST(I,J))
      IF(PRLIST(I,J).EQ.1.) PCD(I,JJ)=0.
      IF(ACLIST(I,J).EQ.0.99) PCD(I,IJ)=0.
 1568 CONTINUE
      PRINT900,ACLIST
C     WRITE GATE OPENINGS,PROBE NUMBERS AND CORRESPONDING AIR CONTENTS
C     AND VELOCITIES
C
      DO 24 J=1,4
      WRITE(6,25)
      WRITE(6,26) J
      WRITE(6,27)
      DO 24 I=1,12
      IJ=2*I+1
      JJ=2*I+2
      WRITE(6,28) I,ACLIST(J,I),PRLIST(J,I),VLIST(J,I),SD(J,IJ),SD(J,JJ)
     1,PCD(J,IJ),PCD(J,JJ)
   24 CONTINUE
   25 FORMAT('1',4X,'GATE OPENING   FT')
   26 FORMAT('+',I18//)
   27 FORMAT('0',4X,'PROBE',4X,'AIR CONTENT',4X,'STAG.PRESSURE',4X,'VELO
     1CITY',4X,'A/C.S.D.(C-)',4X,'PRESS.S.D.(P-)',4X,'C-/(1-C)',4X,'P-/P
     1')
   28 FORMAT('0',I9,F15.2,F17.2,F12.2,F16.3,F18.3,F12.3,F8.3)
      PRINT900,ACLIST
      END
```

```
C     SUBROUTINE TO PROCESS TAPE DATA FROM AVIEMORE SPILLWAY STUDY.
C
      SUBROUTINE TDATA(NDATA,Z1LIST,Z3LIST,NPLS,K,KOUNT,N)
      EXTERNAL KELLEY
      INTEGER*2 NDATA(1)
      INTEGER Z1LIST(1),Z3LIST(1),PML(100),PM,F(30)
      DIMENSION K(1),MPL(100)
      REAL MV
  901 FORMAT('0',7G13.6)
      IF(NPLS.EQ.4) RETURN
C     READ TAPE DATA
C
      CALL PTAPE(NDATA,2000,N,KELLEY)
      DO 61 J=1,N
   61 K(J)=NDATA(J)
      GO TO 500
 2000 WRITE(6,64) (K(J),J=1,N)
   64 FORMAT('0',10(8X,I5))
  500 CONTINUE
C     ELIMINATE SPURIOS TAPE DATA DUE TO POLARITY CHANGE IN DATA LOGGER.
C
      MZ=0
      DO 155 J=1,N
      IF(K(J).EQ.9999.OR.K(J).EQ.-9999) GO TO 156
      GO TO 155
  156 DO 157 I=J,N
  157 K(I)=K(I+1)
      MZ=MZ+1
  155 CONTINUE
      N=N-MZ
C     COMPUTE AVERAGE OF DATA SET
   72 TOTAL=0.
      DO 65 J=1,N
   65 TOTAL=TOTAL&K(J)
      AN=N
      AVE=TOTAL/AN
C     COMPUTE STANDARD DEVIATION
C
      TOTAL=0.
      DO 66 J=1,N
   66 TOTAL=TOTAL&(K(J)-AVE)**2
      SD=SQRT(TOTAL/AN)
C     FIND MAXIMUM AND MINIMUM OF DATA SET
C
      KMAX=-10000
      KMIN=10000
      DO 67 J=1,N
      IF(K(J).GT.KMAX) KMAX=K(J)
      IF(K(J).EQ.KMAX) L1=J
      IF(K(J).LT.KMIN) KMIN=K(J)
      IF(K(J).EQ.KMIN) L2=J
   67 CONTINUE
      KRAN=KMAX-KMIN
      AMAX=KMAX
      AMIN=KMIN
      AGAX=AMAX-AVE
      AGAN=AVE-AMIN
C     ELIMINATE SPURIOUS TAPE READINGS
C
      TD=3*SD
      IF(AGAX.GT.TD) GO TO 68
      IF(AGAN.GT.TD) GO TO 69
      GO TO 70
   68 DO 71 J=L1,N
   71 K(J)=K(J&1)
      N=N-1
      GO TO 72
   69 DO 73 J=L2,N
   73 K(J)=K(J&1)
      N=N-1
      GO TO 72
   70 IF(NPLS.EQ.1.OR.NPLS.EQ.11) Z1LIST(KOUNT)=AVE
      IF(NPLS.EQ.3.OR.NPLS.EQ.33.OR.NPLS.EQ.6) Z3LIST(KOUNT)=AVE
      IF(NPLS.EQ.11.OR.NPLS.EQ.33.OR.NPLS.EQ.6) M=0
      IF(NPLS.EQ.2.OR.NPLS.EQ.22)M=M+1
      IF(NPLS.EQ.1.OR.NPLS.EQ.11.OR.NPLS.EQ.3.OR.NPLS.EQ.33.OR.NPLS.EQ.6
     1) GO TO 661
C     WRITE ACCEPTABLE RANGE LIMITS,AVERAGE,STANDARD DEVIATION,NO. OF
C     ACCEPTABLE READINGS
      GO TO 661
 3000 WRITE(6,74)
   74 FORMAT('0',4X,'READINGS ACCEPTED IN RANGE KMAX TO KMIN')
      WRITE(6,75)
   75 FORMAT('0',4X,'KMAX',6X,'KMIN',6X,'KRAN',3X,'AVERAGE',3X,'STD.DEV.
     1',3X,'NO.ACCEPTED READINGS')
      WRITE(6,76) KMAX,KMIN,KRAN,AVE,SD,N
   76 FORMAT('0',I8,2I10,F10.0,F11.2,I14)
C     ESTABLISH DISPERSION OF DATA ABOUT AVERAGE.
      IF(NPLS.EQ.2.OR.NPLS.EQ.22) GO TO 660
      GO TO 661
  660 KQ=0
      MV=AVE
      PV=AVE
      DO 671 J=1,100
      MPL(J)=0
      PML(J)=0
  671 CONTINUE
  653 KQ=KQ&1
      PM=0
      MP=0
      MV=MV-KRAN/10.
      PV=PV+KRAN/10.
      DO 650 J=1,N
      IF(K(J).GT.MV.AND.K(J).LE.(MV+(KRAN/10.))) GO TO 651
      IF(K(J).LT.PV.AND.K(J).GE.(PV-(KRAN/10.))) GO TO 652
      GO TO 650
  651 MP=MP&1
      GO TO 650
  652 PM=PM&1
  650 CONTINUE
      MPL(KQ)=MP
      PML(KQ)=PM
      IF(PV.GE.KMAX.AND.MV.LE.KMIN) GO TO 654
      GO TO 653
  654 WRITE(6,655)
  655 FORMAT('0',4X,'DATA DISPERSION ABOUT AVERAGE')
      DO 670 J=1,21
  670 F(J)=J-11
      WRITE(6,657) (F(J),J=1,21)
  657 FORMAT('0',2116)
      WRITE(6,658) (MPL(11-I),I=1,10)
  658 FORMAT('0',1016)
      WRITE(6,659) (PML(I),I=1,10)
  659 FORMAT('+',66X,1016)
  661 CONTINUE
      RETURN
      END
```

```
      SUBROUTINE BPLOT(NR,AK,ACLIST,PRLIST,KONT)
      DIMENSION NR(4,28),AK(28,310),ACLIST(4,12),PRLIST(4,12
      DIMENSION TZ(400),TZZ(400)
  900 FORMAT('0',10G13.6)
      LOGICAL*1 ILABEL(3)/'A/C'/
      LOGICAL*1 JLABEL(8)/'PRESSURE'/
      LOGICAL*1 KLABEL(12)/'TIME-SECONDS'/
      PRINT900,NR
      DO 1503 J=3,20,2
      JJ=(J-1)/2
      JOK=J+1
      NRJ=NR(KONT,J)
      NRJJ=NR(KONT,JOK)
      DO 1502 K=1,NRJ
      TZ(K)=AK(J,K)*100.
 1502 CONTINUE
      DO 1504 K=1,NRJJ
      TZZ(K)=AK(JOK,K)
 1504 CONTINUE
      IF(NRJ-NRJJ)1506,1506,1507
 1506 IXINC=NRJJ/20*100+100
      GO TO 1508
 1507 IXINC=NRJ/20*100+100
 1508 ILONG=IXINC+400
      CALL AINIT(ILONG)
      CALL AGRID(100,100,1,2,IXINC,225,2,2)
      CALL AGRID(100,550,1,2,IXINC,225,2,2)
      Z=ACLIST(KONT,JJ)*100.
      PRINT900,Z
      KZ=10*(IFIX(Z/10))
      KKZ=Z-KZ
      IY=145-10*KKZ
      ILO=KZ-10
      YOR=Z-32.5
      CALL ASCA(98,IY,0,100,ILO,10,4,2,4)
      Z=PRLIST(KONT,JJ)
      PRINT900,Z
      KZ=10*(IFIX(Z/10))
      KKZ=Z-KZ
      IY=595-10*KKZ
      ILO=KZ-10
      COR=Z-77.5
      CALL ASCA(98,IY,0,100,ILO,10,4,2,4)
      N=IXINC/100
      CALL ASCA(20,528,100,0,0,10,N,2,2)
      CALL ALAB(25,250,ILABEL,3,2,4)
      CALL ALAB(25,675,JLABEL,8,2,4)
      CALL ALAB(200,560,KLABEL,12,2,2)
      CALL ALINEX(100,5,TZ,NRJ,YOR,10.)
      CALL ALINEX(100,5,TZZ,NRJJ,COR,10.)
      CALL AEND
 1503 CONTINUE
      RETURN
      END
```

5. Water Discharge Programme

Purpose:

To calculate the water discharge from profiles of air concentration and velocity.

Comments:

The programme will accept up to fifty values of air concentration and velocity for each discharge calculation. This capacity could be extended by altering the DIMENSION statement.

Input Data:

	Card	Data	Format
Repeated for each discharge	1	Gate opening, comparative discharge (cusecs)	I1,I4
Repeated for each station and same discharge	2	Station identification, depth increment (in.), number of readings (NC)	I3,F2.2,I2
Repeated for each pair of readings	3	Air concentration, velocity (ft/sec.)	F3.3,F4.1
	Final card of deck	Air concentration at surface, velocity at surface, incremental depth to surface (a value of 0 for air concentration at surface skips this step.)	F3.3,F4.1,F2.2

Output Data:

(a) Gate opening and comparative discharge for each test flow.

(b) Station identification and calculated discharge for each pair of profiles.

```
C**************************************************************************
C
C PROGRAM TO COMPUTE DISCHARGE FROM VELOCITY AND AIR CONCENTRATION PROFILES
C
C**************************************************************************

      INTEGER GO,TD,SN
      DIMENSION ACLIST(50),VLIST(50),AAC(50),AV(50),DQ(50)
   14 READ(5,1) GO,TD
    1 FORMAT(I1,I4)
      WRITE(6,2)
    2 FORMAT('1',4X,'GATE OPENING(FT)',4X,'DISCHARGE(CUSECS)')
      WRITE(6,3) GO,TD
    3 FORMAT('0',I13,I18)
   15 READ(5,4) SN,DY,NC
    4 FORMAT(I3,F2.2,I2)
      WRITE(6,5)
    5 FORMAT('0',4X,'STATION NUMBER')
      WRITE(6,6) SN
    6 FORMAT('0',I3)
      DO 7 J=1,NC
      READ(5,8) AC,V
      ACLIST(J)=AC
      VLIST(J)=V
    7 CONTINUE
    8 FORMAT(F3.3,F4.1)
      DO 9 J=2,NC
      I=J-1
      AAC(I)=(ACLIST(J)&ACLIST(J-1))/2.
      AV(I)=(VLIST(J)&VLIST(J-1))/2.
    9 CONTINUE
      M=NC-1
      DO 10 J=1,M
      DQ(J)=AV(J)*(1-AAC(J))*DY/12.
   10 CONTINUE
      TOTAL=0.
      DO 11 J=1,M
      TOTAL=TOTAL&DQ(J)
   11 CONTINUE
      READ(5,20) DAC,DV,DDY
   20 FORMAT(F3.3,F4.1,F2.2)
      DAAC=(ACLIST(NC)+DAC)/2.
      DAV=(VLIST(NC)+DV)/2.
      DDQ=DAV*(1-DAAC)*DDY/12.
      IF(DAC.EQ.0.) DDQ=0.
      TOTAL=TOTAL+DDQ
      Q=TOTAL*52.
      WRITE(6,12)
   12 FORMAT('0',4X,'COMPUTED DISCHARGE=',8X,'CUSECS')
      WRITE(6,13) Q
   13 FORMAT('+',F30.2)
      IF(SN.EQ.401.AND.GO.EQ.4) CALL EXIT
      IF(SN.EQ.405) GO TO 14
      GO TO 15
      END
```

APPENDIX III

ELECTRONIC CIRCUITRY

Air Concentration Measurement:

The block diagram of the air concentration pier electronics (Figure 2.27, page 88) shows that the electronic equipment required in the pier comprised an oscillator, differential amplifier and rectifier, and a probe selector unit. These three units were specially designed and their circuit diagrams are presented in Figures AIII.1 to AIII.3.

The entire electronic circuitry was mounted on four circuit boards.

The probe selector unit was mounted on one board and consisted of three ternary decode units (shown in Figure AIII.3) - one for each input wire. The oscillator and differential amplifier and rectifier were mounted on a single board. The remaining two boards contained the relay switch circuits for the fourteen test positions (twelve air concentration probes, oscillator monitor, and calibration probe), and the master output switch (R1). A typical switch circuit and master output switch are shown in Figure AIII.4.

Velocity Measurement:

The block diagram of the velocity pier electronics (Figure 2.29, page 90) shows that the electronic equipment required in the pier comprised an oscillator, differential strain bridge amplifier and rectifier, and a probe selector unit. The probe selector unit was identical to that designed for the air concentration pier except that different coding combinations on the three input wires were used. The other two units were specially designed and their circuit diagrams are

presented in Figures AIII.5 and AIII.6.

The electronic circuitry was mounted on four circuit boards - one for the probe selector unit, two for the relay switch circuits, and one for the oscillator, strain bridge amplifier, and master output switch (R2). The circuitry for switch R2 was the same as for switch R1. (Figure AIII.4).

Field Test Cable Specification:

7 core 10 x .010" copper shielded cable, with centre core concentrically shielded.

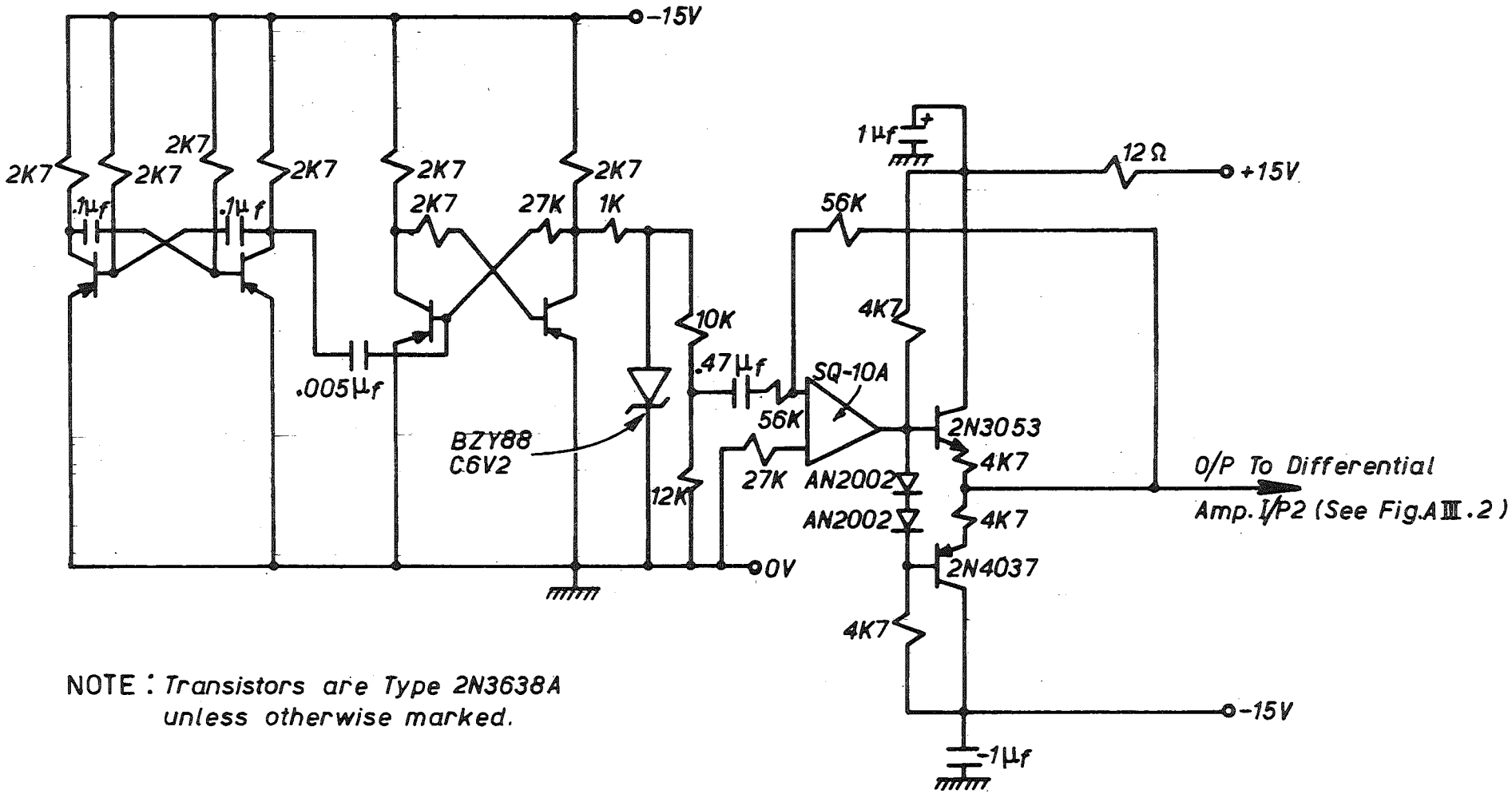

NOTE : Transistors are Type 2N3638A unless otherwise marked.

Fig A III.1: AIR CONTENT PIER OSCILLATOR – CIRCUIT DIAGRAM

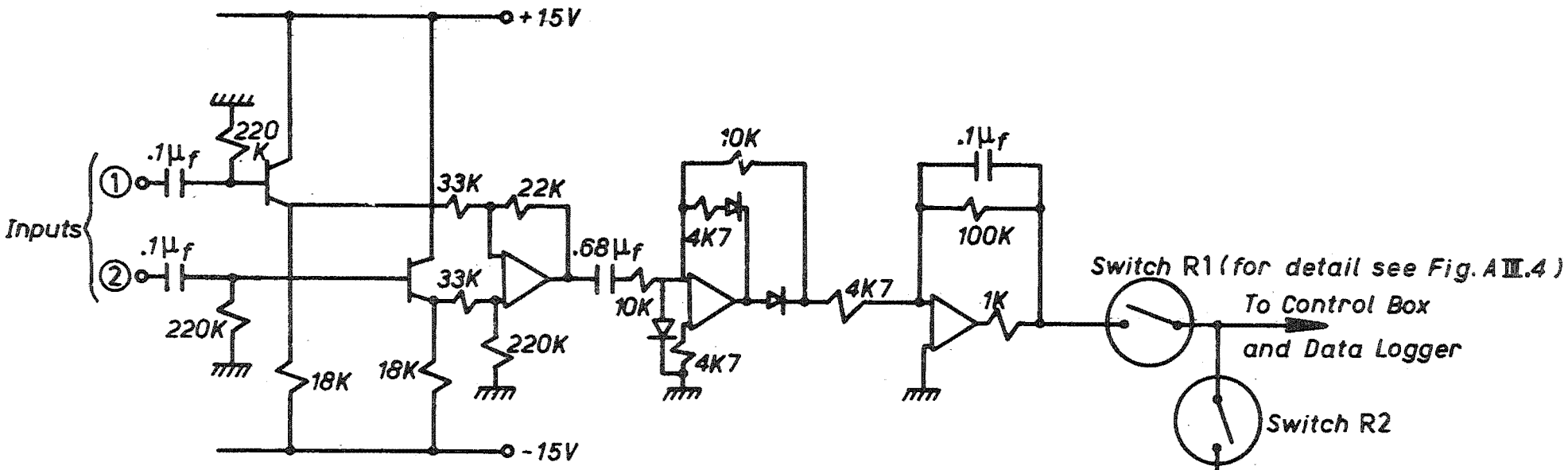

NOTES : 1-All Amplifiers Type μA709
2- " Diodes " AN2002
3- " Transistors " 2N3694

Fig.AIII.2: AIR CONTENT PIER DIFFERENTIAL AMPLIFIER AND RECTIFIER – CIRCUIT DIAGRAM

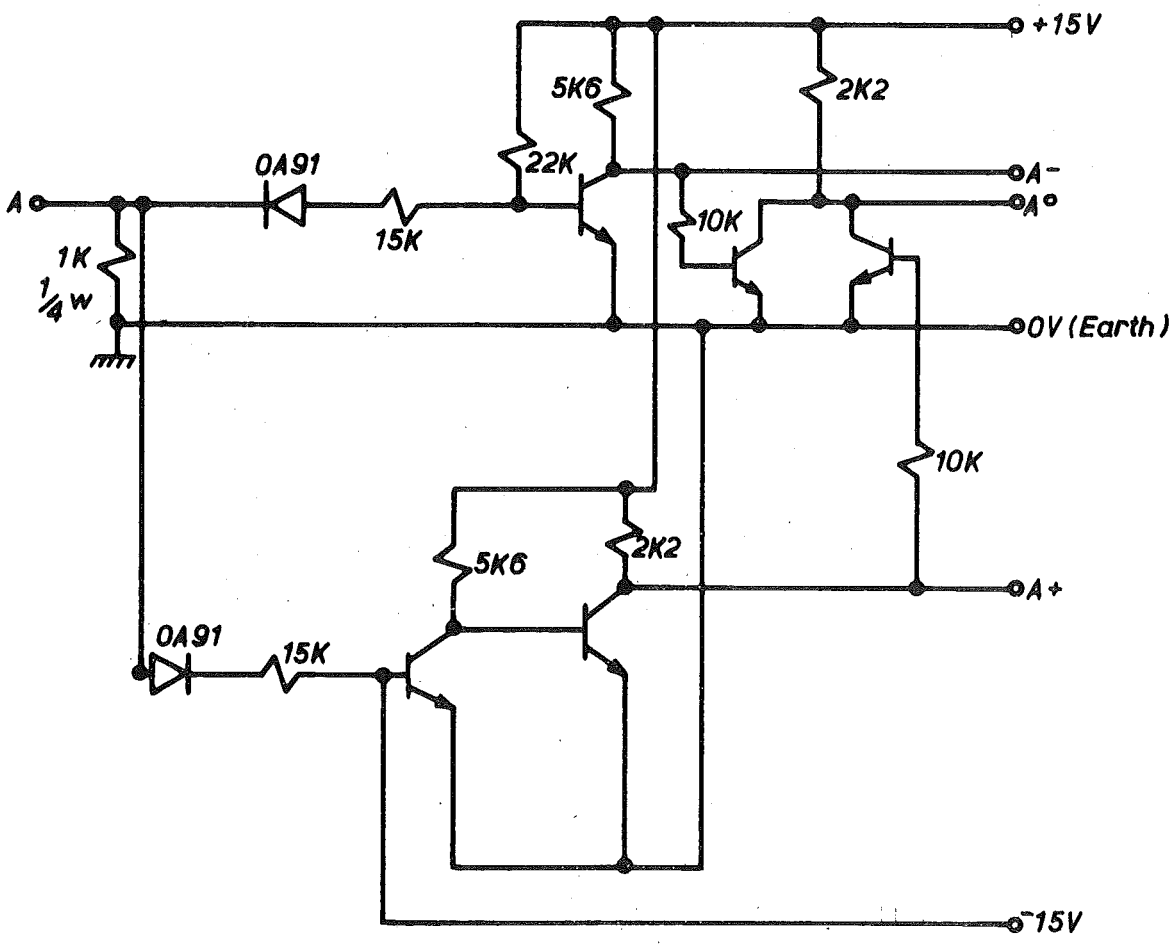

NOTE :-(1) All resistors 1/8 w unless stated otherwise

(2) All transistors Type 2N3643

Fig. A III.3 : AIR CONTENT PIER TYPICAL TERNARY DECODE - CIRCUIT DIAGRAM

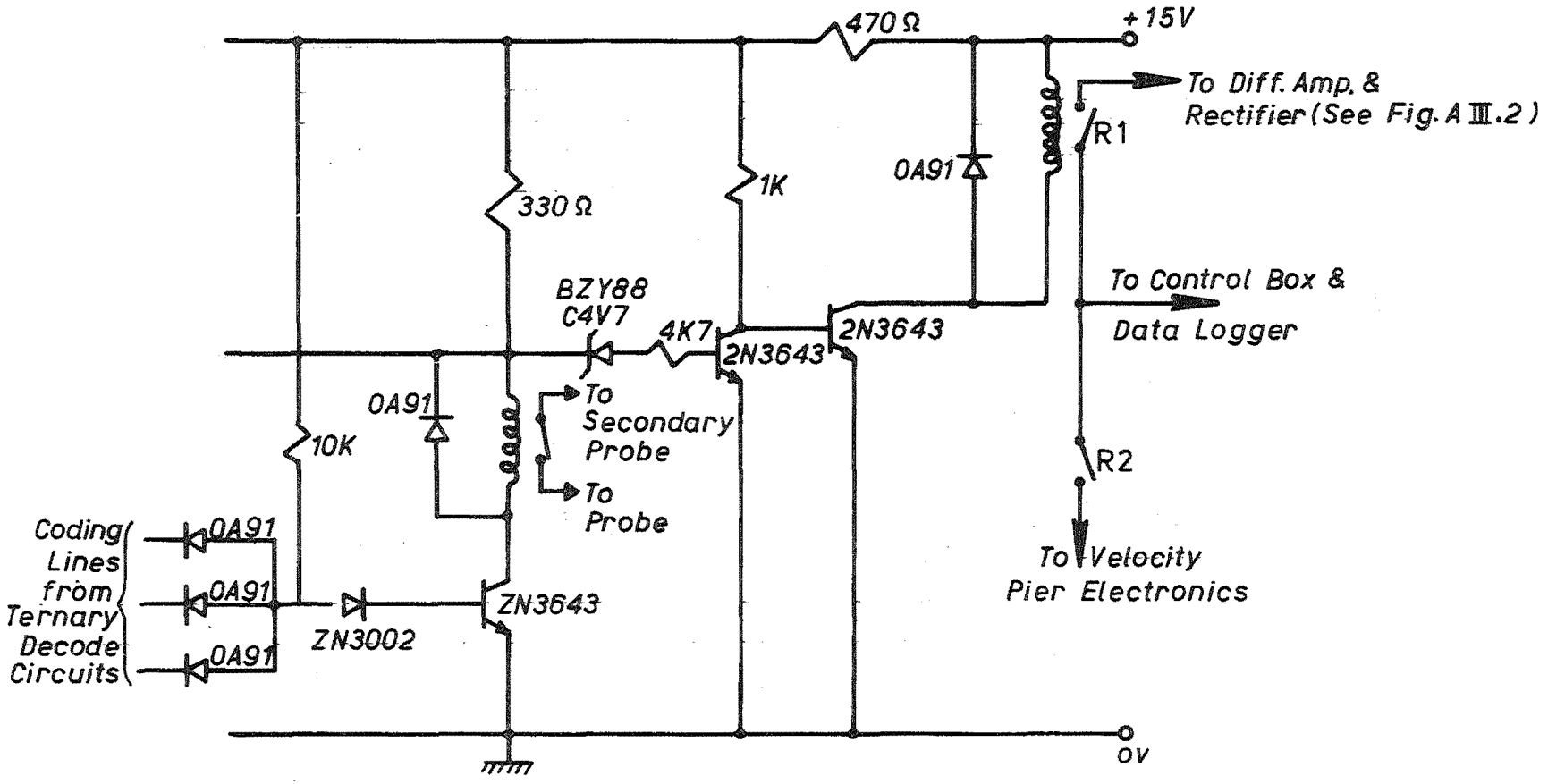

Fig. A III.4: AIR CONTENT PIER TYPICAL RELAY SWITCH AND MASTER OUTPUT SWITCH R1 — CIRCUIT DIAGRAM

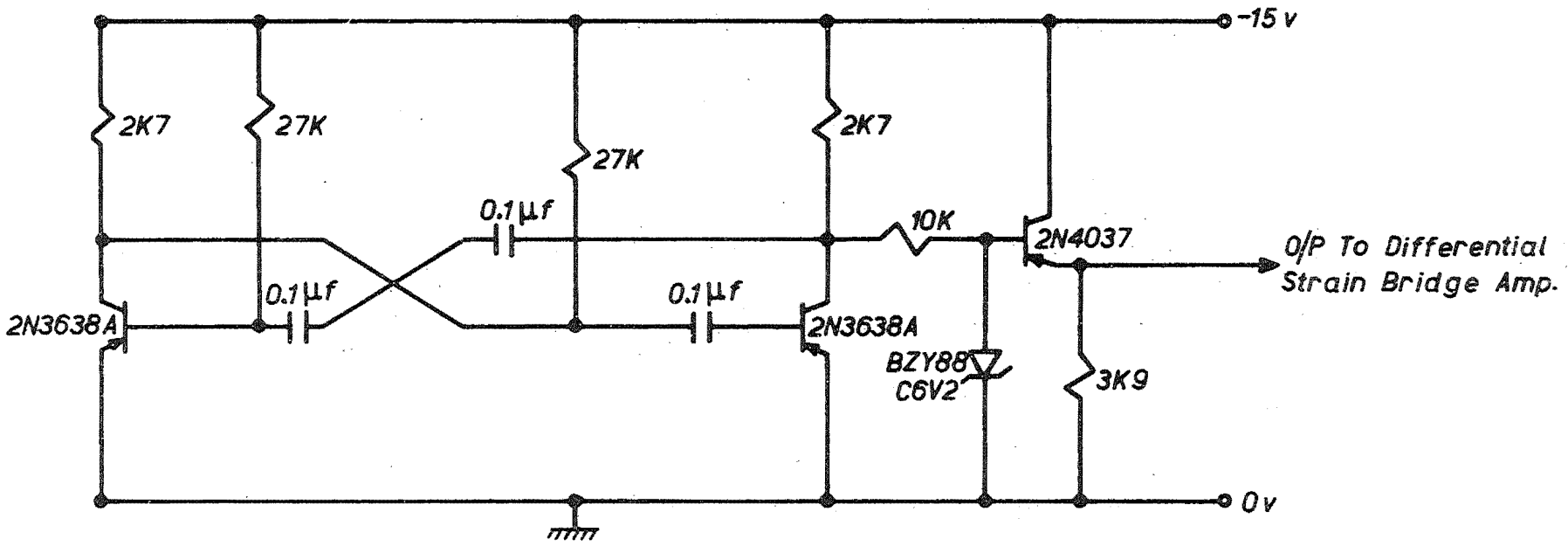

Fig A III.5: VELOCITY PIER OSCILLATOR – CIRCUIT DIAGRAM

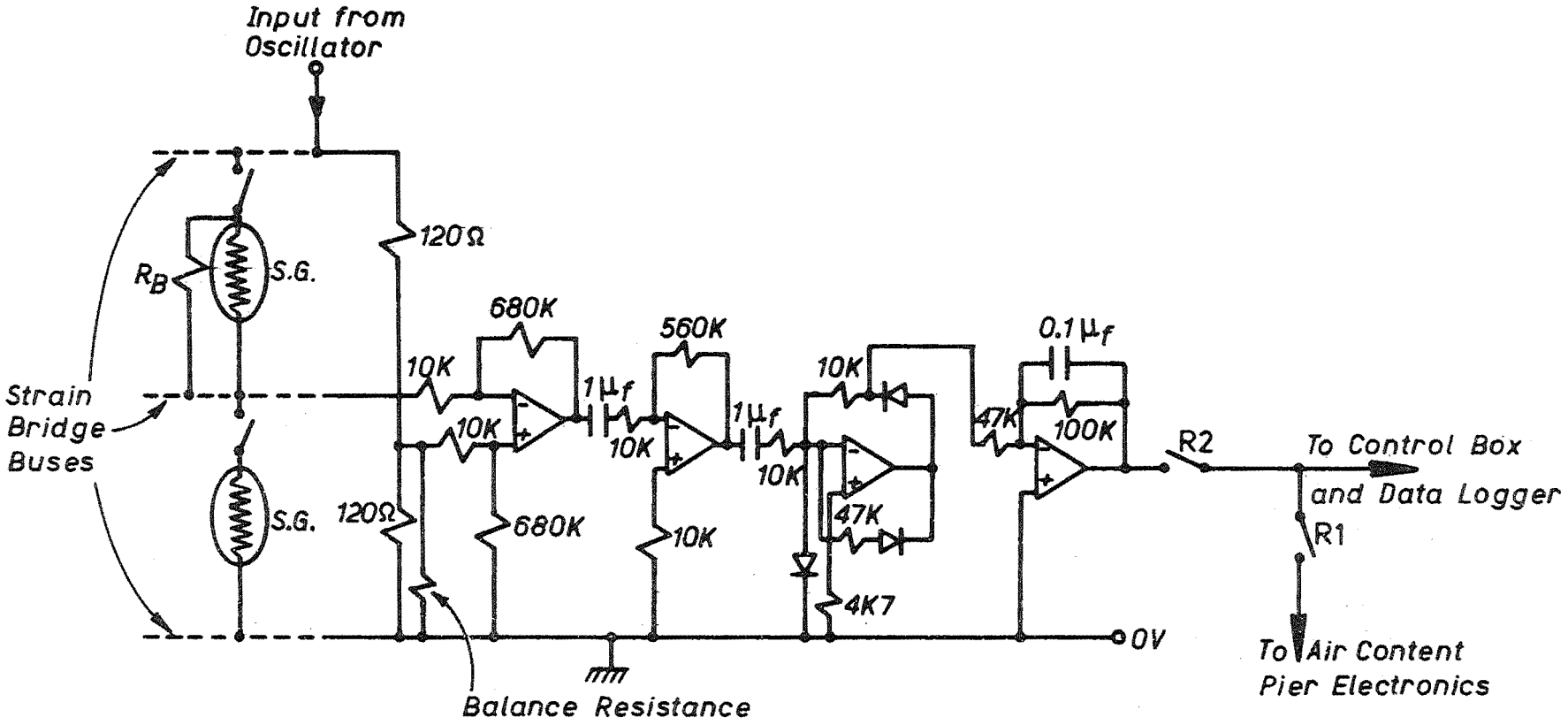

NOTES: 1 - All Amplifiers Type μA709
2 - " Diodes " AN2002
3 R_B is a balance resistance

Fig AIII.6: VELOCITY PIER DIFFERENTIAL STRAIN BRIDGE AMPLIFIER AND TYPICAL STRAIN BRIDGE CIRCUIT DIAGRAM

APPENDIX IV

STRUCTURAL DESIGN OF FIELD TEST UNIT

The structural design of the field test unit was carried out according to the following procedure.

(a) Determine the maximum drag force on the unit.

The drag force, F , on each pier was calculated from the standard equation

$$F = C_D \, A \, \frac{\rho V^2}{2} \qquad \ldots \text{AIV.1}$$

where

C_D is the drag coefficient (estimated to be 0.6)

A is the projected area of the pier normal to the direction of fluid flow

ρ is the fluid density

V is the fluid velocity

The difference in elevation between the normal head water operating level at Aviemore and the bottom recording station was 118 ft. and the drag force on the pier was conservatively calculated as that due to the velocity of pure water falling through this height. The projected area dimensions for each pier were three inches wide by two feet high. The drag force thus determined was 2,200 lb.

(b) Determine the maximum bending moment due to the drag force and the minimum pier section modulus required to withstand it.

The maximum bending moment, M , was calculated from the standard equation

$$M = \frac{FL}{2} \qquad \ldots \text{AIV.2}$$

where

L is the length of the pier (= 2 ft). The bending moment thus calculated was 2,200 lb-ft.

The minimum pier section modulus, Z , was calculated from the standard equation

$$Z = \frac{M}{f} \qquad \ldots \text{AIV.3}$$

where

f is the maximum allowable stress in the pier (= 10.5 tons/sq.in. for steel).

The minimum section modulus thus calculated was 1.12 $in.^3$

(c) Select a suitable pier section to satisfy the requirements of minimum dimensions (specified in Section 3.4.4) and minimum section modulus.

These requirements were satisfied by using a 6" x 3" x 3/16" Rolled Hollow Section. This represents a very strong pier section which will easily withstand the shear due to the drag force.

(d) Determine the minimum thickness of the test unit base plate.

The area dimensions of the base plate were restricted by the size of the spillway station blanking plates to 2' x 2'.

The minimum thickness of the base plate was dependent on the calculation of the minimum plate section modulus to resist the total bending moment due to the drag forces on the two piers. The total bending moment (from b.) above) was 4,400 lb-ft. This moment was assumed to act at the mid-point of a beam two feet long and two feet wide.

The minimum plate section modulus was calculated from Eq. A.IV.3 which gave a value of 2.24 $in.^3$

The minimum thickness of the plate, d , was then calculated from

the standard equation

$$Z = \frac{bd^2}{6} \qquad \ldots \text{AIV.4}$$

where

b is the width of the "equivalent beam". Eq. AIV.4 gave a value for d of 0.75".

This figure represents a very conservative value for the minimum plate thickness, because the plate is bolted down around all four sides. The "equivalent beam" concept assumes the plate to be bolted only at the upstream and downstream edges and free to deform along the sides as a beam.

This justified the adoption of a thinner base than indicated by the above calculation and a plate thickness of $\frac{1}{2}$ inch was adopted.

In subsequent field testing no structural problems of any kind occurred.

The main structural features of the field test unit are shown in Figure 2.24.

APPENDIX V

CALCULATION OF BOUNDARY LAYER DISPLACEMENT THICKNESS

The displacement thickness is defined as the distance by which the boundary layer displaces the whole flow pattern laterally from the solid boundary.

Thus, with reference to Figure AV.1, its value is described by

$$\delta_1 = \frac{1}{U} \int_o^{\delta} (U - u)\, dy \qquad \ldots \text{AV.1}$$

where U is the free stream velocity.

u is the velocity within the boundary layer at distance y from the spillway surface.

δ is the boundary layer thickness.

The velocity profile within the boundary layer may be defined by an equation of the form

$$\frac{u}{U} = \left(\frac{y}{\delta}\right)^n \qquad \ldots \text{AV.2}$$

where the value of n varies from $\frac{1}{7}$ to about $\frac{1}{10}$ with increasing Reynolds Number.

For the comparatively large Reynolds Number of the Aviemore spillway flow, a value for n of $\frac{1}{9}$ was assumed.

Substitution of Eq. AV.2 into AV.1 yields

$$\delta_1 = \int_o^{\delta} \left[1 - \left(\frac{y}{\delta}\right)^{\frac{1}{9}}\right] dy \qquad \ldots \text{AV.3}$$

which, on integration, yields

$$\delta_1 = 0.1\, \delta \qquad \ldots \text{AV.4}$$

Equation AV.4 is applicable to turbulent flows of comparatively large Reynolds Numbers.

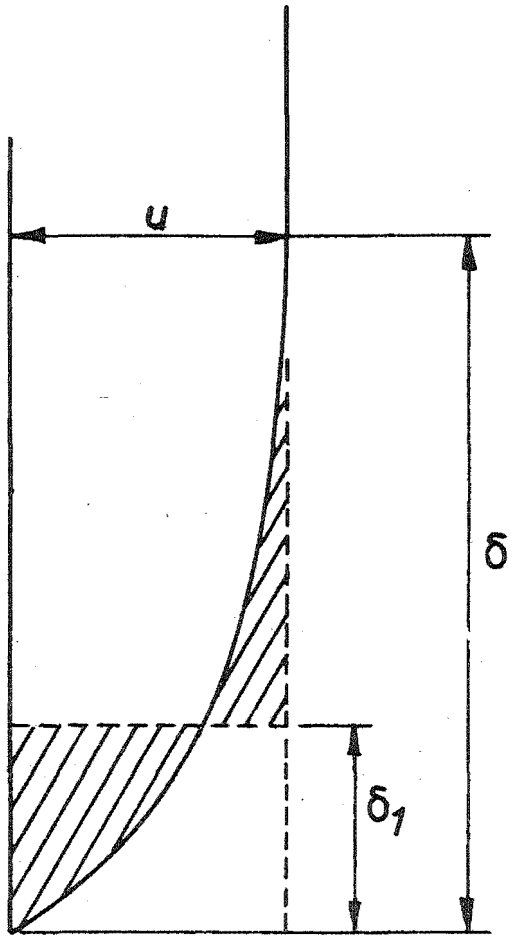

Fig. A V 1 : DEFINITION OF BOUNDARY LAYER DISPLACEMENT THICKNESS.

APPENDIX VI

INTERPRETATION OF EQUATION 2.2.8 WITH RELATION TO INCREASED SECONDARY PROBE RESISTANCE

The derived equation for calculating air concentration is

$$C = \frac{\frac{E_o}{E_s} - z}{\frac{E_o}{E_s} - \frac{(3-z)}{2}} \qquad \ldots 2.2.8$$

It was shown on page 36 that

$$E_p = I R_p = E_o - E_s = E_o - I R_s \qquad \ldots 2.2.4$$

By using Eq. 2.2.4 to eliminate E_o and E_s, Eq. 2.2.8 may be expressed as

$$C = \frac{(R_s + R_p) - z R_s}{(R_s + R_p) - \frac{(3-z)}{2} R_s}$$

i.e.

$$C = \frac{R_s (1-z) + R_p}{R_s (1 - \frac{3-z}{2}) + R_p} \qquad \ldots AVI.1$$

Differentiation with respect to R_s yields

$$\frac{dC}{dR_s} = \frac{\frac{3}{2} R_p (1-z)}{[R_s (1 - \frac{3-z}{2}) + R_p]^2}$$

i.e.

$$\frac{dC}{dR_s} = -\frac{\frac{3}{2} R_p (z-1)}{[R_s (1 - \frac{3-z}{2}) + R_p]^2} \qquad \ldots AVI.2$$

Equation AVI.2 shows that for all values of z not equal to 1, an increase in R_s results in a consequent decrease in the value of C. i.e. A small increase in the resistance of the secondary probe results in a value of air concentration, calculated from Eq. 2.2.8, slightly lower than the true value.